Advances in Planetary Geology

February 1983

NASA

NASA TM-85630

Advances in Planetary Geology

Scientific and Technical Information Branch 1983
National Aeronautics and Space Administration
Washington, DC

CONTENTS

SECTION I

MARTIAN GLOBAL TECTONICS

Richard A. Schultz

ABSTRACT

Scarps, ridges, and graben within the heavily cratered terrain of Mars define distinct groups of structural trends on a regional scale, and a pattern of crustal deformation on a global scale. These trends are the result of regional deformation of the crust, rather than the imposition of a single planet-wide stress system. Centers of deformation are spatially related by a systematic global pattern. As the relative ages of measured structures in the heavily cratered terrain seem to generally predate both the emplacement of Lunae Planum-aged volcanic units and the structural and volcanic activity near Tharsis, this structural pattern is thought to reflect a fundamental global organization of volcanic and tectonic activity. This pattern was developed early in martian history, and served to localize subsequent crustal modification. The earliest manifestation of this pattern was in primarily mechanical deformation of the crust. This was globally asymmetric and most intense in the northern third of the planet; it guided the formation of the planetary dichotomy boundary, much of the original structure of the associated fretted terrain and, in addition to local volcanism, may have contributed to the NE-SW asymmetry of the later Tharsis-related graben sets. The

other major phase of activity was primarily thermal; this produced the extensive volcanic plains of Lunae Planum-age near Tharsis and, to a lesser extent, in Syrtis Major and Hesperia Planitiae. Subsequent, more local activity along this global pattern seems to have contributed to plains volcanism southwest of Hellas, constructional volcanism in the Tharsis region, and modification of surface landforms in areas of fretted terrain.

ACKNOWLEDGMENTS

I am very grateful to Dr. Michael C. Malin, my research advisor, for suggesting the topic and for his exemplary guidance and support.

I also appreciate useful discussions with Dr. Ronald Greeley, Dr. Donal M. Ragan, and Henry Eby, and wish to thank Ron Greeley for the use of the Space Photography Laboratory (Arizona State University), and Robert Strom for access to the Planetary Image Facility (University of Arizona) during the summer of 1981.

TABLE OF CONTENTS

LIST OF TABLES

LIST OF FIGURES

INTRODUCTION

Mars has undergone several episodes of large-scale crustal deformation since its terminal meteoritic bombardment, as suggested by its surface morphology. Perhaps the most fundamental of these is that which gave rise to the planet's distinctive north-south terrain dichotomy. The origin of this dichotomy, as well as the associated fretted and knobby terrains that are commonly used to define its boundary, remains a major enigma in martian geophysical research.

Several other tectonic provinces are regionally important (see Figure 1). Of these, Tharsis is perhaps the youngest and most highly developed. It is marked by extensive plains-forming volcanism (e.g., Lunae, Syria, and Tharsis Plana) and several major volcanic constructs (e.g., Olympus Mons, Tharsis Montes, Alba Patera). Radial fracturing, in the form of graben and canyons, extends into the adjacent terrains. A smaller area of comparable age is Elysium, which is also characterized by large volcanic constructs, volcanic plains, and radial fracturing. An older region of similar, though less intense, activity is centered in Thaumasia; the trends of some structural features near Tharsis (e.g., Echus Chasma and portions of the Valles Marineris) likely follow the trends of older Thaumasia-radial fractures [Frey, 1979]. Detailed studies

Fig. 1. Location map of major features on Mars. Base map of global geology after Scott and Carr [1978].

LOCATION OF MAJOR VOLCANIC AND STRUCTURAL FEATURES MARS GEOLOGY, AFTER SCOTT AND CARR (1978)

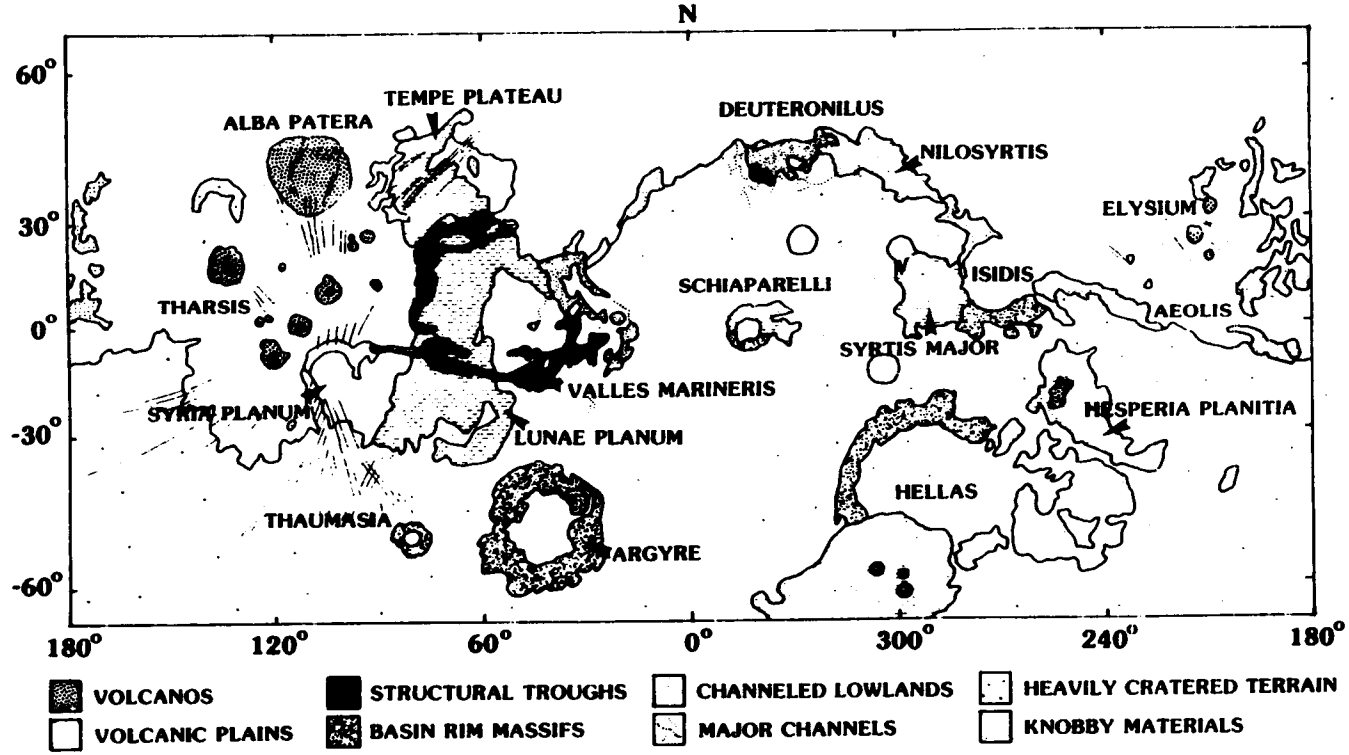

of the structural geology of portions of these areas may be found in Carr [1974], Blasius et al. [1977], and Wise et al. [1979]. Comprehensive reviews of Tharsis and global volcanism can be found in Plescia and Saunders [1979a] and Greeley and Spudis [1981].

Very little is known about the structural history of the heavily cratered terrain of Mars. This area includes over half the surface area of Mars and is probably the most ancient terrain on the planet. The major features developed in and around this terrain are very large multiringed impact basins (e.g., Argyre, Isidis, and Hellas) and relatively smaller impact craters of varying diameters; the Valles Marineris and Tharsis-related graben systems; the Thaumasia rise; and a 2- to 3-km-high discontinuous escarpment, marking the planetary dichotomy boundary, and separating the high-standing, heavily cratered terrain from the lower, smoother cratered plains to the north. The heavily cratered terrain is modified by the development of chaotic terrain [Sharp, 1973], regional systems of outflow channels, interpreted by Sharp and Malin [1975] as possibly being of fluvial origin, and digitate networks of narrow valleys [Pieri, 1980]. Many of these features have been inferred to have formed along older structural trends in the heavily cratered terrain.

Many well defined linear structures and regional trends also can be identified in the heavily cratered terrain. These are recognized in Viking images as scarps, ridges, and graben-like linear depressions; studies of these structures form the basis of this study. The principle objective of this research is to attempt to address the following questions:

1. Are the structures developed in the heavily cratered terrain organized on a global or regional scale, or do they reflect local stress histories?

2. How do these structures relate to the planetary dichotomy boundary and to Tharsis tectonism?

Background

As used in this paper, the term "tectonic" will be restricted to describe those processes that deform the crust of a planet; "structure" will refer to the deformational features formed in the crust by fracture as a result of some tectonic activity.

Of the terrestrial planets and the Moon, only Mercury and the Earth currently show evidence of significant, globally-organized tectonics. Dzurisin [1978] mapped and classified structures on Mercury; based on theoretical work [Melosh, 1977], Dzurisin [1978] and Melosh and Dzurisin [1978] suggested that the orthogonally trending lineaments represented conjugate shear fractures resulting from tidal despinning of the planet. Similar orthogonal

lineament trends have also been suggested for the Moon [Fielder, 1961; Strom, 1964]; however, the lack of significant strike-slip displacement along these fractures, as well as the angles between them, argues against such a model for their formation.

Martian lineaments were suggested by studies of Mariner IV images [Binder, 1966] and later missions [Binder and McCarthy, 1972; Wilson et al., 1973; Schultz and Ingerson, 1973]. The most comprehensive pre-Viking study of lineament patterns was that of Harp [1976], who utilized the extensive Mariner 9 data set.

Schultz and Ingerson [1973] first mentioned possible difficulties in identifying a global structural pattern if regional deformation were superimposed upon it; such regional structures might have been produced or enhanced by the formation of fractures radial to large impact basins [Casella, 1976; Melosh, 1976]. Gifford [1981] studied the distribution and trends of well developed mare-type wrinkle ridges located in relatively isolated regions of inferred volcanic plains. Although the origin of wrinkle ridges is unclear, they seem to have been produced through some combination of volcanic and tectonic processes, and may locally follow pre-existing structural trends [Young et al., 1973; Lucchitta, 1976]. The martian wrinkle ridges studied by Gifford [1981] are restricted to local geologic units and, to date, no attempt has been

made to infer whether these features follow any globally organized pattern, although relations to regional Tharsis tectonism have been suggested [Plescia and Saunders, 1979b; Wise et al., 1979; Phillips and Lambeck, 1980; Gifford, 1981; Plescia and Saunders, 1981].

The nearly orthogonal set of lineament trends suggested by Binder [1966], Binder and McCarthy [1972], Wilson et al. [1973], and Harp [1976] are oriented symmetrically to both the present rotation axis and the equator; these trends were interpreted as conjugate shear fractures, based on the model developed by Vening-Meinesz [1947] and expanded upon by Melosh [1977]. Acquisition of systematic high resolution images by the Viking Orbiter spacecraft now makes possible a reexamination of these martian linear features.

STRUCTURAL MAPPING

Summary of Approach

A reconnaissance survey of possible structural features in the heavily cratered terrain of Mars was undertaken; the resulting inventory of possible structures from various parts of the planet comprise the basic observations. These features, after morphologic studies, were plotted in azimuth-frequency (rose) diagrams to identify dominant trends and to facilitate comparisons of features from widely separated locations on the planet. In this study, north and south latitude will be given in positive or negative degrees, respectively; longitude increases from 0° to 360° to the west.

Coverage

Selected areas of Mars were chosen for detailed study on the basis of the availability of sufficient images of roughly comparable and uniform resolution in a given area. These areas are shown in Figure 2.

The surface of Mars has been divided into 30 broad regions for mapping purposes. Maps of each of these regions are termed "Mars Charts" (abbreviated MC), which are assigned a number, and "quadrangles," which are named. A quadrangle can be subdivided into four parts, designated NE, NW, SE, and SW. Images used in this study are those

acquired by the Viking Orbiter spacecraft; these can be studied in either of two digitally-produced map projections: rectilinear or orthographic. Rectilinear images preserve the perspective of terrain features as viewed and recorded by the Orbiter, commonly from an oblique angle. These images are useful for identifying structural features. The viewing angle of a scene can be artificially changed from oblique to vertical using digital image processing techniques; this new version is called an orthographic projection. Although the terrain is somewhat distorted, these altered versions are useful for measuring the lengths and azimuths of structures, as well as for making mosaics of multiple images. Many such mosaics were compiled at the Jet Propulsion Laboratory in Pasadena, California, and are identified by a sequential four-digit number affixed to a 211- prefix (e.g., JPL mosaic 211-5501).

Preference was given to areas that contained either prominent structural features or some desirable location within the heavily cratered terrain. For example, data were taken from within the Ismenius Lacus Quadrangle because certain structures there locally parallel, and often merge with, elements of the fretted terrain marking the planetary dichotomy boundary. On the other hand, structures in close proximity to major impact basins (e.g., Hellas) were <u>not</u> included, in order to evaluate structural

Fig. 2. Coverage map of study regions within the heavily cratered terrain.

STUDY AREAS WITHIN THE HEAVILY CRATERED TERRAIN MARS GEOLOGY, AFTER SCOTT AND CARR (1978)

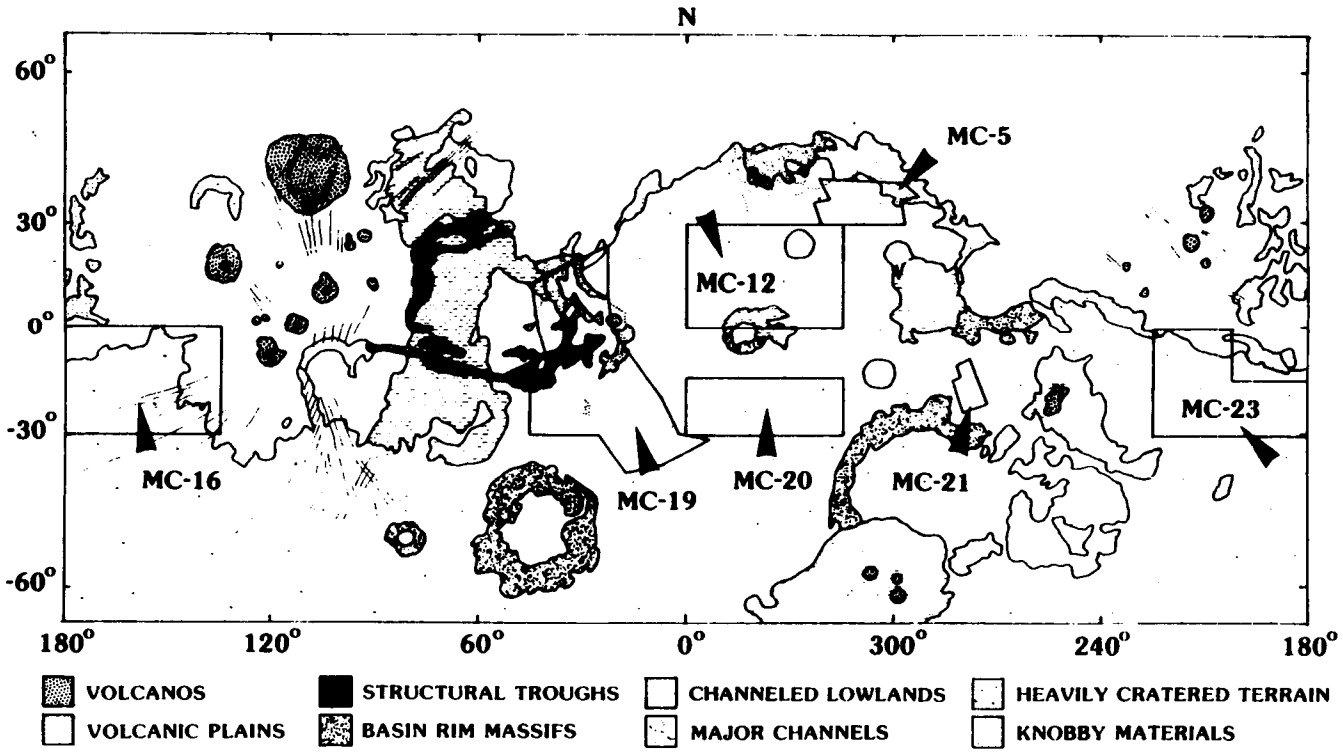

trends in the heavily cratered terrain produced from endogenic processes. The results are generally representative of the heavily cratered terrain north of the equator. The areas studied include regions located near Tharsis, but in the heavily cratered terrain (MC-16); near the Elysium volcano-tectonic province (MC-23); in areas of extensive channeling (MC-19); within the heavily cratered terrain (MC-20 and MC-12); adjacent to fretted terrain (MC-5, 211-5741); and between Isidis and Hellas basins (Viking Orbiter frames 625A01 through 625A08 in MC-21).

Many graben sets extend from Tharsis deep into the heavily cratered terrain; no effort was made to map the most obvious of these structures, as they appear to be generated from a well defined regional source [Wise et al., 1979]. Although in the heavily cratered terrain the orientations of Tharsis-related graben could conceivably reflect a composite of Tharsis-generated stress trajectories and movement along pre-existing structural trends, structures located elsewhere would most likely define such older trends more precisely and with less "noise" from later, superimposed deformations. Analysis of the trends of Tharsis-related graben, however, are useful in estimating how much of their development, if any, was influenced by older structural trends, once these have been isolated.

Morphology

Three general types of features were studied: scarps, ridges, and graben. Examples are shown in Figures 3 and 4. The scarp illustrated in Figure 3a is typical of many well developed structures elsewhere in the heavily cratered terrain. It defines a distinct break in topography of both the surrounding plains and the transected crater; virtually no lateral offset or displacement normal to the trend of the scarp can be detected in the vicinity of the crater. Similar scarps in other regions may be somewhat less strongly defined, but the general characteristics of a continuous topographic break are maintained.

As the form of scarps have little similarity to features interpreted as lava flow fronts [Greeley and Spudis, 1981], they are here thought to represent fault scarps; the lack of lateral offsets of transected craters suggests predominantly vertical or nearly vertical motion. Many of these structures are here interpreted as scarps associated with normal faults, although an origin as high-angle reverse faults is not precluded.

Ridges are somewhat less common in the heavily cratered terrain than scarps. Figure 3b shows a prominent ridge. It is located on what is now an irregular plateau; note the graben-like linear trough that transects the

Fig. 3. Examples of scarps and ridges measured in this study. Note the pronounced topographic expression of the westwardly facing scarp in Figure 3a and the ridge in Figure 3b; this ridge was transected by one of the Tharsis-related Memnonia Fossae. Scale bars represent 100 km; north towards the top. Viking Orbiter frames 637A75 (3a) and 637A82 (3b).

a. Scarps in the heavily cratered terrain

b. Ridges in the heavily cratered terrain

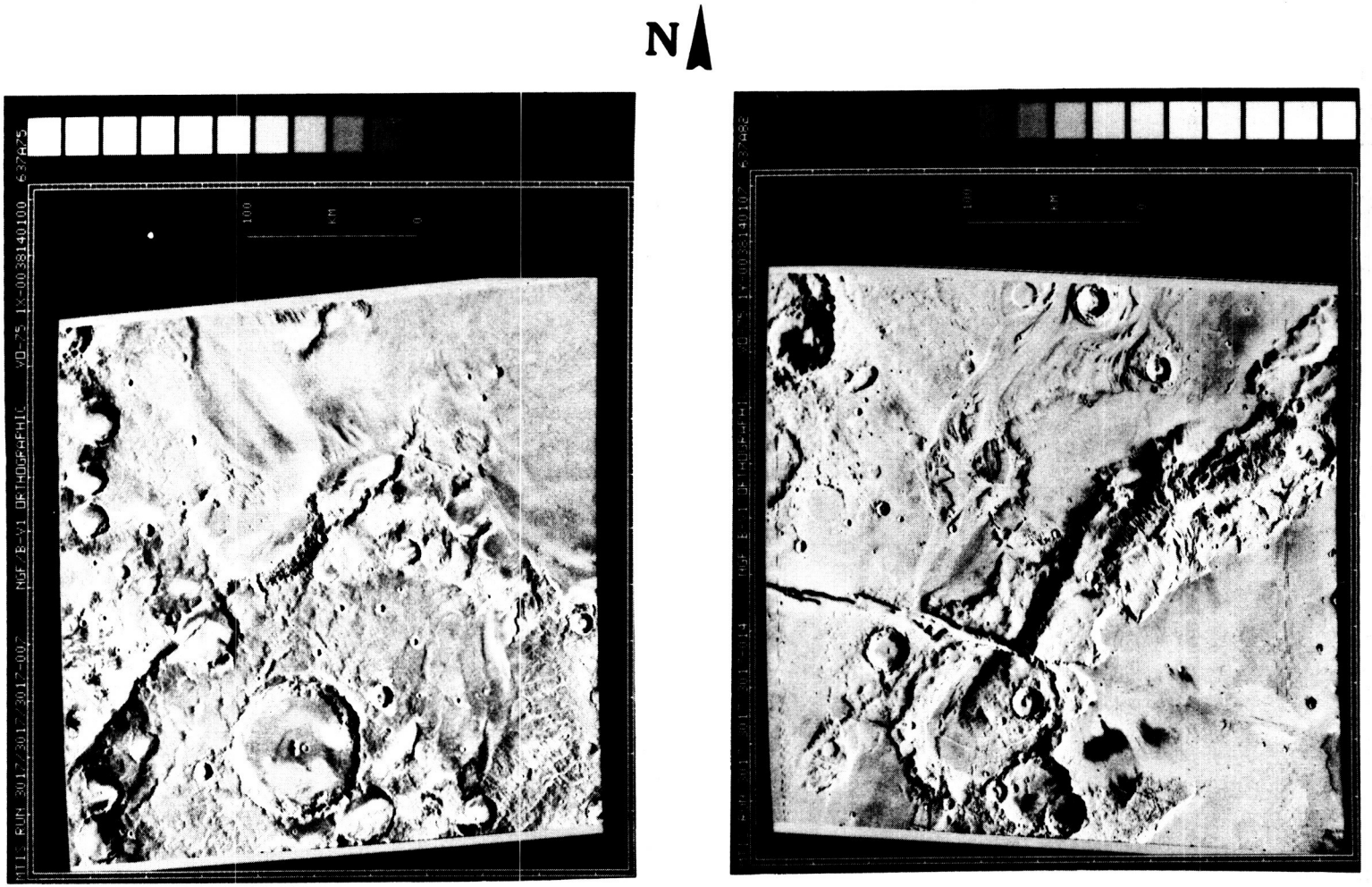

a 637A75 b 637A82

ridge: it is a member of the Memnonia Fossae that are radial to Tharsis.

The origin of these ridges is unclear. They seem unrelated to volcanic processes, and appear to deform crater walls and floors. Their cross-sectional profiles vary from asymmetric in fresher examples to more symmetrical in some heavily furrowed examples (both types can be seen in Figure 3b). In addition, some isolated curvilinear ridges of similar morphology are arranged in circular patterns suggesting that they are massifs associated with partially preserved crater rims. If crater rims represent structurally uplifted crustal material, then it is possible that the ridges might represent modified fault scarps.

Graben can be identified with reasonable confidence on Mars. Perhaps the best examples are the morphologically crisp graben radiating from Tharsis. A few of these are included in Figure 3b at lower left; they are commonly long, linear depressions with nearly vertical walls that may occur singly or in subparallel sets. Where graben transect other features with relief, a portion of this relief can frequently be seen on the down-dropped floor of the graben.

Many other graben occur in the heavily cratered terrain far from Tharsis. Two subparallel sets of these are shown in Figure 4. Although less sharply defined

than those around Tharsis (and others near Elysium), they are similar in both morphology and their subparallel arrangements. In some instances (e.g., Figure 4a), narrow digitate valleys appear to merge with the graben or follow parallel or subparallel trends. Pieri [1980] suggested that such valleys might develop along older structural trends; if so, they might aid in identifying very subdued graben.

Other, somewhat more subtle graben lack the associated valley networks (Figure 4b). The particular examples shown here strike into a mountainous escarpment, suggested by Saunders et al. [1978], Schultz and Glicken [1979], and Schultz et al. [1982] to represent an inner ring of a Ladon multiring basin. Such transectional relationships can be used to infer relative ages of structure-forming events.

In addition to the three general types of structures discussed above, two others were examined; shown in Figures 5 and 6, these are polygonal crater wall scarps and channel wall scarps, respectively. Polygonal crater wall scarps are straight rim wall segments that combine with other portions of the crater rim to give an angular or polygonal appearance in planimetric view. For the craters examined in this study, these wall scarps do not seem to be associated with wall terracing and slumping; generally,

Fig. 4. Graben of the heavily cratered terrain are shown in Figures 4a and 4b. Such graben commonly occur as subparallel sets and are reminiscent of the morphologically crisper Thaumasia Fossae south of Tharsis. Note the development of digitate valleys in Figure 4a that locally trend normal to graben trends, and the apparent disruption of Ladon basin-related mountains (arrow) in Figure 4b. Scale bars represent 100 km; north towards the top. Viking Orbiter frames 650A20 (4a) and 650A14 (4b).

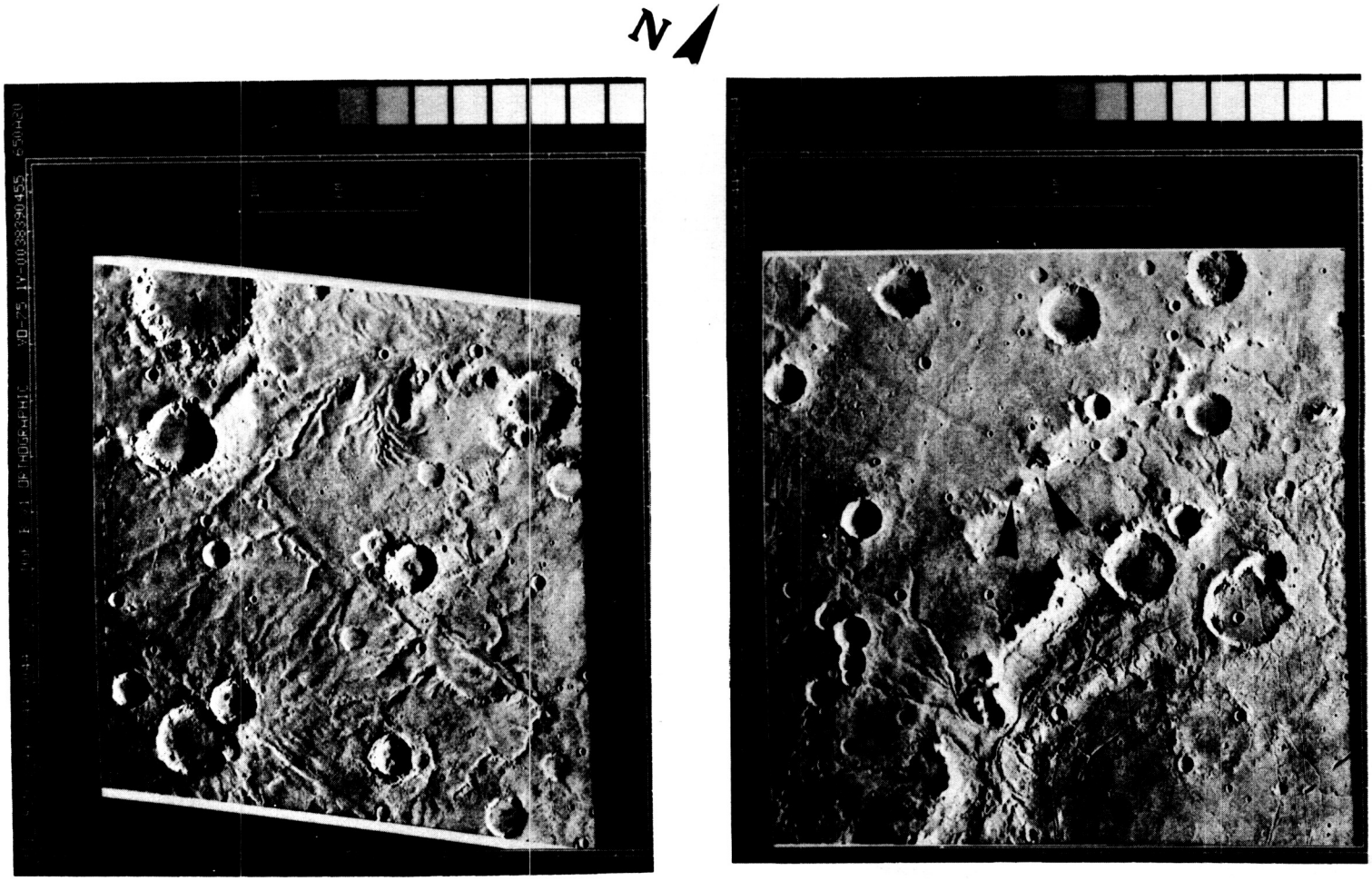

a 650A20 b 650A14

Fig. 5. Polygonal crater wall scarps (arrows) in MC-21. Note the similarity of trends between crater wall scarps and the trends of nearby ridges and scarps. Scale bar represents 100 km; north towards the top. Viking Orbiter frame 625A08.

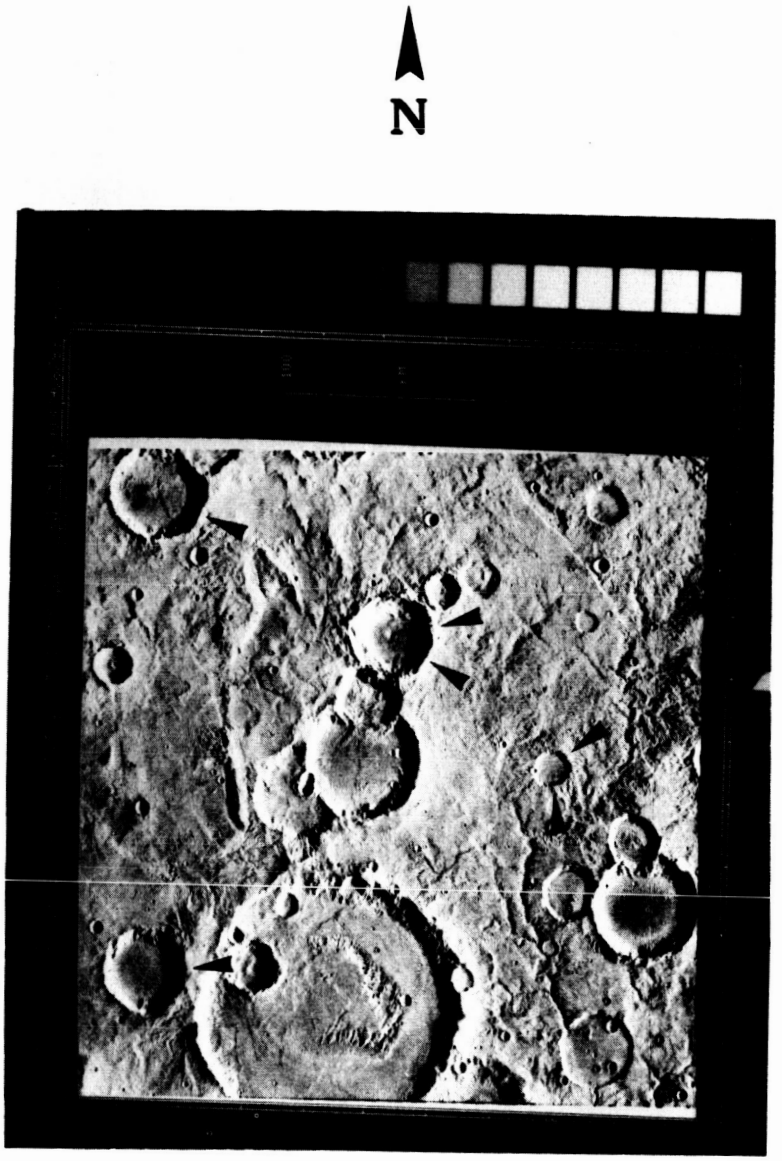

625A08

Fig. 6. Channel wall scarps are illustrated in Figures 6a and 6b. Note the prevalence of linear escarpments forming the boundaries of the channels (arrows), and the subtle scarp that parallels a channel wall scarp in Figure 6b (arrow). Scale bar represents 100 km; north towards upper right. Viking Orbiter frames 651A53 and 651A56.

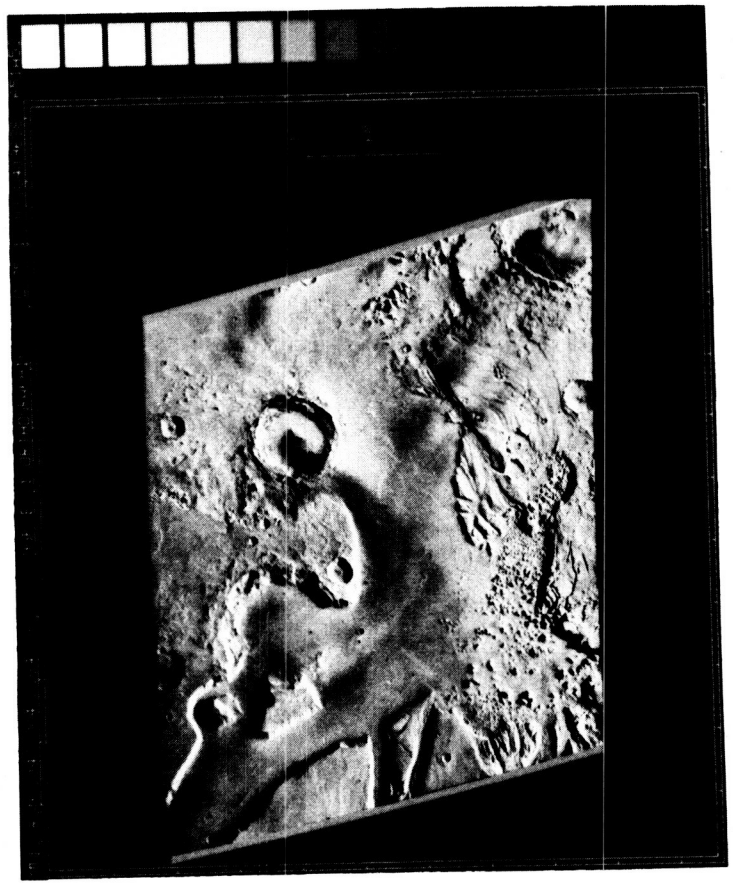

a 651A53

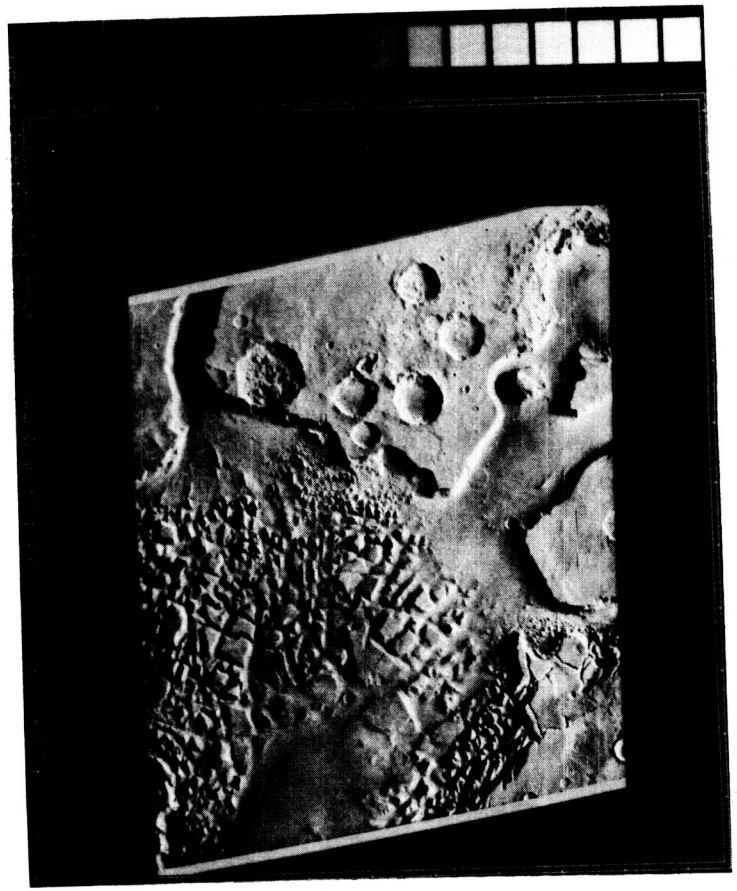

b 651A56

failure of crater rim walls results in scalloped, rather than linear, rim wall segments.

Channel wall scarps are the second subclass of structures investigated. Examples of these are given in Figure 6. It has been suggested that many of the large outflow channels and some sections of chaotic terrain, as well as fretted channels and portions of fretted terrain, might in part be guided by regional structural trends [Sharp and Malin, 1975]. Figure 6a shows a portion of a typical channel in the Margaritifer Sinus region (MC-19). Many of the mesas are bounded by parallel scarps (arrows) of various orientations; "fretting" may also locally parallel these scarps. This is illustrated in Figure 6b, where inter-mesa troughs form a rectilinear pattern that may parallel some of the enclosing scarps (arrows). In Figure 6b a north-facing scarp located at center right (arrow) parallels the channel wall scarp to the south.

"Structure," as used here, refers to a morphologic feature with significant topographic expression to be identified, and whose surface expression is sufficiently distinct to allow genetic classification, based on terrestrial analogs (e.g., graben). Specific examples of structural features used in this analysis are reviewed below; it is important to point out the main limitation of this approach: the observations are systematically biased in favor of the most prominent or easily

recognizable structures. This approach limits the sensitivity of the data to small-scale changes in trend or the detection of transectional relationships (used to infer relative ages). Although many subtle or less familiar structural features were probably neglected, this approach results in a collection of features composed solely of structures resulting from crustal deformation (of unspecified scale) and whose origin (and hence, possible relations to principal stress trajectories) can be inferred.

The linear features illustrated in Figures 3 through 6 and discussed above are assumed to be morphologic expressions of well defined subsurface structural trends. This is a limiting assumption, as any features that do not follow correlatable regional trends will contribute to scattering of the data when they are plotted; it is also probable that many other structures, of different surface expression, were not included in the mapping effort. For the purpose of this research, however, which is to outline the dominant structural trends (if any) based on these structures, the overall effect of these assumptions is probably minor.

Procedure

Viking Orbiter images (5" x 5" contact prints) for each area of interest were obtained for study. Data

recorded for each structure in an image included the Viking Orbiter frame number(s), the mosaic number (if applicable), the MC quadrangle in which the structure was located, its latitude and longitude, length, width, strike (and face direction, if a scarp), its morphologic class, and the solar incidence angle for each image. Elevations of selected scarps and ridges were estimated from orthographically projected images using shadow lengths.

In general, rectilinear versions of the images were used in locating and identifying structural features, as these have been minimally processed. All measurements were made on the orthographic prints to assure uniformity of scale and orientation. Latitude and longitude were "rounded" to the nearest degree, as was strike; length and width were measured to the nearest kilometer. Accuracy of the strike measurements is estimated at ± 2°.

Results

Initial manipulation of the observations was in the form of rose diagrams, of which two types were employed: azimuth-frequency, displaying the number of structures oriented in a given general direction; and total length-azimuth, displaying the cumulative length of these structures compared to their azimuthal distribution. One azimuth frequency and one total length-frequency diagram were prepared for each of the regions studied; in some

instances, separate diagrams for each morphologic type represented (e.g., scarps and graben) were made if sufficient numbers of each were available to make such a breakdown statistically meaningful.

Before discussing the trend distributions for each region, some comments on the applicability and limitations of rose diagrams are necessary. Data from trends in MC-16 provide an illustrative example (see Figure 7). Each of the diagrams was constructed using 5° bins (e.g., 1°-5°, 6°-10°). This results in some trend maxima whose precise strike directions are not known, due to the arbitrary bin size. Two conventions were employed to accommodate this: if a solitary peak occurs (as at N2W in Figure 7a), then a "mean" trend is assigned to represent the trends in that bin [Batschelet, 1965]; if two roughly comparable peaks occur adjacent to one another (as at N30E), the value assigned is shifted to an average value between them.

Results of the statistical analysis for each study region follow, as well as discussions of the relations between trends, morphology of the structures included in these trends, relative ages, and possible observational biases. Interpretation and correlation of these trends appear in a later section.

Memnonia Quadrangle (MC-16). Figure 7 shows the distribution of mapped structural trends in this quadrangle. Most of the structures strike between N2W and

Fig. 7. Rose diagrams for the Memnonia Quadrangle (MC-16), all structures.

a. Azimuth-frequency

b. Total length-frequency

STRUCTURAL TRENDS: MEMNONIA QUADRANGLE

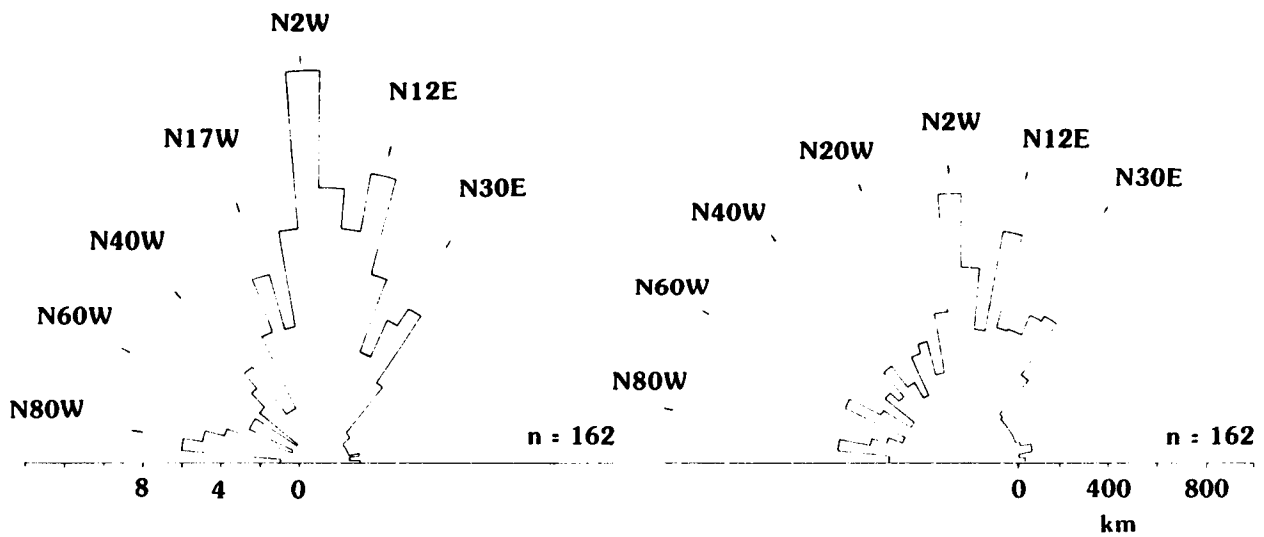

a AZIMUTH - FREQUENCY

b TOTAL LENGTH - AZIMUTH

N12E, and the scarps and ridges possessing these trends show the greatest relief of any in the quadrangle. Some of these structures are shown in Figure 8: note the abrupt terminations on both the east and west faces of the mountainous terrain, the apparent truncation of a crater at A, and the Tharsis-related graben (Memnonia Fossae) at B, members of which transect all structural trends in the area. The height of the prominent ridge at C, as inferred from apparent shadow length measurements, is over 3.5 km.

Other well developed trends illustrated in Figure 7 are those of N30E, N40W, N60W, and N80W. Those structures trending N80W, though, are much more subdued than structures trending in other directions; in the absence of significant numbers of fault intersections, assignment of a greater relative age is difficult.

Aeolis Quadrangle (MC-23). The Aeolis Quadrangle lies adjacent to and west of Memnonia. Approximately three fourths of the quadrangle was mapped in this study, as very little of the heavily cratered terrain is located in the excluded quadrant.

Many broad, linear troughs are developed in the northern portions of the quadrangle. One of these, Al-qahira Vallis, is shown in Figure 9 and is composed of linear escarpments bounding a flat floor; other troughs form a regular interconnecting network, suggesting

structural control. The main reach of Al-qahira resembles the Alpine Valley northeast and radial to the Imbrium basin on the Moon [Mutch, 1972]; although a basin-related origin is not necessarily suggested for this system, structural control of its development seems likely.

The statistical distribution of structural trends in MC-23 is given in Figure 10. Three prominent trends are suggested by the azimuth-frequency diagram: N50W, N6E, and N22E; the N38E trend apparently contains a few long structures, as suggested in Figure 10b.

Arabia Quadrangle (MC-12). The Arabia Quadrangle occupies the north-central portion of the heavily cratered terrain (see Figure 2), approximately midway between the fretted terrain on the planetary dichotomy boundary to the northeast, and the extensively channeled Margaritifer Sinus region to the southwest. Extensive scarp development occurs in the northeastern corner of the quadrangle; these scarps become fewer to the southwest.

Two main structural provinces can be identified from the number per unit area, uniformity of azimuthal trend, and topographic expression. The northeast corner of the northeast portion of the quadrangle contains a large number of long, high scarps with relatively crisp morphologies, most of which are subparallel to one another. As these are continuous with very similar structures in the Ismenius Lacus Quadrangle (MC-5) to the northeast, this

Fig. 8. Ridges and scarps in Memnonia locally exhibit pronounced relief. Flows with low-albedo surfaces emanating from Tharsis can be seen at right; note the apparent crater truncation by the scarp at A, and one of the Memnonia Fossae graben at B. Height of the ridge at C is estimated at 3.7 km. Scale bar represents 100 km; north towards upper right. Viking Orbiter frames 639A11 and 639A12.

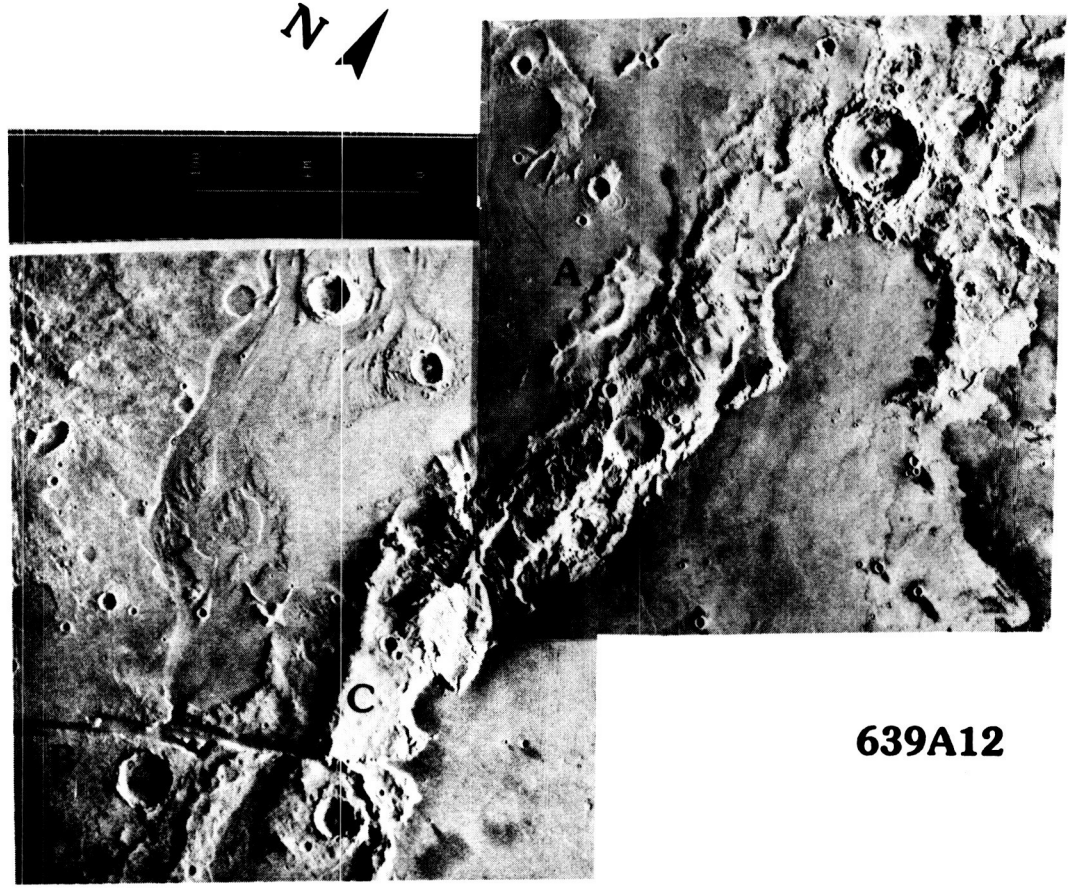

639A12

639A11

Fig. 9. Possible structural troughs in the Aeolis Quadrangle (MC-23) are generally straight, developed along regular trends, and have flat floors; the system shown here is Al-qahira Vallis. Scale bar represents 100 km; north towards upper right. Viking Orbiter frames 596A47 and 596A50.

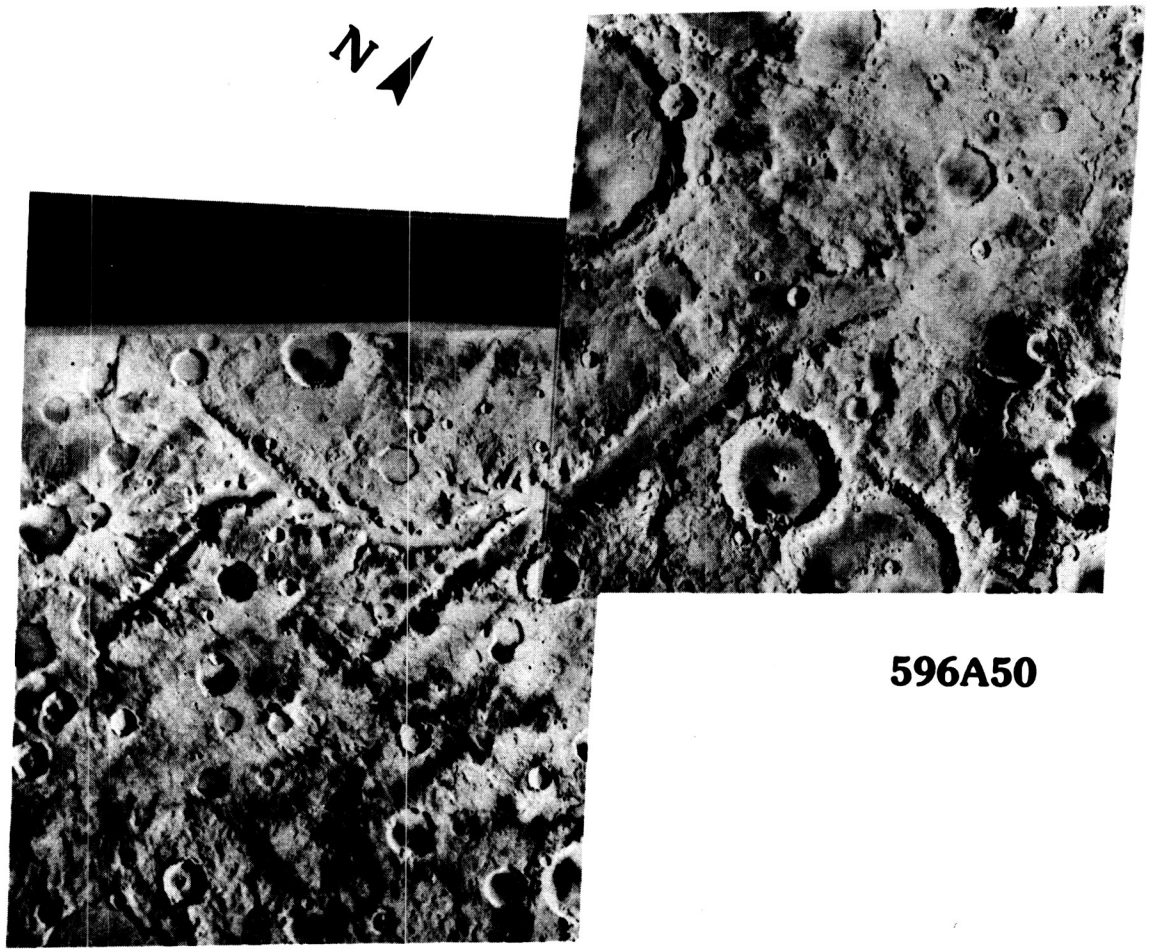
N
596A50
596A47

Fig. 10. Structural trends in the Aeolis Quadrangle (Mc-23).

a. Azimuth-frequency diagram

b. Total length-frequency diagram

STRUCTURAL TRENDS: AEOLIS QUADRANGLE

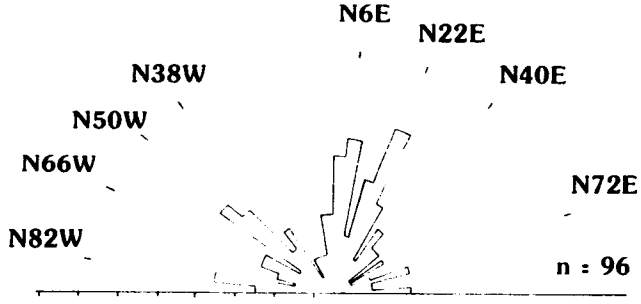

a AZIMUTH - FREQUENCY

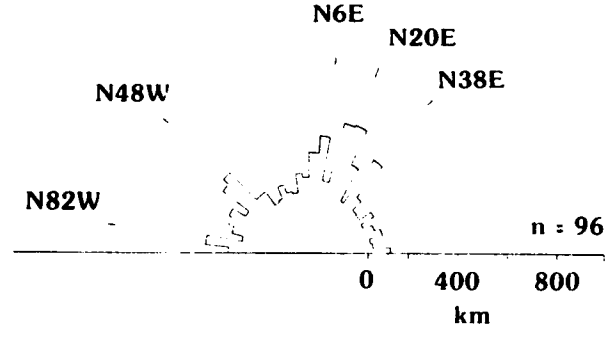

b TOTAL LENGTH - AZIMUTH

region, between 30,325; 20,325; 30,315; and 20,315, will be considered jointly with MC-5 and separately from the rest of MC-12. The boundary of this region, hereafter referred to as MC-12 NE-NE, and the remainder of the quadrangle is abrupt. Northeast of this boundary, the scarps are prominently developed; to the southwest, very little structural deformation is apparent.

The structures in Arabia can be seen to follow a number of preferred directions. Figure 11 illustrates these trends; NNW-trending structures in MC-12 NE-NE are excluded from these diagrams. Structures of equivalent orientation, N17W, are prominent elsewhere in the quadrangle and, indeed, numerically dominate all other trends. Whether the boundary previously referred to represents a change in the intensity of faulting or a major difference in material properties is unclear; the important observation is that this N17W trend is well expressed throughout the quadrangle, regardless of apparent differences in topographic expression along the trend.

In the western portion of the Arabia Quadrangle, two prominent trends occur, centered at N30W and N45W. The azimuthal variation about both trends is broad (±5°); a somewhat tighter clustering is found in their total length-azimuth distributions. Although structures trending N17W are more numerous than either of the other

westerly trends, the total length-azimuth data suggest a more equitable relationship with respect to length.

Structures trending N62W and N72W appear to be numerically less significant than any of the three previous trends discussed above; examination of the total length data, however, seems to imply that both of these trends are related to a small number of relatively long structures trending approximately N68W. An examination of the data shows that most of the features with a similar trend are scarps, although a few are graben. These structures are extremely subdued and frequently support superposed valley networks. In addition, transectional relationships with other structures seem to suggest that many of these N68W-trending structures are the oldest linear features in the quadrangle.

It is apparent from Figure 11 that no well defined "conjugate sets" of orthogonally-oriented structures are represented in this quadrangle. Although some trend sets do appear to be nearly orthogonal (e.g., N45W and N42E), their member structures are restricted to local occurrences. For example, a block-like mesa might trend N45W and be bounded on one side by a short scarp oriented normal to the long direction of the block; if only three sides of the block are well expressed (as commonly occurs), these data might be recorded as two relatively long scarps at N45W with one short scarp at N45E. Although such

Fig. 11. Structural trends in the Arabia Quadrangle (MC-12).

a. Azimuth-frequency distribution

b. Total length-azimuth distribution

STRUCTURAL TRENDS: ARABIA QUADRANGLE

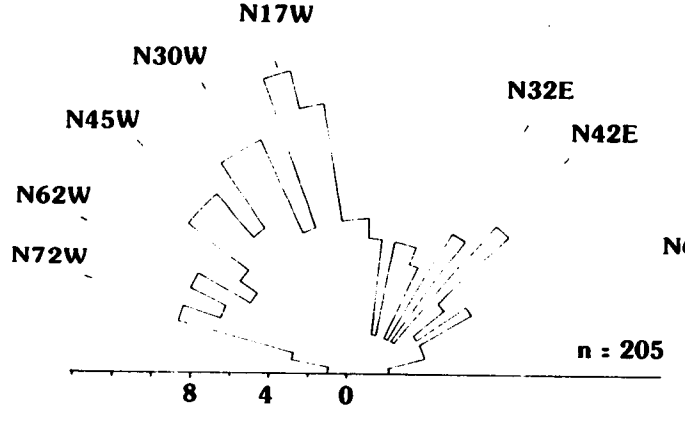

a AZIMUTH - FREQUENCY

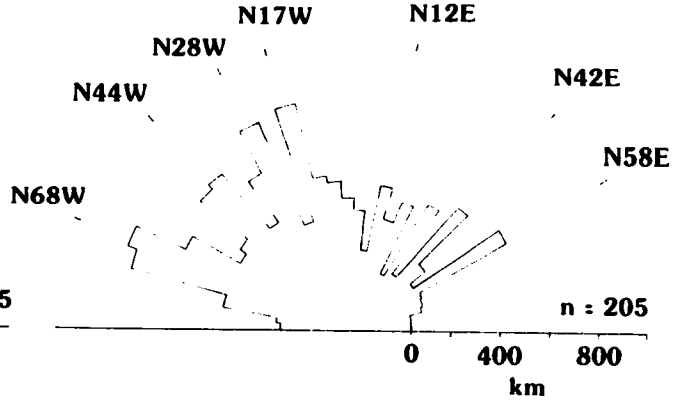

b TOTAL LENGTH - AZIMUTH

trends might be taken as evidence of conjugate shear sets, these approximately orthogonal structures need not have resulted as shear fractures. Rather, such locally orthogonal trends might result as an artifact of faulting along a single major structural trend.

In summary, several well defined structural trends can be isolated: the most subdued scarps and graben are cumulatively the longest in the quadrangle and trend approximately N68W; these are transected by structures of most other trends. Although the N45W and N30W trends are quantitatively important, structures trending N17W are dominant in total numbers and are slightly greater in total length than these other westerly trends. Easterly trends cluster much more tightly about a given azimuth than the westerly trends, although they seem to be less important.

Ismenius Lacus Quadrangle (MC-5). The Ismenius Lacus region, lying northeast of Arabia and adjacent to well developed fretted terrain, contains perhaps the most prominent display of subparallel linear scarps on the planet. Figure 12 illustrates some typical examples. The long, linear scarp that displaces the crater at A and whose sense of displacement changes from west to east at B strikes approximately N28W; the prominent scarp at C strikes N13W. Very little lateral (i.e., strike-slip) displacement can be observed along these scarps, and given

the sharp, linear faulting of the crater at A, these structures are thought to reflect dominantly vertical to nearly vertical motion.

Structures included in the azimuth-frequency and total length-azimuth diagrams shown in Figure 13 are those from JPL mosaic 211-5741 and MC-12 NE-NE. The dominantly unimodal distribution of structural trends in Figure 13 is striking; aside from small peaks centered near N32E and N42W, the majority of azimuths (irrespective of their lengths) cluster about a N19W trend. Examination of the length data, however, shows that the longest structures generally trend approximately N28W, and that the N18W and N42W trends contain similar numbers of structures of similar total length. It appears, therefore, that the predominant structural trend in this region, based on the large number of long structures, is N28W; the N42W and N18W trends, then, contain a moderate number of moderately long structures and a great amount of very short structures, respectively. Many such scarps in the easternmost portions of the quadrangle often are parallel to, and locally merge with, linear depressions of the fretted terrain.

Margaritifer Sinus Quadrangle (MC-19). JPL mosaic 211-5821 was used in conjunction with USGS subquadrangle mosaic MC-19 SW to study some of the extensively channeled portions of the heavily cratered terrain. A variety of

Fig. 12. Scarps near the fretted terrain in the Ismenius Lacus Quadrangle (MC-5) show pronounced topographic relief: height of the scarp at A is greater than 1 km. Note the subdued expression of the scarps in Figure 12b and apparent crater transections (arrows). Scale bar represents 100 km; north towards the top. Viking Orbiter frames 569A29 and 569A30.

N

a 569A29

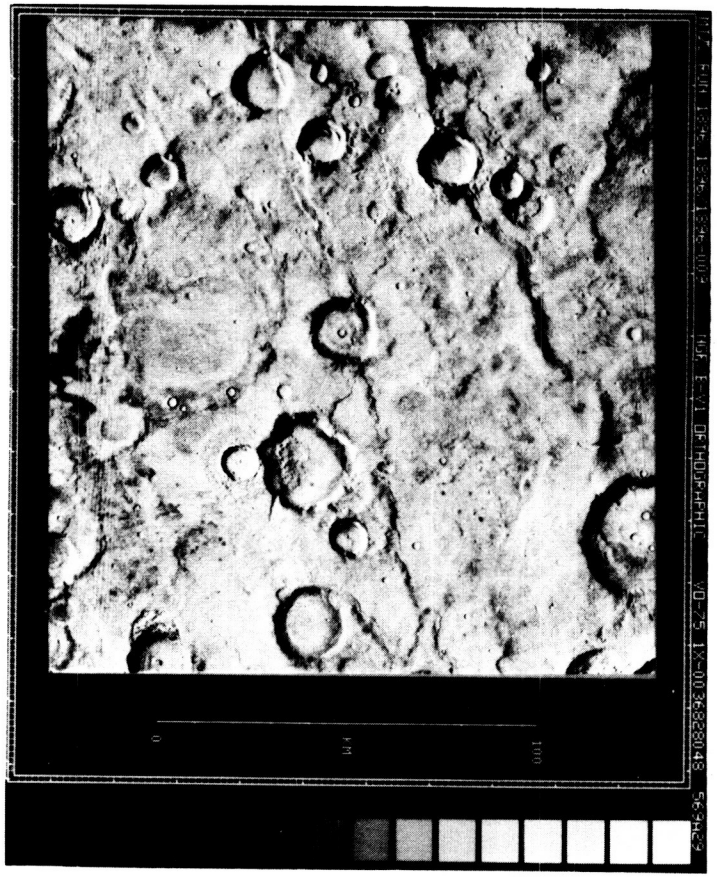

b 569A30

Fig. 13. Structural trends in the Ismenius Lacus Quadrangle (MC-5).

a. Azimuth-frequency distribution

b. Total length-azimuth distribution

STRUCTURAL TRENDS: ISMENIUS LACUS QUADRANGLE

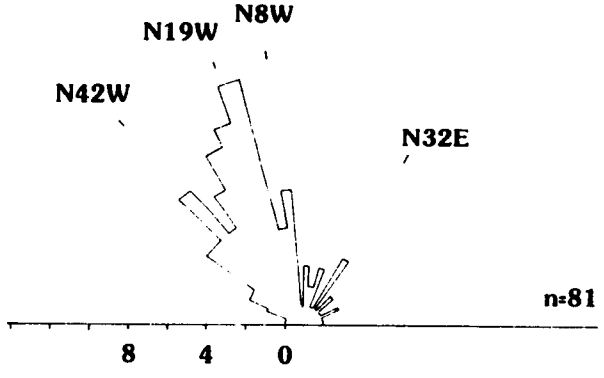

a AZIMUTH-FREQUENCY

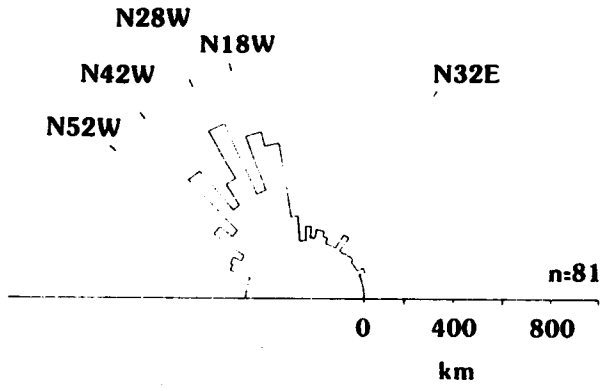

b TOTAL LENGTH-AZIMUTH

terrain types are found in the region, including, from north to south, the heavily channeled regions south of Chryse, the easternmost reaches of the Valles Marineris, zones of large-scale chaos formation (Aureum, Margaritifer, Iani Chaos), and regions of valley networks (e.g., Ladon Valles). The extreme southern end resembles more "typical" heavily cratered terrain as seen elsewhere (as in MC-20), and possesses a pronounced topographic "grain" resulting from generally northeasterly-trending scarps and valleys.

Trends for all structures measured in this region are given in Figure 14. A generally bimodal distribution of trends is apparent: a northwesterly group and a northeasterly group. Structures comprising these two trends are dissimilar in both relative age and in morphologic type. All graben recorded in the region were compiled and are plotted in Figure 15: they have a strong maximum trend near N78W, along with some minor easterly trends. These subdued graben were consistently transected by other structures, suggesting a relatively early formation. All other structures were similarly compiled and are presented in Figure 16. Note the predominance of northeast trends, the maximum of which is more precisely defined by the length data in Figure 16b as being near N32E. Other strong maxima are at N42W and N18W.

It is probable that the structures plotted in each of Figures 15 and 16 span a range of relative ages. It is significant, however, that the earliest structures, the graben, show a pronounced peak in one direction, whereas later structures seem to be preferentially developed along a distinctly different set of trends.

Sinus Sabaeus Quadrangle (MC-20). Images from the southern half of the Sinus Sabaeus Quadrangle were examined for features suggesting structural trends; this area lies south of MC-12 (see Figure 1), directly east of the Margaritifer Sinus region, and northwest of Hellas basin. It is very heavily cratered and has been the site of prevalent structural deformation in the form of scarps, ridges, and graben.

Figure 17 shows the structural trends for this area. The scale of this diagram has been doubled in order to improve its clarity. An anomalous peak occurs in the total length-azimuth plot (Figure 17b): it is a single graben-like trough, 585 km long, that might be concentric (and related) to Hellas. A smaller peak at N68W, also composed of a very few long structures, is consistent with a Hellas-radial orientation.

The remaining trends, however, show no clear relationship to either Hellas (aside from their relative proximity) or Isidis basins and might represent regional trends. These are N42W, N28W, N32E, N56E, and N80E, all of which

Fig. 14. Structural trends in the Margaritifer Sinus Quadrangle (MC-19) and vicinity show a bimodal distribution. Note the changes in relative importance of longer structures in the N12E, N28E, and N78W groups.

a. Azimuth-frequency distribution

b. Total length-azimuth distribution

STRUCTURAL TRENDS: MARGARITIFER SINUS QUADRANGLE

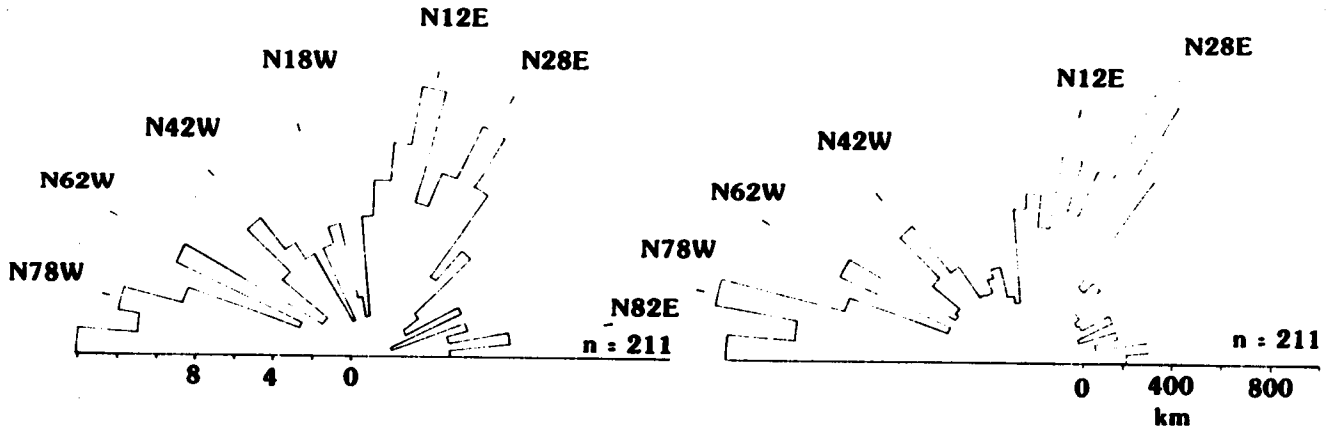

a AZIMUTH-FREQUENCY

b TOTAL LENGTH - AZIMUTH

Fig. 15. Graben trends in MC-19 and vicinity cluster about a strong N78W peak; smaller N11E and N28E trends are also present.

a. Azimuth-frequency distribution

b. Total length-frequency distribution

TRENDS OF GRABEN: MARGARITIFER SINUS QUADRANGLE

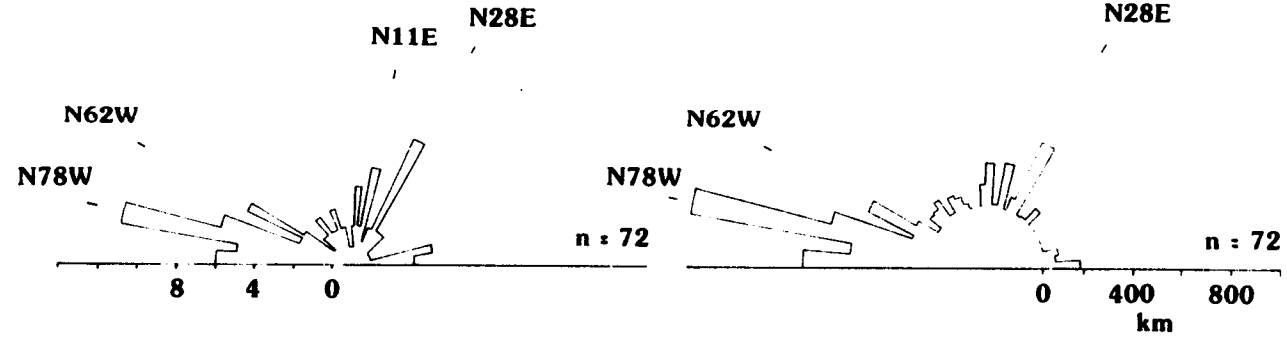

a AZIMUTH - FREQUENCY

b TOTAL LENGTH - AZIMUTH

Fig. 16. Channel wall scarps, ridges, and scarps in MC-19 and vicinity generally transect the graben in Figure 15; note the predominance of northeast trends and the cluster near N32E in the length data.

a. Azimuth-frequency distribution

b. Total length-azimuth distribution

TRENDS OF CHANNEL WALL SCARPS, RIDGES, AND SCARPS: MARGARITIFER SINUS QUADRANGLE

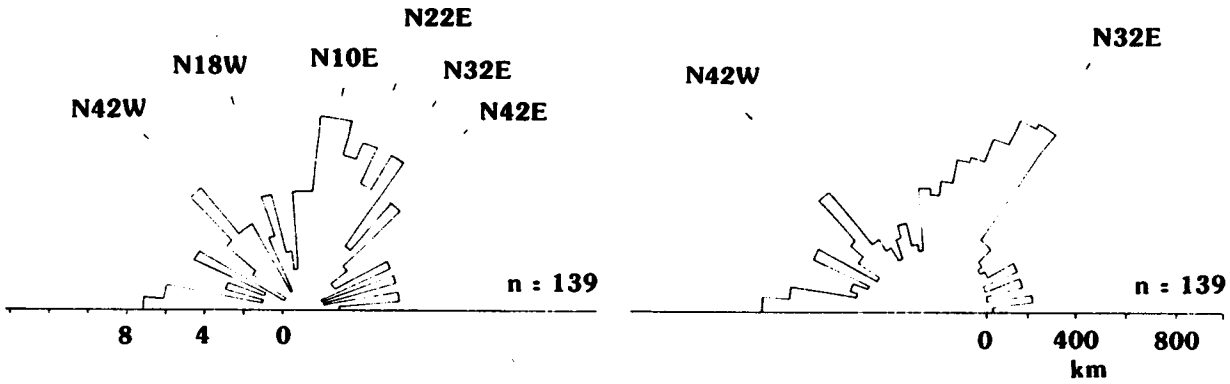

a AZIMUTH - FREQUENCY

b TOTAL LENGTH - AZIMUTH

Fig. 17. Structural trends in the Sinus Sabaeus Quadrangle (MC-20).

a. Azimuth-frequency distribution

b. Total length-azimuth distribution

STRUCTURAL TRENDS: SINUS SABAEUS QUADRANGLE

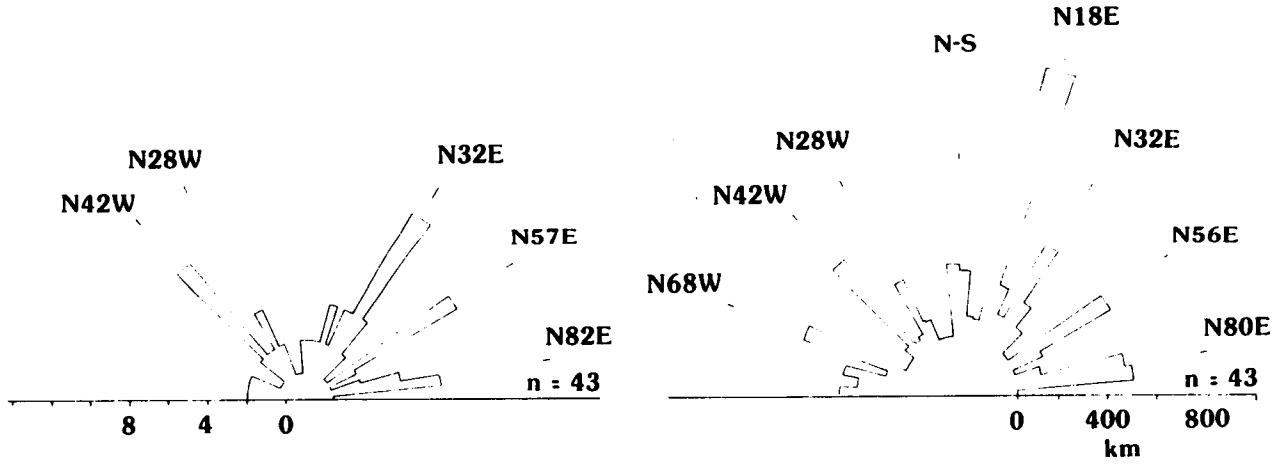

a AZIMUTH - FREQUENCY

b TOTAL LENGTH - AZIMUTH

seem roughly comparable in total numbers and lengths of their included structures. There appears to be no strong correlation between morphologic type and structural trend.

Iapygia Quadrangle (MC-21). A small portion of the heavily cratered terrain lying approximately midway between the Hellas and Isidis basins was selected for study. This area contains a large number of craters whose planimetric forms are polygonal rather than circular. Some of these are shown in Figure 5; note that, in many cases, the linear scarps that form the sides of the crater polygons run parallel to one another in various sets. Moreover, the craters that are the most strongly polygonal fall within a specific size range (here, 10 to 30 km) and relative age class, in that very young craters with extensive ejecta deposits do not show pronounced polygonality; those of intermediate age are the best developed, and only a few of the oldest show evidence of linear rim segments.

Meteor Crater in Arizona is perhaps the best terrestrial example of a crater of this type. Shoemaker [1974] has suggested that the squarish shape of the crater resulted from its development in a target with strong regional structural trends. Indeed, both subparallel sides of the crater are aligned with the directions of preexisting structural trends: a northeast-trending joint set and a northwest-trending system of normal faults.

Although some martian linear crater wall segments appear to result from superposition of two or more craters, it is apparent that many polygonal craters, especially those isolated from others, seem likely to have been produced in a manner analogous to that of Meteor Crater; that is, impact into a target with previously developed local or regional structural trends.

In addition to polygonal crater wall scarps, other structures were measured, including scarps, graben, and a few ridges. These data were combined with those trends derived from measurements of polygonal wall scarps; the composite azimuth-frequency diagram for this region is presented in Figure 18. As this diagram includes structures of unrelated lengths (polygonal crater wall scarps are related to their parent crater diameters; regional structures are independent of crater diameter), no composite total length-azimuth plot was produced. In order to compare data on polygonal crater wall scarps and regional structures separately, however, azimuth-frequency and length-frequency diagrams for these are given in Figures 19 and 20, respectively.

Several main trend directions are suggested in the composite plot (see Figure 18). Possible regional trends, as inferred from Figure 20, are N62W, N48W, N32W, and N2-6E; although the statistics are poor for non-crater

Fig. 18. Composite azimuth-frequency diagram for a portion of the Iapygia Quadrangle (MC-21). Included are data from polygonal crater wall scarps and non-crater structures. Radial scale has been doubled to improve clarity; data derived from Viking Orbiter frames 625A01 to A08.

STRUCTURAL TRENDS: IAPYGIA QUADRANGLE

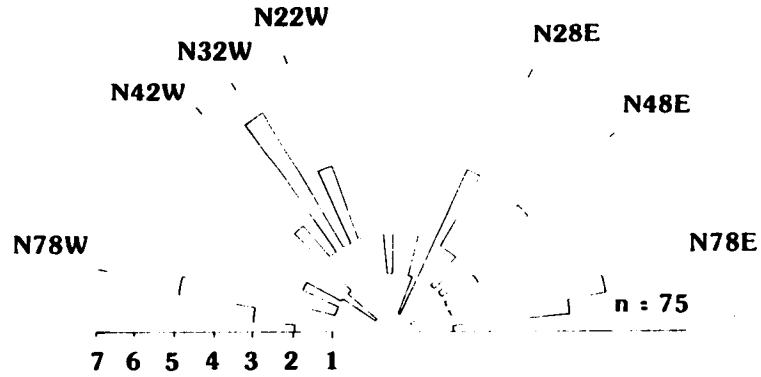

AZIMUTH - FREQUENCY DISTRIBUTION

Fig. 19. Trends of polygonal crater wall scarps in MC-21. Radial scale has been doubled; Viking Orbiter frames 625A01 to A08.

a. Azimuth-frequency distribution

b. Crater diameter-azimuth distribution

TRENDS OF POLYGONAL CRATER WALL SCARPS: IAPYGIA QUADRANGLE

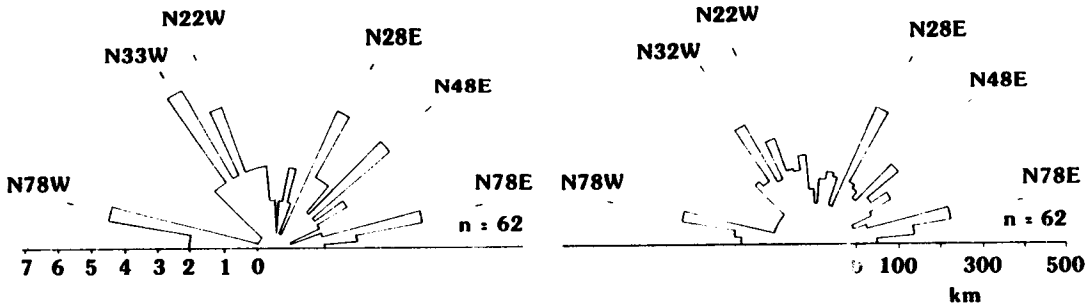

a AZIMUTH - FREQUENCY

b CRATER DIAMETER - AZIMUTH

Fig. 20. Trends of non-crater structures in MC-21. Radial scale has been doubled; Viking Orbiter frames 625A01 to A08.

a. Azimuth-frequency distribution

b. Total length-azimuth distribution

TRENDS OF NON-CRATER STRUCTURES: IAPYGIA QUADRANGLE

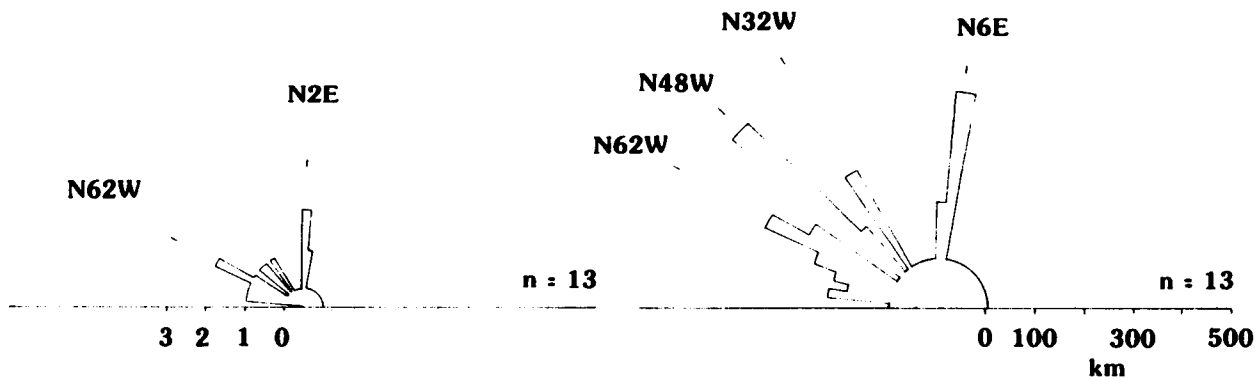

a AZIMUTH - FREQUENCY

b TOTAL LENGTH - AZIMUTH

structures, a coincidence of crater- and non-crater-derived trends near N32W seems possible.

As this region lies between the Hellas and Isidis basins, crustal structure is probably complex, and components of some larger structural pattern are probably less clearly indicated. The data do, however, provide some information on at least the local structure of the area.

Potential Biases

When a few trends in a rose diagram adjoin, the human eye is drawn preferentially to them; the possibility then exists that numerically significant but isolated trends might be overlooked or de-emphasized. Another bias is introduced during compilation of the data for the diagram. Trends of north-south and east-west do not fit into any 5° bin; consequently, they were assigned to the adjacent eastern bin (e.g., N90W added to N85-89W; N0E to N1-5E).

As only the most obvious structural features were documented in this study, many more subtle structures were probably missed. In some areas (e.g., Memnonia), subdued graben-like troughs locally parallel the trends of Tharsis-related graben; such subdued features were excluded from this study. As the number of such features was small, the error introduced is relatively minor. In other areas of extensive lava plains (e.g., Aeolis),

many structures were undoubtedly concealed; however, it is possible that some rather linear lava flow front scarps were included in the statistics; if so, they should contribute to scatter.

None of these potential biases significantly affect the detection of prominent regional structural trends. The regional rose diagrams are thus reasonably reliable estimates of structural trends in the quadrangles studied.

Summary

Generalized azimuth-frequency diagrams for each area studied were plotted on the coverage map of Figure 2 and are presented here in Figure 21. Individual trends vary widely from location to location; very few trends can be continuously traced with confidence through more than two study areas. Comparison of these trends with the principal stress trajectories of Banerdt et al. [1981] reveals very little correlation; the trends appear too variable to result from imposition of such a single stress field. It was hoped that the representation of structural trends in such a manner might suggest some systematic variations with latitude and longitude, distance from Tharsis, the planetary dichotomy boundary, or major impact basins; none of these seems unambiguously to be the case. Rose diagram comparisons such as these appear to be of limited usefulness in evaluating regional trends from

Fig. 21. Azimuth-frequency distributions for structural features in the heavily cratered terrain.

REGIONAL STRUCTURAL TRENDS WITHIN THE HEAVILY CRATERED TERRAIN

MARS GEOLOGY, AFTER SCOTT AND CARR (1978)

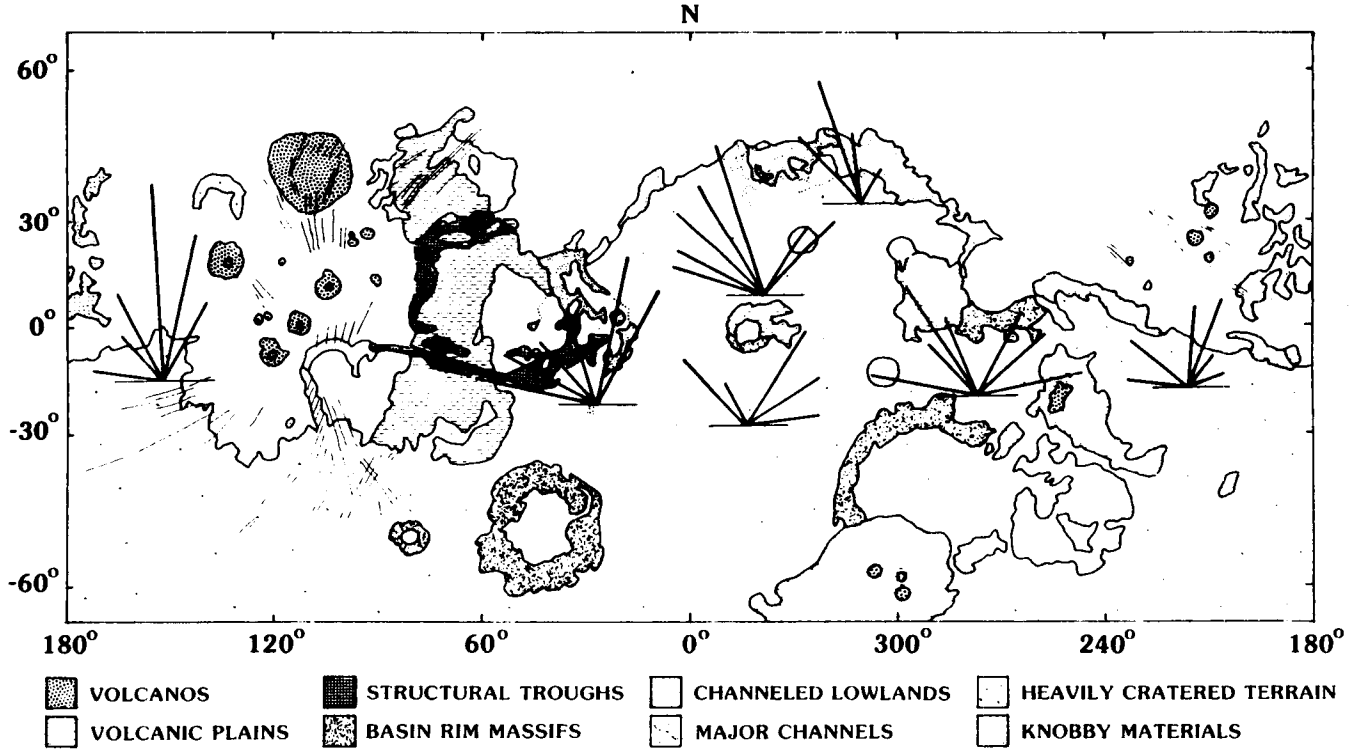

measurements of rather isolated structural features.

Consequently, the regional rose diagrams were used to identify prominent regional trends; these trends were then replotted on stereographic projections of Mars. This method has the advantage of combining a large portion of the original data into single plots covering the entire planetary surface, without significant distortion. Following brief reviews of previous work, principal stress directions on a sphere, and stereonet techniques, the method and its results will be presented.

SYNTHESIS AND TECTONIC ANALYSIS

Previous Work

Deformation of planetary crusts occurs as a response to the stresses imposed upon them. If brittle fracture occurs, it may be possible to infer the orientations of the maximum and minimum principal stresses. This has been used successfully on Earth [Anderson, 1951; Hafner, 1951; Engelder and Geiser, 1980] and has met with some success on Mercury [Melosh and Dzurisin, 1978], the Moon [Melosh and McKinnon, 1978; Golombek, 1979], and Mars [Carr, 1974; Wise et al., 1979; Phillips and Lambeck, 1980; Banerdt et al., 1982].

The approach adopted here was to extend the dynamic classification of faults developed by Anderson [1951] to planetary scale problems. This technique can be applied to tectonic problems on any planet (or satellite) whose outer crust deforms by brittle failure near the surface and is not excessively mobile (the "one-plate" planets of Solomon, 1978). In principle, it is possible to preserve evidence of tectonic activity that occurred very early in a planet's history; the complication, however, is that results of subsequent events may also be preserved. Although studies of fault-trends have been performed for portions of Mars [Masson, 1977; Frey, 1979], to date such studies

have not addressed early global tectonism or the formation of the planetary dichotomy boundary.

Stress and Faulting on a Globe

In this study, the maximum principal stress, σ_1, will be taken to be compressive; the minimum principal stress, σ_3, will be taken to be tensile. Using this convention and given the condition that one of the three mutually perpendicular principal stresses must be vertical, the orientations of the principal stresses to the resulting principal planes of faulting can be specified. Central to Anderson's [1951] classification of faults is the assumption of one vertical principal stress. For normal faults, this stress is equal to the overburden pressure. As this parallels the gravitational acceleration vector, this vertical principal stress parallels the line directed radially outward from the center of mass of the planet through the piece of rock being stressed. It is apparent, then, that for normal fault-producing stresses, σ_1 will be radial to the planet's center, and the intermediate and minimum principal stresses will be perpendicular to this and thus tangent to the surface of the planet.

For normal faulting, the maximum principal stress is parallel to the gravitational acceleration vector, and the intermediate and minimum principal stresses are

tangential to the surface being deformed; faulting may occur along either of the two principal planes for uniform, homogeneous rock. Anisotropies will alter this somewhat, but on a planetary scale it is found that the effect of these irregularities seems small compared to the scale of the deformation.

A total of 890 structures were measured in this study. Of these, scarps constituted 61%; graben, 16%; channel wall scarps, 9%; polygonal crater wall scarps, 8%; and ridges, 6%. Very little evidence of strike-slip movement was observed for any of these structures. Many show evidence of differential vertical motion, and the majority of the structures studied are inferred to reflect dominantly vertical motion. It is thought that this motion resulted from normal faulting, as the structures locally parallel and grade into one another; this interpretation is not necessarily conclusive, however, and local high-angle reverse faulting is not ruled out.

Principal stress directions and potential fault planes for normal, reverse, and strike-slip faulting are shown in Figure 22 (a, c, and e after Hobbs et al., 1976, p. 329). It is emphasized that the stress poles described here need not coincide with the geographical poles of the planet: the stress trajectories may rotate to any position to match planetary structural trends. It is interesting also that the only stress spheroid with uniquely defined axes

Fig. 22. Stress trajectories and faulting on local and planetary scales are illustrated for the three common fault types. For local stresses (Figures 22 a, c, and e), one principal stress direction is vertical. This vertical stress follows the gravitational acceleration vector and is radial to the planet's center, thus defining a planetary stress system based on near-surface stress directions. Stress poles need not coincide with geographic poles.

a. Local stresses resulting in normal faulting
b. Planetary stresses resulting in normal faulting
c. Local stresses resulting in strike-slip faulting
d. Planetary stresses resulting in a zone of conjugate shear fractures. Lateral displacement can occur when σ_1 is equatorially directed.
e. Local stresses resulting in reverse or thrust faulting
f. Planetary stresses resulting in a zone of reverse or thrust faulting

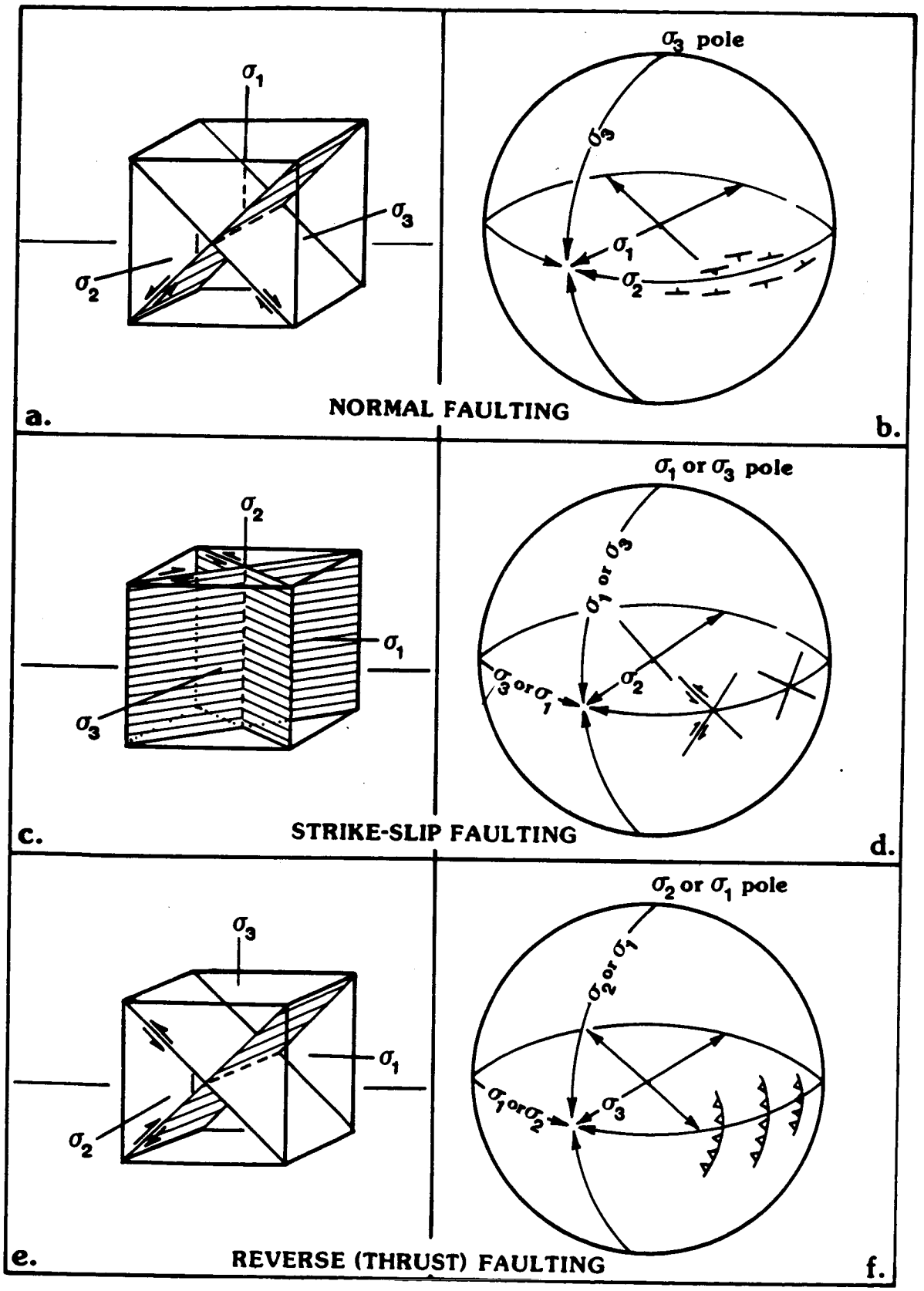
σ1
σ3
σ2
a.
σ3 pole
σ3
σ1
σ2
b.
NORMAL FAULTING
σ2
σ1
σ3
c.
σ1 or σ3 pole
σ1 or σ3
σ3 or σ1
σ2
d.
STRIKE-SLIP FAULTING
σ3
σ1
σ2
e.
σ2 or σ1 pole
σ2 or σ1
σ1 or σ2
σ3
f.
REVERSE (THRUST) FAULTING

is that for normal faulting; for the other cases, even though the radial (i.e., local vertical) principal stress direction is fixed, directions of the other two can vary between the pole and equator. Reconsideration of faults as "radial" or "tangential" follows the ideas originally formulated by Suess in 1885 (see Suess, 1904).

It can be seen that the trends of normal faults and graben produced from these stresses will be parallel to the "stress equator," that is, σ_2. This is analogous to uniaxial tension directed along the σ_3 axis. The stress spheroid for strike-slip faulting would produce conjugate sets of fractures; no relative motion across these fractures would occur if σ_3 were equatorial, but significant lateral displacement will occur along these fractures if the maximum principal stress (σ_1) were parallel to the equator. Assuming the stress poles coincide with the planet's poles of rotation, an analogous stress state might be imposed on a planet through a change in its rotation rate (e.g., the tidal despinning concept of Melosh, 1977). If the intermediate and maximum principal stress directions are tangential to the surface of the planet and σ_3 is vertical, thrust faulting may occur; this stress condition could be met by planetary contraction [Melosh, 1977].

In order to evaluate whether planetary stress systems similar to these have been active on a planet, it is useful

to plot the major structural trends on stereographic projections. This has been done for the trends identified in the regional rose diagrams for structures in the heavily cratered terrain of Mars. Before discussing these results, however, a review of stereonet concepts and procedural methods will be presented.

Review of Stereonet Concepts and Applications

Stereographic projections, commonly referred to as stereonets, are graphic representations of a sphere that allow problems in three-dimensional geometry to be manipulated and solved on a two-dimensional sheet of paper. These projections can be thought of as being roughly analogous to an image of a globe, complete with lines of longitude and latitude, traced onto a flat surface. Discussion of techniques and applications of the stereonet can be found in Ragan [1973] and Hobbs et al. [1976].

As the stereographic projection represents a sphere, two hemispheres are superimposed on the net. The lower hemisphere is most commonly used in structural geology, whereas the upper hemisphere is primarily used in mineralogy (see Phillips, 1960); the choice is arbitrary and is selected according to the needs of the particular problem being studied. Structural data plotted on the upper and lower hemispheres are usually symmetric; while not true for plotting fault planes, symmetry is an asset,

for example, when plotting the poles to crystal faces.

Stereonets have the property of representing planes in space as (curved) lines on the net, and lines in space as points on the net. In addition, the orientation and position of any plane, when plotted as a great circle, can be specified by a single point, the pole. Small circles can be specified by their center points and the "radius" of the circle. A pole is the normal to the plane, passing from the center of the sphere through its surface; the point at which the normal pierces the sphere is projected onto the stereonet as a point. As both hemispheres of the net are symmetric, the normal to the plane pierces both the upper and lower hemispheres, resulting in two poles, 180° apart, either one of which is 90° from the plane; either one of these poles by itself can specify the attitude of the plane. The technique of plotting poles to planes instead of the planes themselves results in a great simplification of three-dimensional geometric problems and has the additional advantage of generating patterns on the resulting pole plot. In many cases, complicated deformational structures, when plotted in this fashion, can be isolated and readily identified by some recognizable pattern of poles on the stereonet. Thus, complex spatial relationships between planes can be analyzed with greater efficiency through the patterns generated with this technique.

Two types of stereographic projections are commonly used in structural geology: the Wulff net and the Schmidt equal area net. The Wulff net is an equiangular projection, whereas Schmidt nets conserve area. The property of having constant area per unit distance on a Schmidt net is useful for analyzing clusters of poles for diagnostic patterns. When poles to planes are plotted on an equal area net, a contour diagram can be constructed to reveal regions of maximum and minimum density of points (see Ragan, 1973, pp. 112-114). The maxima derived from contouring can produce the patterns characteristic of specific types of deformation, such as folding about an axis or the development of planar fabric in rocks.

Faults in terrestrial situations are represented on a stereonet as great circles, defined by their azimuth in degrees from north and their dip, measured down from the horizontal. The direction of movement relative to reference points defines the type of displacement along a fault. Normal faulting, for example, involves downward motion relative to the local vertical, commonly taken as the gravitational acceleration vector and, hence, the maximum principal stress. By definition, the trend of a normal fault or graben locally follows the direction of the intermediate principal stress (σ_2); the fault plane thus defined begins in the planet's outer crust parallel to σ_2 and can be thought of as extending radially inward

to the center of the planet. This argument can also be applied to strike-slip and reverse faulting. Thus, any fault with a measurable strike represents a portion of some great circle that locally follows the strike of the fault, and that passes through the center of the planet. As such a plane can be represented on a stereonet by either one of its poles, any structural trend on a planet, in defining a great circle, can be plotted on a stereonet as a point.

Lines of longitude and latitude on a globe can be thought of as being analogous to great and small circles on a Wulff or Schmidt net. The similarity between planetary position, with coordinates in latitude and longitude, and poles to planes on a stereonet can be exploited, in that structural trends of widely separated locations on a planet might be compared and analyzed at a planetary scale using such a net.

Two types of diagrams can be used to analyze a system of great circle trends: beta-diagrams and pi-diagrams. Beta-diagrams involve the plotting of all great circles on a single equal area net, and are interpreted after construction of a contour diagram of the resulting great circle intersections. Inherent in a construction of this type are several sources of significant error. The entire great circle must be plotted to great accuracy, and the point of intersection of two similarly trending great

circles (i.e., ± 10° in azimuth) cannot be precisely located. As the number of intersections increases much faster than the total number of great circles plotted, a false sense of confidence can result, in that many of the intersections are artifacts of the plotting process. Spurious numbers of intersections, leading to spurious maxima, can often result as a byproduct of the "artificial" intersections.

An alternative method of analyzing a large number of structural trends is that of the pi-diagram. Instead of drawing the entire great circle, only its pole is recorded on the stereonet. This greatly reduces clutter, spurious concentrations, and plotting error while increasing the clarity of any resulting patterns and clusterings of points. Further, the method is flexible, in that, given one pole, both the opposite pole and the parent plane can be determined with great rapidity and accuracy. Thus, pi-diagrams represent a more efficient way of simultaneously analyzing a large number of structural trends on a global scale.

Methodology

Rose diagrams for each of the regions studied were used to identify prominent structural trends. Of the 890 total structures mapped in the heavily cratered terrain, 603 were members of 43 well defined trends and were selected for analysis on a stereonet.

One Schmidt equal area net was used to plot the poles of structures whose trends were close to the maxima defined from the 21 rose diagrams. The 43 principal structural trends plotted using this technique are given in Table 1; the 9 marked by an asterisk contained too few members (≤ 3) to plot, leaving 34 usable trends.

For each structural trend, the data on latitude, longitude, and strike were taken for each of the structures whose strikes were comparable to the mean trend. As the prominent trends were grouped in 5° boxes, there were usually enough data for each trend to give a meaningful pattern on the stereonet. The data for each trend were plotted as follows: each Schmidt net was centered at Mars geographical coordinates 0° latitude, 360° longitude; the conceptual upper hemisphere of the stereonet was used to simulate this hemisphere of Mars more realistically. The latitude and longitude of each structure were located on the net to the nearest degree, and an "x" was centered on this point. To include the strike on such a projection, the transparent overlay on which these points were located was rotated the appropriate number of degrees of strike; the "x" then represented a point on the nearest underlying great circle. Having defined the great circle for this structure, the upper hemisphere pole was determined by counting off 90° along the equator and marked by a point; the overlay was then rotated back into its original

TABLE 1. Regional Structural Trends

MC Quad	Trend	MC Quad	Trend	MC Quad	Trend
16	N80W	12	N72W	21	N78W(?)
	N60W		N62W		N32W*
	N40W		N45W		N22W*
	N17W		N30W		N28E*
	N2W		N17W		N48E*
	N12E		N12E(?)		N78E*
	N30E		N42E		
			N58E	23	N82W
19	N78W				N66W
	N62W	5	N42W		N50W
	N42W		N19W		N38W
	N18W		N8W*		N6E
	N12E				N22E
	N28E	20	N68W*		N40E*
			N42W(?)		
			N28W*		
			N32E		
			N57E		
			N82E		

* Trends contained 3 members or less
(?) Produced scatter on pi-diagram

position, the "x" erased, and the next datum plotted. Once all the data for each trend were plotted, the resulting groupings were contoured on a separate overlay using a Kalsbeek counting net (see Ragan, 1973).

It was found that the poles to most of the trends identified in the rose diagrams formed rather tight clusters; three pi-diagrams produced significant scatter and are queried in Table 1: these were not used in subsequent analyses. Using the contoured pi-diagrams, one best-fit pole was selected for each of the 31 structural trends that produced compact clusterings; this pole and its projection in the opposite hemisphere, the parent structural trend identified in the rose diagrams, and the number of structures contained in each diagram are listed in Table 2. These derived data comprise the documented poles to the best defined structural trends in each of the regions studied in the heavily cratered terrain, and form the basis for subsequent diagrams and analyses.

Results

All of the 62 derived best-fit poles (31 on each of the two hemispheres) to the measured regional structural trends were plotted the upper hemisphere of another Schmidt equal area net, centered at martian coordinates, 0,360. This diagram is shown in Figure 23a; note that filled

TABLE 2. Best-fit Poles to Prominent Structural Trends in the Heavily Cratered Terrain of Mars

MC Quad	Trend	Lat., Long.	Lat., Long.	n
16	N80W	64,146	-64,326	13
16	N60W	63,94	-63,274	6
16	N40W	40,90	-40,270	6
16	N17W	14,68	-14,248	21
16	N2W	0,240	0,60	43
16	N12E	8,239	-8,59	22
16	N30E	22,226	-22,46	20
19	N78W	50,344	-50,164	32
19	N62W	46,326	-46,146	11
19	N42W	38,298	-38,118	23
19	N18W	17,299	-17,119	12
19	N12E	10,112	-10,292	25
19	N28E	22,112	-22,292	33
12	N72W	55,210	-55,30	15
12	N62W	56,230	-56,50	16
12	N45W	42,240	-42,60	33
12	N30W	26,246	-26,66	30
12	N17W	12,246	-12,66	36
12	N42E	42,90	-42,270	14
12	N58E	58,100	-58,280	10
5	N42W	30,212	-30,32	24
5	N19W	18,220	-18,40	35
20	N32E	24,44	-24,224	10
20	N57E	42,32	-42,212	5
20	N82E	58,16	-58,196	6
23	N82W	68,158	-68,338	7
23	N66W	54,150	-54,330	8
23	N50W	40,130	-40,310	11
23	N38W	38,120	-38,300	6
23	N6E	4,292	-4,112	13
23	N22E	21,272	-21,92	17

symbols represent poles plotting on the upper hemisphere of the net, whereas open symbols represent poles on the lower hemisphere. The absence of points near the center of the net and the regular, symmetrical distribution of points about the center is striking; their pattern can be enhanced by contouring the points as in Figure 23b.

The pi-diagrams presented in Figure 23 suggest a unifying pattern to the poles of prominent structural trends in the heavily cratered terrain. These poles define a pair of small circles, one on each of the upper and lower hemispheres of the net, which are superimposed here as a byproduct of the plotting process. The composite small circle shown in Figure 23 has a statistical center near 0,360 and a radius of 60 ± 10°.

In order to represent these small circles in a form perhaps more familiar to geologists, the derived poles were also plotted on a Schmidt net centered at 0,270; this results in a 90° westward rotation of the small circles while preserving their coordinates on the planet. This new projection is shown as poles in Figure 24a and as contoured data in Figure 24b. Note that the two small circles can be resolved using this projection: they lie at opposite sides of the net and have geometric centers near -8,360 and 8,180. In this projection, an additional concentration of poles trends north-south along the 270° (and 90°) meridian.

The 0,360 projection of the small circle zones does not precisely resolve the centers of the zones. Shifting the center of the projection from 0,360 to 0,270 reveals that the small circle geometric centers are located at ± 8° from the "equator." This new projection is thus used to resolve the north-south components of the small circle centers. Any east-west components, however, are not resolved; when the data are replotted on a polar stereographic projection, these components can be found. The geometric centers of the visually determined best-fit small circles to the pole data, based on all three projections, are located at -8,356 and 8,176.

Although the physical meaning of great circles is familiar to geologists, the concept of "small circle tectonics" may seem somewhat unconventional. Tectonic activity that leads to small circle traces is common on planetary surfaces, however. Very large impact basins, for example, directly affect a large portion of the surface of a planet. The outer rim of such a basin generally defines a circle in planimetric view and an arc in cross section; this arc would plot on a stereonet as a small circle, assuming the center of the basin lies on the primitive.

Perhaps a more familiar example is that of terrestrial subduction zones. The subducting lithosphere is planar; the arcuate shape of the associated trench results from

Fig. 23. Pi-diagrams of poles to structural trends, centered at 0,360; upper hemisphere of Schmidt equal area net. Filled symbols denote poles plotting on the upper hemisphere; open symbols, lower hemisphere poles. The poles define a zone approximating a small circle, with a geometric center near 0,360 and radius of 60 ± 10°.

a. Pi-diagram of derived poles

b. Contour diagram of Figure 23a data

POLES TO STRUCTURAL TRENDS,
HEAVILY CRATERED TERRAIN, MARS

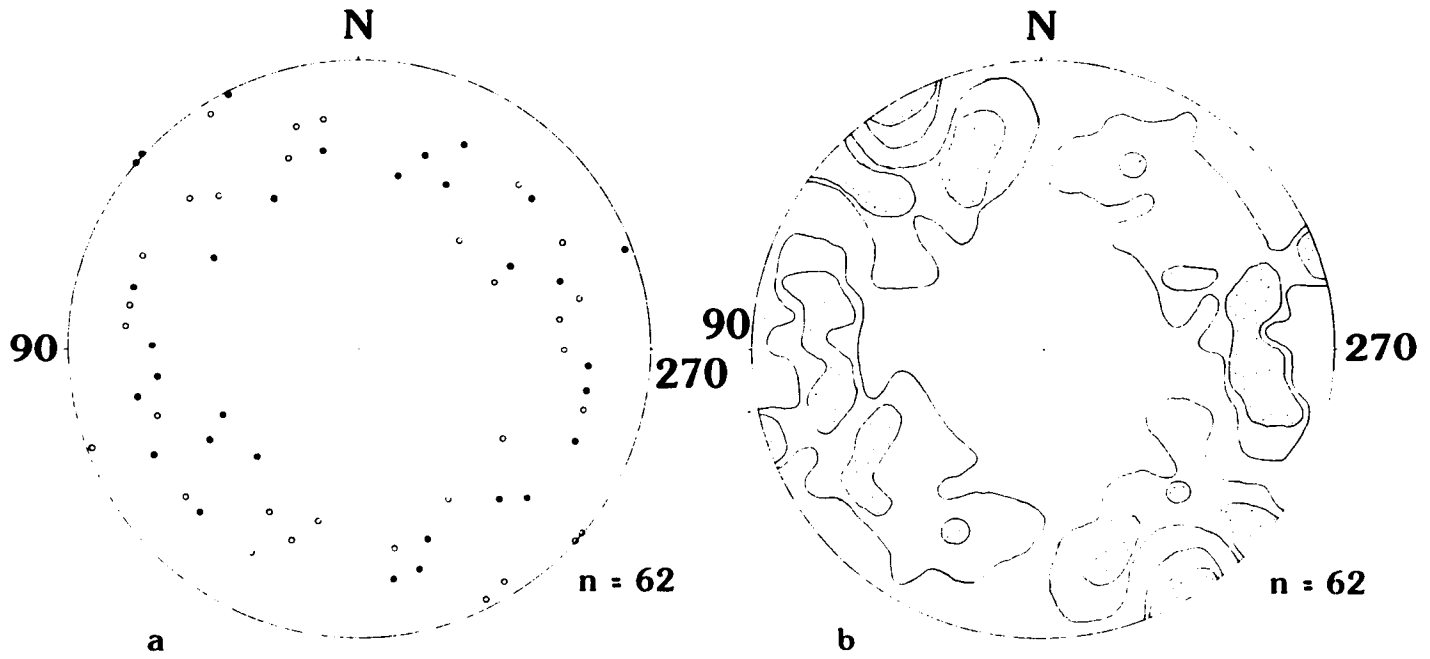

SCHMIDT EQUAL AREA NET
UPPER HEMISPHERE
PROJECTIONS CENTERED AT 0, 360

• :Upper Hemisphere ◦ : Lower Hemisphere

Fig. 24. Pi-diagrams of poles to structural trends, centered at 0,270; upper hemisphere of Schmidt Equal Area Net. These diagrams represent a 90° westward rotation of the projection shown in Figure 23, using the same data. Note resolution of the zone into two small circle traces, and a medial north-south-trending cluster of points.

a. Pi-diagram of derived poles

b. Contour diagram of Figure 24a data; geometric centers of small circles lie near -8,360 and 8,180.

POLES TO STRUCTURAL TRENDS,
HEAVILY CRATERED TERRAIN, MARS

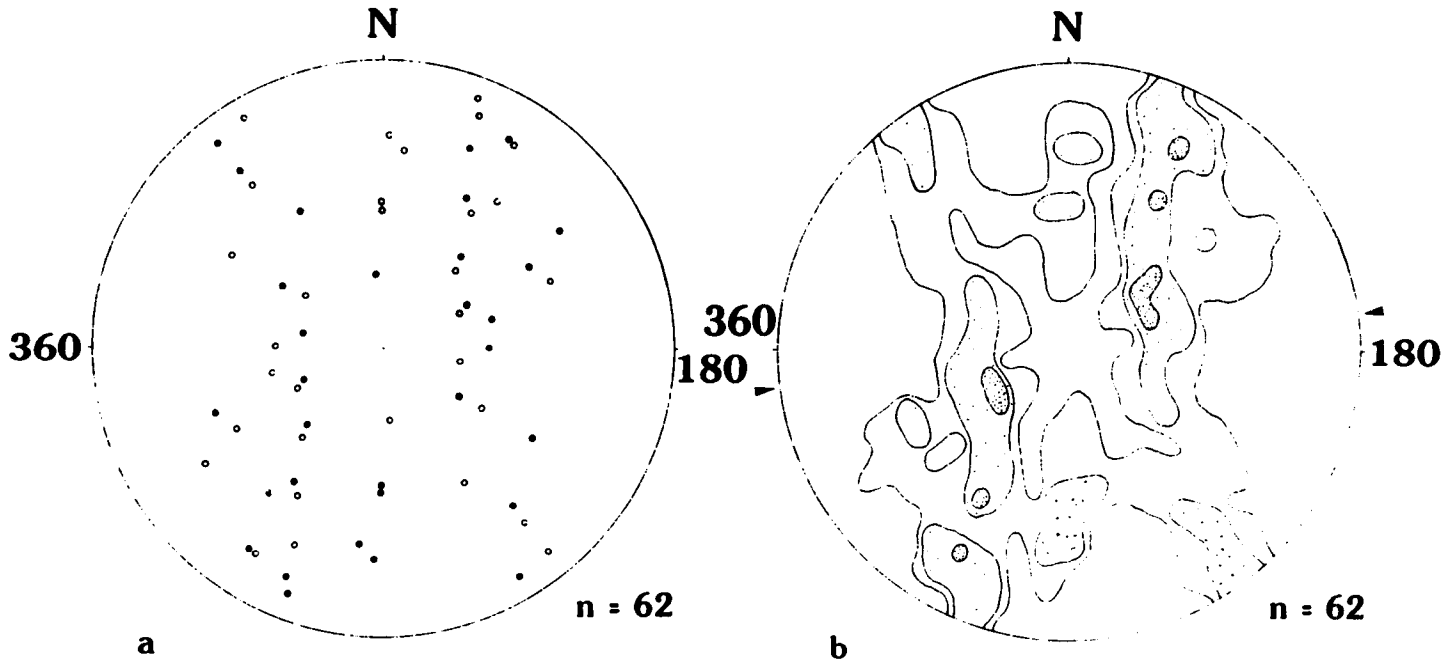

SCHMIDT EQUAL AREA NET,
UPPER HEMISPHERE
PROJECTIONS CENTERED AT 0, 270

• : Upper Hemisphere : Lower Hemisphere

the intersection of this plane with the curved surface of the Earth [Frank, 1968]. As these planes can be projected through only a portion of the globe, they form arc segments of small circles and can be plotted as such on a stereonet. It is significant here that the center of this small circle, defined by the arcuate trace of a subducting planar lithosphere, has little physical meaning aside from serving to locate the small circle on the planet, using geographical coordinates. In the previous example of an impact basin, the center corresponded to the physical center of the basin. Thus, in considering "small circle tectonics," the center may or may not be physically significant; the important activity is marked by the small circle zone.

One final example will be presented here, that of the large-scale movement of lithospheric plates on the Earth. Although termed "plate tectonics," the lithosphere behaves more like "spherical caps" on a sphere (see Hobbs et al., 1976, pp. 447-457); relative motion between plates (as inferred from patterns of transform faults) can be specified by movement along small circles; i.e., by an angular displacement around an Euler pole of rotation. Here, the center of the small circle (the Euler pole) is a derived quantity and may not physically exist.

Undoubtedly, other examples could be cited; it is thus not unrealistic to postulate some tectonic process that gives rise to a pattern of small circles. As with

studies of ocean trenches and mountain belts in the last century, a pattern of structures must first be recognized before possible modes of origin can be explored.

DISCUSSION

The small circles recognized in the pi-diagrams of Figures 23 and 24 have been plotted on the Scott and Carr [1978] geologic map of Mars. As most of the poles fall within 10° of a best-fit small circle, this 20°-wide circular zone was plotted in Figure 25 for both small circles; these zones are elongate in the north-south direction because of the distortions inherent in the Mercator projection of the geological base map.

A strong correspondence between the location of the small circle zones on the planet and the sites of major volcanism can be seen in Figure 25. Plains-forming volcanism, such as that of Lunae Planum, the Tempe Plateau, Alba, Tharsis, Syrtis Major Planitia, Hellas, and Hesperia Planum and, to a lesser extent, constructional volcanism as in Alba, Tharsis, and Tyrrhenia Patera, appears spatially related to the position of these small circle zones. The inferred volcanic plains of Schiaparelli and Elysium do not fall within either small circle zone; the position of these volcanic regions may be due to something other than the global pattern defined here.

In addition to these primary units, several areas of modified, heavily cratered terrain appear to be associated with the small circle zones. One is Tempe Plateau. Its easternmost reaches are characterized by heavy modification

of plateau materials; this portion of the plateau is near one of the two small circle zones. The western margin of the plateau is similarly disrupted; one section of the northerly-trending medial zone of poles is located near this area.

The most widespread and intense activity associated with these small circle zones is in the areas where the zones converge. The best example of this is Tharsis; the activity at Hesperia, Syrtis Major, and the east-Hellas surficial modification are also notable. The volcanic plains southwest of Hellas seem somewhat anomalous, although the locations of the inferred calderas and the general direction of volcanic plains correspond very well to that of the associated small circle.

The poles to structural trends in the heavily cratered terrain represent centers of regional deformation: no single planet-wide stress system seems capable of producing the observed structural trends. The poles to these trends, however, are rather uniformly distributed within well defined small circle zones, comprising 44% of the surface area of Mars.

It is suggested here that these small circle zones represent statistical loci of tectonic activity that affected much of the martian crust in a systematic way. As the relative ages of measured structures in the heavily cratered terrain seem in general to predate the emplacement

Fig. 25. Global small circle zones of tectonic activity are superimposed on a Mercator projection of Mars geology, from Scott and Carr [1978]. Note the apparent localization of major plains-forming and constructional volcanism along the zones.

LOCI OF REGIONAL STRUCTURAL TRENDS WITHIN THE HEAVILY CRATERED TERRAIN

MARS GEOLOGY, AFTER SCOTT AND CARR (1978)

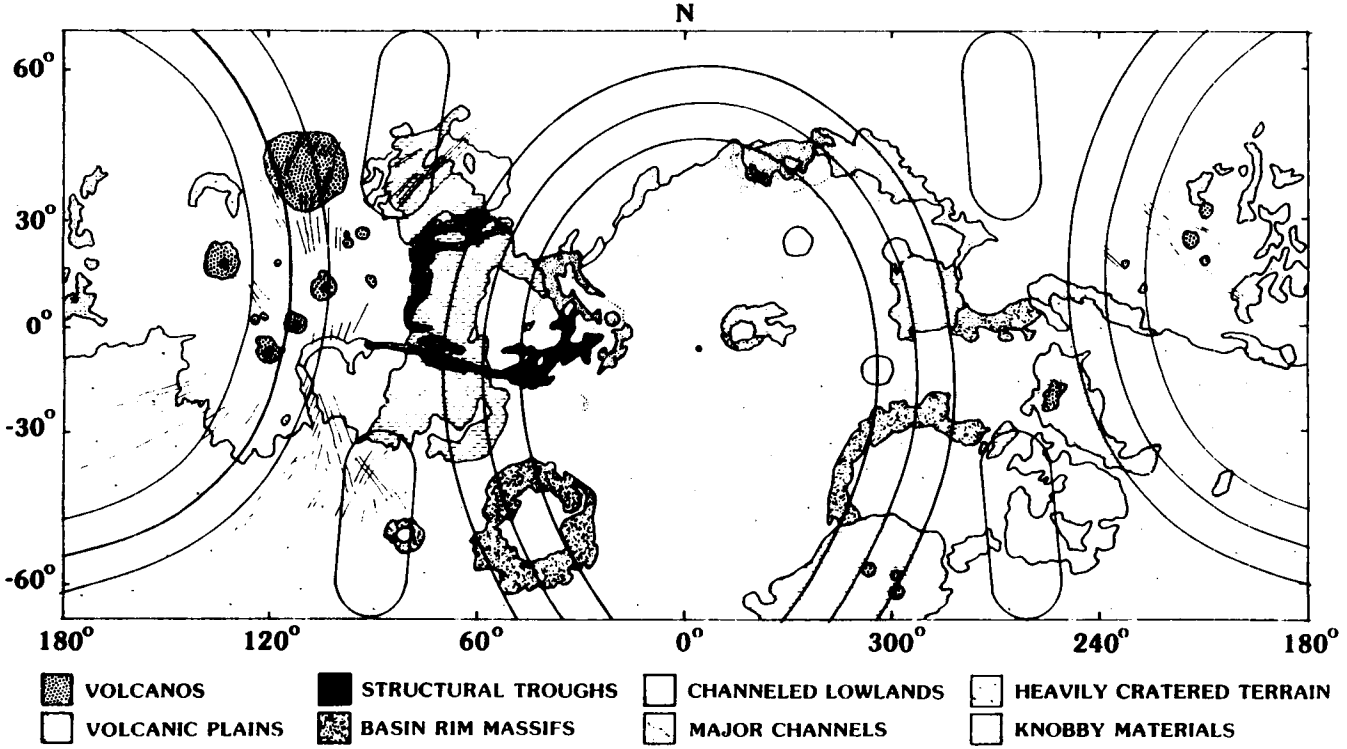

• GEOMETRIC CENTERS OF SMALL CIRCLE ZONES: -8,356 and 8,176

of the Lunae Planum-aged volcanic plains, as well as the structural and volcanic activity near Tharsis, these small circle zones and associated pole groups are thought to reflect a global organization of volcanic and tectonic activity that was developed early in martian history. This apparent global organization seems to have controlled the development of plains and constructional volcanism and may have contributed to the formation of portions of the fretted terrain.

The region of knobby terrain east of Hellas basin exhibits evidence of extensive modification of surface materials [Squyres, 1979]. This area is also associated with one of the southerly-trending medial zones of poles identified in Figure 24. A third region of intensely modified surface materials is Deuteronilus Mensae. This is the "type area" of fretted terrain of Sharp [1973] and is perhaps the most heavily modified portion of the planetary dichotomy boundary; it also seems to be associated with one of the small circle zones.

As the inferred tectonic pattern is uniformly globally defined, some other mechanism must have combined with this to create the asymmetries of the current martian crust. One of these asymmetries is the concentration of tectonic activity near the convergence of the two small circle zones near the present location of Tharsis; the other principal asymmetry seems to predate the Tharsis

localization: that of the formation of the planetary dichotomy boundary.

Activity in the vicinity of Tharsis seems to have largely obliterated or obscured the planetary dichotomy boundary in that area. Portions of the dichotomy boundary that appear the least obscured lie in the Nilosyrtis and Aeolis regions. Coordinates of the northernmost extent of the heavily cratered terrain for Nilosyrtis and Aeolis Mensae were plotted on a Schmidt Equal Area Net; the trends of these coordinates lie on a well defined small circle, which is shown in Figure 26, and centered at 66,180. There is also a possible small circle with a center at -66,360, symmetric to the dichotomy boundary small circle.

These hypothetical small circles have been superimposed onto a Mercator geologic map showing the global tectonic small circle zones, and are presented in Figure 27. The northern small circle is the best approximation of the present position of the planetary dichotomy boundary, based on the results of this research; the southern small circle is derived from symmetry arguments on the stereonet. Several important relationships between the best-fit small circles and global geology are apparent in Figure 27. Prominent structural trends seem to parallel the trace of the northern small circle, including the Aeolis, Nepenthes, and Nilosyrtis Mensae. Kasai Vallis

Fig. 26. The best-fit curve to the planetary dichotomy boundary is a small circle centered at 66,180. A corresponding small circle is centered at -66,360. Schmidt Equal Area Net, upper hemisphere; projection centered at 0,270.

BEST - FIT CURVE
MARS PLANETARY DICHOTOMY BOUNDARY

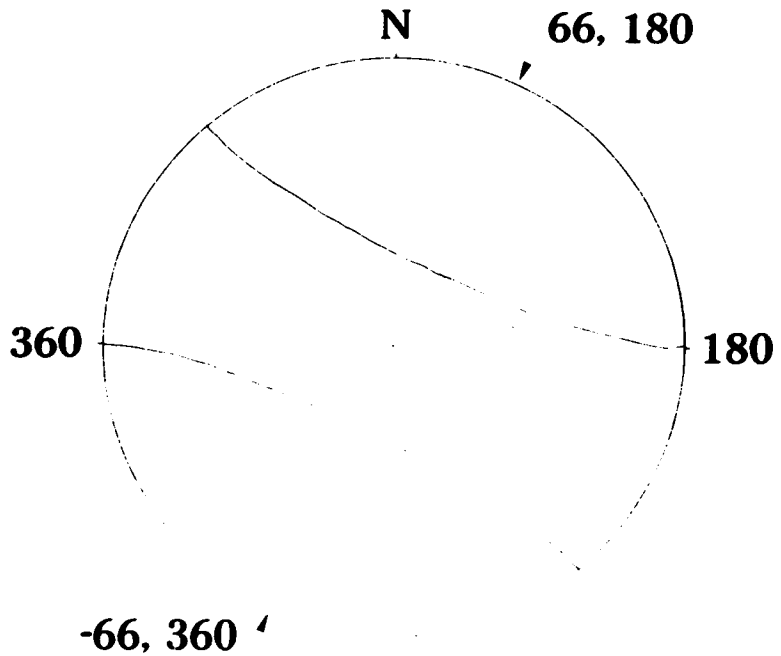

SCHMIDT EQUAL AREA NET,
UPPER HEMISPHERE
PROJECTION CENTERED AT 0, 270

Fig. 27. Best-fit small circle to the planetary dichotomy boundary plotted on Mercator projection of martian geology. Note the correlation of volcanic and structural features.

BEST-FIT CURVE, PLANETARY DICHOTOMY BOUNDARY

MARS GEOLOGY, AFTER SCOTT AND CARR (1978)

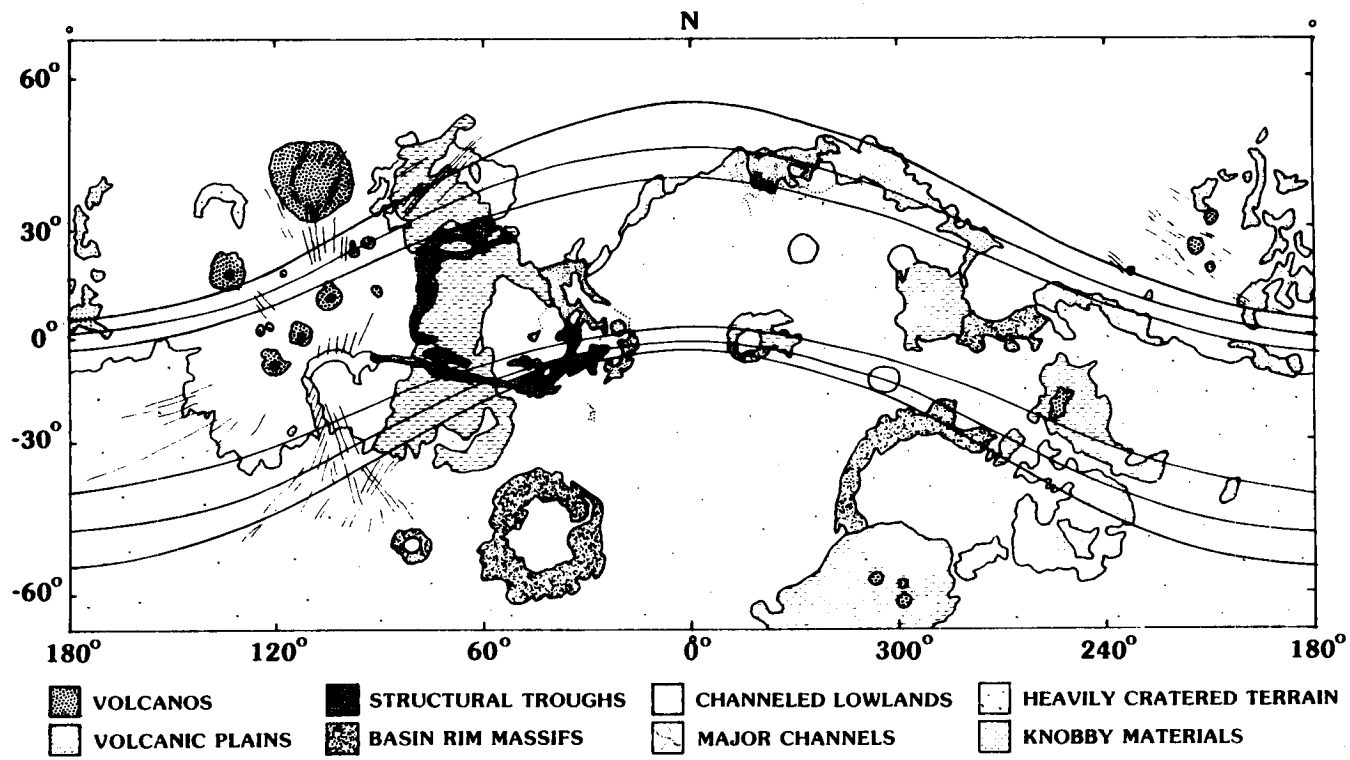

° GEOMETRIC CENTERS OF SMALL CIRCLE ZONES: 66, 180 and -66, 360

and the broad trough adjacent and to the north, which separates Tempe Plateau from the Lunae Planum to the south, also parallel this small circle. The trends of the older Tharsis volcanos, including Ceraunius Tholus and Uranius, Biblis, and Ulysses Paterae and, to a lesser extent, the general northeast-southwest trends of the Mareotis, Tempe, and Memnonia Fossae near Tharsis all seem to be aligned along this small circle. In addition, the position of the possible ash flow tuffs [Malin, 1979; Scott and Tanaka, 1982] in Memnonia and Aeolis seem to parallel this trend.

The southern small circle also mirrors trends in the southern heavily cratered terrain, although these are less pronounced than those to the north. The main activity located along this small circle is the volcanism east of Hellas (Hadriaca Patera) and that associated with Huygens and Schiaparelli; in addition, the trend of trough and furrow terrain, as mapped by McCauley [1978], tends to lie along this small circle. The most noticeable, perhaps, is the change in trend of the Valles Marineris as they pass from Lunae Planum into the heavily cratered terrain to the east; the abrupt shift from WNW to NE trends might reflect some contribution of the southern small circle to visible structural trends.

Recall that the poles to structures such as those near Valles Marineris defined the original small circle

zones; if these structures also parallel another small circle, then there may be a strong linkage between the two. Indeed, the poles to the oldest graben in MC-19 (N78W) lie southwest of Tharsis and in Deuteronilus Mensae: the global small circle zones and the planetary dichotomy boundary small circles intersect in both these areas. In addition, when the centers of the dichotomy boundary small circles are plotted on Figure 27, they lie within one of the global small circle zones.

It seems possible, then, that tectonism along the planetary dichotomy boundary small circles was perhaps the earliest manifestation of activity that was organized according to the global small circle zones; this phase of activity mostly resulted in mechanical deformation of the crust, and was most intense in the north. The other major phase of activity involved the extrusion of extensive volcanic plains along the traces of the global small circle zones; this was followed by more localized activity, especially near Thaumasia and Tharsis, and in structural control of landform modification, as of the fretted terrain in Deuteronilus Mensae.

SUMMARY AND CONCLUSIONS

Studies of structural trends in the heavily cratered terrain of Mars provide important information and insight into the distribution, relative timing, and intensity of crustal deformation on a global scale. The technique employed here involved measurements of the locations and and trends of structural features; these were compiled into rose diagrams on a region-by-region basis in order to isolate prominant structural trends. The best-fit poles to these trends were then determined and plotted on a stereographic projection that enabled the points plotted on the stereonet to correspond directly to planetary coordinate positions. The pattern of poles using this procedure revealed a set of small circles on the stereonet; these were then transferred to their corresponding positions on the planet.

Structural trends within the heavily cratered terrain are the result of regional deformation of the crust: no single global stress system (e.g., Tharsis loading or flexure) is indicated. The centers of deformation are spatially related on a global scale by a set of well defined small circle zones, which are associated with major structural and volcanic terrains. These global small circle zones probably reflect an early, fundamental pattern in the martian crust. Activity was principally expressed

as brittle, structural deformation of the crust, and was asymmetrically disposed. The most intense activity occurred in the north and produced the planetary dichotomy boundary, and may have contributed to the NE-SW elongation of the later Tharsis-related graben. Later activity was primarily thermal and resulted in the extrusion of Lunae Planum-age volcanic plains along the trends of the small circle zones, in addition to local faulting. Like the previous episode, this activity was also asymmetrically distributed; the most intense activity occurred in the region now known as Tharsis. Structures such as the Tharsis-related radial graben and the Valles Marineris probably resulted from regional stresses that were later superimposed upon this global system.

Substantial problems remain to be solved. This model does not address the localization of volcanism at Elysium or at Olympus Mons; nor does it account for the trends of the Tharsis Montes and the Claritas Fossae crustal block, or the Phlegra Montes. Further, models of crustal deformation resulting from Tharsis-induced loading stresses should perhaps address the potentially troublesome problem of a crust with strong preexisting structural trends and zones of weakness. These observations do suggest, however, that many regional structures within the heavily cratered terrain developed as a consequence of global tectonic processes.

REFERENCES

Anderson, E. M., The Dynamics of Faulting (2nd. ed.), 206 pp., Oliver and Boyd, Edinburgh, 1951.

Banerdt, W. B., R. J. Phillips, N. H. Sleep, and R. S. Saunders, Thick-shell tectonics on one-plate planets: Applications to Mars, submitted to J. Geophys. Res., 1981.

Batschelet, E., Statistical Methods for the Analysis of Problems in Animal Orientation and Certain Biological Rhythms, 57 pp., Amer. Inst. Biol. Sci., Washington, D.C., 1965.

Binder, A. B., Mariner IV: Analysis of preliminary photographs, Science 152, 1053-1055, 1966.

Binder, A. B., and D. W. McCarthy, Mars: The lineament system, Science 176, 279-281, 1972.

Blasius, K. R., J. A. Cutts, J. E. Guest, and H. Masursky, Geology of the Valles Marineris: First analysis of imaging from the Viking 1 Orbiter Primary Mission, J. Geophys. Res. 82, 4067-4091, 1977.

Carr, M. H., Tectonism and volcanism of the Tharsis region of Mars, J. Geophys. Res. 79, 3943-3949, 1974.

Casella, C. J., Evolution of the lunar fracture network, Bull. Geol. Soc. Am. 87, 226-234, 1976.

Dzurisin, D., The tectonic and volcanic history of Mercury as inferred from studies of scarps, ridges, troughs,

and other lineaments, J. Geophys. Res. 83, 4883-4906, 1978.

Engelder, T., and P. Geiser, On the use of regional joint sets as trajectories of paleostress fields during the development of the Appalachian Plateau, New York, J. Geophys. Res. 85, 6319-6341, 1980.

Fielder, G., Structure of the Moon's Surface, 226 pp., Pergamon Press, New York, 1961.

Frank, F. C., Curvature of island arcs, Nature 220, 363, 1968.

Frey, H., Thaumasia: A fossilized early forming Tharsis uplift, J. Geophys. Res. 84, 1009-1023, 1979.

Gifford, A. W., Ridge systems of Mars, M.S. Thesis, George Washington University, Washington, D.C., 1981.

Ginberg, M., and D. Pieri, Martian valley orientations and regional structural controls (abstract), NASA Tech. Memo. 82385, 95-97, 1980.

Golombek, M. P., Structural analysis of lunar grabens and the shallow crustal structure of the Moon, J. Geophys. Res. 84, 4657-4666, 1979.

Greeley, R., and P. D. Spudis, Volcanism on Mars, Rev. Geophys. Space Phys. 19, 13-41, 1981.

Hafner, W., Stress distributions and faulting, Geol. Soc. Am. Bull. 62, 373-398, 1951.

Harp, E. L., Fracture systems of Mars, Proc. First Intern. Conf. on the New Basement Tectonics, Utah Geol.

Assoc., 389-408, 1976.

Hobbs, B. E., W. D. Means, and P. F. Williams, An Outline of Structural Geology, 571 pp., John Wiley and Sons, New York, 1976.

Lucchitta, B. K., Mare ridges and related highland scarps--Result of vertical tectonism? Proc. Lunar Sci. Conf. 7th, 2761-2782, 1976.

Lucchitta, B. K., Geologic map of the Ismenius Lacus Quadrangle of Mars, Map I-1065, U.S. Geol. Surv., 1978.

Malin, M. C., Mars: Evidence of indurated deposits of fine materials (abstract), NASA Conf. Publ. 2072, 54, 1979.

Masson, P., Structure pattern analysis of the Noctis Labyrinthus-Valles Marineris regions of Mars, Icarus 30, 49-62, 1977.

McCauley, J. F., Geological map of the Coprates Quadrangle of Mars, Map I-897, U.S. Geol. Surv., 1978.

Melosh, H. J., On the origin of fractures radial to lunar basins, Proc. Lunar Sci. Conf. 7th, 2967-2982, 1976.

Melosh, H. J., Global tectonics of a despun planet, Icarus 31, 221-242, 1977.

Melosh, H. J., and D. Dzurisin, Mercurian global tectonics: A consequence of tidal despinning? Icarus 35, 227-236, 1978.

Melosh, H. J., and W. B. McKinnon, The mechanics of ringed basin formation, Geophys. Res. Lett. 5, 985-988, 1978.

Mutch, T. A., Geology of the Moon (revised ed.), 391 pp., Princeton University Press, Princeton, 1972.

Phillips, F. C., The Use of Stereographic Projection in Structural Geology (2nd. ed.), 86 pp., Edward Arnold Ltd., London, 1960.

Phillips, R. J., and K. Lambeck, Gravity fields of the terrestrial planets: Long-wavelength anomalies and tectonics, Rev. Geophys. Space Phys. 18, 27-76, 1980.

Pieri, D. C., Martian valleys: Morphology, distribution, age, and origin, Science 210, 895-897, 1980.

Plescia, J. B., and R. S. Saunders, The chronology of the martian volcanos, Proc. Lunar Planet. Sci. Conf. 10th, 2841-2859, 1979a.

Plescia, J. B., and R. S. Saunders, Tectonism of the Tharsis region (abstract), NASA Tech. Memo. 80339, 47-49, 1979b.

Plescia, J. B., and R. S. Saunders, Tectonics of the Tharsis region, Mars (abstract), in Papers Presented to the Third International Colloquium on Mars, 202-204, 1981.

Ragan, D. M., Structural Geology: An Introduction to Geometrical Techniques (2nd. ed.), 208 pp., John Wiley and Sons, New York, 1973.

Saunders, R. S., L. E. Roth, C. Elanchi, and G. Schubert, Topographic confirmation of 500 km degraded crater north of Ladon Valles, Mars (abstract), NASA Tech.

Memo. 79729, 157-159, 1978.

Schultz, P. H., and H. Glicken, Impact crater and basin control of igneous processes on Mars, J. Geophys. Res. 84, 8033-8047, 1979.

Schultz, P. H., and F. E. Ingerson, Martian lineaments from Mariner 6 and 7 images, J. Geophys. Res. 78, 8415-8427, 1973.

Schultz, P. H., R. A. Schultz, and J. L. Rogers, The structure and evolution of ancient impact basins on Mars, J. Geophys. Res., in press, 1982.

Scott, D. H., and M. H. Carr, Geologic map of Mars, Map I-1083, U.S. Geol. Surv., 1978.

Scott, D. H., and K. L. Tanaka, Ignimbrites of Amazonis Planitia region of Mars, J. Geophys. Res. 87, 1179-1190, 1982.

Sharp, R. P., Mars: Fretted and chaotic terrains, J. Geophys. Res. 78, 4073-4083, 1973.

Sharp, R. P., and M. C. Malin, Channels on Mars, Geol. Soc. Am. Bull. 86, 593-609, 1975.

Shoemaker, E. M., Synopsis of the geology of Meteor Crater, in Guidebook to the Geology of Meteor Crater, Arizona, Shoemaker and Kieffer (eds.), 1974.

Solomon, S. C., On volcanism and thermal tectonics on one-plate planets, Geophys. Res. Lett. 5, 461-464, 1978.

Squyres, S. W., The distribution of lobate debris aprons and similar flows on Mars, J. Geophys. Res. 84, 8087-8096, 1979.

Strom, R. G., Analysis of lunar lineaments, I-Tectonic map of the Moon, Arizona Univ. Lunar and Planetary Lab. Commun. 2, 205-221, 1964.

Suess, E., The Face of the Earth (translated from the original German), vol. 1., 604 pp., Clarendon Press, Oxford, 1904.

Vening-Meinesz, F. A., Shear patterns of the Earth's crust, Trans. Amer. Geophys. Union 28, 1-61, 1947.

Wilson, R. C., E. L. Harp, M. D. Picard, and S. H. Ward, Chaotic terrain of Mars: A tectonic interpretation from Mariner 6 imagery, Geol. Soc. Am. Bull. 84, 741-748, 1973.

Wise, D. U., M. P. Golombek, and G. E. McGill, Tharsis Province of Mars: Geologic sequence, geometry, and a deformation mechanism, Icarus 38, 456-472, 1979.

Young, R. A., W. J. Brennan, R. W. Wolfe, and D. J. Nichols, Volcanism in the lunar maria, Apollo 17 Prelim. Sci. Rep., 31-1 to 31-11, 1973.

SECTION II

A COMPARISON OF THE ORIGIN AND EVOLUTION OF A CIRCULAR AND AN IRREGULAR LUNAR MARE

James L. Whitford-Stark

Abstract of A Comparison of the Origin and Evolution of a circular and an irregular lunar mare by James Leslie Whitford-Stark, Ph.D., Brown University, June 1980.

Five related studies of the origin and evolution of lunar maria are presented. They all relate photogeologic and remote-sensing studies and are summarized as follows:-

1) The stratigraphy and eruption styles of basalts within Oceanus Procellarum are outlined. Four major volcanic phases were identified: The Repsold Formation(3.75 ± 0.5 b.y.) of titanium-rich basalts confined to the surface of northwest Procellarum (but probably underlying most of the mare) and occuring as dark mantle deposits around Sinus Aestuum. The Telemann Formation(3.6 ± 0.2 b.y.) of probably V.L.T. basalts occuring at the Aristarchus Plateau, northern Procellarum, and as scattered outcrops in the southeast. The Hermann Formation(3.3 ± 0.3 b.y.) of intermediate basalts occupying large areas of central and southeast Procellarum. Finally the Sharp Formation(2.7 ± 0.7 b.y.) of titanium-rich basalts preferentially erupted from vents at the mare/highland boundary. These basalts cover 1,700,000 km^2, average 550 m in thickness, and have an estimated volume of 0.87 x 10^6 km^3. Three large volcanic complexes(Rümker Hills, Aristarchus Plateau, Marius Hills) were sources for many of the basalts.

2) Oceanus Procellarum is hypothesized to have formed as a large sector graben consequent to the Imbrium basin-forming event. The origin of floor-fractured craters and graben are shown to be related to the thickness of mare fill. Graben formation terminated at 3.3 ± 0.3 b.y. while mare ridge production took place from at least the time of eruption of the Telemann Formation(3.6 ± 0.2 b.y.) till after the deposition of the youngest basalt. Positive

gravity anomalies are shown to be associated with Rima Sirsalis - a major tectonic feature of the lunar surface - and the young Sharp Formation basalts.

3) The filling of the ancient 900 km diameter, circular Australe basin is described. Four major episodes of basalt eruption ranging in age from early Imbrian to Eratosthenian were recognized. These basalts cover an area of 320,000 km^2, average about 750 m in thickness, and have a total volume of approximately 0.24×10^6 km^3. Flood-style eruptions were from at least 197 vents on crater floors. The youngest basalts occur in an annulus near the outer basin edge. North-south aligned mare ridges are present but there are no graben. The multi-ring basin morphology of Australe is reflected by basalt thickness variations. Extra-basin craters and basins contributed a substantial portion of the basin fill.

4) The evolution and basalt fill of the young, multi-ringed Imbrium basin is described. Ten major units, separable in age and chemistry have been defined. Surface basalts range in age from 3.75 ± 0.05 to 2.5 ± 0.3 b.y. and in chemistry from VLT to titanium-rich. The 850,000 km^2 of surface basalts form a small part of the total Imbrium basin fill estimated at 2.2×10^6 km^3. Mare ridge production took place from at least 3.5 ± 0.25 b.y. to less than 3.0 b.y. ago, while graben production terminated at 3.3 ± 0.3 b.y. ago.

5) A comparison of the origin and evolution of a circular and

irregular lunar mare is made based on the results described in the previous four papers. Data obtained from landing sites and other maria are combined with the photogeologic and remote-sensing analyses to decipher the histories of lunar maria. Eruptions of dissimilar composition were found to have taken place synchronously both within and between maria. The tectonic evolution of Imbrium and Procellarum was found to be similar except in the distribution of the deformed products. Currently available petrogenetic models for basalts were found to be inadequate.

PREFACE

Introduction: The aquisition of remote-sensing data from lunar orbit, the refinement of earth-based techniques, and the return of lunar samples has led to an unprecedented increase in our knowledge of the Moon in the last 15 years. This thesis represents an attempt to synthesize remote-sensing, sample, and photogeologic information in order to decipher the mode and nature of the basalt filling of the lunar maria. In particular, it emphasizes the similarities and differences between the origins and basalt-filling sequences of a circular and an irregular mare; the former represented by Mare Imbrium and the latter by Oceanus Procellarum.

The five papers are presented in a chronologic order with respect to the time at which the data-gathering for each was completed. The reader may thereby be able to trace the development of the author's thinking on the subject. Three of the papers were written in collaboration with my thesis advisor, James W. Head III, who contributed to the final organization of the manuscripts and offered many ideas as to their content. The data-gathering and much of the content was, however, the product of the author.

The first paper, following the guidelines of the American Commission on Stratigraphic Nomenclature, defines the filling sequence of Oceanus Procellarum. The second paper describes the tectonic evolution of that mare. Paper 3 changes to a description of the fill of a very degraded multi-ring basin; Australe. Paper 4 defines the filling sequence of the youthful, multi-ringed Imbrium basin where, unlike Australe, basalt eruption appears to have closely followed the basin-forming event. The final paper

compares the information from the previous four and incorporates the work of other lunar scientists in an attempt to define the major characteristics of the evolution of lunar maria. The main conclusions are that basin-filling by basalts was considerably more complex than was envisaged as little as five years ago but that tectonic processes were simply related to the basin fill and lithosphere thicknesses.

Papers 1 and 3 were previously published and cannot be reprinted in this publication. However, the titles and abstracts are included to present a continuum.

ACKNOWLEDGEMENTS

The majority of the work presented in this thesis was performed under NASA Grant NGR-40-002-116 though some of the early data collection was begun under an N.E.R.C. grant to Gilbert Fielder at the University of Lancaster. Photographs were supplied by the N.S.S.D.C. Maryland.

I would like to thank the many teachers and colleagues whose interactions with the author have influenced the material herein presented, including: A. Brown, M.J. Cintala, C.S. Exley, G. Fielder, P.A. Floyd, R.J. Fryer, B.R. Hawke, P.C. Hess, G. Hulme, R. Macdonald, P.J. Mouginis-Mark, C.M. Pieters, H. Pinkerton, R.A. Roach, S. Self, M. Settle, R.S.J. Sparks, P.D. Spudis, R. Todhunter, L. Wilson, and C.A. Wood. Most particularly, I would like to thank J.W. Head III for his supervision and assistance in the preparation of this thesis.

The reprinted version of my thesis is dedicated to the late Thomas (Tim) A. Mutch who served as an exemplary advisor on my thesis committee shortly prior to his tragic death.

TABLE OF CONTENTS

STRATIGRAPHY OF OCEANUS PROCELLARUM BASALTS: SOURCES AND STYLES OF EMPLACEMENT.

James L. Whitford-Stark

and

James W. Head, III

Dept. of Geological Sciences

Brown University

Providence, Rhode Island 02912, USA.

Abstract

The basalts within Oceanus Procellarum have been named the Oceanus Procellarum Group and subdivided into four major geologic units on the basis of morphology, spectral reflectance, and other remote sensing information in order to develop a framework of regional stratigraphy for the largest lunar mare. The oldest mare basalt unit identified, the Repsold Formation (low albedo, blue color, high crater density, very weak 3.8 cm radar backscatter, and a weak 1 μm reflectance) crops out in NW Procellarum and may be correlative with Apollo 11 and 17 high titanium basalts. The next youngest unit, the Telemann Formation (red, higher albedo, high crater density, high D_L values, and an average to strong 1 μm reflectance) extends over wide areas of Procellarum and crops out as extensive surface units and as local patches surrounding earlier, topographically higher, units. Numerous large sinuous rilles in the Aristarchus Plateau were a major source for some of these deposits. Pyroclastic deposits forming the dark red mantle were also emplaced at the Aristarchus Plateau during these eruptions. The Hermann Formation (intermediate color, low albedo, intermediate crater density, and average to strong 1 μm reflectance) occurs as extensive plains developed from less voluminous eruptions from sources at the Marius Hills complex, the Rümker Hills, and in Nubium, Cognitum, and near Delisle. The youngest unit, the Sharp Formation(very low albedo, blue color, low crater density, and a strong 1 μm reflectance) is volumetrically small and is derived primarily from vents near the highland/mare boundary. Many Sharp Formation members have

associated sinuous rilles. Basalts of the Hermann Formation were sampled by Apollo 12, those of the Telemann Formation may be similar to the Luna 24 VLT basalts, while those of the Repsold Formation may be comparable with the Apollo 11,17 and Luna 16 samples. The Sharp Formation, the youngest basalts, remain unsampled. The total volume of Procellarum basalts is estimated at 8.7×10^5 km^3(about 10% of the total mare volume). The relative volumes of the individual formations are not reflected by the surface area covered because the youngest flows tend to be thin and widespread. For example, the Sharp Formation has a surface area of 720,000 km^2 but an estimated volume of only 1.8×10^4 km^3 while the Repsold Formation has a present surface area of only 22,000 km^2 but an estimated volume of 2.1×10^5 km^3. The vast majority of lavas in Procellarum were extruded early in the phase of lava flooding, prior to about 3.5 b.y.

THE TECTONIC EVOLUTION OF THE OCEANUS PROCELLARUM BASIN

James L. Whitford-Stark

and

James W. Head III

Dept. of Geological Sciences

Brown University

Providence, R.I. 02912 U.S.A.

ABSTRACT

The stratigraphy and emplacement styles of Oceanus Procellarum basalts are briefly reviewed. Procellarum is divided into three sections, each with a different degree of mare flooding and mare ridge pattern; the center is deeply flooded with a central parallel ridge zone, the southeast is shallow with reticulate ridges, and the north is intermediate with polygonal ridges. Gravity, magnetic and photogeologic data indicate Rima Sirsalis and its mare extension to Tobias Mayer W to be an important tectonic feature of the lunar surface; possibly a dike-intruded normal fault with relative downward motion to the west. Graben formation is shown to have terminated during the emplacement of the Hermann Formation basalts(3.3 $\pm$ 0.3 b.y.). Basalt flooding of circum-mare craters appears to have been more common in craters cut by graben than those with floor fractures. Mare ridges exhibit regular offsets, are rarely cross-cutting, were formed over a long time period(at least 0.5 b.y.), and some post-date the deposition of the youngest basalts. Post-emplacement basalt downwarping of the mare surface has in places reversed the original topography and elsewhere emphasized that topography. A small positive gravity anomaly appears to correlate with the youngest Procellarum basalts while older units have no anomalies. The Procellarum topographic low is hypothesized to have originated as a large sector-graben with movements on faults radial and concentric to the Imbrium impact basin.

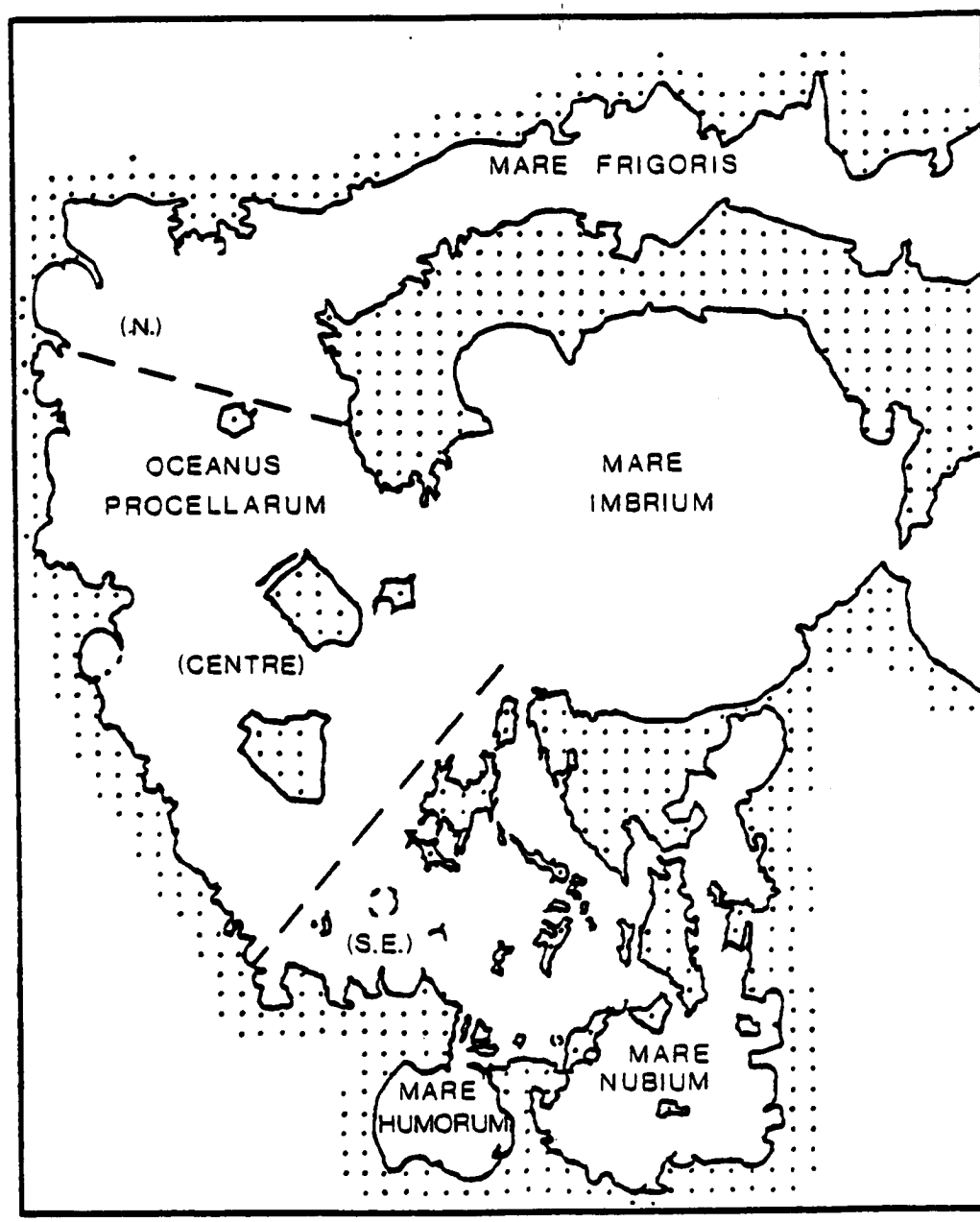

Figure 1 Diagram of the maria near the western limb of the Moon, showing the tripartite subdivision of Oceanus Procellarum. Highlands and volcanic complexes are demarcated by dots.

1) Introduction

The lunar maria can be subdivided into regular and irregular groups. The regular maria are approximately circular (e.g., Mare Crisium) and appear to result from the basalt-infilling of large impact basins. The shape of the irregular maria does not appear to have resulted from the simple flooding of single basins. Oceanus Procellarum is the largest of these irregular maria, with a surface area of about 1,700,000 km^2, and lies near the western limb of the near side of the Moon (Figure 1).

Oceanus Procellarum has been mapped as a number of separate quadrangles by the U.S.Geological Survey and these maps have been combined to form part of the geological map of the near side of the Moon (Wilhelms and McCauley,1971). More recently, syntheses of remote-sensing data relating to Oceanus Procellarum have been made by Pieters et al (1980) and Whitford-Stark and Head (1980). The former deals with the detailed description of the part of Procellarum centered on the Flamsteed area while the latter describes the stratigraphic sequence of basalts infilling the entirety of Procellarum. The present paper briefly reviews the stratigraphic sequence and describes and interprets the structural development of Oceanus Procellarum by combining information derived from photogeological analyses, and geochemical and geophysical remote-sensing.

2) Summary of Stratigraphy

a. Stratigraphic Units

A formal lithostratigraphy for the basaltic materials within Oceanus Procellarum has been recently compiled (Whitford-Stark and Head, 1980). The Oceanus Procellarum Group was subdivided into four formations (Figure 2) and a number of member units. The oldest (3.75 $\pm$ 0.05 b.y.), Repsold Formation has defining characteristics which include a blue color on combined ultraviolet-

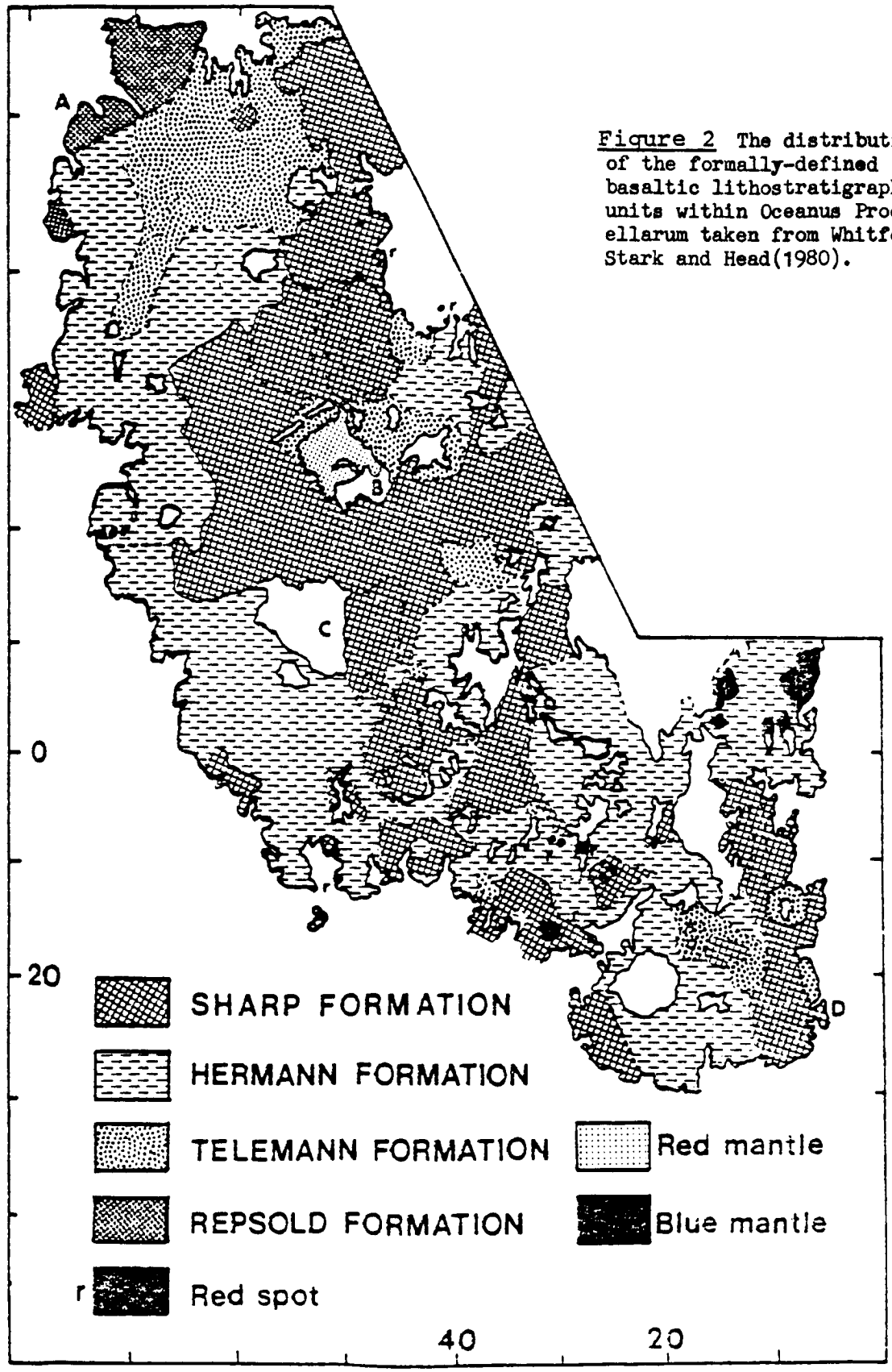

Figure 2 The distribution of the formally-defined basaltic lithostratigraphic units within Oceanus Procellarum taken from Whitford-Stark and Head(1980).

infrared photographs (Whitaker,1972), a very low albedo - 0.069 to 0.0793 (Pohn and Wildey,1970), and a high impact crater density. Pieters (1978) tentatively assigned materials of the Repsold Formation the spectral characteristics of the Luna 16 mare basalts, including; a medium-high ultraviolet/ visible ratio, a low albedo, and a weak 1μm reflectance. The Repsold Formation is characterized by a weak 3.8 cm radar reflectance (Zisk et al, 1974). On the basis of age and similar spectral characteristics, the Repsold Formation was considered (Whitford-Stark and Head,1980) to be similar to Apollo 11 and 17 high titanium basalts. The Telemann Formation which overlies the Repsold Formation has defining characteristics which include less than 2 wt% TiO_2 (Johnson et al, 1977; Pieters, 1978), a red color on combined UV/IR photographs (Whitaker, 1972), a high albedo - 0.074 to 0.102 (Pohn and Wildey,1970), an average to strong 1 μm reflectance (Pieters,1978), and a high crater density. It is also characterized by a medium 3.8 cm radar backscatter (Zisk et al,1974) and a low thorium content - about 2.5 ppm (Haines et al,1978). Combined crater degradation/ density data (Boyce and Johnson,1978) indicate an age of 3.6 ± 0.2 b.y. for the Telemann Formation. Both the Repsold and Telemann Formation basalts have complementary pyroclastic materials; the former including the blue dark mantling materials of Sinus Aestuum and the latter, the red mantling materials of the Aristarchus Plateau. The Hermann Formation with crater degradation/ density data (Boyce and Johnson,1978) indicating an age of 3.3 ± 0.3 b.y. appears to postdate the Telemann Formation. A TiO_2 content of 1.0 to 5.0 wt% (after Pieters,1978) or less than 2 wt% to 6 wt% (Johnson et al,1977), a low albedo - 0.074 to 0.085 (Pohn and Wildey,1970), a reddish-intermediate-bluish color on combined UV/IR photographs (Whitaker,1972), an average to strong 1 μm reflectance (Pieters,1978), and an intermediate crater density all serve to define the Hermann Formation. Orbital gamma-ray data suggest that the Hermann Formation has low concentrations of K, Th, and U (Arnold et al,1977)

UNIT	SURFACE AREA (km^2)	% Area	Original Maximum surface area (km^2)	Estimated av. thickness (m)	Volume (km^3)	% Volume
Sharp Formation	720,000	42.55	720,000	25	1.8×10^4	2.07
Hermann Formation	770,000	45.51	1,490,000	150	2.2×10^5	25.35
Telemann Formation	180,000	10.64	1,670,000	250	4.2×10^5	48.39
Repsold Formation	22,000	1.30	1,692,000	125	2.1×10^5	24.19
Total	1,692,000	100.00	1,692,000	550	8.7×10^5	100.00

TABLE 1

while the 3.8 cm radar indicates it to have a generally low backscatter (Zisk et al,1974). The youngest basaltic materials in Procellarum are represented by the Sharp Formation with an estimated crater degradation/density age of 2.7 ± 0.7 b.y. (Boyce and Johnson,1978) though Young (1977) indicates that parts of the Sharp Formation may be as young as 1.77 ± 0.2 b.y. Defining characteristics of the Sharp Formation include a TiO_2 content of 3 to 11 wt% (Johnson et al,1977; Pieters,1978), a very low albedo - 0.069 to 0.079 (Pohn and Wildey,1970), a blue color on combined UV/IR photographs (Whitaker,1972), a strong 1 μm reflectance band where observable (Pieters,1978), a low crater density, and, in places, topographic boundaries. Characterizing features of the Sharp Formation include the common presence of well-defined sinuous rilles, the presence of sharply-defined rimless pits, outlines commonly controlled by topographic highs in the form of mare ridges, and a thorium content of about 9 ppm (Haines et al,1978).

There also exists the possibility of non-mare basalts underlying and interfingering with the mare basalts. These non-mare basalts have been correlated with the spectrally anomalous features called "red spots" and equated with KREEP volcanism (Malin,1974) and/or other highland basalt types (Head and McCord,1978). Some of these red spots are domed structures (Head and McCord,1978) while others in southeast Procellarum take the form of plains units and hummocky uplands (Wood and Head,1975). Hawke and Head(1978) have proposed that KREEP basalts were emplaced as extrusive materials over a time range extending from prior to 4.1 b.y. ago to the period of extrusion of the basin-filling mare basalts.

b. Distribution, thicknesses and volumes of basalts.

Table 1 and Figure 2 taken from Whitford-Stark and Head (1980) indicate the areas occupied by each formation, their estimated average thicknesses,

the relative proportion of the total fill each represents, and their areal distribution. The original surface area of each formation was calculated assuming that each underlies the younger basalt units. Various methods have been employed to estimate the average thickness of each formation and other estimates have been made by Marshall(1961), Baldwin (1970), Neukum and Horn (1976), De Hon (1978,79), and Hörz(1978). The basalt fill is not uniformly thick but rather varies from feather thin at the mare/highland boundary to several kilometers over large pre-fill craters. With an estimated average thickness of 550 m and an area of approximately 1,700,000 km^2, the Procellarum basalts represent nearly 9.5 % of the 10 x 10^6 km^3 volume and 25 % of the area of mare basalt estimated (Head,1975) to occur at the lunar surface.

Outcrops of the Repsold Formation are presently confined to the extreme northwest of Procellarum (Figure 2) and the dark mantle materials of Sinus Aestuum. The Telemann Formation is most extensively developed in northern Procellarum and around the Aristarchus Plateau. In southeast Procellarum the Telemann Formation occurs as small patches near the mare/highland boundary and at mare ridge crests. The Hermann Formation is the most extensive of the units occuring over most of the surface except in northern Procellarum. The Sharp Formation occupies an extensive area of central Procellarum and extends eastward into Mare Imbrium and southwards into the Flamsteed region (Pieters et al,1980). In addition, the Sharp Formation was preferentially emplaced near the Mare/highland boundary where it occurs in a number of isolated outcrops. Although areally extensive, the Sharp Formation is volumetrically small (Table 1).

c. Eruption Styles

The main eruptive centers within Procellarum are the three large volcanic complexes - the Aristarchus Plateau/ Harbinger Mts. (40,000 km^2), the

VOLCANIC COMPLEX	SINUOUS RILLES	LOW DOMES	STEEP DOMES	CONES
Marius Hills	20	135	127	59
Aristarchus Plateau - Harbinger Mts.	36	3	-	-
Rümker Hills	-	30 (1)	-	-

Table 2. Volcanic features of the Procellarum igneous complexes. (1) after Smith (1974).

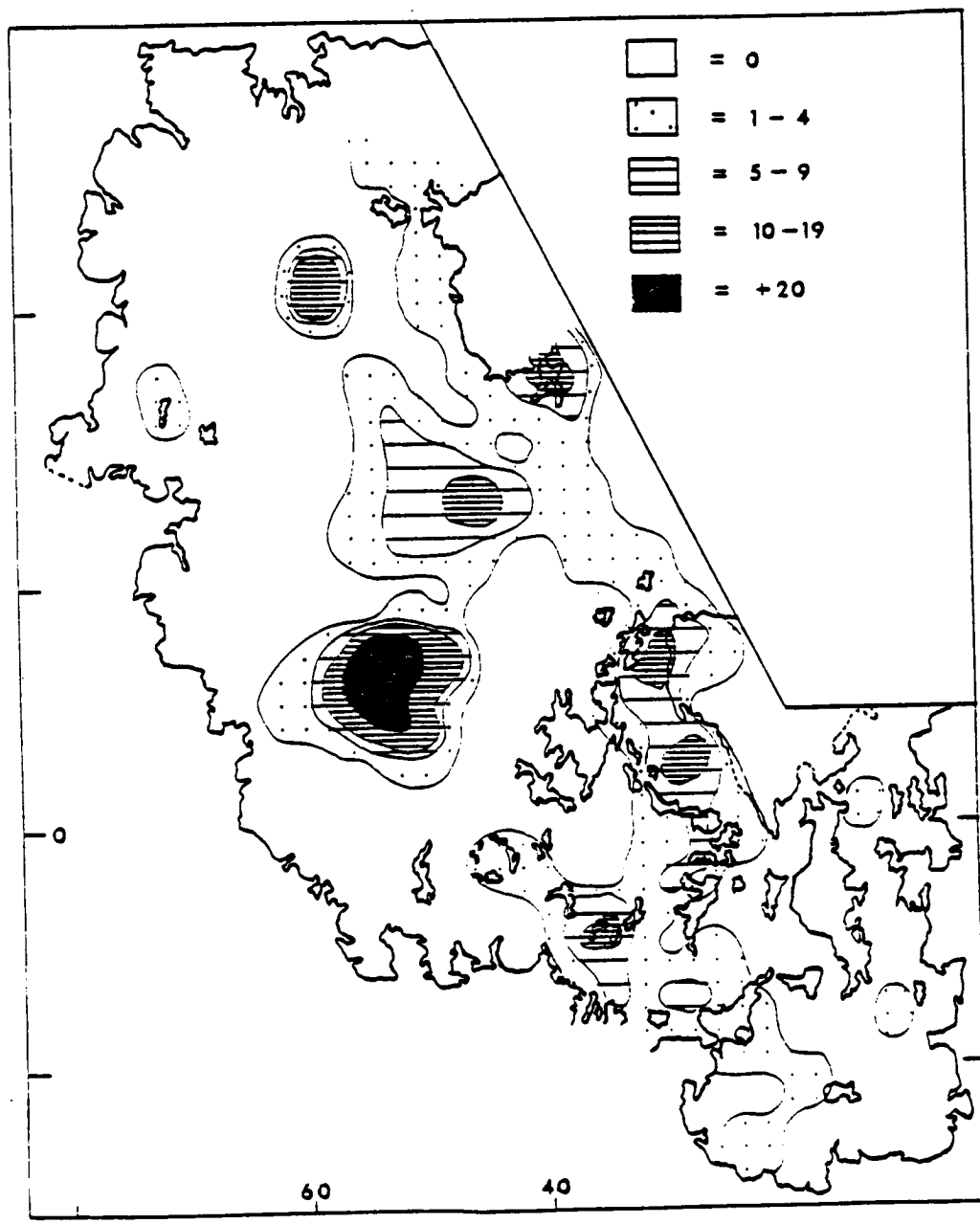

Figure 3 Isopleth map of the distribution of identifiable volcanic vents within Oceanus Procellarum. The key indicates the number of vents per 5° by 5° square.

Marius Hills (35,000 km^2), and the Rümker Hills (5,000 km^2) - whose different eruption styles have been described by Whitford-Stark and Head (1977). The different volcanic structures within these complexes are shown in Table 2. Figure 3 shows the distribution of identified volcanic centers within Procellarum. The three complexes are clearly demarcated but, in addition, other concentrations can be recognized at the southern end of the Heraclides Promontory (40 W, 35 W) and to the west of Copernicus in the south Imbrium basin (30W, 5 to 15 N). The Heraclides group comprises the Gruithuisen domes (Head and McCord,1978) and a number of sinuous rille source craters while the south Imbrium group comprises a series of low-profile domes (Hackman,1962; Schmitt et al,1967).

Previous mapping (Whitford-Stark and Head,1980) established that the youngest unit within Procellarum, the Sharp Formation, was primarily erupted from sinuous rille source craters located at the mare/highland boundary although some, such as the Flamsteed Basalt Member (Pieters et al,1980), were erupted from vents near the eastern edge of the Marius Hills. This association of flows with rilles is typical of plains-style eruptions (Greeley,1976). Similar rille-associated flows form large parts of the Hermann Formation; a unit that can be shown (Whitford-Stark and Head,1980) to have been particularly derived from the Marius Hills and possibly the Rümker Hills. The sinuous rilles, and their source craters, of the Telemann Formation are much larger than those of the Hermann Formation (up to 5 km diameter as against $\ll 1$ km) implying much greater eruption rates for the former (Whitford-Stark and Head, 1977; Head and Wilson,1980). These Telemann Formation rilles are particularly associated with the Aristarchus Plateau/Harbinger Mts. No vents have been identified within the limited surface exposure of the Repsold Formation. This may be a function of erosion of this early mare unit or, by analogy with Mare Australe (Whitford-Stark,1979), may reflect an early flood-type eruption

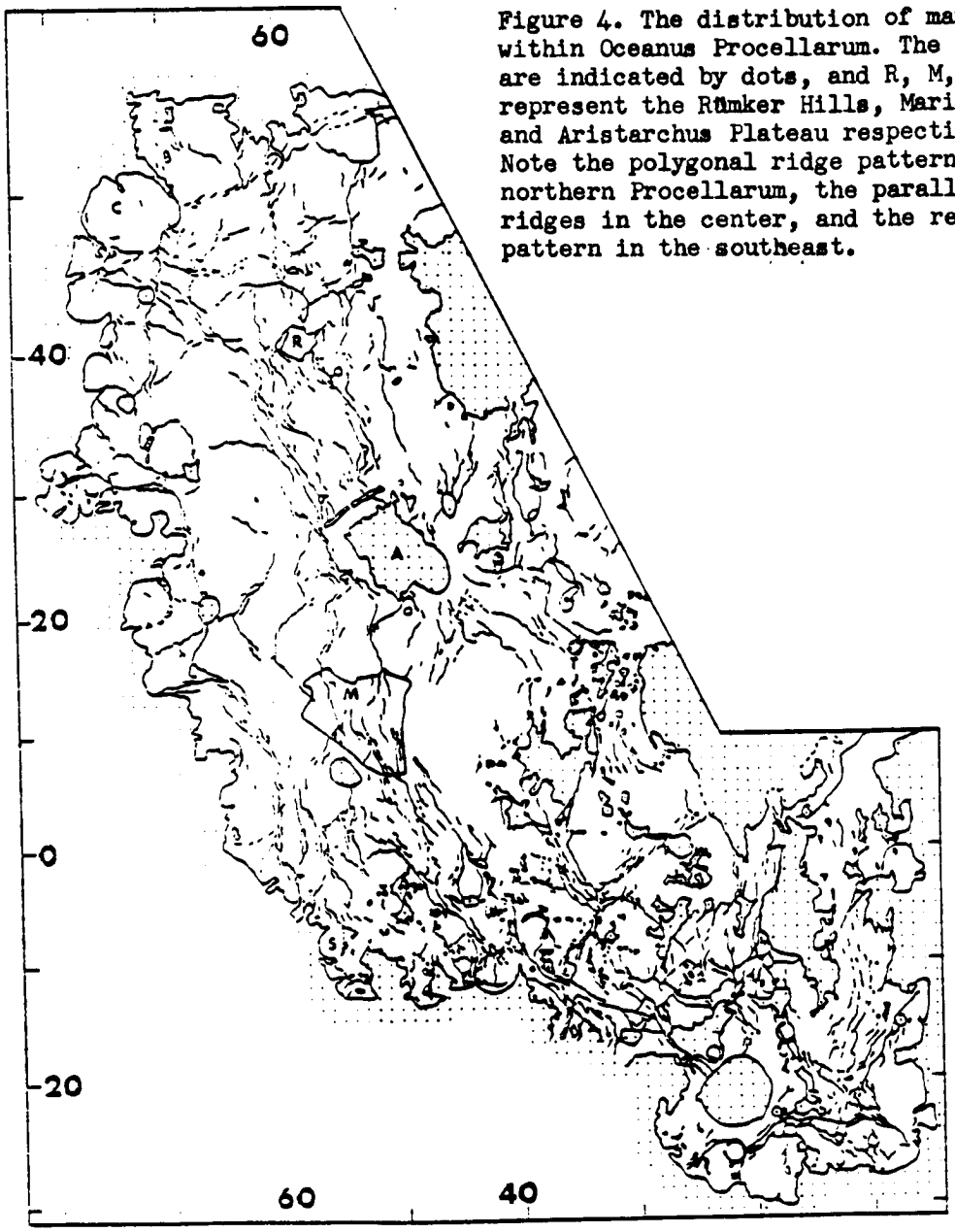

Figure 4. The distribution of mare ridges within Oceanus Procellarum. The highlands are indicated by dots, and R, M, and A, represent the Rümker Hills, Marius Hills, and Aristarchus Plateau respectively. Note the polygonal ridge pattern in northern Procellarum, the parallelism of ridges in the center, and the reticulate pattern in the southeast.

style.

3) Tripartite subdivision of Procellarum

The tripartite subdivision of Procellarum(Figure 1) was established by Whitford-Stark and Head (1977b) based on physiographic differences between each. The central section is characterized by the three large igneous complexes and is generally devoid of highland remnants. This scenario was believed to reflect a thick mare fill. The northern section has a few highland remnants, particularly in the northwest, but its most distinctive characteristic is the polygonal mare ridge pattern (Figure 4) rather than the linear ridge alignment of central Procellarum. This polygonal pattern could reflect sub-basalt topography (Maxwell et al,1975), which together with the highland "islands", suggests that northern Procellarum is shallower than central Procellarum. The southeast section of Procellarum is characterized by mare lavas separated by abundant interspersed remnants of highlands (Figure 5). This abundance of pre-mare topography suggests a thin mare fill. Estimates of the average fill thickness in southeast Procellarum include 1.1 km (Marshall,1961), 1.4 km (De Hon,1978), 500 to 750 m (Hörz,1978), and 400 m (De Hon,1979; Pieters et al,1980).

The boundary between the southeast and central sections is represented by a line connecting Sirsalis E and Tobias Mayer W. Radar data shows a topographic drop of 100 m to the northwest of the lineament (Pieters et al,1980). Magnetic data (Anderson et al,1977) indicates a strong linear magnetic anomaly associated with Rima Sirsalis - the highland extension of the topographic lineament - and there is also a linear gravity high associated with Rima Sirsalis (Sjogren,1974). In these respects Rima Sirsalis is unique among the lunar graben that have been the subject of remote-sensing analyses. These features suggest that the lineament is a normal fault, downdropped to the

northwest and perhaps intruded by an igneous dike. The fact that the youngest flows in the Flamsteed region cover the lineament with no apparent deflection in flow direction (Pieters et al,1980) suggests that the presently observed topographic variation across the lineament has arisen since the emplacement of the mare basalts. The distinctive variation in highland remnants between central and southeastern Procellarum suggests, however, that movement on the fault also predated mare emplacement. The height difference of the mare surface between central and southeastern would have to have been removed prior to the emplacement of the Sharp Formation. The extensive deformation of the early Hermann but not the late Hermann Formation (Whitford-Stark and Head,1980) suggests that major movement on the fault had occured prior to the emplacement of the late Hermann Formation. Basalts of the late Hermann Formation would therefore have been responsible for removing the topographic differences either side of the fault. This scenario might explain the presence of the Marius Basalt Member of the Hermann Formation to the west of the Flamsteed area but the Cognitum Basalt Member to the east (Pieters et al,1980). Vertical movement on this fault might also account for the largely missing western ring mountain of Mare Imbrium and also the greater degree of flooding in central Procellarum. In essence, central Procellarum is a sector graben which collapsed along faults initiated by the Imbrium impact. The northern equivalent of the Sirsalis lineament which presumably downdropped Proceelarum on its southeast side has not been identified and is merely inferred from the Imbrium ring gap. The lack of similar geophysical anomalies associated with other graben may be a function of the instrument resolution (since Sirsalis is one of the largest) or it may mean that Sirsalis is unique in being intruded by dense basaltic material. If the latter is the case, it would imply that the graben predated intrusion of basaltic material and were not initiated by those intrusions. If central Procellarum, prior to mare flooding, had the

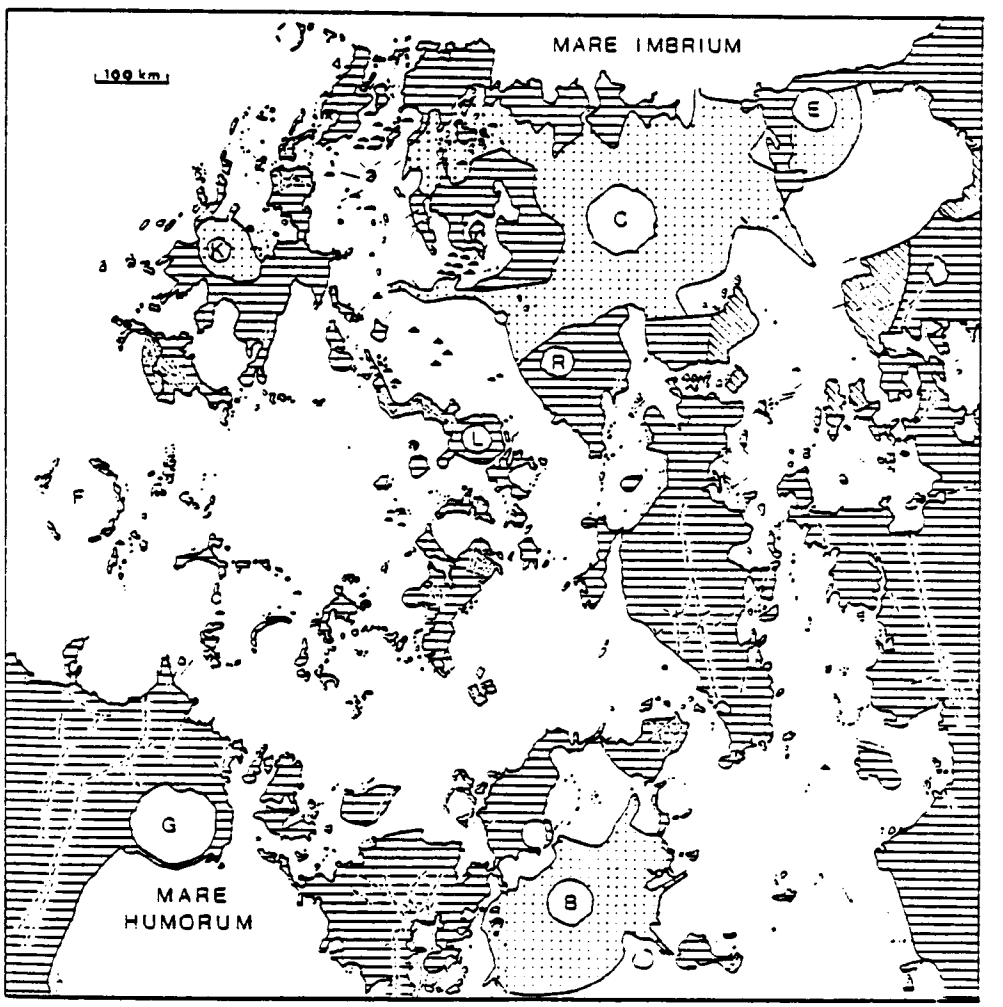

Figure 5 Large scale map of southeast Procellarum showing the highlands(horizontal ruling), crater ejecta blankets(dotted), dark mantle material(diagonal ruling), cones(triangles), domes(hemispheres), graben (dash-dot lines), and fractures(solid lines). B is the crater Bullialdus, C is Copernicus, E is Eratosthenes, F is Flamsteed P, G is Gassendi, K is Kepler, R is Reinhold, and L is Lansberg.

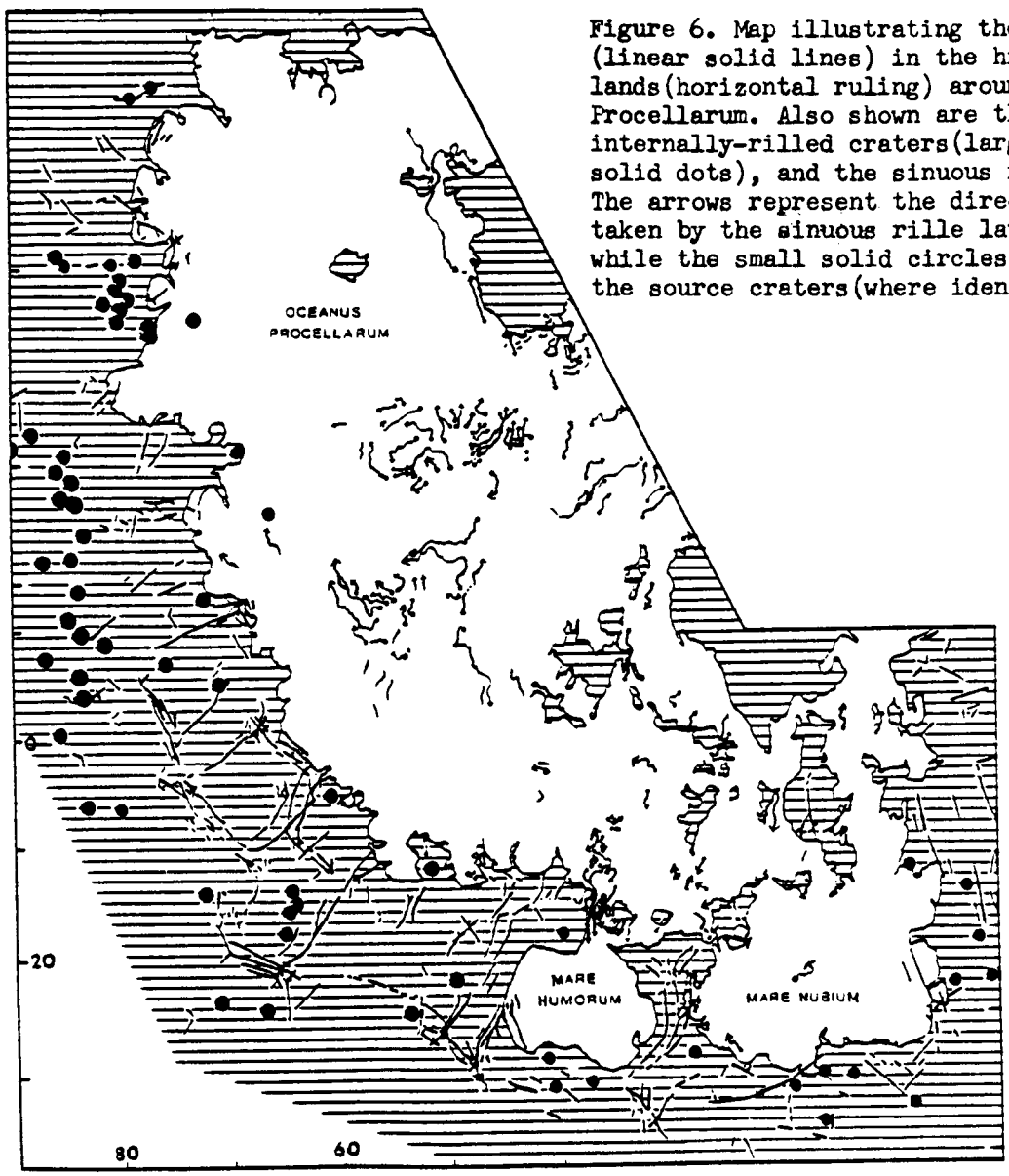

Figure 6. Map illustrating the graben (linear solid lines) in the highlands (horizontal ruling) around Procellarum. Also shown are the internally-rilled craters (large solid dots), and the sinuous rilles. The arrows represent the directions taken by the sinuous rille lavas while the small solid circles are the source craters (where identiable).

surface topographic characteristics of southeast Procellarum, then the net throw on the faults may have been of the order of a kilometer or greater.

4) Tectonic evolution

a) Graben

Linear graben are clearly related to the emplacement of mare basalts, they being found only within and around the maria (Whitford-Stark,1974) and both cut and are flooded by mare basalts. Mason et al (1976) have hypothesized that the graben resulted from posthumous movements on fracture patterns formed in the lunar lithosphere by the basin-forming impacts. These movements are believed (Quaide,1965; Solomon and Head,1979) to result from tensional stresses produced close to the mare/highland boundary as a result of the basalt load within the maria. Figure 6 shows the large tectonic graben within and around Procellarum while Figure 5 shows the fractures, too small to be depicted on Figure 6, that occur within southeast Procellarum. Particularly apparent from Figure 6 is the annulus of graben around Mare Humorum. The lack of a similar well-developed graben annulus to Mare Nubium suggests a lesser basalt thickness within that mare; a suggestion supported by isopach maps of basalt thickness (De Hon,1979). The linears developed within the highlands to the east of 0^{o} are clearly radial to Mare Imbrium. Some of these linears may be tectonic but many appear to be of sedimentary origin caused by erosion of the pre-Imbrian terrain and deposition of the Imbrium ejecta blanket (Head,1976). The other prominent graben system in Figure 6 is that developed within the highlands to the southwest of Procellarum. The longest of these graben, Rima Sirsalis, extends some 450 km into the highlands from the edge of Procellarum. More commonly, the graben are restricted to within 250 km of the mare/highland boundary and appear to divide the highlands up into approximately 725,000 km^2 blocks. The presence of these extensive graben to the southwest of Procellarum

is again supportive of a thick basalt fill within central Procellarum, while the thinner fill in northern Procellarum is reflected by the lesser graben development in the highlands adjacent to that area.

The width of Rima Sirsalis is remarkably constant, generally varying between two and three kilometers (Figure 6); notable departures from these average values occur where Rima Sirsalis is joined by another slightly offset graben and where it tapers to a point at its furthest distance from Procellarum. It seems unlikely that two cross-cutting graben could have been produced in the same tensional environment, rather it would seem that at least two different generations of graben are present to the southwest of Procellarum. Rima Sirsalis appears to cut and therefore be younger than all the graben along its path though it is flooded by mare basalts at its northern extremity. McGill (1971) has determined that the graben wall slopes cluster around 60° while he calculated that Rima Sirsalis walls sloped at 68°. Assuming 68° and that Sirsalis is symmetrical, with an average width of 2.75 km the two walls would converge at a depth of about 3.5 km. A more detailed analysis of graben by Golombek(1979) supports this convergence depth and he has proposed that this depth reflects the thickness of the lunar megaregolith.

Lucchitta and Watkins (1978) determined the southwest Procellarum graben to be among the youngest on the Moon and suggested that their formation terminated at about 3.6 $\pm$ 0.2 b.y. ago. The present authors have established that the graben around Procellarum are flooded by the Sharp Formation and late part of the Hermann Formation but cut the early part of the Hermann Formation; the Hermann Formation was estimated (Whitford-Stark and Head,1980) to have an age of 3.3 $\pm$ 0.3 b.y., in general agreement with the results of Lucchitta and Watkins(1978).

Although graben parallel to the mare/highland boundary can be adequately explained by basalt loading of the lunar lithosphere, the graben normal to the

boundary are difficult to explain by this same mechanism. It is possible that these normal graben were produced by the Imbrium impact event (Mason et al, 1976), alternatively they may represent the surface expression of subsurface dikes. This latter interpretation would be analagous to that proposed (Pollard and Holzhausen,1979)to explain similar structures developed over terrestrial dikes, would be consistent with the formation of the graben during the period of emplacement of mare basalts, would explain the magnetic and gravity anomalies associated with Rima Sirsalis (Anderson et al, 1977), and may offer an explanation for the volcanic cone-like structure (McCauley, 1973) of the crater Sirsalis J (59 W, 13.5 S).

In addition to the large graben, there are within the mare fractures usually less than 50 km in length and a few hundred meters in width. In southeast Procellarum (Figure 5) these fractures are common to basalts of the Hermann Formation but also occur in the younger Sharp Formation. Their production therefore continued after the termination of graben production. To the west of Copernicus these fractures are associated with low profile domes, but more particularly cone-like structures are aligned along the fractures. It therefore appears probable that at least some of these fractures were fissures from which basalts were erupted.

The Straight Wall (Rupes Recta) is most probably a dip-slip fault (Fielder 1963) produced by loading of the mare basalts on the lunar lithosphere. The Straight Wall is located in eastern Mare Nubium, is 120 km in length has a height of 340 $\pm$ 50 m, and has a slope of less than 48° (Fielder, 1963). It would seem that this fault is also younger than the graben since it cuts the young basalts of the Sharp Formation.

b) Internally-rilled craters

Internally-rilled craters are those whose floors are punctuated by

fractures in various patterns (Whitford-Stark,1974; Schultz,1976). These fractures appear to have been produced by forces acting entirely within the confines of the enclosing crater and most likely resulted from the volcano-tectonic modification of impact craters(Schultz,1976; Hall et al,1979) although regional isostatic adjustment associated with mare emplacement (Bryan et al, 1975) and isostatic rebound (Baldwin,1968) have also been proposed to account for this phenomenon.

To investigate the thickness of basalt fill in, or sill thickness beneath the floors of,floor-fractured craters, the floor-fractured craters to the west of Procellarum were analysed by the method outlined in Whitford-Stark (1979). In brief,

$$t = \left(\frac{Df - De}{Dr - Dt}\right) De$$

where t is the fill thickness, Df and Dr are the measured floor and rim crest diameters respectively, $De = 0.684 \times Dr^{0.41}$ (Wood and Andersson,1978), and $Dt = 0.728Dr - 9.86$ (R.Roth,personal communication,1979) where the curves for De and Dt are the depths of excavation and original floor diameter of fresh Tycho-type craters. That is, the thickness values obtained assumes that the measured crater had the characteristics of a fresh Tycho-type crater at the time of filling. A total of 132 craters in excess of 18 km diameter were investigated by this method; of these, 38 were classified as being floor-fractured (Figure 6). Figure 7 compares frequency plots for the floor-fractured and non-floor-fractured craters. Although the two plots are not identical, no systematic differences can be observed between them; both sets of craters have similar fill thicknesses - up to in excess of 3.5 km. Since the craters were probably not fresh at the time of filling, the fill thicknesses were recalculated based on the degradation state of the enclosing crater. Wood (1979) has proposed that in the 1 to 5 classification scale of lunar craters,

where 1 is the youngest and 5 the oldest, that the 2,3,4, and 5 class craters are 23%, 40%, 59%, and 76% degraded respectively. For example, a class 4 crater with a calculated fill thickness of 3.09 km has a recalculated fill thickness of 1.27 km after taking into account the degradation state. In effect, the recalculated value is the excess of fill thickness that a crater has in comparison with a similarly degraded, unfilled,Tycho-type crater of the same size. The recalculated fill thicknesses are plotted in Figure 8. The recalculated floor-fractured craters still exhibit a wide, though reduced, range of fill thicknesses. The non-floor-fractured craters exhibit as wide a range of values but they do show a strong peak at 400 to 700 m. If the floor-fractured craters do owe the origin of their fractures to volcanotectonic uplift, it is not readily apparent from Figures 7 and 8 how much movement has taken place. If both the floors of floor-fractured and non-floor-fractured craters in this area have been uplifted by similar amounts, the presence of fractures may simply reflect the cohesiveness of the floor material- fractures forming most readily in a cohesive substrate.

A further feature of both figures 7 and 8 is that the craters of both groups with the thickest fill tend to be partly or completely lava-flooded. In these cases, such as the example of the crater Cruger(67 W, 16.5 S), it is possible that the basaltic floor materials cover previously-formed floor fractures. The craters which are non-rilled but apparently contain a thick basaltic fill, such as Cruger, were evidently flooded at a late stage in the development of Procellarum. The fill of these craters floods the graben earlier shown to have been produced prior to the emplacement of the late Hermann Formation. Thus the basaltic crater fill is equivalent in age to the late Hermann Formation or the Sharp Formation. The low albedo and blue color of the floor material of the crater Grimaldi(67 W, 5 S) suggests that it is a titanium-rich basalt of the Sharp Formation. The presence of this young basalt

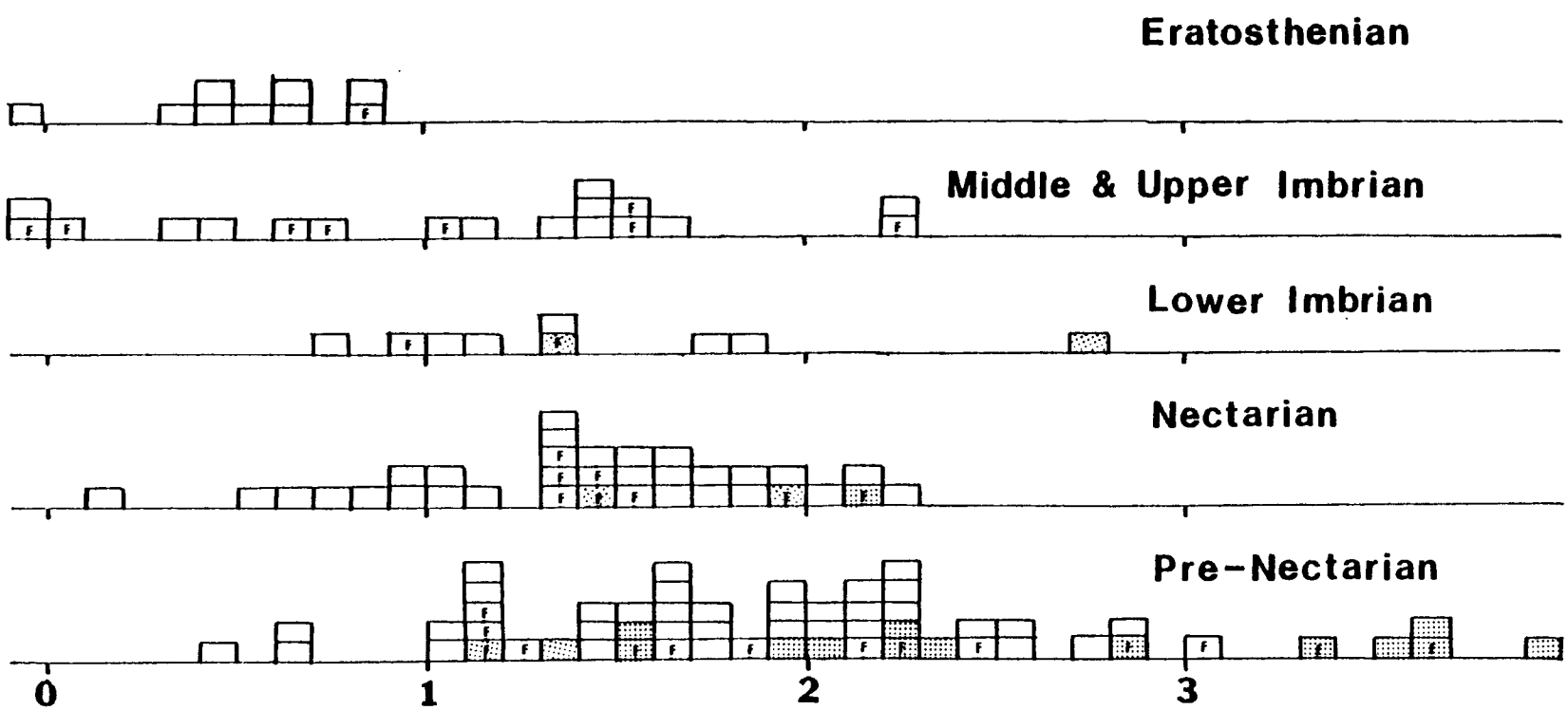

Figure 7 Histograms illustrating the fill thicknesses calculated for large craters in the highlands to the west of Procellarum assuming that the craters were fresh Tycho-type at the time of infilling. F indicates floor-fractured craters, shading represents basalt-flooded craters, and each box represents one crater within the specified 100 m thickness interval.

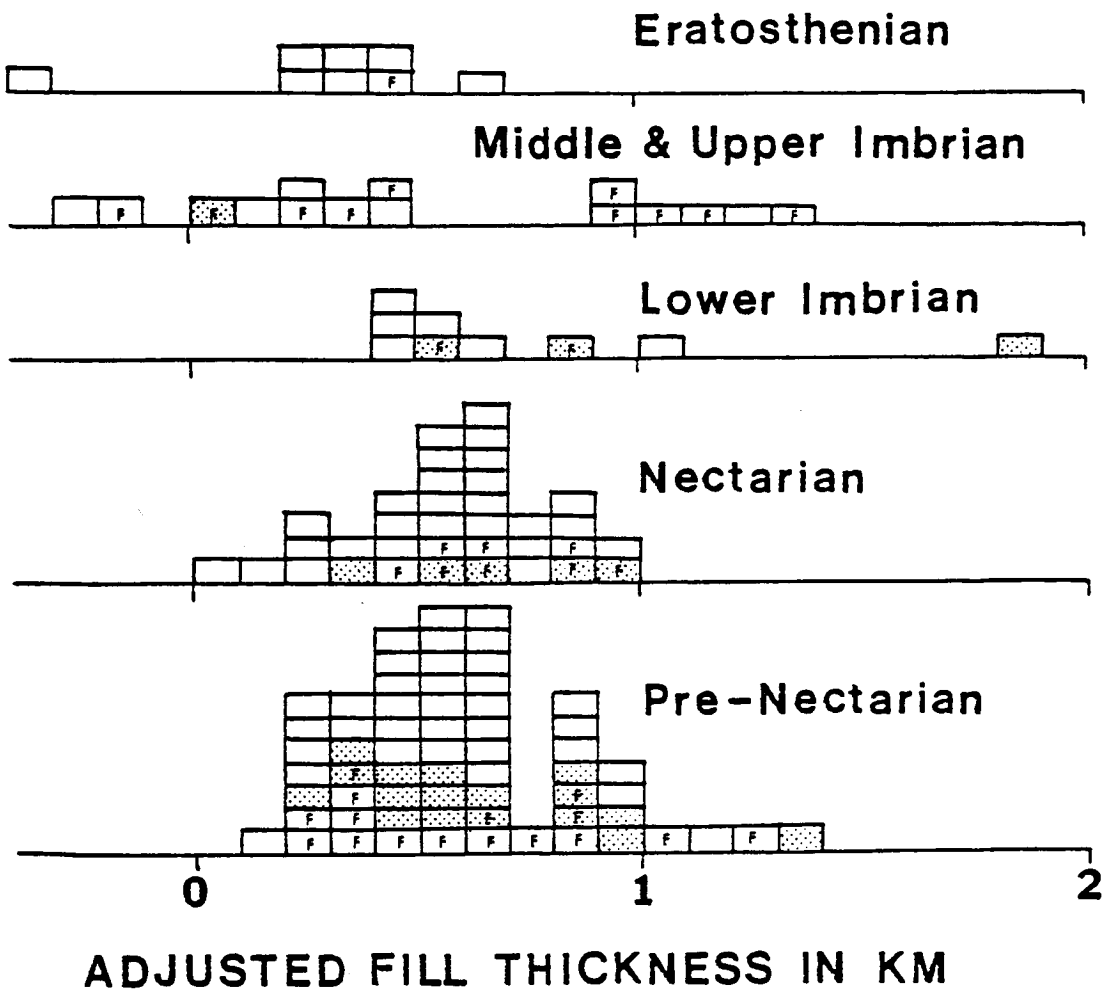

Figure 8 Histograms illustrating fill thicknesses for large craters to the west of Procellarum recalculated on the basis that they were variously degraded at the time of infilling(see text for detailed description). Key as for figure 7.

in the circum-mare craters supports the view(Solomon and Head,1979) that a tensional environment existed in this area as a result of lithosphere loading by the earlier mare basalts. This appears to be the most logical explanation for highland craters which correspond in age, and probably composition, with the least voluminous of the Procellarum basalt units(Whitford-Stark and Head, 1980). The previously-formed graben faults may have acted as pathways for magma which were tapped by the as yet unflooded craters, a suggestion supported by the location of both the internally-rilled and flooded craters within the limits of the area containing graben(Whitford-Stark,1974). Indeed, many of the craters which have been partly flooded by basalts lie on graben and are not internally-rilled(e.g., Hedin and Ricciolli). This observation does not lend support to the viewpoint (Schultz,1976) that flooded craters were floor-fractured prior to basalt emplacement. In addition, if floor-fracturing were a precursor to basalt flooding, one might expect to see some floor-fractured, unflooded craters in Mare Australe, yet in that mare all the craters are either flooded, or non-flooded and non-floor-fractured (Whitford-Stark,1979)

In addition to the large floor-fractured craters there is also a group of small floor-fractured craters classified as types IV and V by Whitford-Stark(1974) and included within Class IV of Schultz(1976). The small craters studied in the present analysis (Figure 6) have a mean diameter of 13.68 km, tend to occur in groups, and are often intersecting. Some of these craters have similar sizes and are elongate in the same direction as adjacent non-floor-fractured Orientale secondary craters. The small size of these craters appear to be more consistent with floor-fracturing by the cooling of an originally molten floor surface than by tectonic motion. It is possible that this molten material could have been Orientale impact melt though, again, adjacent unfractured craters do not lend support to this mode of origin,since the distribution of impact melt would be expected to be more uniform. Cooling

of volcanic material would more readily account for the scattered distribution of these small floor-fractured craters.

c) Mare ridges

After craters, mare ridges have been the lunar surface features with the most numerous different interpretations of their origin. This stems largely from the fact that similar features are lacking or not obvious on Earth. Most hypotheses consider the ridges to be volcanic, tectonic, or volcanotectonic. Typically the ridges consist of a broad arch from 1 to 20 km wide, often capped by an irregular, steep wrinkle ridge. Some arches reach several hundred kilometers in length and range in height from a few to several hundred meters (Strom,1971). Although mare ridges often terminate at the mare/highland boundary, in some instances they can be traced into the adjacent highlands (e.g.,Whitford-Stark, 1979). Parts of the ridge system within Procellarum have been the object of studies by Tjia(1970), Wilson (1970), Colton et al(1972), Young (1972), Lucchitta (1977), and Raitala (1978).

Figure 4 shows the distribution of mare ridges over the entirety of Procellarum. In southeast Procellarum the ridges exhibit a pronounced reticulate pattern with preferential alignments in NW-SE, NE-SW directions corresponding to the alignments of the "lunar grid" (Fielder and Kiang,1962). To the northwest of the boundary between southeast and central Procellarum the ridge system exhibits a greater degree of parallelism. The system is dominated by a central group of sub-parallel ridges which passes through the Marius Hills complex, skirts the western side of the Aristarchus Plateau and continues to the Rümker Hills (Figure 4). This same ridge system can be traced through the southern part of southeast Procellarum as far as the crater Bullialdus (22.5 W, 21 S). The fact that the ridge system passes around the Aristarchus Plateau but through the Marius and Rümker Hills (Whitford-Stark and Head, 1977) may

reflect a different near-surface structure at the Plateau.Other features of the ridge system in central Procellarum include a pattern which postdates and is radial to the crater Seleucus (66.5 W, 21 N), and a group of ridges which continue the circular outline of Mare Imbrium.

In northern Procellarum the central ridge system disappears and is replaced by a polygonal ridge pattern. In the eastern part of northern Procellarum and in the adjacent Mare Frigoris, the ridges are parallel with or normal to the mare/highland boundary (Whitford-Stark and Fryer, 1975). In northwestern Procellarum a mare ridge completes the outline of the largely buried crater Repsold C.

A notable feature of the mare ridges is that they rarely cross-cut one another. A rare example occurs to the immediate north of the Rümker Hills where a northeast trending ridge cuts a northwest trending ridge. Another feature of the mare ridges is their common en echelon arrangement and, as noted by Tjia(1970), those ridges which strike between north and east predominantly exhibit dextral en echelon offset while those striking between north and west exhibit a predominantly sinistral en echelon pattern. Radar analysis of maria Serenitatis and Crisium (Peeples et al, 1978) clearly shows the local higher relief of subsurface layers directly beneath the arches. Together, these features strongly indicate that the majority of ridges are tectonic in origin, most likely being compressional folds. The coherence between the surface arches and the locally high relief of the subsurface layers at depths in excess of 1.5 km in Mare Serenitatis does not lend support to the interpretation (Bryan,1973) for their origin by localized compression of a relatively thin crust uncoupled from the underlying structure and topography. A compressional origin for the ridges does,however, provide a mechanism to account for the central ridge system in central Procellarum, located furthest from, and parallel with, the mare/highland boundary in a position where the

basalt fill might be expected to be thickest. The lack of ridges within the Aristarchus Plateau could be accounted for by its being a non-coherent, less readily-deformable block than the mare surface. On the other hand, the presence of ridges within both the Marius and Rümker Hills suggests that a significant thickness of mare-related materials overlies highland crust at those localities. At other localities, such as within the crater Flamsteed P (Pieters et al,1980) and the ridge system completing the outline of Repsold C, the ridges appear to have originated more through local stresses resulting from the disposition of the pre-existing topography, that is, either by distortion of the basalts where they are draped over buried rim crests or by subsidence of basalts within large craters. The reticulate pattern in southeast Procellarum, the polygonal pattern in northern Procellarum, and the radial pattern around Seleucus appear difficult to explain by compressional forces. On Earth such patterns are usually produced by tensional forces,though within the mare the reticulate and polygonal patterns could be produced by compression if two maximum horizontal principal stress directions arise from the sinking of a rectangular or oblong basin. The radial pattern around Seleucus may be related to vertical forces (Schultz,1976) acting during the formation of the fractured floor of that crater. Another feature of ridges is that they rarely extend far into the ejecta blankets of pre-ridge, large (greater than 30 km diameter) craters. The intense brecciation of the surface in the vicinity of large craters presumably inhibited the coherency of the stress distribution.

The wrinkle ridges which are often associated with the arches exhibit no predictable pattern; they occur in linear trends, form zig-zag patterns, move from one side of the arch to the other, and in places extend out onto the flat mare surface (Lucchitta,1977). Lucchitta (1977) came to the conclusion that the wrinkle ridge and arch appear to be only indirectly related and suggested that the wrinkle ridges might not even be structural in origin but

UNIT	Present Surface area (km^2)	% of total area	Length of ridges (km)	% of total ridge length	% area divided by % ridge length
Sharp Formation	194,346	48.56	3,205	45.18	1.07
Hermann Formation	187,000	46.73	3,271	46.11	1.01
Telemann Formation	18,843	4.71	618	8.71	0.54
Total	400,189	100.00	7,094	100.00	1.00

Table 3. Morphometry of the basalt units and mare ridges in the Flamsteed region (Pieters et al,1980) of Oceanus Procellarum.

rather volcanic. A volcanic origin for the ridges has been proposed by Fielder (1961) and Strom (1971). In support of his volcanic interpretation, Strom cites the location of bright hills overlying ridges, circular plateau along ridges, and the presence of short flows from ridges. To these might be added the source craters of sinuous rilles in the Herigonius region of southeast Procellarum (Greeley and Spudis,1978) and a line of vents along a ridge to the north of the crater Kreiger(45.5 W, 29 N) in northern Procellarum (Lucchitta,1977). There seems little doubt that volcanism was associated with the mare ridges, it is less obvious that the ridges were actually produced by volcanism.

Although the predominantly non-cross-cutting nature of ridges and their regular offsets suggests that they were produced within a uniform stress field, there is less information on how long that stress field was operative. Muehlberger (1974) in a study of ridges in Mare Serenitatis believed their formation to be continuing to the present. Schaber (1973) and Bryan (1973) have shown that mare ridges grew between the emplacement of successive flows in Mare Imbrium while Greeley(1971) has documaneted a similar situation in the Marius Hills. In an attempt to investigate the time period of ridge formation, a detailed investigation has been made of the Flamsteed region (Pieters et al, 1980). Because of the difficulties in accurately defining the lateral limits of the ridges because of their low profiles, the lengths of individual ridge segemnts within each Formation were measured (Table 3). Another difficulty arises from the ridge size being being close to or below the resolution of the spectral vidicon images. Thus although a ridge may be within the Sharp Formation it could be composed of Telemann Formation material. An example was found (Pieters et al,1980) where basalts of the Sharp Formation were guided by and partly flooded the lower portions of a ridge composed of Hermann Formation material. A thin lava cover over ridges would thus overemphasize the

ridge population of the younger unit. In Table 3 the most significant column is that of %area of basalt/ % length of ridges. It clearly shows that in terms of the area occupied by each formation there is a progressive decrease in ridge development with decrease in age. This is partly a reflection of the fact that the early units would probably have been covered by younger units had they not been topographic highs at the time of deposition of the younger units. However, it also implies that deformation to produce ridges of the Telemann Formation material took place before the deposition of the overlying Hermann Formation. At the same time, the presence of ridges within the youngest Sharp Formation implies that ridge production also postdated the emplacement of that unit. However, the barriers to basalt flow provided by some ridges in the Flamsteed region (Pieters et al,1980) and in other parts of Procellarum (Whitford-Stark and Head,1980) indicates that the major ridge systems were produced prior to the emplacement of the Sharp Formation and probably before the end of emplacement of the Hermann Formation. Subsequent production of ridges has been minor, though it may continue to the present.

To summarize, ridges were produced over a period extending from at least 3.6 $\pm$ 0.2 to 2.7 $\pm$ 0.7 b.y. ago in an apparently uniform stress field. Their formation may continue to the present and, in this respect, they differ from graben whose production terminated prior to the eruption of late mare basalts. It therefore would appear that the graben and ridges are not concomitant phenomena, an argument supported by the presence of ridges but not graben in Mare Australe (Whitford-Stark,1979).

d) Evolution of the present surface topography

The present surface topography of Procellarum in part reflects original depositional slopes and in part the tectonic modification of those slopes (Scott et al, 1978). The gross topography of Procellarum can be ascertained

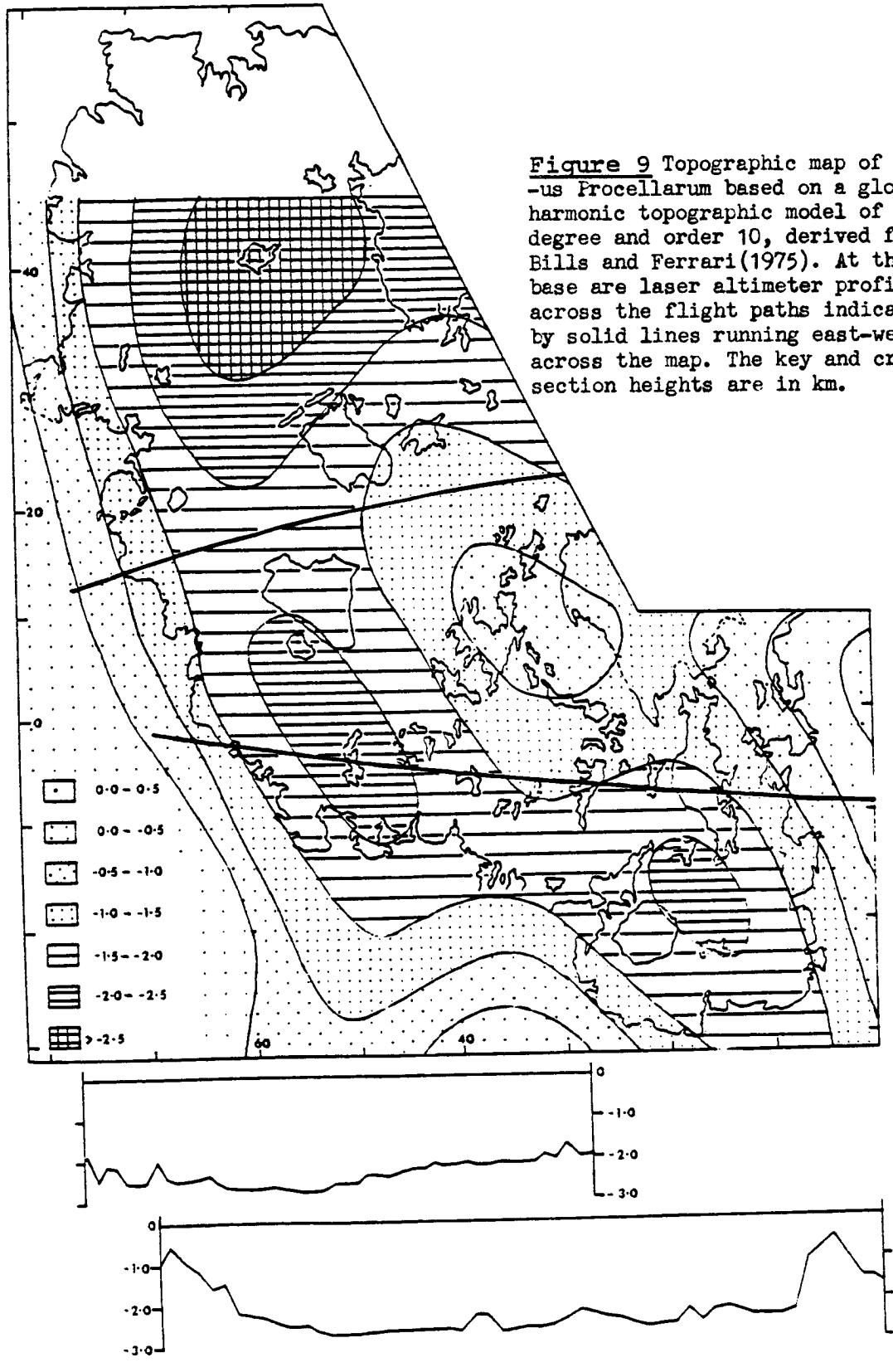

Figure 9 Topographic map of Ocean -us Procellarum based on a global harmonic topographic model of degree and order 10, derived from Bills and Ferrari(1975). At the base are laser altimeter profiles across the flight paths indicated by solid lines running east-west across the map. The key and cross-section heights are in km.

Figure 10. Contour map of Oceanus Procellarum. The downslope directions are indicated by the tick marks while the contour interval is approximately 100 m (see text). Highlands are indicated by the dotted pattern. The map was compiled from the Lunar Topographic Orthophotomaps, Radar data supplied by S.H. Zisk, and the Lunar Aeronautical charts, augmented by laser altimetry data. The coverage and resolutions of the different data sets are indicated in the key.

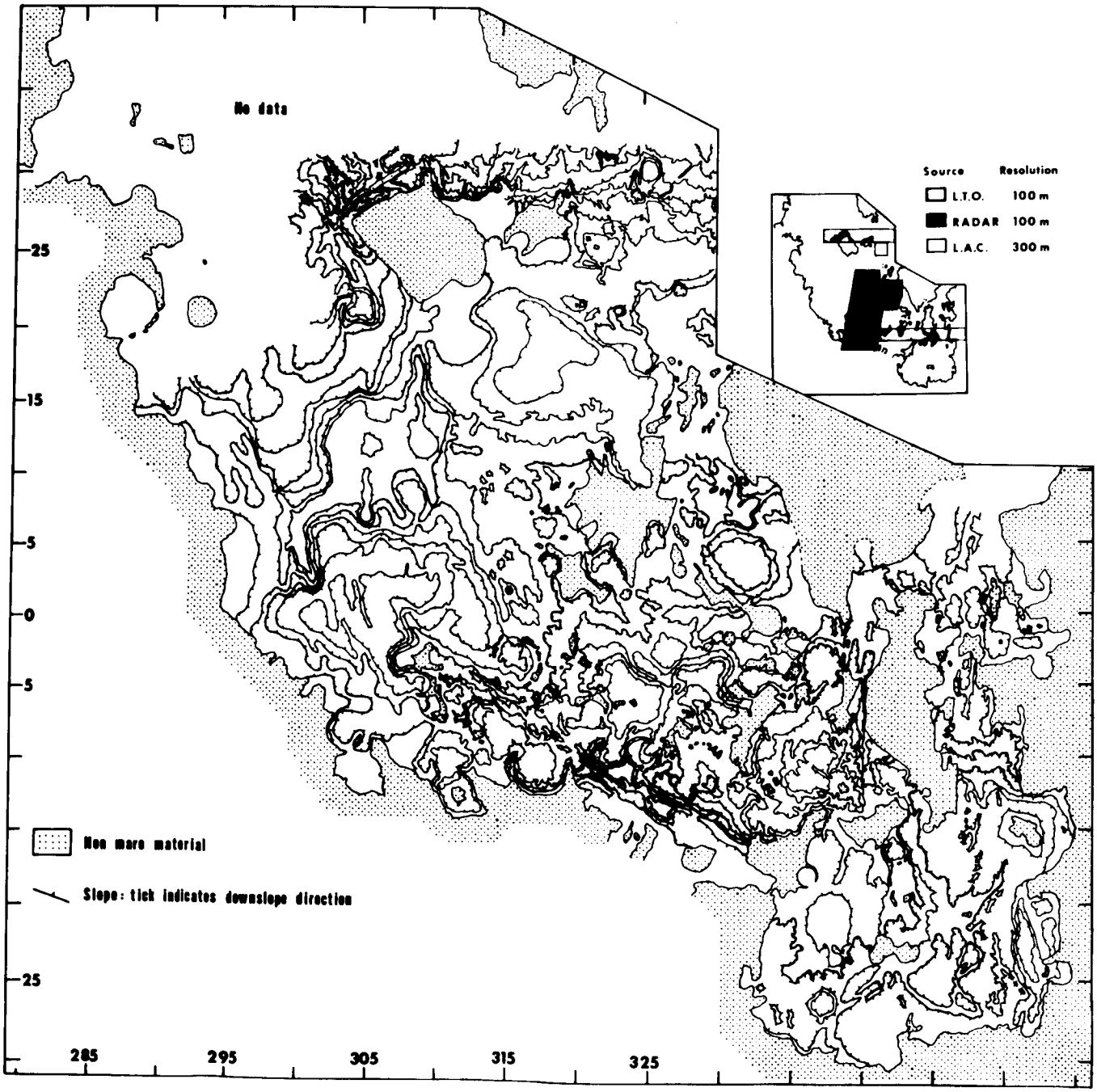

from Figure 9,which is based on the map by Bills and Ferrari(1975) and is part of a global harmonic topographic model of degree and order 10. Particularly apparent from this figure are the topographic lows associated with the Rümker Hills in northern Procellarum and the area to the southwest of the Marius Hills. A topographic high appears to correlate with the area of mare domes to the west of Copernicus. In northern Procellarum the sinuous rilles (Figure 6) are largely tangent to the topographic low,suggesting that the low results from subsidence rather than reflecting original depositional slopes. The load which induced that subsidence was probably that of the Rümker Hills themselves. Likewise, the low to the southwest of the Marius Hills does not appear to correlate with the directions of local sinuous rilles and again probably results from post-emplacement subsidence. If the basalts within both lows were originally erupted to a near hydrostatic level, subsidence of the order of 0.5 to 1.5 km is required near the center of Procellarum.

Figure 10 represents a preliminary attempt to define more accuratley the slopes within Procellarum. The map has been compiled from the Lunar Topographic Orthophotomaps which in places have a contour interval of 50 m, the profiles of the laser altimeters, and radar topographic maps with a contour interval of 100 m. Areas not covered by the previous were mapped using the LAC charts which have a contour interval of 300 m. Several difficulties were encountered in compiling the information from these various sources. For example, many of the contours on the early LAC charts do not match at the map boundaries while the 300 m contour interval on these maps appears to be closer to a 100 m interval when compared with the more accurate orthophotomaps of the same areas. In view of these difficulties, the absolute heights of the contours have been omitted from Figure 10; however, the interval between each is believed to be close to 100 m within the mare areas.

A comparison of sinuous rille directions (Figure 6) with slope

directions (Figure 10) shows that there are places where the rilles parallel the slope direction and places where they are normal to the slopes. If there had been no topographic alteration of the mare surface since the eruption of the sinuous rille basalts then it is to be expected that the rilles would be normal rather than parallel to the contours. This is in part constrained by the contour interval since the rille lavas probably flowed down very shallow slopes (e.g.,Hulme 1973). Additionally tectonic subsidence could have emphasized the local slope or inverted that slope(Scott et al,1978). It is not as likely, however, that the sinuous rilles would have originally paralleled the contour lines. Such a situation is found to the southeast of the Aristarchus Plateau and east of the Marius Hills. Both these areas have surface flows of the youngest Sharp Formation. It is therefore postulated that relative subsidence of parts of Procellarum postdated the emplacement of these youngest basalt units. In other areas with older basalts such as to the north and west of the Aristarchus Plateau, in the south Imbrium basin, and northwest of the Marius Hills, the rilles are normal to the contours. These and others appear to have originally been basinal areas which have sunk further following basalt emplacement and, as Scott et al (1978) note, not a contradiction in that the younger basalt surfaces appear more deformed than older. For example, in the crater Letronne the early Telemann Formation is preserved at a higher topographic level at the crater edge than the younger basalts at the crater center.

The Lunar Topographic Orthophotomaps also show that there are significant absolute height variations between the presently defined basinal areas. For example, relative to the 1,730,000 km datum, the floor of Letronne has a height of 5.9 km while Mare Cognitum has a height of 5.2 km. Some of the highest mare areas as shown on the LTO's are the mare ridges in the Herigonius region at 6.3 km. In contrast, the mare surface to the immediate northwest of the

Figure 11. a) Bouguer gravity data for Oceanus Procellarum using the twelth degree and order spherical harmonic and gravity models(after Ferrari and Bills, 1976). Values are in milligals. Note the generally low, uniform values for the mare area.

b) Lunar gravity at 100 km altitude derived from a mass point model(after Sjogren, 1974). Values are in milligals. Note the mascons over Imbrium and Humorum and the linear gravity high associated with Rima Sirsalis in the lower left.

c) Positive(+) and negative(-) linear gravity anomalies in Oceanus Procellarum interpreted by Scott(1974) based on data from the Apollo missions. These linear trending anomalies were believed by Scott to correspond to the trends of mare ridges.

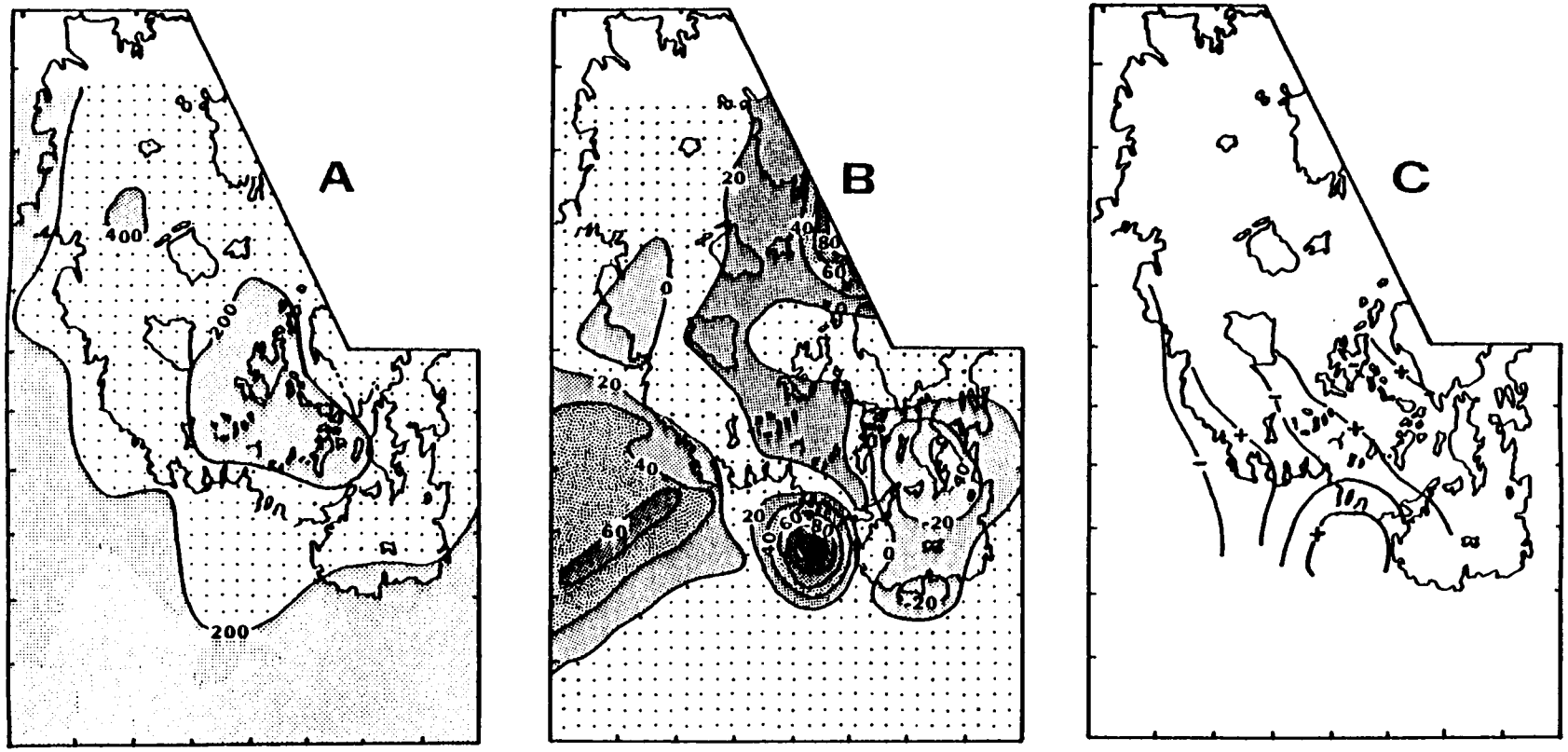

Figure 11

Aristarchus Plateau is only 5.0 km. It would appear on the basis of the present analysis that, if the mare basalts were originally erupted to a consistent hydrostatic level, that level was close to 6.0 km with respect to the 1,730,000 km datum. Values now lower than this would suggest local subsidence, while values higher would suggest uplift. As noted in the previous section on mare ridges, the majority of localized, rather than regional subsidence and uplift,appears to have predated the completion of emplacement of the Hermann Formation.

5) Gravity anomalies

Oceanus Procellarum has been described as enigmatic (Scott,1974) in terms of its gravitational properties,since there are no large anomalies nor any anomalies that appear to be associated with surface features. Figure 11a shows a portion of the Bouguer gravity map of the Moon on which the only correlation appears to be high values associated with the mare and lower values associated with the highlands. A small gravity high to the northwest of the Aristarchus Plateau lies within the youngest Sharp Formation and, from the alignment of sinuous rilles toward this location, appears to have been a topographic, perhaps basinal, low in the past.

The 100 km altitude gravity anomalies depicted in Figure 11b can be better correlated with surface features. Immediately obvious are the large positive anomalies associated with Mare Humorum and Mare Imbrium - the so-called mascons. A further gravity high to the west of Humorum represents the outer limit of the Orientale mascon anomaly,though superimposed upon this there is a linear gravity high which, like the magnetic anomaly in this same area, appears to correlate with the location of Rima Sirsalis. Within Procellarum itself there is a negative anomaly centered on the Fra Mauro area and a smaller negative anomaly in western Procellaum that could correlate

with the ejecta from the crater Cavalerius. The negative anomaly over Fra Mauro extends to Mare Nubium and lends further support to the prediction (De Hon, 1979) of a thin basaltic fill within that mare. The slight positive anomaly that extends over the rest of Procellarum almost exactly matches the distribution of the major part of the youngest Sharp Formation. A previous analysis of the Flamsteed region (Pieters et al,1980) also showed a strong correlation between positive gravity anomalies and the location of the Sharp Formation. It was suggested that the lack of strong anomalies associated with earlier units resulted from their having undergone at least partial isostatic readjustment while the Sharp Formation basalts had not.

Figure 11c shows the interpreted(Scott,1974) gravity highs and lows obtained by combining the data obtained from several spacecraft. Scott (1974) concluded that the axial trends of these anomalies correlated with the axial trends of the mare ridge systems(Figure 4), the highs corresponding to the ridges and the gravity lows to the intervening topographic lows. Scott also noted that a westward shift of 1° to 2° of the gravity axes would produce a better correlation. The correlation of positive anomalies with ridges was thought by Scott(1974) to result from dike intrusion into fractures and faults beneath the ridges.

The apparent lack of large positive gravity anomalies within Oceanus Procellarum is therefore believed to result from the partial isostatic compensation of the early basalt units. This period of compensation is reflected by the mare ridges and graben which formed largely prior to the emplacement of the youngest part of the Hermann Formation. Younger units, such as the Sharp Formation, have not been compensated and thus exhibit small positive gravity anomalies. Other gravity highs appear to be associated with the intrusion of dense basaltic material, such as along Rima Sirsalis, while gravity lows are correlated with the less dense ejecta blankets of large

craters and the fractured, older highland megaregolith.

6) Evolution of Oceanus Procellarum

The irregular shape of Procellarum indicates that the original cavity that was infilled by mare basalts was not a single impact cavity at the time of that infilling. It has been proposed (Cadogan,1974) that the western border of Procellarum corresponds to a ring fracture of an early 2,400 km diameter basin called Gargantuan, cenetered at 23N, 29W. This basin was subsequently largely destroyed by the formation of the Imbrium impact cavity within its northwestern quadrant. Prior to its destruction, Gargantuan had been flooded by KREEP basalts (Cadogan,1974). Some difficulties are encountered with this scenario; for example, it is difficult to account for the present variation in height of highland topography around what was the basin without employing post-Imbrium formation alteration of that topography. Specifically, the highlands are topographically high in the southeast quadrant of what would have been the Gargantuan basin(Fra Mauro area) but are completely buried in the central Procellarum area (except at the Aristarchus Plateau) which is equidistant from the proposed basin center. This implies to the present authors that the height alteration of highlands underlying central Procellarum postdated the formation of the Imbrium impact cavity or that the Fra Mauro material ejected to the west of Imbrium was deposited in a basinal area. The evidence for vertical tectonics at the Aristarchus Plateau and the Rima Sirsalis extension suggests that central Procellarum was tectonically lowered on major faults.

It has been argued (Whitford-Stark and Fryer,1975) that the irregular Mare Frigoris cavity may have been initiated the the movement of crustal blocks along faults initiated by the formation of the Imbrium impact cavity. It is possible that Procellarum owes its origin, in part, to a similar

mechanism. As an alternative to the Gargantuan basin hypothesis, it is suggested that the western boundary of Procellarum and the northern boundary of Frigoris are defined by ring faults produced by the Imbrium impact event and that the present height variations around Procellarum result from tectonic motion along faults radial and concentric to the Imbrium impact cavity. Recent analysis of orbital geochemical data (Spudis,1979) also indicates that KREEP volcanism was not confined to the Imbrium-Procellarum area and instead was probably moonwide. It is therefore not necessary to invoke a huge early basin to account for the KREEP around Procellarum. Moreover, the correlation of KREEP with the ejecta blankets of the craters Archimedes, Timocharis, and Lambert within Mare Imbrium (Metzger et al,1979) suggests that such material forms a shallow subsurface layer beneath the mare basalts. The presence of KREEP materials as basaltic fragments within Apollo 15 samples and their crystallization ages of 3.9 b.y. led Hawke and Head (1978) to suggest that the KREEP basalts were extruded just subsequent to the Imbrium impact, again making some of the arguments for the existence of Gargantuan superfluous. In Procellarum, KREEP basalts appear to both predate, and were erupted simultaneously with, mare basalts (Whitford-Stark and Head,1980).

In its early (during the Nectarian period) history Procellarum is envisaged as a highland area punctuated by a number of smaller impact basins such as Humorum, Cognitum, and Nubium, which had been partly flooded by KREEP and mare basalts. The formation of the Imbrium impact cavity led to gross modifications of this highland topography with central Procellarum being down-dropped with respect to other areas. It is suggested that this major tectonic activity was synchronous with, or postdated, the draping of the terrain by the Imbrium ejecta. This ejecta in turn was overlain by the subsequent ejecta deposits from the Orientale basin.

The earliest, recognizable, apparently extensive,post-Imbrium basin

formation basalts erupted in Oceanus Procellarum were the titanium-rich basalts and pyroclastic rocks of the Repsold Formation (3.75 ± 0.05 b.y.) (Whitford-Stark and Head,1980). These were overlain by the extensive, possibly VLT, basalts of the Telemann Formation(3.6 ± 0.2 b.y.) which were in part derived from the Aristarchus Plateau. It is not known whether the Aristarchus Plateau was also a source for the older Repsold Formation but the spectral characteristics of the floor of Aristarchus crater could be those of a titanium-rich basaltic impact melt excavated from beneath the Telemann Formation(Whitford-Stark and Head,1980). The Aristarchus Plateau did, however, exist as a topographic high at the time of eruption of the Telemann Formation as is evidenced by the outward-pointing directions of sinuous rilles and the fact that the Telemann Formation is not there covered by younger basalts. Although the Aristarchus Plateau appears to be fault-bounded(Whitford-Stark and Head 1977), it is not possible to distinguish whether the Plateau remained as a topographic high as the rest of central Procellarum was downdropped or the Plateau was downdropped and later re-elevated.

The surface materials at the Rümker and Marius Hills appear to belong to the Hermann Formation (3.3 ± 0.3 b.y.) though it is not possible to distinguish whether they were also eruption sites for older basalts. These areas remained as topographic highs through the eruption of the younger Sharp Formation(2.7 ± 0.7 b.y.). The major period of isostatic re-adjustment of Procellarum appears to have taken place during the eruption of the Hermann Formation intermediate basalts since the formation of graben and major period of ridge formation appears to have terminated at this time though ridges continued to form at a later date.

The final episode of basaltic magmatism within Procellarum was that of eruption of the titanium-rich Sharp Formation basalts from locations predominantly at the mare/highland boundary. Many of the craters in the adjacent

highlands, such as Zupus and Cruger, appear to have been infilled with basalts at this time. The subsequent history of Procellarum has been that of the formation of Copernican-aged impact craters and continuous very slow subsidence of the basaltic fill. Presently observed positive gravity anomalies appear to be associated with graben and the youngest, uncompensated Sharp Formation. Alinear magnetic anomaly also appears to be associated with Rima Sirsalis, while negative gravity anomalies and other magnetic anomalies appear to be related to crater ejecta blankets and the highlands(Hood et al,1979).

ACKNOWLEDGEMENTS

This work was begun several years ago under the guidance of Gilbert Fielder. Sean Solomon and Lynn Hall provoked the authors into structuring their ideas. Stan Zisk provided contoured radar maps. Sam Merrell, Nancy Christy, and Sally Bosworth are thanked for their assistance in manuscript preparation. This work was performed under NASA grant NGR-40-002-116.

REFERENCES

Anderson,K.A., R.P.Lin, R.E.McQuire, and J.E.McCoy, Linear magnetization feature associated with Rima Sirsalis. Earth Planet.Sci.Lett.34, 141-151, 1977.

Arnold,J.R., A.E.Metzger, and R.C.Reedy, Computer-generated maps of lunar composition from gamma-ray data.Proc.Lunar Sci.Conf.8th. 945-948,1977.

Baldwin,R.B., Rille pattern in the lunar crater Humboldt, J.Geophys.Res. 73, 3227-3229, 1968.

Baldwin,R.B.,A new method of determining the depth of the lava in lunar maria, Pub.Astr.Soc.Pacific, 82, 857-864, 1970.

Bills,B.G. and A.J.Ferrari, Frontispiece, Proc.Lunar Sci.Conf.6th, 1975.

Boyce,J.M. and D.A.Johnson, Ages of flow units in the far eastern maria and implications for basin-filling history.Proc.Lunar Planet.Sci.Conf.9th, 3275-3283, 1978.

Bryan,W.B., Wrinkle ridges as deformed surface crust on ponded mare lava, Proc.Lunar Sci.Conf.4th, 93-106, 1973.

Bryan,W.B.,P.A.Jezek, and M.L.Adams, Volcanic and tectonic evolution of crater Goclenius, western Mare Fecunditatis,Proc.Lunar Sci.Conf.6th,2563-2569, 1975.

Cadogan,P.H., Oldest and largest lunar basin? Nature, 250, 315-316, 1974.

Colton,G.W., K.A.Howard, and H.J.Moore, Mare ridges and arches in southern Oceanus Procellarum, Apollo 16 Preliminary Science Report,29.90-29.93,1972.

De Hon,R.A., Maximum thickness of materials in the western mare basins,Lunar and Planetary Science IX, The Lunar and Planetary Institute,Houston, Texas 229-231, 1978.

Ferrari,A.J. and B.G.Bills, Frontispiece, Proc.Lunar Sci.Conf.7th., 1976.

Fielder,G., Structure of the Moon's Surface, Pergamon Student Ed.N.Y.266p.1961.

Fielder,G., Topography and tectonics of the lunar straight wall. Planet.Space Sci. 11, 23-30, 1963.

Fielder,G. and T.Kiang, The segmental structure of wrinkle ridges and the lunar grid system, Observatory, 82, 8-9, 1962.

Golombek,M.P., Structural analysis of lunar grabens and the shallow crustal structure of the Moon. J. Geophys. Res. 84, 4657-4666, 1979.

Greeley,R., Lava tubes and channels in the lunar Marius Hills. The Moon, 3, 289-314, 1971.

Greeley,R., Modes of emplacement of basalt terrains and an analysis of mare volcanism in the Orientale basin, Proc.Lunar Sci.Conf.7th.,2747-2759,1976.

Greeley,R. and P.D.Spudis, Mare volcanism in the Herigonius region of the Moon, Proc.Lunar Planet.Sci.Conf.9th.,3333-3349, 1978.

Hackman,R.J., Geologic map and sections of the Kepler region of the Moon, U.S.Geol.Survey Misc.Inv.Map I-355, 1962.

Haines,E.L.,M.I.Etchegaray-Ramirez, and A.E.Metzger, Thorium concentrations in the lunar surface.II, Deconvolution modeling and its application to the regions of Aristarchus and Mare Smythii, Proc.Lunar Planet.Sci.Conf.9th., 2985-3013, 1978.

Hall,J.L.,J.W.Head, and S.C.Solomon, Lunar floor-fractured craters: Quantitative test of hypotheses for their origin, Reports of Planetary Geology Program,1978-1979, NASA-TM-80339, 129-131, 1979.

Hawke,B.R., and J.W.Head, Lunar KREEP volcanism: Geologic evidence for history and mode of emplacement,Proc.Lunar Planet.Sci.Conf.9th.,3285-3309, 1978.

Head,J.W., Lunar mare deposits: Areas,volumes, sequence, and implications for melting in source areas, Origins of Mare Basalts, The Lunar Science Institute, Houston,Texas 66-69, 1975.

Head,J.W. and T.B.McCord, Imbrian-age highland volcanism on the Moon: The Gruithuisen and Mairan domes, Science, 199, 1433-1436. 1978.

Head,J.W. and L.Wilson, The formation of eroded depressions around the sources

of lunar sinuous rilles: Observations, Lunar and Planetary Science XI, The Lunar and Planetary Science Institute,Houston,Texas.426-428,1980.

Hood,L.L.,P.J.Coleman,Jr., and D.E.Wilhelms, The Moon: Sources of the crustal magnetic anomalies, Science, 204, 53-57, 1979.

Hörz,F., How thick are lunar mare basalts? Proc.Lunar Planet.Sci.Conf.9th., 3311-3331, 1978.

Hulme,G., Turbulent lava flow and the formation of lunar sinuous rilles, Modern Geology, 4 107-117, 1973.

Johnson,T.V., J.A.Mosher, and D.C.Matson, Lunar spectral units: A northern hemisphere mosaic, Proc.Lunar Sci.Conf.8th.,1013-1028, 1977.

Lucchitta,B.K., Topography, structure, and mare ridges in southern Mare Imbrium and northern Oceanus Procellarum,Proc.Lunar Sci.Conf.8th.,2691-2703,1977.

Lucchitta,B.K. and J.A.Watkins, Age of graben systems on the Moon, Proc.Lunar Planet.Sci.Conf.9th., 3459-3472, 1978.

Malin,M.C., Lunar red spots: Possible pre-mare materials, Earth Planet.Sci. Lett. 21, 331-341, 1974.

Marshall,C.H., Thickness of the Procellarian System, Letronne region of the Moon, U.S.Geol.Survey Prof.Paper 424-D,208-211, 1961.

Mason,R.,J.E.Guest, and G.N.Cooke, An Imbrian pattern of graben on the Moon, Proc.Geol.Ass. 87, 161-168, 1976.

Maxwell,T.A., F.El-Baz, and S.H.Ward, Distribution, morphology,and origin of ridges and arches in Mare Serenitatis, Geol.Soc.Amer.Bull.,86,1273-1278, 1975.

McGill,G.E., Attitude of fractures bounding straight and arcuate lunar rilles, Icarus, 14, 53-58, 1971.

Metzger,A.E., E.L.Haines,M.I.Etchegaray-Ramirez, and B.R.Hawke, Thorium concentrations in the lunar surface: III.Deconvolution of the Apenninus region, Proc.Lunar Planet.Sci.Conf.10th., 1701-1718, 1979.

Muehlberger, W.R., Structural history of southeastern Mare Serenitatis and

adjacent highlands, Proc.Lunar Sci.Conf.5th.,101-110,1974.

Neukum,G. and P.Hörn, Effects of lava flows on crater populations, The Moon, 15, 205-222, 1976.

Peeples,W.J., W.R.Sill,T.W.May,S.H.Ward, R.J.Phillips, R.L.Jordan, E.A.Abbott, and T.J.Killpack, Orbital radar evidence for lunar subsurface layering in maria Serenitatis and Crisium, J.Geophys.Res.,83, 3459-3468, 1978.

Pieters,C.M., Mare basalt types on the front side of the Moon: A summary of spectral reflectance data, Proc.Lunar Planet.Sci.Conf.9th.,2825-2849,1978.

Pieters,C.M.,J.W.Head, J.B.Adams, T.B.McCord, S.H.Zisk, and J.L.Whitford-Stark, Late high titanium basalts of the western maria: Geology of the Flamsteed region of Oceanus Procellarum, J.Geophys.Res. in press, 1980.

Pohn,H.A. and R.L.Wildey, A photoelectric photographic study of the normal albedo of the Moon, U.S.Geol.Survey Prof.Paper 599-E, 1970.

Pollard,D. and G.Holzhausen, On the mechanical interaction between a fluid-filled fracture and the Earth's surface, Tectonophysics, 53, 27-57,1979.

Quaide,W.L., Rilles, ridges, and domes - clues to maria history, Icarus, 4, 374-389, 1965.

Raitala,J., Tectonic pattern of mare ridges of the Letronne - Montes Riphaeus region of the Moon, The Moon and Planets, 19, 457-477, 1978.

Schaber,G.G., Lava flows in Mare Imbrium: Geologic evaluation from Apollo orbital photography, Proc.Lunar Sci.Conf.4th., 73-92, 1973.

Schmitt,H.H., N.J.Trask, and E,M,Shoemaker, Geologic map of the Copernicus quadrangle of the Moon, U.S.Geol.Survey Misc.Inv.Map I-515, 1967.

Schultz,P.H., Floor-fractured lunar craters, The Moon, 15, 241-273, 1976.

Scott,D.H., The geologic significance of some lunar gravity anomalies, Proc. Lunar Sci.Conf.5th., 3025-3036, 1974.

Scott,D.H., J.A.Watkins, and J.M.Diaz, Regional deformation of mare surfaces, Proc.Lunar Planet.Sci.Conf.9th., 3527-3539, 1978.

Sjogren,W.L., Frontispiece, Proc.Lunar Sci.Conf.5th, 1974.

Smith,E.I., Rümker Hills: A lunar volcanic dome complex, The Moon,10, 175-181, 1974.

Solomon,S.C. and J.W.Head, Vertical movement in mare basins: Relation to mare emplacement, basin tectonics, and lunar thermal history, J.Geophys.Res., 84, 1667-1682, 1979.

Spudis,P.D., The extent and duration of lunar highland volcanism, in, Reports of Planetary Geology Program,1978-1979, NASA-TM-80339, 270-272, 1979.

Strom,R.G., Lunar mare ridges, rings and volcanic ring complexes, Modern Geology, 2, 133-158, 1971.

Tjia,H.D., Lunar wrinkle ridges indicative of strike slip faulting, Geol.Soc. Amer.Bull., 81, 3095-3099, 1970.

Whitaker,E.A., Lunar colour boundaries and their relationship to topographic features: A preliminary survey, The Moon, 4, 348-355, 1972.

Whitford-Stark,J.L., Internal origin for lunar rilled craters and the maria? Nature, 248, 573-574, 1974.

Whitford-Stark,J.L., Charting the Southern Seas: The evolution of the lunar Mare Australe, Proc.Lunar Planet.Sci.Conf.10th.,2975-2994, 1979.

Whitford-Stark,J.L. and R.J.Fryer, Origin of Mare Frigoris, Icarus,26, 231-242, 1975.

Whitford-Stark,J.L. and J.W.Head, The Procellarum volcanic complexes: Contrasting styles of volcanism, Proc.Lunar Sci.Conf.8th.,2705-2724, 1977.

Whitford-Stark,J.L. and J.W.Head, Oceanus Procellarum: Volcanic and tectonic evolution, Lunar Science VIII, The Lunar Science Institute,Houston, Texas, 1011-1013, 1977b.

Whitford-Stark,J.L. and J.W.Head, Stratigraphy of Oceanus Procellarum basalts: Sources and styles of emplacement, J.Geophys.Res., in press 1980.

Wilhelms,D.E. and J.F.McCauley, Geologic map of the nearside of the Moon, U.S.Geol.Survey Misc.Inv. Map I-703, 1971.

Wilson,G., Wrench movements in the Aristarchus region of the Moon, Proc.Geol. Ass.Lond. 81, 595-608, 1970.

Wood,C.A., Crater degradation through lunar history, Lunar and Planetary Science X, The Lunar and Planetary Institute,Houston,Texas,1373-1375,1979.

Wood,C.A. and G.Andersson, New morphometric data for fresh lunar craters, Proc.Lunar Planet.Sci.Conf.9th., 3669-3689, 1978.

Wood,C.A. and J.W.Head, Geologic setting and provenance of spectrally distinct pre-mare materials of possible volcanic origin, Origin of Mare Basalts, The Lunar Science Institute,Houston,Texas, 189-193, 1975.

Young,R.A., Lunar volcanism: Mare ridges and sinuous rilles, Apollo 16 Preliminary Science Report, 29.79-29.80, 1972.

Young,R.A., The lunar impact flux: Radiometric age correlation, and dating of specific lunar features, Proc.Lunar Sci.Conf.8th., 3457-3473,1977.

Zisk,S.H., G.H.Pettengill, and G.W.Catuna, High-resolution radar maps of the lunar surface at 3.8 cm wavelength, The Moon, 10, 17-50, 1974.

Charting the Southern Seas: The evolution of the lunar Mare Australe

James L. Whitford-Stark

Department of Geological Sciences

Brown University

Providence, R. I. 02912

Abstract

Mare Australe, an approximately 900 km diameter basin of impact origin located near the southeast limb of the moon, has been subjected to at least four major episodes of basalt eruption ranging in age from early Imbrian to Eratosthenian. These basalts cover an area of 320,000 square km, average about 750 m in thickness, and have a total volume of approximately 240,000 cubic km. The basalts were emplaced largely in flood eruptions from at least 197 vents located on post-basin impact crater floors. The youngest basalts occur in an annulus near the outer edge of the basin. The fill thickness apparently reflects a multi-ring structure for the post-impact morphology of the Australe basin despite the fact that this basinal structure was largely destroyed by smaller impacts before eruption of the present surface basalts. The thin basaltic fill was not sufficient a load to produce tectonic rilles, but mare ridges are present and exhibit a prominent north-south alignment.

THE STRATIGRAPHY OF MARE IMBRIUM

J. L. WHITFORD-STARK

and

J. W. HEAD III

Department of Geological Sciences

Brown University

Providence, R. I. 02912

ABSTRACT

Photogeologic and remote-sensing data have been combined to characterize the chemistries and eruption styles of the Mare Imbrium basalts. Ten major units, seperable in terms of age and chemistry, have been recognized. These units range in age from 3.75 $\pm$ 0.15 to 2.5 $\pm$ 0.3 b.y. and in chemistry range from V.L.T. to titanium-rich basalts. The 850,000 km^2 of surface basalts are believed to form a small portion of the total Imbrium basin fill estimated at 2.2 x 10^6 km^3; the earliest units being totally buried. KREEP and titanium-rich basalts were possibly early infil materials. The surface basalts were preferentially erupted near the periphery of Imbrium. Mare ridge production took place over a period extending from at least 3.5 $\pm$ 0.25 b.y. to less than 3.0 b.y. ago, while graben formation terminated at 3.3 $\pm$ 0.3 b.y. Faults extending from the Imbrium basin into the surrounding highlands appear to have been the eruption sites for young, titanium-enriched, circum-mare basalts.

Introduction

Mare Imbrium is an approximately circular expanse of basalt with a radius of about 540 km, located on the near side of the moon. It has been the site of one sample return (Apollo 15) and one Lunokhod mission. The ejecta from the Imbrium basin-forming event has been employed as the lower marker horizon for the Imbrian System (e.g., Wilhelms and McCauley, 1971), thus the basaltic fill of the basin is Imbrian and post-Imbrian in age.

The purpose of the present analysis was to characterize the basalt units in Imbrium from photogeologic criteria and employ remote sensing data to identify their compositions and geophysical properties.

Geophysical characteristics:

The lunar gravitational field, determined by various means (e.g., Muller and Sjogren, 1968; Ferrari and Anada, 1977; Sjogren *et al.*, 1971; Ferrari, 1977), exhibits a positive anomaly (mascon) over Mare Imbrium and negative anomalies over Sinus Iridum and the Apennine Mountains. The Bouguer anomaly over Imbrium is +350 milligals at 100 km altitude (Thurber and Solomon, 1978), comparable to anomalies over Serenitatis and Crisium. The non-uniqueness of the inversion of the gravity data has resulted in a number of contradictory models to account for the mascons (summarized by Thurber and Solomon, 1978) but the most likely model is one that assumes both mantle relief and a near-surface mass excess (mare fill). Both Bills and Ferrari (1977) and Thurber and

Solomon (1978) derived values of between 25 km and 35 km for the crustal thickness beneath Imbrium, compared with an average lunar crustal thickness of about 70 km. Ferrari et al. (1978) proposed that the Apennine region is isostatically uncompensated and is underlain by a crust 10 km thicker than the lunar crustal mean. Additionally, Thurber and Solomon(1978) argued that a minimum of 3 km basalt thickness is required in the Imbrium basin, assuming that it is the sole source of the superisostatic mass.

Maps of the lunar magnetic field show the Imbrium area to have a low, fairly uniform (range 0.4 γ) field strength (Sharp et al., 1973; Russell et al., 1974). The strength recorded at the Apollo 15 site was the lowest (3.4 ± 2.9 γ) obtained surface value (Hood et al., 1979) but it did exhibit a strong radial component (Schubert et al., 1974). The anisotropy of the Apollo 15 field has been suggested to be possibly associated with deep faults concentric to the Imbrium impact basin (Schubert et al., 1974) or to a lower electrical conductivity beneath the mare as a result of more rapid cooling of the submare mantle and the depletion of radioactive elements relative to the sub-highland mantle (Dyal and Daily, 1979).

Lunar altimetry data (Kaula et al., 1973) shows that the Imbrium surface has a mean elevation of -4.1 km relative to a 1738 km radius sphere, while harmonic analysis indicates a -2.0 to -2.5 km altitude relative to a 1737.42 km radius sphere (Bills

and Ferrari, 1975). The altimetry data suggest that the surface of Imbrium is at a higher elevation than both Serenitatis and Crisium, however, only the southern part of Imbrium was overflown by Apollo (Lucchitta and Boyce, 1979).

Radar studies of Imbrium (Schaber et al., 1970; Schaber et al., 1975) show that the average intensity of the 3.8 and 70 cm polarized and depolarized returns varies both with age and composition of the surface basalt units; increasing with increasing age and decreasing with increased iron and/or titanium content.

Orbital geochemistry:

Gamma-ray data for the Apollo 15 groundtrack over southern Imbrium was deconvolved (Metzger et al., 1979a) to produce thorium values of 3.4 to 3.6 ppm for the southeast Imbrium surface, 1.7 ppm for Palus Putredinis, and + 9.0 ppm for the ejecta blankets of Timocharis, Archimedes, Autolycus and Lambert. The high Th values (relative to mare basalts) for the Imbrium surface were attributed to a 20-24% admixture of medium K Fra Mauro basalt to the regolith. The gamma-ray data also indicate a general increase of TiO_2 wt% along the groundtrack from east to west with values of 0.8 to 1.7% in the east to greater than 4.2% in the west (Metzger et al., 1979b). This is matched by a similar Fe wt% variation for the same area of from 10 to 14% and a potassium variation of 1500 to 2300 ppm (Metzger et al., 1979b; Bielefeld et al., 1976).

X-ray fluorescence data is only available for the extreme

southeast corner of Imbrium but appears to show that at this location the mare surface has a very low Al/Si ratio (< 0.29), a low Mg/Si intensity ratio of 0.64 to 0.69, and a low Mg/Al intensity ratio of 1.07 to 1.16 (Andre et al., 1977). These compare with Mg/Si values of + 1.0 and Mg/Al values of + 1.3 for Serenitatis and Tranquillitatis (Bielefeld, 1977). Combined with the gamma-ray data, the evidence from the XRF data indicates that the Imbrium flows are Fe-rich, Mg-poor, medium to high titanium basalts. The present authors will show that these compositions do not represent the entirety of the Imbrium surface basalts.

Data from the α -particle experiment show an increased decay rate for ^{210}Po at the edge of Imbrium ($4.6 \pm 3.1 \times 10^{-3}$ cts/sec) relative to the center ($2.3 \pm 4.2 \times 10^{-3}$ cts/sec) (Bjorkholm et al., 1973). These values are about half those of Mare Fecunditatis but equivalent to those of Serenitatis and Procellarum.

The low surface resolution of the orbital geochemical experiments and the incomplete coverage of Imbrium preclude detailed comparison of the derived data with individual surface units. At these low resolutions, however, it is apparent that there are geochemical differences in the surface materials of the mascon maria and non-mascon maria.

Basalt stratigraphy:

The U. S. Geological Survey quadrangle maps of the Im-

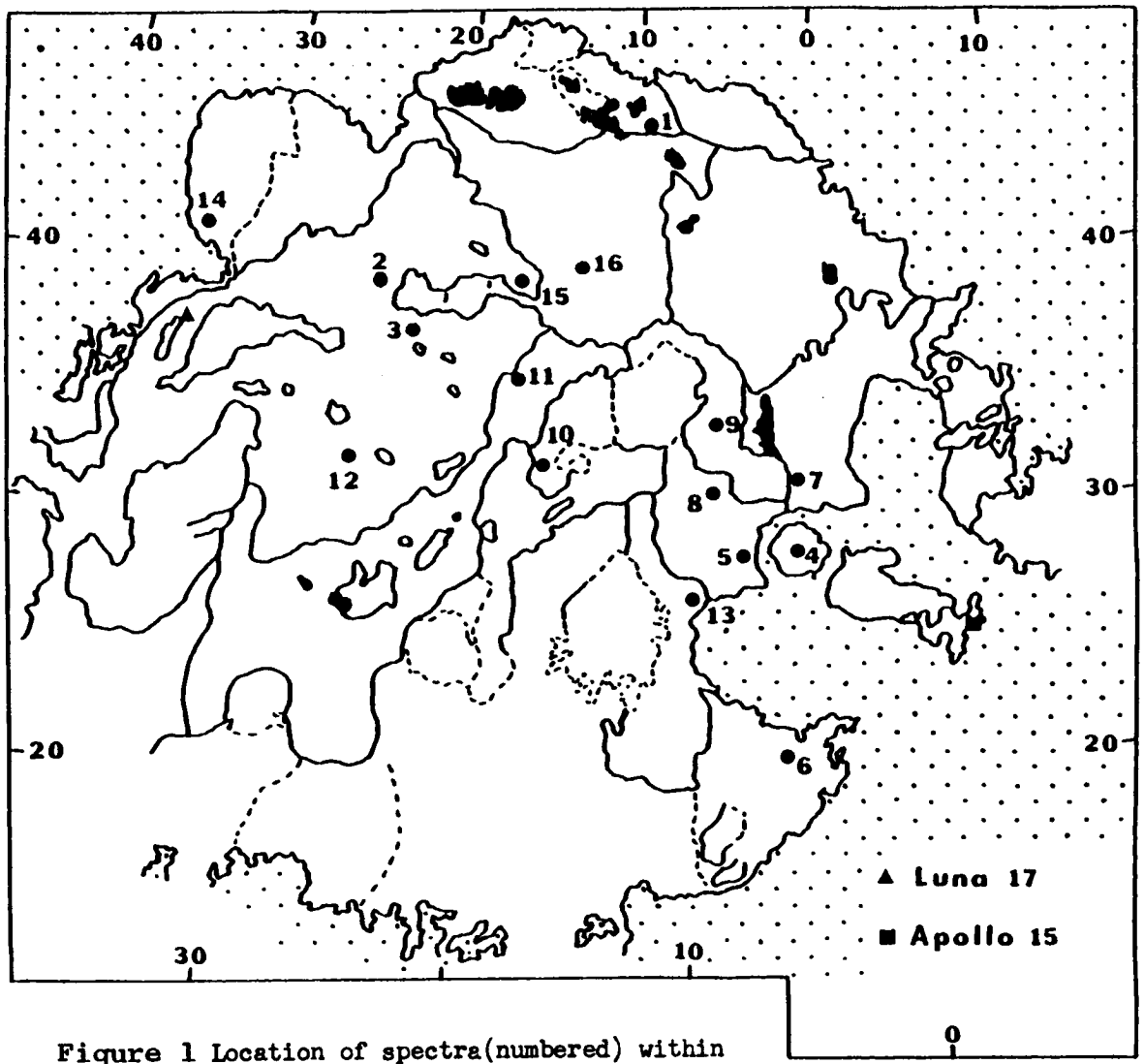

Figure 1 Location of spectra(numbered) within Mare Imbrium. Co-ordinates and basalt types are given in Table 1. Also shown are two Imbrium landing site locations, outlines of the various basalt units(see fig.2) and the surrounding highlands(stipled).

Number	Spectra locations	Spectrum type
1	47 10N 9 50W	LIG
2	41 05N 25 00W	hDSA
3	38 45N 22 40W	hDSA
4	29 55N 4 00W	LIG
5	29 45N 6 40W	LIG
6	21 30N 5 05W	mIG
7	32 30N 4 30W	LIG
8	32 10N 8 20W	LBS
9	35 25N 7 30W	hDSA
10	34 00N 16 00W	LBS
11	37 00N 17 45W	hDSA
12	34 00N 25 00W	hDSA
13	27 50N 9 45W	mIG
14	42.3N 34.3W	LBG
15	41.1N 17.2W	hDSA
16	41.7N 14.5W	LBS

Table 1 Spectra locations and types as illustrated in figure 1a. The spectra type is based on Pieters(1978) while individual spectra are described by Pieters and McCord(1976).

brium area have been combined into the geological map of the near side of the moon by Wilhelms and McCauley (1971) while Soviet maps have been published by Markov et al. (1974). The stratigraphic relationships of the youngest basalts in Imbrium have been mapped by Fielder and Fielder (1971), Schaber (1973), Todhunter (1975), and Saito (1977) while Boyce and Dial (1975) determined the relative ages of the surface units.

The present analysis combines data from spectral reflectance measurements, spectral vidicon imagery, color photography, albedo measurements, crater statistics, lunar sample analyses, and photogeologic analysis of Lunar Orbiter, Apollo, and earth-based photographs to determine the stratigraphic evolution of Mare Imbrium. Spectral reflectance measurements employed were those of Charette et al. (1974), Pieters and McCord (1976), and Pieters (1978); the surface locations of the areas investigated are shown in figure 1 and tabulated in table 1. Multispectral vidicon imagery employed was that of McCord et al. (1976, 1979) and Johnson et al. (1977a, b). Color photography was from Whitaker (1972), while albedo values were derived from Pohn and Wildey (1970).

The basalt units mapped within Imbrium are illustrated in figure 2; Unit 1 representing the oldest and Unit 10 the youngest flows. A further unit designated as obscured is masked by ejecta from the craters Copernicus and Eratosthenes. The surface areas

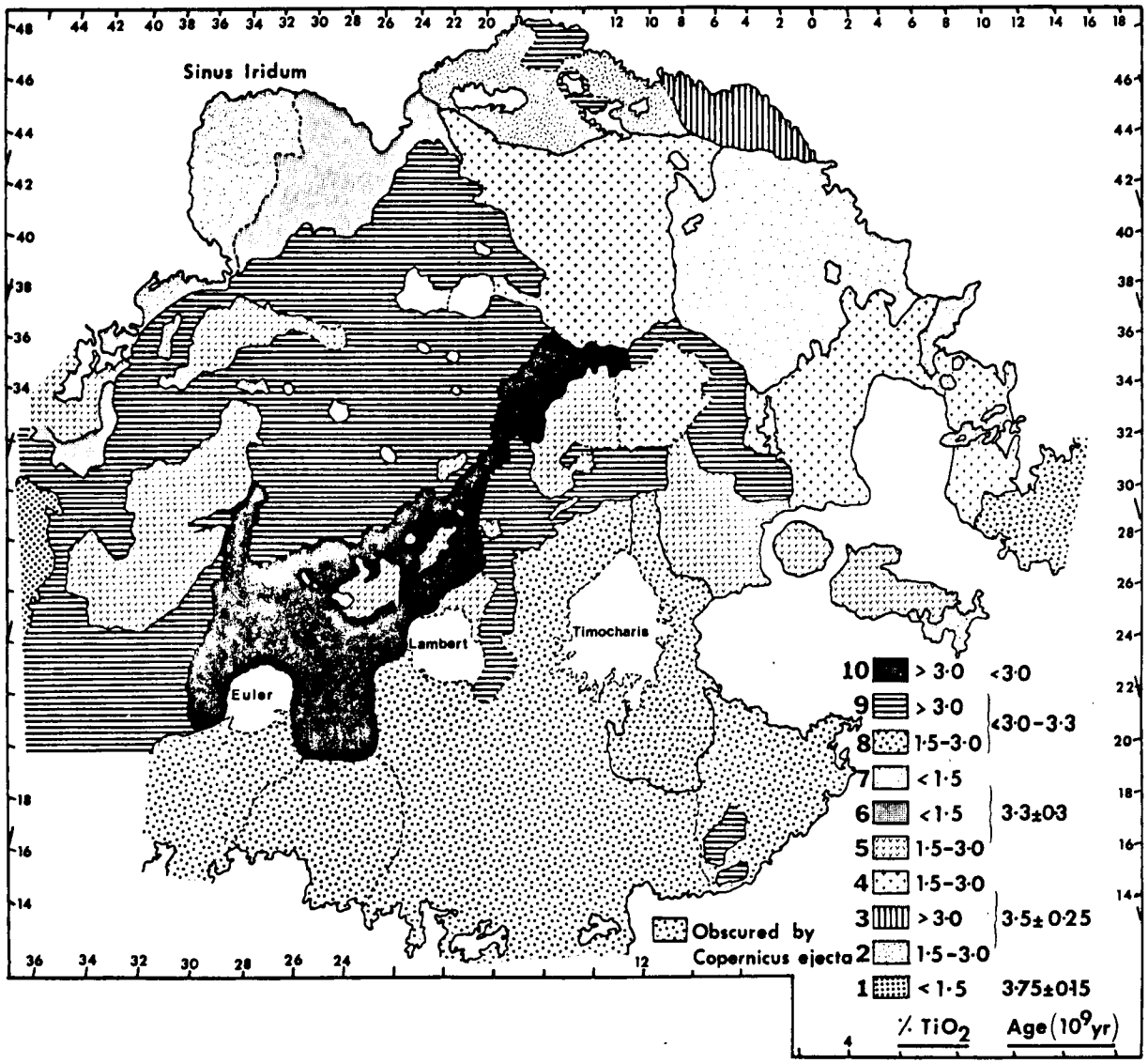

Figure 2 Subdivisions of the basalt units in Mare Imbrium based on photogeologic and remote-sensing data. The units are ranked in terms of relative age from 1 to 10; 10 being the youngest and 1 the oldest. Also indicated in the key are the approximate TiO_2 concentrations based on Johnson et al (1977).

Unit	Area ($\times 10^5$ km^2)	% total area
Obscure	1.98	23.35
10	0.77	9.08
9	2.24	26.42
8	0.38	4.48
7	0.55	6.49
6	0.16	1.89
5	0.83	9.79
4	1.20	14.15
3	0.07	0.83
2	0.21	2.48
1	0.09	1.06
Total	8.48	100.00

Table 2 Areas of the basalt units within Mare Imbrium defined in this paper.

occupied by each unit are outlined in table 2.

Unit 1:

This unit occurs to the extreme west of the area mapped and is part of the Oceanus Procellarum infill. Unit 1 has been described in detail by Whitford-Stark and Head (1980) and, although apparently the oldest unit exposed at the surface near Imbrium, it is not the oldest surface unit in Procellarum. Similarly it does not appear to be as old as mare basalts returned from some landing sites (e.g., Turner, 1977; Nyquist, 1977). Although the evidence is rather circumstantial, it is proposed that the earliest mare basalt units erupted in Imbrium are nowhere exposed at the surface, but rather have been covered by younger basalts. This conclusion negates attempts to define a period between basin formation and lava filling on the basis of crater counts (e.g., Hartmann, 1967) on surface basalts.

Unit 2:

Although spectral reflectance data (Pieters and McCord, 1976; Pieters, 1978) indicate Unit 2 to be similar to Unit 4 located immediately to the south, relative dating (Boyce and Dial, 1975) suggests Unit 2 to be slightly older than Unit 4 while vidicon imagery shows Unit 2 to have, on average, a higher TiO_2 content (McCord et al., 1976; Johnson et al., 1977a). According to Pieters (1978), Unit 2 has a TiO_2 content of less than 1.5 wt% while according to Johnson et al. (1977b) it has a TiO_2 con-

Figure 3. Lunar Orbiter photograph of northeast Imbrium showing the sinuous rilles developed within Unit 3. The abrupt termination to the south(arrow) results from flooding by a younger Unit 7 flow. Scale bar is 20 km.

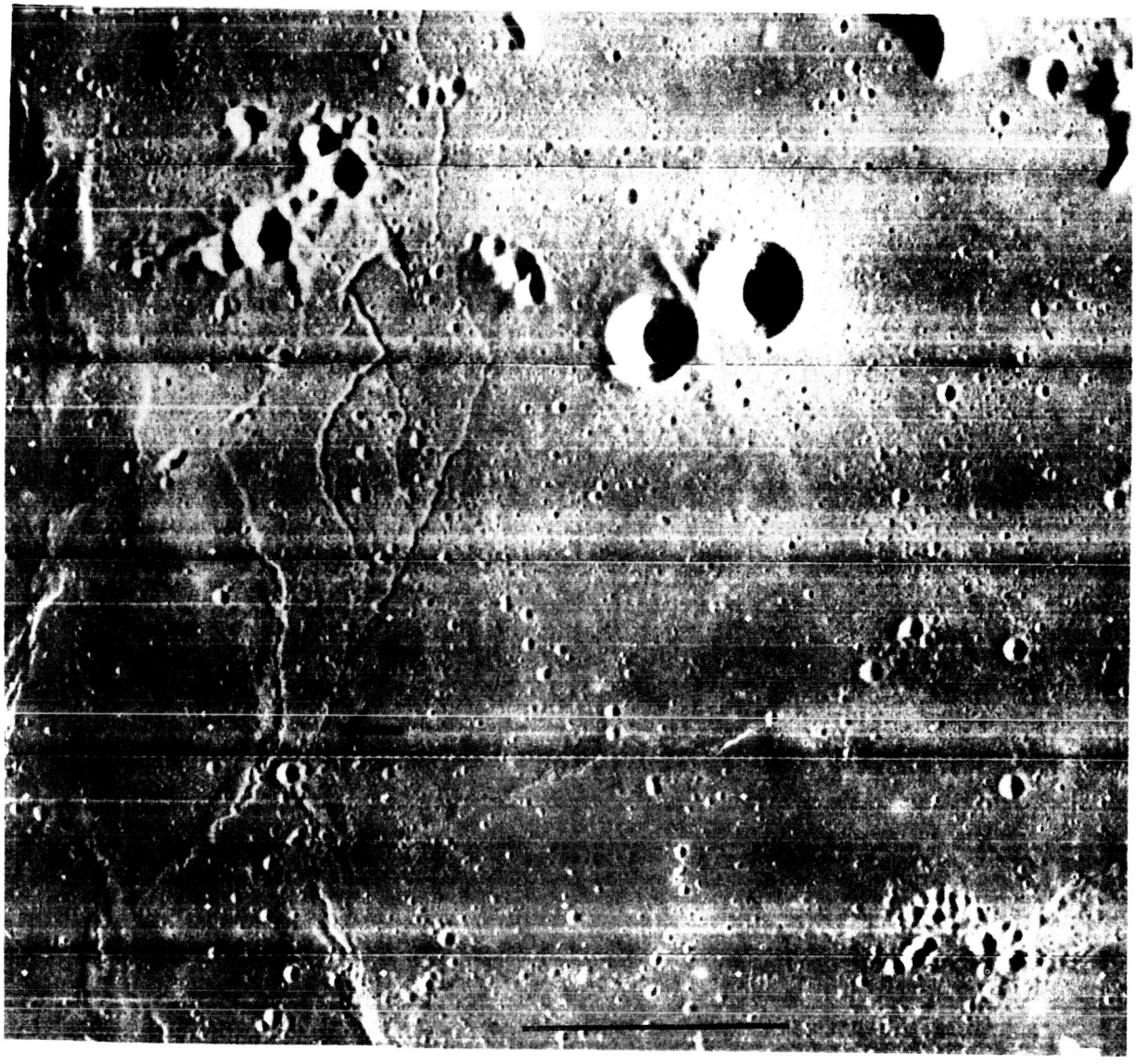

tent generally less than 2.0 wt%, but locally exhibits values of 2.0 to 3.0 wt%. Unit 2 is defined (see Head et al., 1978) by a high albedo (0.09 to 0.102) (Pohn and Wildey, 1970), a reddish color on infrared-ultra-violet composite photographs (Whitaker, 1972), a low u.v./visible ratio (less than 0.99) (Pieters, 1978), and a high crater density. D_L values (see Soderblom and Lebofsky, 1972 for discussion) are greater than 250, a value which suggests an age of 3.5 ± 0.25 b.y. (Boyce, 1976). A spectrum obtained within Unit 2 (figure 1, table 1) exhibits a strong 1 μm band (Pieters, 1978) indicative of a high Fe^{2+} content in the glass, pyroxene, or olivine (Adams and Ralph, 1977). The available data thus characterizes Unit 2 as being a relatively old, low-titanium, possibly iron-rich basalt.

Unit 3:

Located solely in northeast Imbrium, Unit 3 has been previously described (Pieters, 1978) as a low titanium basalt. Vidicon imagery and u.v.-i.r. photography, however, show the unit to be a medium to high (2.0 to 6.0 wt% TiO_2; Johnson et al., 1977b) with spectral characteristics similar to Unit 9. High D_L values (+250) (Boyce and Dial, 1975) and the abrupt termination of a rille within Unit 3 at the boundary with Unit 7 (figure 3) demonstrate Unit 3 to be older than Unit 9. Unit 3 also differs from Unit 9 in having a high albedo (0.09 to 0.108; Pohn and Wildey, 1970). It was not possible to separate units 2 and 3

on the basis of relative age (3.5 ± 0.25 b.y.) so they could represent synchronous eruptions of basalts with differing compositions.

Unit 4:

Two different spectra have been obtained for Unit 4 (figure 1, table 1) which may imply that it is laterally inhomogeneous. Spectrum 7 is, however, from an area partly obscured by ejecta from the nearby crater Aristillus. It is therefore believed that spectrum 16 is more representative of the Unit. Unit 4 occurs in three areas of northeast Imbrium which are separated by flows of younger basalts. It is quite possible that the three areas were, therefore, originally continuous. Spectral reflectance and vidicon imagery denote Unit 4 to be a low titanium basalt with less than 1.5 wt% TiO_2 (Pieters, 1978) to less than 2.0 wt% TiO_2 (Johnson et al., 1977b). The unit has a high albedo (0.09 to 0.102; Pohn and Wildey, 1970) while combined u.v.-i.r. photographs show it to have a reddish color (Whitaker, 1972). A strong 1 μm band in the spectra implies a high Fe^{2+} glass, olivine, or pyroxene concentration (Pieters, 1978) while D_L values in the range 250-320 (Boyce and Dial, 1975) again indicate an age in the 3.5 ± 0.25 b.y. range, but at the younger end of the range than Units 2 and 3. The available evidence thus suggests that Unit 4 is a low titanium possibly high FeO basalt with a relatively old age.

Figure 4. Lunar Orbiter photograph of sinuous rilles within Unit 5 in western Imbrium. Note their elongate source craters and abrupt termination to the east(right) where they have been flooded by younger Unit 9 and 10 flows. Flow margins are arrowed. Scale bar is approximately 20 km.

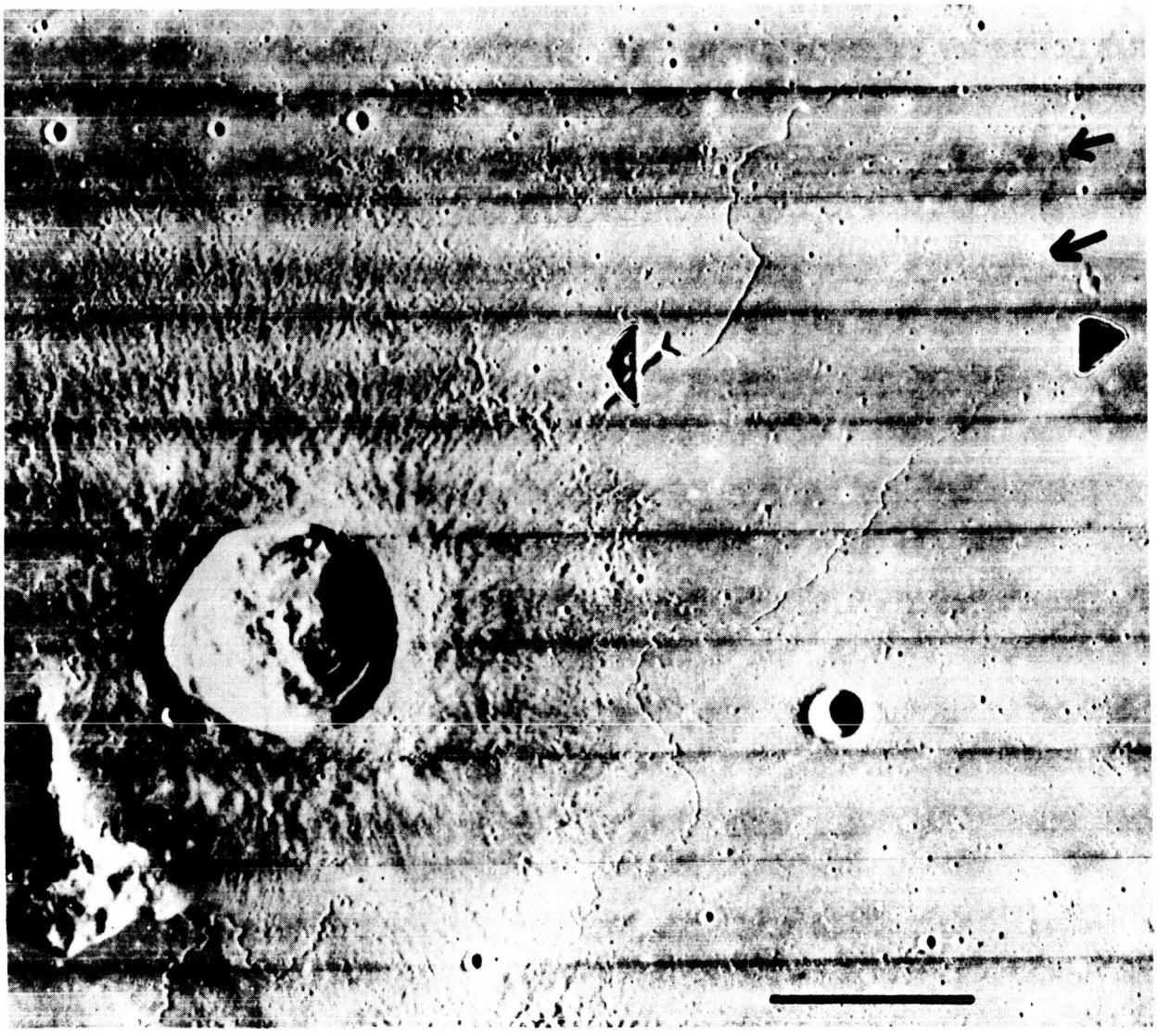

Unit 5:

Unit 5 is present as a number of spatially separate areas across a central band of Imbrium (figure 2). The separate occurrences appear to be of approximately the same age (3.3 ± 0.3 b.y.; after Boyce and Dial, 1975) and were possibly originally continuous since intervening areas are occupied by younger units. The greater original extent of Unit 5 is documented by the abrupt termination of sinuous rilles at the boundaries with younger units (figure 4). The small size of many of the occurrences of Unit 5, however, makes correlation a formidable task. Indeed, a spectrum taken on the floor of Archimedes (27N, 4W) and immediately west of Archimedes differ from those taken near central Imbrium (Pieters and McCord, 1976). Those in the east appear to have a slightly higher TiO_2 content (1.5 to 3.0 wt%) than those in the west (less than 2.0 wt%) (Johnson et al., 1977b). Additionally, those in the east have a weaker 1 μm absorption band (Pieters, 1978). The albedos of the separate areas vary from 0.09 to 0.106 (Pohn and Wildey, 1970). Part of Unit 5 in western Imbrium has been described in detail as part of the Procellarum stratigraphic column (Whitford-Stark and Head, 1980).

Luna 17 apparently landed somewhere near the boundary between Units 5 and 9 in western Imbrium at $38^{\circ}17'N$, $35^{\circ}W$ (Alekseyev et al., 1973). The surface traversed by Lunokhod 1 was found to be relatively flat with 1° to 2° slopes, broken by mare

	Luna 17	Surveyor 5	Surveyor 6
Si	20	17.1 ± 1.2	18.5 ± 1.4
Fe	12	3.8 ± 0.4	3.9 ± 0.6
Ca	8	5.5 ± 0.7	5.2 ± 0.9
Al	7	6.4 ± 0.4	6.5 ± 0.4
Mg	7	2.8 ± 1.5	3.7 ± 1.6
Ti	4	2.0 ± 0.5	1.0 ± 0.8
K	1	n.d.	n.d.
Na	-	0.47 ± 0.15	0.6 ± 0.24

Table 3 Comparison of the Luna 17 surface preliminary geochemical analysis (from Kocharov et al, 1971) and the surface analyses at the Surveyor 5 and 6 sites (Turkevich ,1971) in Mare Tranquillitatis and Sinus Medii respectively. All three are mare sites. Values are in atom percent.

ridges 200 to 400 m in height (Florenskii et al., 1971). A preliminary analysis of the basalts at the landing site presented by Kocharov et al. (1971) is given in table 3 and indicates, along with spectral evidence, that Unit 5 is a low titanium, FeO-enriched basalt.

Unit 6:

Units 6 and 7 were difficult to separate in terms of vidicon characteristics and geological boundaries but D_L values (Boyce and Dial, 1975) denote an area occupied by Unit 6 to be older; D_L values of 250 to 320 as against less than 250. Pieters (1978) has also typified Unit 6 as having a less strong 1 μm band than Unit 7. Unit 6 has a high albedo (0.09-0.106; Pohn and Wildey, 1970), a red color (Whitaker, 1972), and a low or very low titanium content (less than 1.5 wt%; Johnson et al., 1977b).

Unit 7:

Like Unit 6, Unit 7 appear to be a low to very low titanium basalt (Johnson et al., 1977a). It is possible to define Unit 7 extremely well since it occurs at the Apollo 15 landing site in addition to occupying large areas of northeast Imbrium and Sinus Iridum.

Although spectra indicate the Apollo 15 area to have a very low titanium content, compositional data on returned samples (table 4) exhibit TiO_2 contents in excess of 1.5 wt% TiO_2.

	Apollo 15 Olivine basalt	Apollo 15 Pigeonite basalt	Apollo 15 Green glass
SiO_2	44.08	47.98	44.14
TiO_2	2.28	1.80	0.37
Al_2O_3	8.38	9.44	7.81
FeO	22.74	20.23	21.05
MnO	0.32	0.30	-
MgO	11.30	8.74	16.72
CaO	9.27	10.43	8.41
Na_2O	0.27	0.32	0.13
K_2O	0.04	0.06	0.03
Cr_2O_3	0.85	0.48	0.33
Total	99.53	99.78	98.99

Table 4 Analyses of basalts and green glass from the Apollo 15 site in Mare Imbrium (from Papike and Vaniman, 1978). Values are in wt%.

These values are higher than those which define the Very Low Titanium basalts (less than 1.0 wt% TiO_2; Papike and Vaniman, 1978) and may indicate incorrect calibration of the vidicon data or, more possible, dilution of the regolith TiO_2 content by incorporated low TiO_2 green glass (table 4). Statistical analysis of geochemical analyses by Pratt et al. (1977) showed that all barring two basalt samples (15385 and 15388) fell into but two compositionally distinct groups designated olivine-normative and quartz-normative basalts. In a review of Rb-Sr chronology, Nyquist (1977) was unable to separate the two groups in terms of age; the QNB's having an age of 3.35 ± 0.09 b.y. and the ONB's an age of 3.36 ± 0.04 b.y. He did note, however, that Papanastassiou and Wasserburg (1973) suggest the possibility that samples 15085 (ONB) and 15682 (QNB) might be slightly older than the other samples.

In spite of the arguments by Ma et al. (1978) that the green glass and the Apollo 15 basalts are geochemically unrelated, they do appear to be of similar age and were both derived by volcanic processes (Delano, 1979). Geochemical analyses of the green glasses led Delano (1979) to propose that they were derived from five separate magma sources. Furthermore, layering within the walls of Hadley Rille (Howard et al., 1972) suggests the presence of several flow units beneath the Apollo 15 site. Other pyroclastic deposits with different spectral properties to

the green glass have also been identified in the Apollo 15 area (Hawke et al., 1979).

Areas of Unit 7 in Sinus Iridum and northeast Imbrium could not have been derived from the same vents as that (those) at the Apollo 15 site since they are separated by regions of older basalt. This serves to emphasize that the basalts of Imbrium, like those of Australe (Whitford-Stark, 1979), were derived from a multiplicity of sources. Additionally, spectral differences between the Iridum and Hadley areas (Pieters and McCord, 1976) suggest that, if the apparent low TiO_2 of the Hadley regolith does indeed result from an admixture of green glass, the Iridum surface may be composed of true VLT basalts.

Unit 8:

Located to the east of the crater Timocharis and on the boundary between Imbrium and Serenitatis (figure 2), Unit 8 appears to be composed of low to intermediate TiO_2 basalt with a 1.5 to 3.0 wt% TiO_2 content (Johnson et al., 1977a, b; Pieters and McCord, 1976). The unit has a high albedo of 0.09 to 0.108 (Pohn and Wildey, 1970) and a reddish color (Whitaker, 1972). Unit 8 predates the Copernican aged crater Timocharis since secondary craters from the latter cover it. D_L values (Boyce and Dial, 1975) indicate an age of less than 3.0 to 3.3 b.y. for the unit.

Unit 9:

This is the most areally extensive (table 2) of the units herein defined in Imbrium. That part of the unit to the west side of Imbrium has been described in detail by Whitford-stark and Head (1980) as part of the Procellarum stratigraphic column. Unit 9 comprises medium to high titanium basalts with TiO_2 contents in excess of 3.0 wt% (Johnson et al., 1977a, b; Pieters, 1978). The basalts have a bluish color (Whitaker, 1972), a very low albedo (0.079 to 0.09; Pohn and Wildey, 1970), and weak 3.8 and 70 cm radar returns (Schaber et al., 1975). Pieters (1978) concluded, on the basis of an average 2 μm band absorption, that the regolith of Unit 9 was either enriched in glass relative to the Apollo 11 regolith, or it contained a FeO-rich glass.

Although Unit 9 forms a fairly continuous blanket over western Imbrium, sinuous rilles within it indicate it to have been derived from several sources. This has probably resulted in the lateral inhomogeneity of TiO_2 content as determined by spectral reflectance (Pieters and McCord, 1976). D_L values of less than 250 (Boyce and Dial, 1975) denote a relatively young age for Unit 9. Schaber (1973) suggests an age of 3.0 ± 0.4 b.y. for parts of Unit 9 which correspond to his Phase 1.

Unit 10:

The youngest basalts within Imbrium have been combined

(figure 2) into a single unit although many separate flows (Todhunter, 1975) appear to define two main eruptive phases (Schaber, 1973; Todhunter, 1975). Spectrally, Unit 10 is similar to Unit 9 (Pieters, 1978) and is a medium to high titanium basalt with a low albedo (0.079 to 0.096; Pohn and Wildey, 1970), a bluish color (Whitaker, 1972), and has low 3.8 and 70 cm radar returns (Schaber et al., 1975). D_L values for Unit 10 are generally less than 190 (Boyce and Dial, 1975) implying ages of less than 3.0 b.y. Schaber (1973) derived ages of 2.7 ± 0.3 b.y. and 2.5 ± 0.3 b.y. for his two phases which comprise Unit 10, but Todhunter (1975) obtained older ages for the same unit by the D_L method; her age for the youngest unit being 3.2 ± 0.5 b.y.

Obscured area

A large part of southern Imbrium (figure 2) is covered by ejecta from the craters Copernicus and Eratosthenes. Although Pieters (1978) mapped this area as being an intermediate basalt regolith, the high resolution vidicon images (McCord et al., 1976) show many of the contrasting spectral properties to be related to Copernican rays. Similarly D_L values (Boyce and Dial, 1975) indicate a variety of ages for this area, as do geological relationships such as the flooding of Euler ejecta and numerous sinuous rilles. Since geochemical and flow boundaries cannot be uniquely defined at present, the entire area has been left as a

single undifferentiated unit.

Flow thicknesses, depth of flooding, and crater degradation:

Several different techniques have been employed to determine flow thickness and flooding depths of the lunar maria (e.g., Marshall, 1961; Baldwin, 1970; Neukum and Horn, 1976; Hörz, 1978; DeHon, 1979; Head, 1979; Whitford-Stark, 1979), most of which require a detailed knowledge of local topographic variation. Within Imbrium such information is available for areas covered by Lunar Topographic Orthophotomaps but large areas of Imbrium are not so covered. The present authors have therefore devised a technique for determining basalt thicknesses for application to areas where there is no topographic information.

It was first assumed that the measured craters had rim heights equivalent to similarly-sized fresh lunar craters which follow the relationship:-

1) $$R = 0.036\ D^{1.014} \quad \text{(where } D < 17 \text{ km)}$$

and

2) $$R = 0.236\ D^{0.399} \quad \text{(where } D > 17 \text{ km)}$$

where R is the rim height and D is the rim crest diameter in kilometers (Pike, 1977). Further expressions have been calcula-

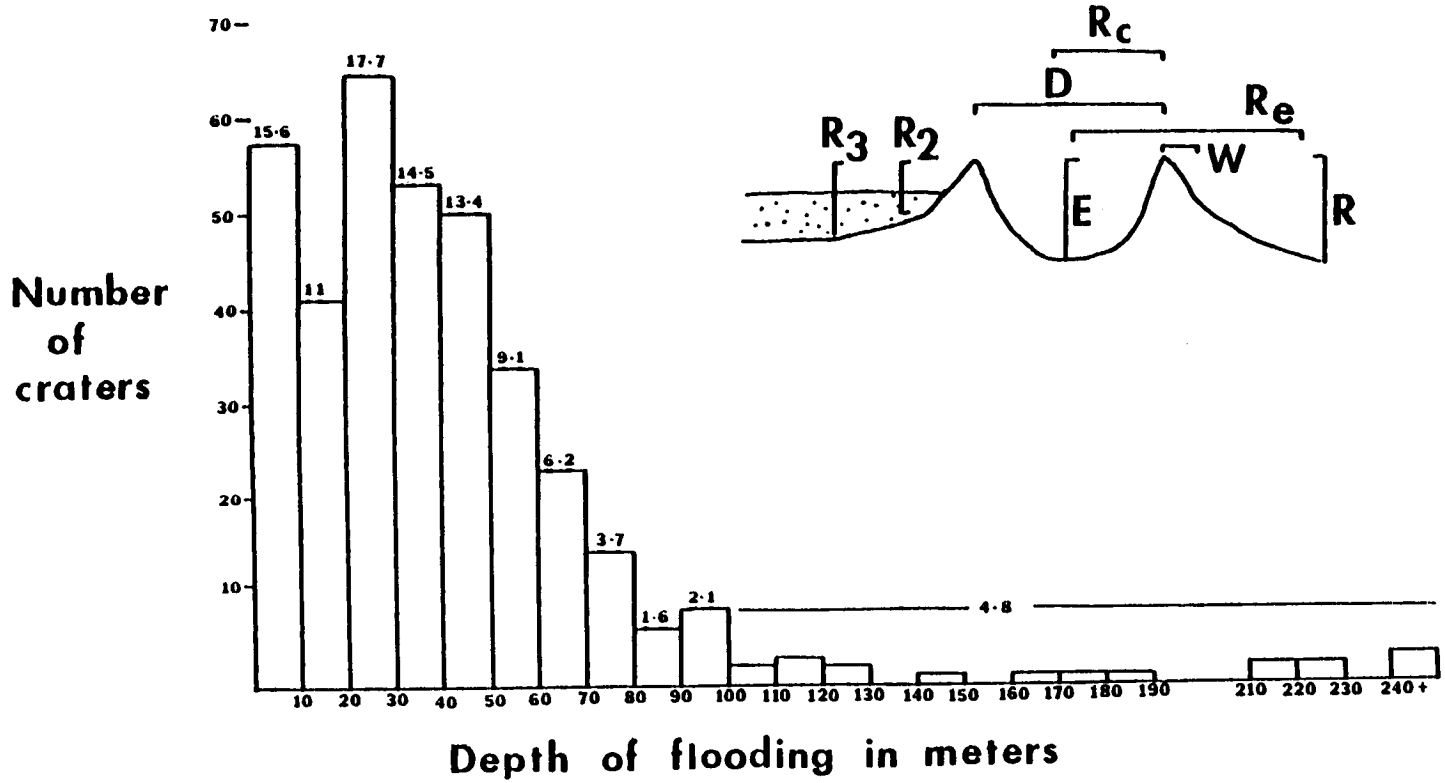

Figure 5 Histogram showing the depth of flooding of 372 craters within Mare Imbrium. The number above the blocks indicate the percentage of the total population which fall within the specified depth of flooding range. The inset diagram indicates parameters employed in equations 1 through 9 of the text.

ted defining the rim width and ejecta blanket radius as functions of crater diameter and radius as:-

3) $$W = 0.257\ D^{1.011} \qquad (\text{where } D < 17 \text{ km})$$

and

4) $$W = 0.467\ D^{0.836} \qquad (\text{where } D > 17 \text{ km})$$

and

5) $$Re = 2.248\ Rc^{1.006}$$

where W is the flank width, D is the crater diameter (Pike, 1977), Rc is the crater radius and Re is the radius of continuous ejecta measured from the crater center (Moore et al., 1974) (see figure 5). By substitution of equations 3, 4, and 5 into equations 1 and 2 it is possible to define the rim height as a function of ejecta width or flank width, whichever is applicable. For example:-

6) $$R_2 = 0.036 \left(\exp \left(\frac{\log \frac{W}{0.257}}{1.011} \right) \right)^{1.014} \qquad (\text{where } D < 17\text{km})$$

and

$$7) \quad R_2 = 0.236 \left(\exp \left(\frac{\log \left(\frac{W}{0.467} \right)}{0.836} \right) \right)^{0.399} \quad \text{(where } D > 17 \text{ km)}$$

which define the rim height (R_2) as a function of flank width (W), and

$$8) \quad R_3 = 0.036 \left(2 \exp \left(\frac{\log \left(\frac{Re}{2.348} \right)}{1.006} \right) \right)^{1.014} \quad \text{(where } D < 17 \text{ km)}$$

and

$$9) \quad R_3 = 0.236 \left(2 \exp \left(\frac{\log \left(\frac{Re}{2.348} \right)}{1.006} \right) \right)^{0.399} \quad \text{(where } D > 17 \text{ km)}$$

which define the rim height (R_3) as a function of ejecta radius (Re). If a crater has been flooded then R_2 or R_3 should be less than R. The same applies if the crater is old since the ejecta blanket will become less readily definable on photographs. The difference between derived values of R and R_2 or R_3 is thus a function of the depth of flooding of the crater and/or its age. Inaccuracies arise from the actual measurements on the craters and the scatter in expressions 1 through 5 (defined in Pike, 1977). In essence, the technique artificially gives the measured crater the rim height of a crater of lesser diameter. The authors believe this to be viable within the accuracy limits of equations 1, 3, and 5 since, for small craters, these relation-

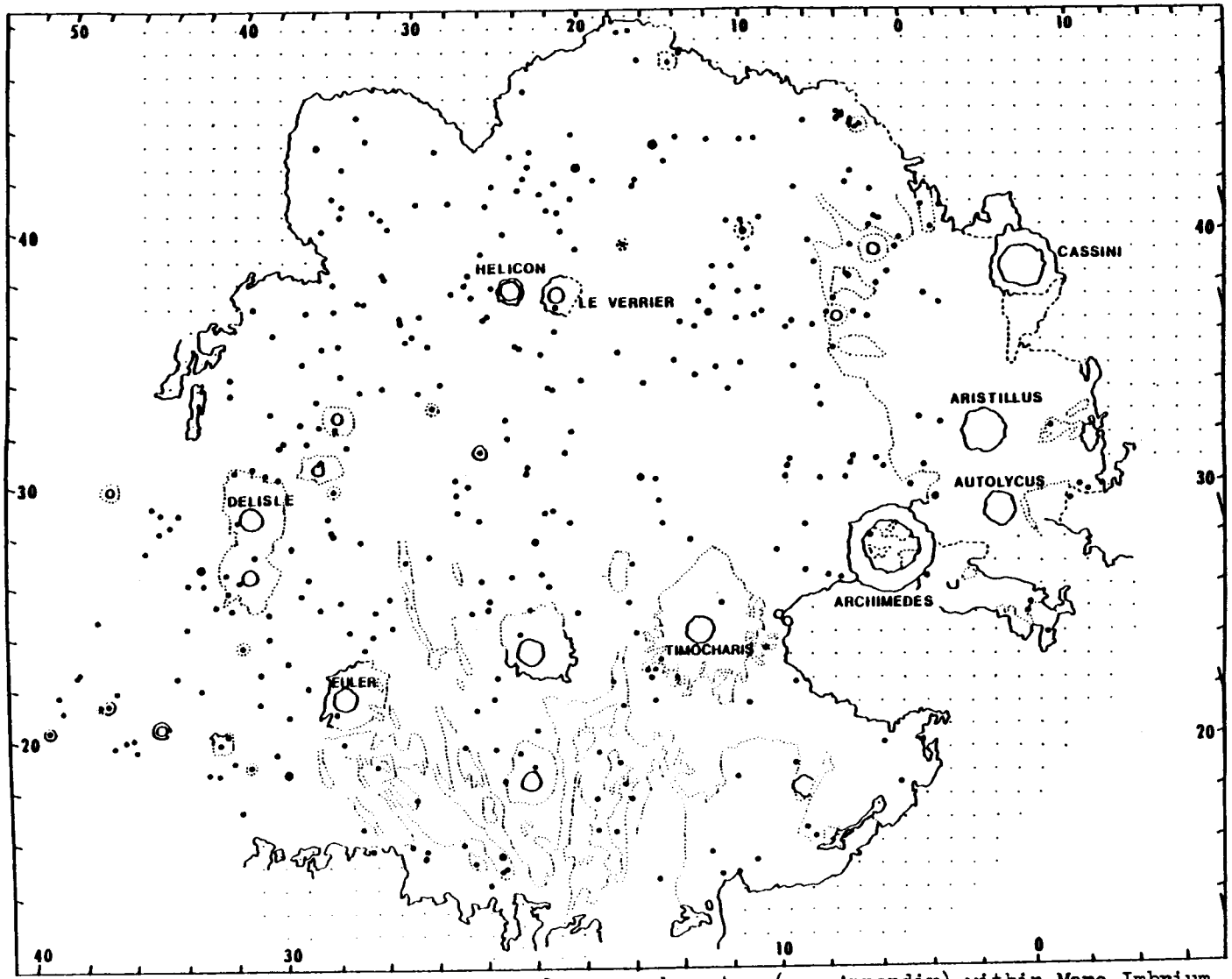

Figure 6 Locations of measured craters(see Appendix) within Mare Imbrium.

ships are reasonably linear. It works less well for larger craters employing equations 2 and 4 since they are non-linear. Thus the computational error estimate increases for larger craters while the measurement error increases for smaller craters. For example, based solely on the quoted (Pike, 1977) errors for equations 1 through 5, the approximate errors in derived rim heights for a 2 km, 10 km, and 50 km diameter crater are ± 5 m, ± 50 m, and ± 180 m respectively. Comparison of the calculated rim height differences and photographs indicates that craters with differences in excess of 20 m appear to have been partly flooded.

A total of 372 craters within Imbrium (figure 6) were measured and the derived thickness values are plotted in figure 5 and tabulated in the Appendix. The calculated rim heights obtained from equations 6 through 9 were compared with the rim heights measured from the Lunar Topographic Orthophotomaps available for Imbrium and are plotted in figure 7. Although a fair degree of scatter was obtained, there appeared to be no systematic under- or overestimate of rim heights. Furthermore, a plot of depth of flooding against crater diameter (figure 8) indicates little bias resulting from crater size variations.

Of the craters measured, nearly 27% appeared to be unflooded or fresh (figure 5) while the greatest rim height differences were measured at the craters Wallace and Archimedes K (300 to 350 m). There were four structures that did not have well-

defined flanks; the ring Lambert R, a ring to the immediate north of Aristillus, a degraded crater to the immediate west of Mt. Huygens, and Sinus Iridum. Assuming these structures to be completely flooded fresh craters, minimum flooding thicknesses of 1.2, 0.9, 0.85, and 2.1 km respectively were calculated on the basis of equation 1. These structures, plus possibly Archimedes and Cassini, are the only visible craters within Imbrium which could postdate the formation of the Imbrium basin and pre-date the eruption of mare basalts. This is supported by the spectral vidicon imagery data which indicates that the majority of the craters in Imbrium have spectral responses of mare, rather than highland, craters. Exceptions appear to be the craters Piko K, Tobias Mayer GA, Eratosthenes A and B, and Wallace B, which have responses more typical of highland material. They are all located near the mare edge or the sub-basalt extension of an inferred Imbrium ring. Their calculated excavation depths are 640, 920, 1200, 1080, and 750 meters, assuming them to be fresh craters and employing the expression:-

10) $$E = 0.196\ D^{1.010} \quad (\text{for } D < 17 \text{ km})$$

where E is the depth and D is the rim crest diameter in kilometers (Pike, 1977). It is therefore concluded that the lack of large (greater than 35 km diameter), partly buried craters within

Figure 7. Comparison of actiual (maximum) crater rim heights derived from the Lunar Topographic Orthophotomaps with the average values predicted from equations 6 through 9 of the text. Although there is an extremely good agreement between the two data sets, there appears to be a tendency to preferentially underestimate the predicted average rim height. If consistent, this would result in an overestimate of relative basalt thicknesses determined from the difference between the measured rim height and that of a fresh crater.

Figure 7

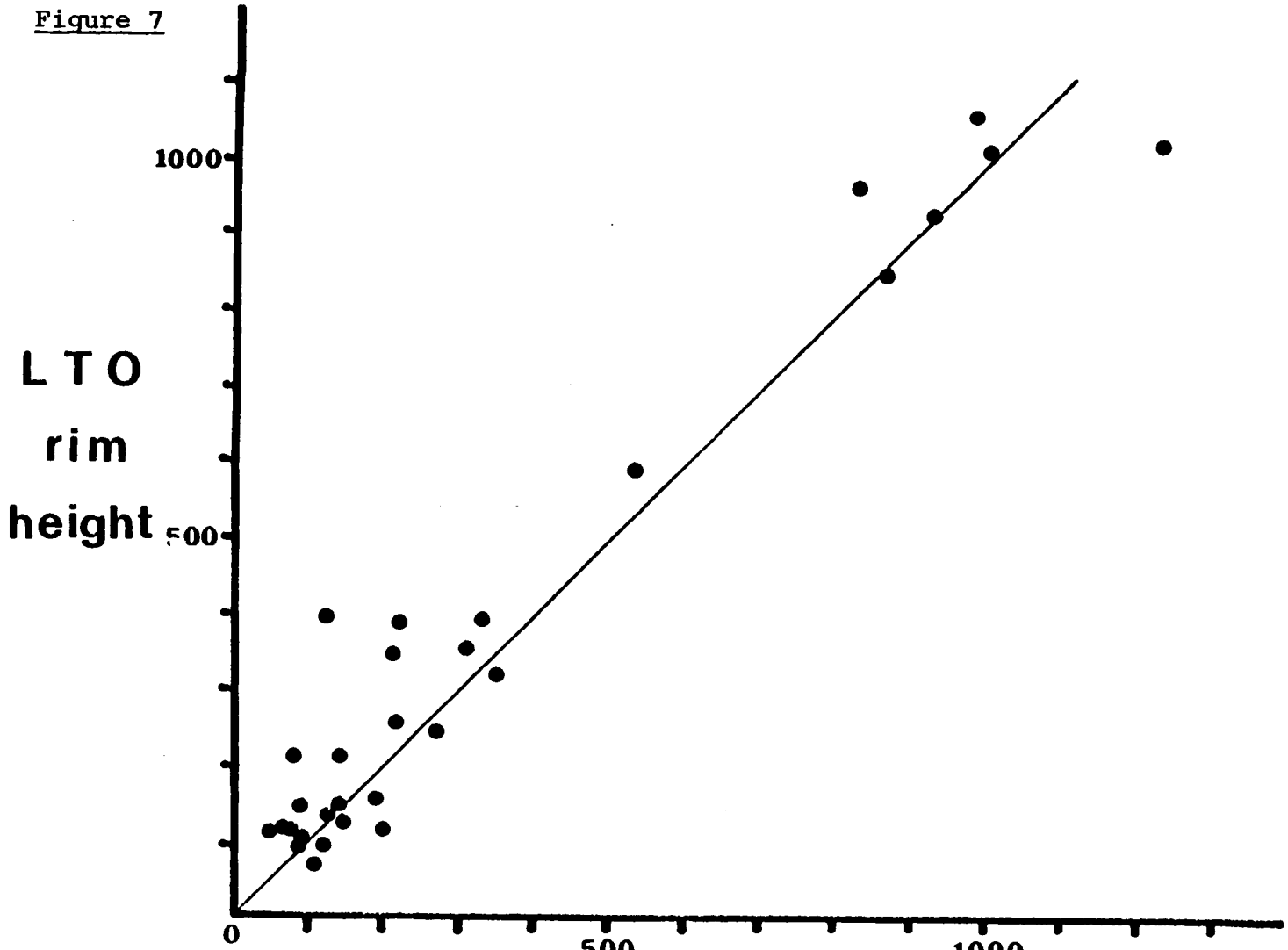

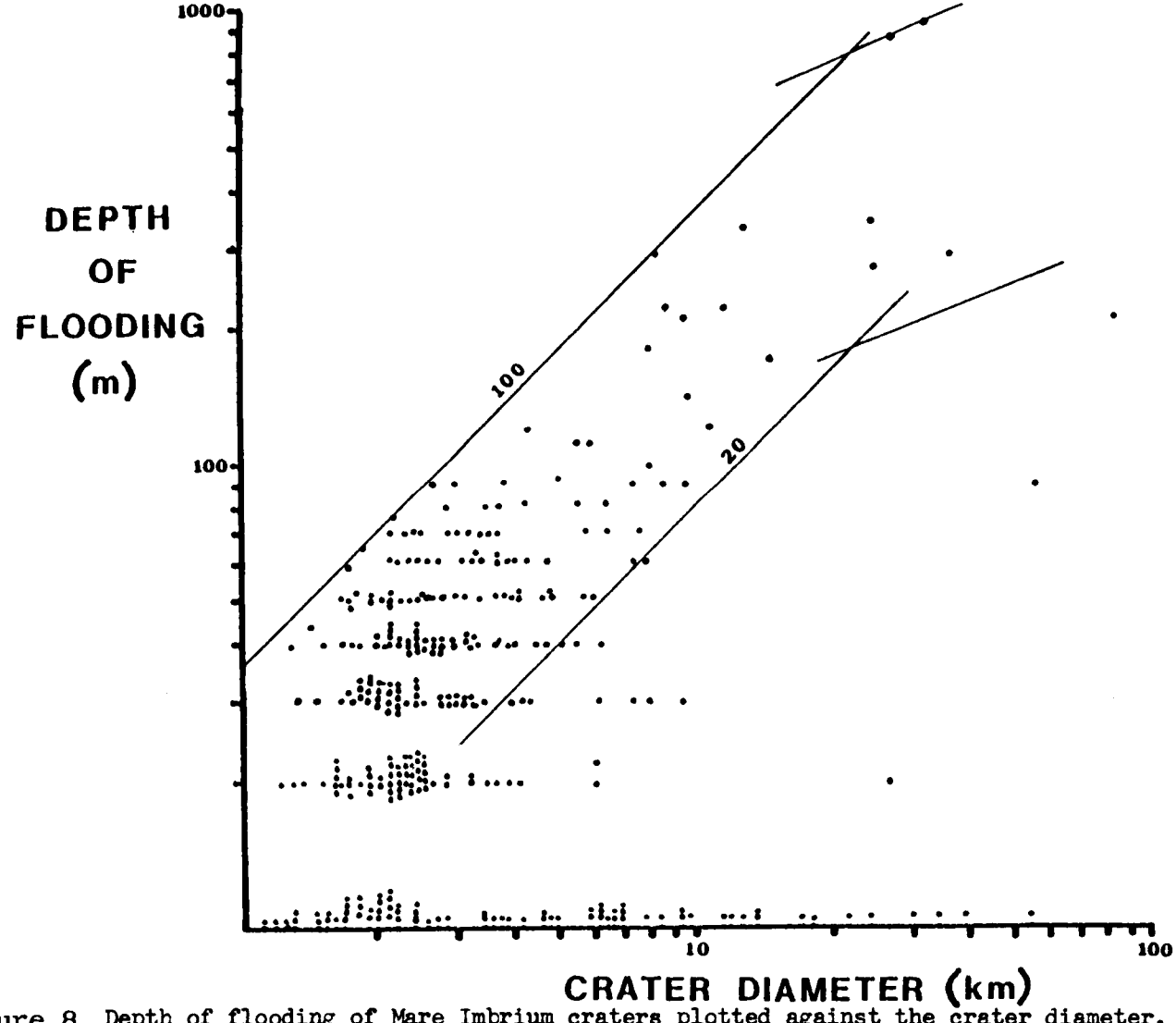

Figure 8 Depth of flooding of Mare Imbrium craters plotted against the crater diameter. The horizontal linearity of data points results from rounding to the nearest 10 m interval. Data points immediately above the horizontal axis represent zero flooding. Curves for 20 and 100% flooded craters are also shown.

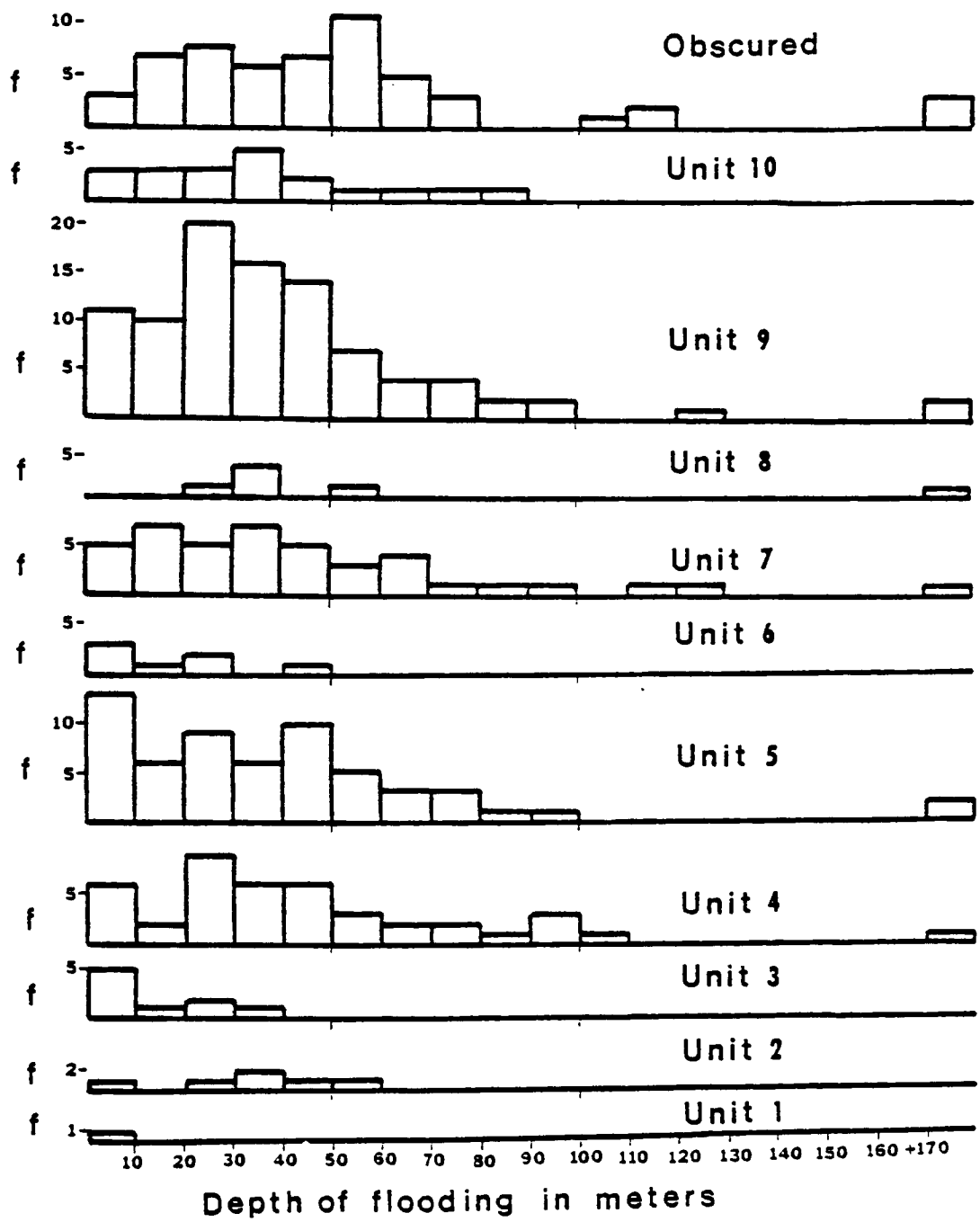

Figure 9 Histograms showing the depths of flooding for each of the basalt units within Mare Imbrium. The frequency(f) is the number of data points(flooded craters) within each unit. Note that there is no significant depth of flooding peak for any unit but rather a spread from zero to 110 m with mean values in the range of 30 to 40 m.

Unit	Mean depth in meters	Greatest depth in meters	Other data
10	29.0	80 (max)	10-63(2)
9	35.7	35	60 (1)
8	61.67	30	
7	41.19	48	30(1)
6	14.29	40(max)	
5	36.78	82	
4	38.81	60	
3	10	30(max)	
2	23.3	50(max)	
1	10	10(max)	

Table 5 Estimated thicknesses of the basalts in Mare Imbrium. The mean depth represents the mean of all the values derived for a particular unit and tabulated in the Appendix. The greatest depth represents the maximum values (max) if there were no depths greater than 100 m recorded for that unit, or the highest value divided by the number of previous units if greater than 100 m. The values in the third column represent thicknesses derived by Neukum and Horn(1) and Schaber(2) for sites within the respective units.

Imbrium indicates that the mare basalts are everywhere in excess of 950 meters in thickness except near the basin edges and over the submerged rings.

When depth of flooding was plotted as a function of the basalt unit which surrounds the buried crater (figure 9) it was found that a wide spread of depth values occurred for each unit. It was also found, however, that approximately only 4% of the measured crater population had been flooded to a depth in excess of 100 meters. The most commonly derived flooding values were 30 to 50 meters and are similar to the average values of 30 to 35 meters derived by Schaber (1973) for the heights of the Unit 10 flow fronts. The height range of the lobes determined by photogrammetric methods was 10 to 63 meters (Schaber, 1973). Similar estimates of the thicknesses of the flows are derived if the means of the data set for each unit are taken (table 5). These values would imply that the surface units of Imbrium are generally less than 100 meters in thickness and each could therefore be the product of a single eruptive phase.

Neukum and Horn (1976) have investigated the effects of lava flooding on crater frequency curves for an area of southwest Imbrium (Unit 9) and derived a thickness estimate of about 60 m for the surface unit and approximately 200 m for earlier units. They also derive a value of 30 m for the depth of flooding at the Apollo 15 site. Similarly, Eggleton et al. (1974) derived values

Figure 10. Histograms showing the diameters of fresh and flooded craters within each basalt unit of Mare Imbrium. Note that there is no prefered concentration of fresh craters in the youngest units or flooded craters in the oldest units, as might be expected. This has important ramifications for crater-counting techniques since an incorrect identification of crater age would overestimate the age of the surface unit if the measured crater were flooded rather than fresh.

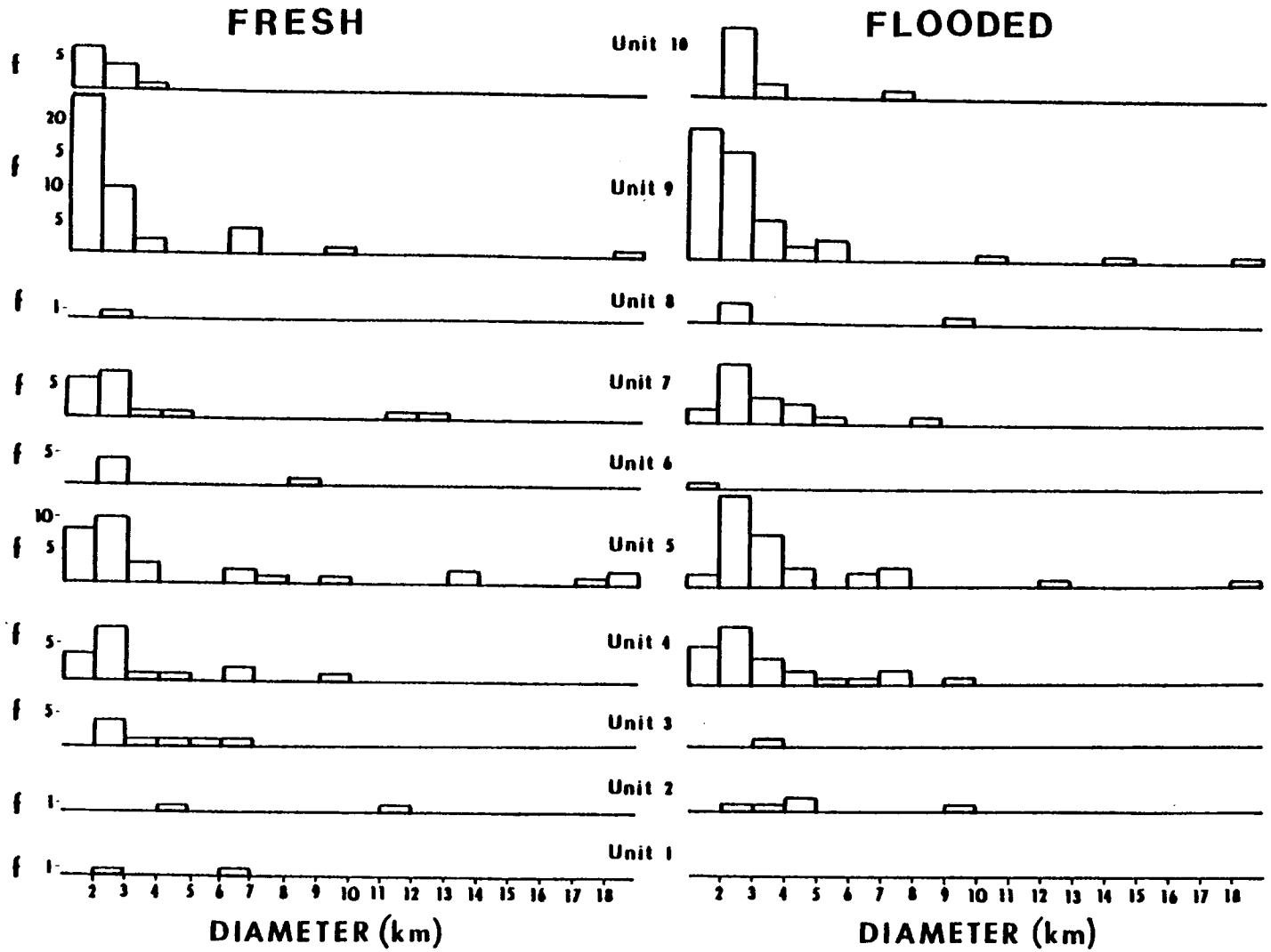
FRESH
FLOODED
Unit 10
Unit 9
Unit 8
Unit 7
Unit 6
Unit 5
Unit 4
Unit 3
Unit 2
Unit 1
f
5
20
10
1
2 3 4 5 6 7 8 9 10 11 12 13 14 15 16 17 18
DIAMETER (km)
DIAMETER (km)

Figure 10

of 75 to 100 m for the depth to a planar layer in northwestern and central Imbrium.

The process of partial flooding of impact craters poses problems for age determinations of the mare surface by crater counting since if the crater is regarded as being on, rather than being flooded by, a younger unit, an artificially older age would result for that unit. Figure 10 compares the frequencies of flooded and unflooded (< 20 m flooding) craters on each unit. It can be seen that a significant number of apparently flooded craters occurs within each unit.

Although the depth of flooding of visible surface craters enable estimations of the surface layer thickness in Imbrium, they do not permit determination of the total basalt pile thickness. Previously DeHon (1979) has calculated a minimum 1.5 km thickness for central Imbrium based on crater flooding, Thurber and Solomon (1978) estimated a minimum basalt fill of 3 km based on geophysical arguments, while Settle and Head (1976) estimated an original depth of 8 to 27 km for the Imbrium impact cavity based on their estimated ejecta volume and assuming a spherical cap geometry for the excavation. More recently, Head (1979), by artificially flooding contour maps of unflooded basins, has estimated that the outer shelves of multi-ring basins are covered by around 2 km of fill while the average thickness within the peak ring is between 4 and 5 km and may locally be as high as 8 km.

An alternative method to determining the depth of crater flooding to estimate fill thickness is to determine the depth of excavation of craters which appear to have pierced or not pierced mare basalts. Metzger et al. (1979) have argued that the craters Autolycus, Archimedes, Timocharis and Lambert have excavated KREEP-rich highland basalts. Lambert, the smallest of these, was estimated to have excavated to a depth of 3.7 km. At present there are diverse opinions as to whether the KREEP basalts pre-date the Imbrium impact event or both pre- and post-date it (see Schultz and Spudis, 1979). At least in Oceanus Procellarum, non-mare, though not necessarily KREEP, basalts were erupted simultaneously with mare basalts (Head and McCord, 1978) and would argue in favor of the latter interpretation.

On the basis of spectral vidicon imagery, the two craters Helicon and Le Verrier in central Imbrium appear to have ejecta blankets not inconsistent with mare basaltic material. That is, the ejecta from Le Verrier has characteristics similar to nearby Unit 4 and also has a low albedo. If this interpretation is eventually supported by spectral reflectance data, the excavation depths of these craters must be less than the basalt thickness. Employing:-

11) $E = 1.044\ D^{0.301}$ (for $D > 17$ km; Pike, 1977)

where E is the depth and D the diameter in kilometers, Le Verrier excavated to a depth of nearly 2.6 km while Helicon excavated to 2.7 km. It has been previously shown, however, that Helicon has been flooded by nearly 300 m of fill. A minimum thickness for the fill in the Helicon region is therefore 3.0 km. Furthermore, since both craters post-date the Iridum impact, the ejecta from the latter event must underlie the craters and contribute to the Imbrium fill. The calculated depths of the craters represent the minimum depth of excavation since equation 11 describes the present crater shape rather than the size of the transient cavity prior to modification by such processes as rebound and slumping (Settle and Head, 1977). Settle and Head (1979) found that craters 15 to 30 km in diameter had reconstructed depths greater than those predicted by small-crater morphology. Employing equation 10 therefore, the minimum excavation depths and thus minimum fill thicknesses are increased to 4.3 and 5.2 km for Le Verrier and Helicon respectively.

Taking a circular radius commensurate with the total surface area of basalt (8.5×10^5 km^2) and assuming a parabaloid with a depth of 5 km at the center, a minimum estimate of 2.2×10^6 km^3 is obtained for the total volume of fill within the Imbrium basin. This value represents approximately one fifth of the total volume of basalt (Head, 1975) estimated to occur on the moon.

Eruption style:

The surface basalts within Imbrium can be separated into three types; 1) those with flow lobes and channels, 2) those with sinuous rilles, and 3) those with neither of the previous characteristics. These groups are believed to represent three distinct eruptive styles.

Basalts with lobes and channels are limited to flows of Unit 10. They appear to represent a unique eruption style on the moon (Schaber et al., 1976) and have been analysed in great detail. Flows of Unit 10 extend some 600 km from their sources, have widths of the order of 40 to 60 km, thicknesses of 10 to 60 m, and were emplaced on low slopes ($\sim$0.0023; Schaber, 1973). Based on laboratory analyses of returned samples (Murase and McBirney, 1970) and geometric properties of the flows, the basalts had eruption viscosities of the order of 10 Pas (Hulme, 1974), yield strengths of about 100 to 400 N/m^2 (Hulme, 1974; Moore et al., 1978), and flow velocities of 1 to 14 km/hr (Hulme, 1974; Moore and Schaber, 1975). All these characteristics are satisfied by basalts with exremely rapid eruption rates; Hulme (1974) has estimated flow rates of 8×10^4 m^3/s and an emplacement period of about 6 days assuming constant flow, while Schaber (1973) derived a value of about 10 days.

In excess of 50 sinuous rille segments have been identified in Imbrium (figure 11) and their lengths are plotted as a

Figure 11. The location of volcanic features and graben structures within Mare Imbrium. Also shown are islands of highland material (solid shading) corresponding to portions of the Imbrium rings. Note the preferential development of volcanic features between the innermost ring of islands and the mare edge.

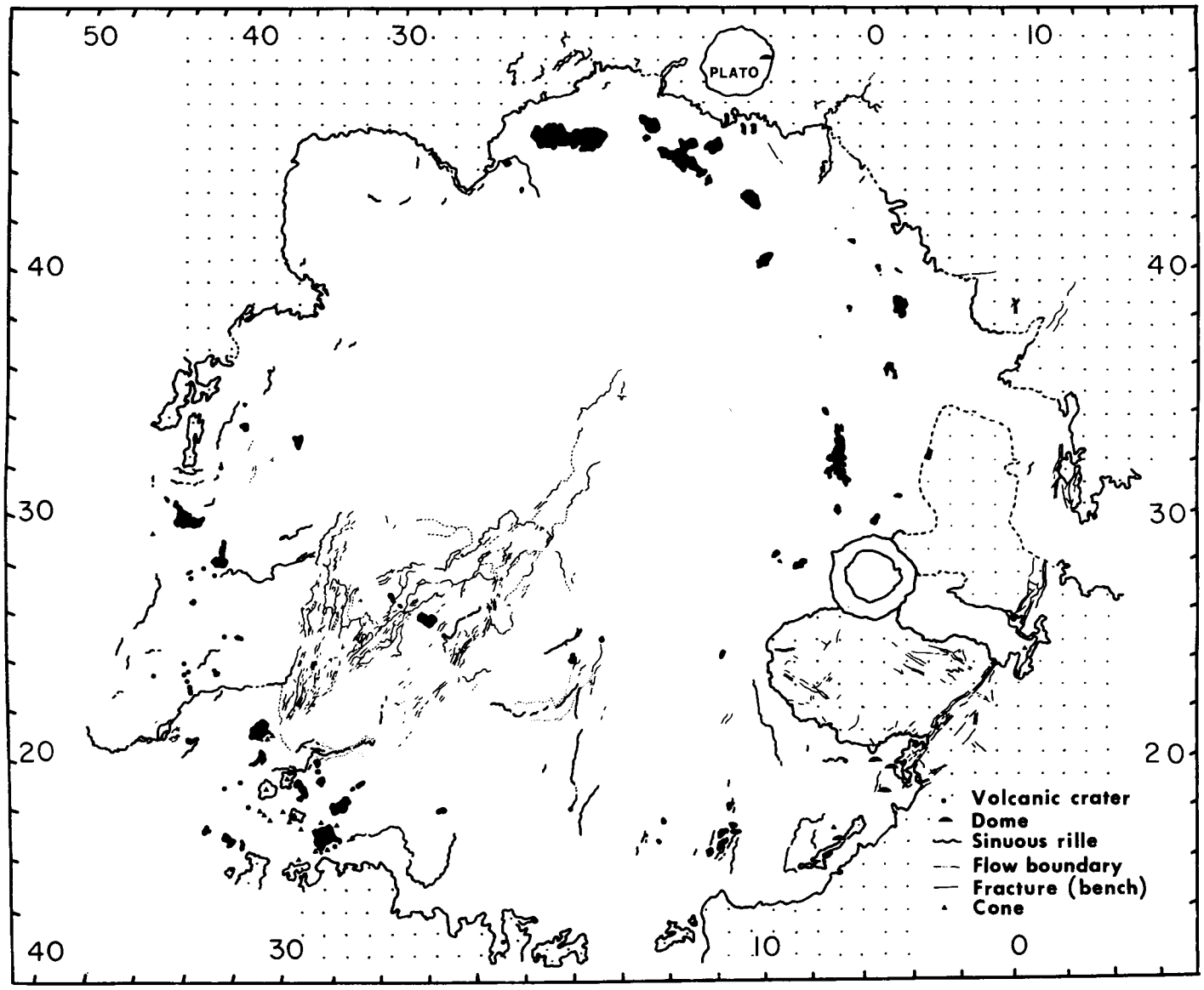
50
40
30
0
10
PLATO
40
30
20
40
30
10
0
Volcanic crater
Dome
Sinuous rille
Flow boundary
Fracture (bench)
Cone

Figure 12. Histogram of total sinuous rille lengths in each of the basalt units of Mare Imbrium. Note rilles are lacking in Units 1, 4, and 10. 0 represents the obscured area of figure 2. Since old units have been partially flooded by younger, these represent minimum values for each unit.

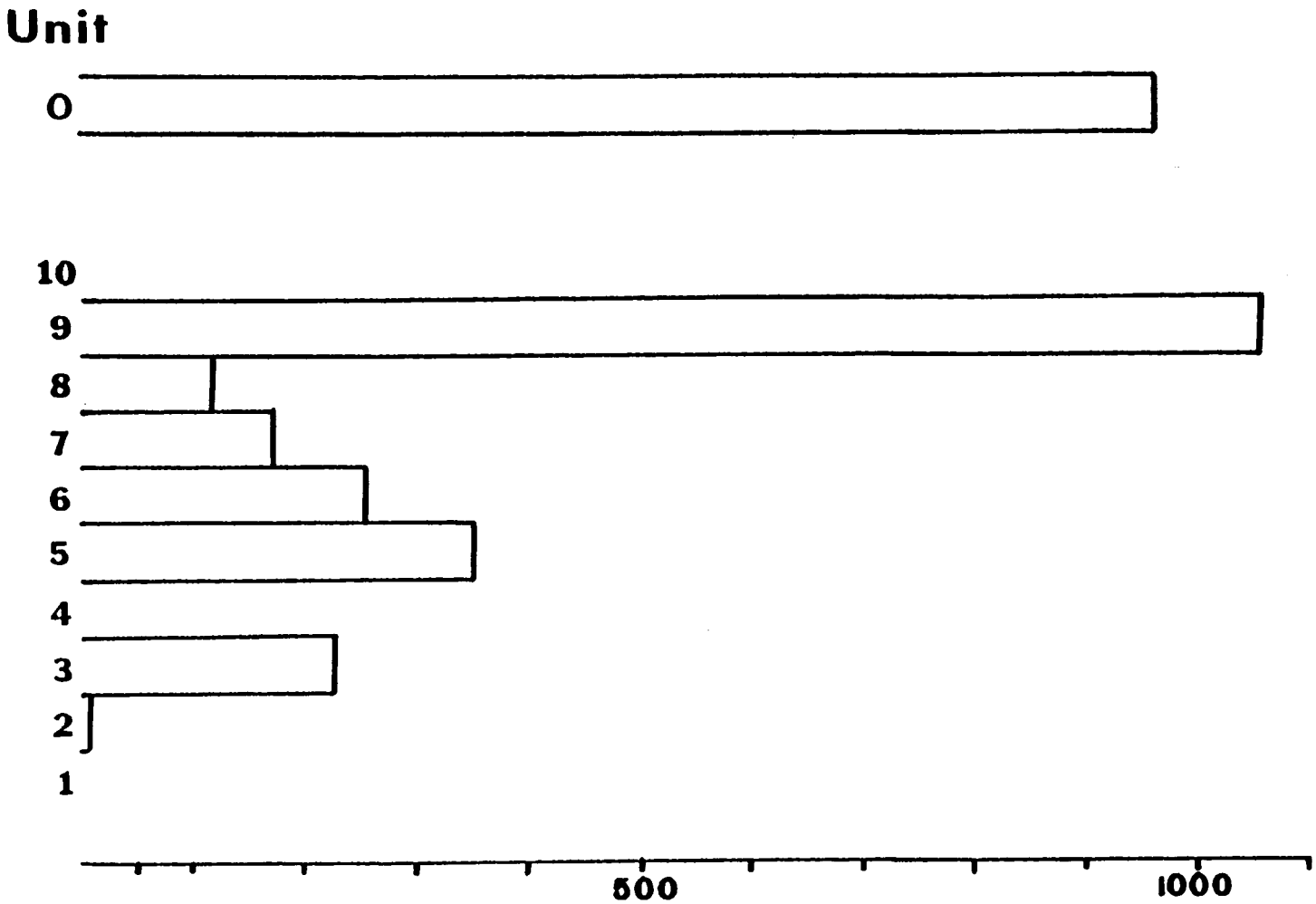

Figure 12

Figure 13. Plot of the depth of flooding(see Table 5) versus sinuous rille density for basalt units within Mare Imbrium. Also indicated by different symbols are the relative TiO_2 concentrations of each unit. Note intermediate units are relatively thick and depleted in rilles, titanium-rich units are thin and have high rille densities, while titanium-depleted basalts share the characteristics of both.

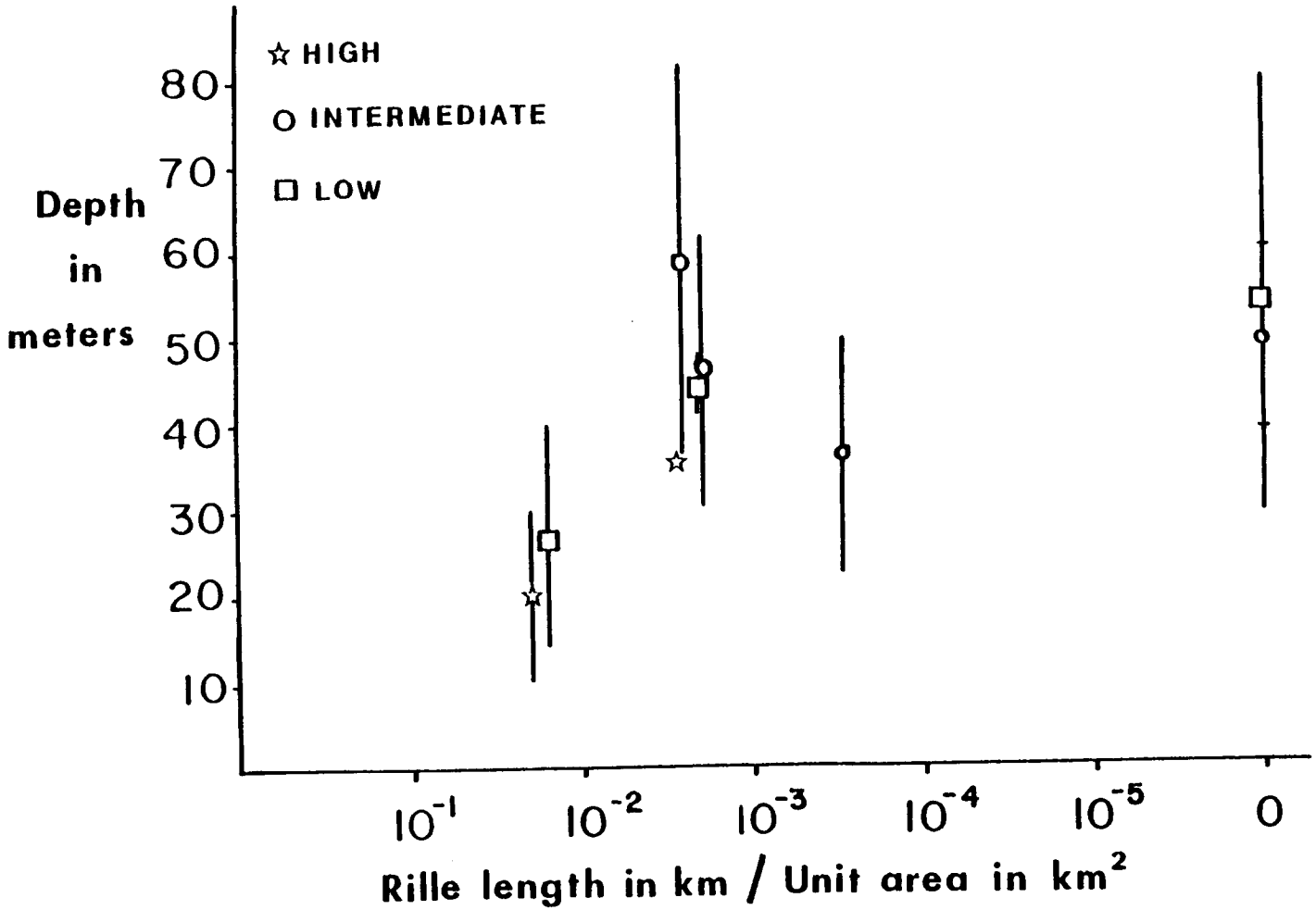
☆ HIGH
O INTERMEDIATE
□ LOW
Depth in meters
80
70
60
50
40
30
20
10
10^{-1}
10^{-2}
10^{-3}
10^{-4}
10^{-5}
0
Rille length in km / Unit area in km^2

Figure 13

Unit	Rille length/Unit area	Titanium concentration
3	3.0×10^{-2}	high
6	2.0×10^{-2}	low
9	4.7×10^{-3}	high
5	4.2×10^{-3}	Intermediate
7	3.1×10^{-3}	low
8	3.0×10^{-3}	Intermediate
2	4.7×10^{-4}	Intermediate
1	0	Low
10	0	high
4	0	Intermediate

Table 6 Lengths of sinuous rilles within each basalt unit of Mare Imbrium divided by the area of that unit. The relative titanium concentrations are on the right. The data are ranked with the units having the greatest rille density at the top. Unit 1 is undervalued because all the rilles within it do not occur within the area mapped while Unit 10 had a different eruption style which led to the formation of channels rather than rilles.

function of the unit in which they occur in figure 12. Neglecting rilles within the obscured area, rilles are most prevalent within Unit 9. This is undoubtedly partly a function of age since the rilles of progressively older units become more degraded and flooded. Rille lengths were therefore calculated as a function of the exposed area of the unit in which they occur (Table 6). Neglecting Unit 10 which has been previously shown to have experienced a unique eruptive style and Unit 1 which does not have rilles in the mapped area, rille density does not appear to be correlated with unit age and there is but a slight preference for intermediate units to be relatively rille-depleted.

Both Hulme(1973) and Carr(1974) independently proposed that sinuous rilles were produced by lava erosion through thermal incision. Hulme and Fielder(1977) state that the presence of meanders along the rilles is a result of turbulent flow. They furthermore imply that rilled flows were emplaced on steeper slopes than rille-less flows of similar eruption rate. In an analysis of a Marius Hills flow, Hulme(1973) derived an eruption rate of 4×10^4 m^3/s, a mean depth of lava of 10 m, a mean flow velocity of 8 m/s, and an emplacement period of approximately one year assuming continuous eruption. These values suggest that

rilled flows are thinner, were erupted at lesser rates, and were emplaced over a significantly longer time period than channeled flows of similar volume.

Basalts which contain neither channels nor rilles may either have never had such features or those features may have been degraded or buried. Flows lacking such features are produced by flood eruptions, are usually thick (+20-30 m), and tend to bury their own vents (Greeley,1976). Unit 4, lacking both rilles and channels, appears to be one of the thicker flows (Table 5) and covers an extensive part of the surface area within the inner ring of Imbrium; both features favoring a flood-style eruption.

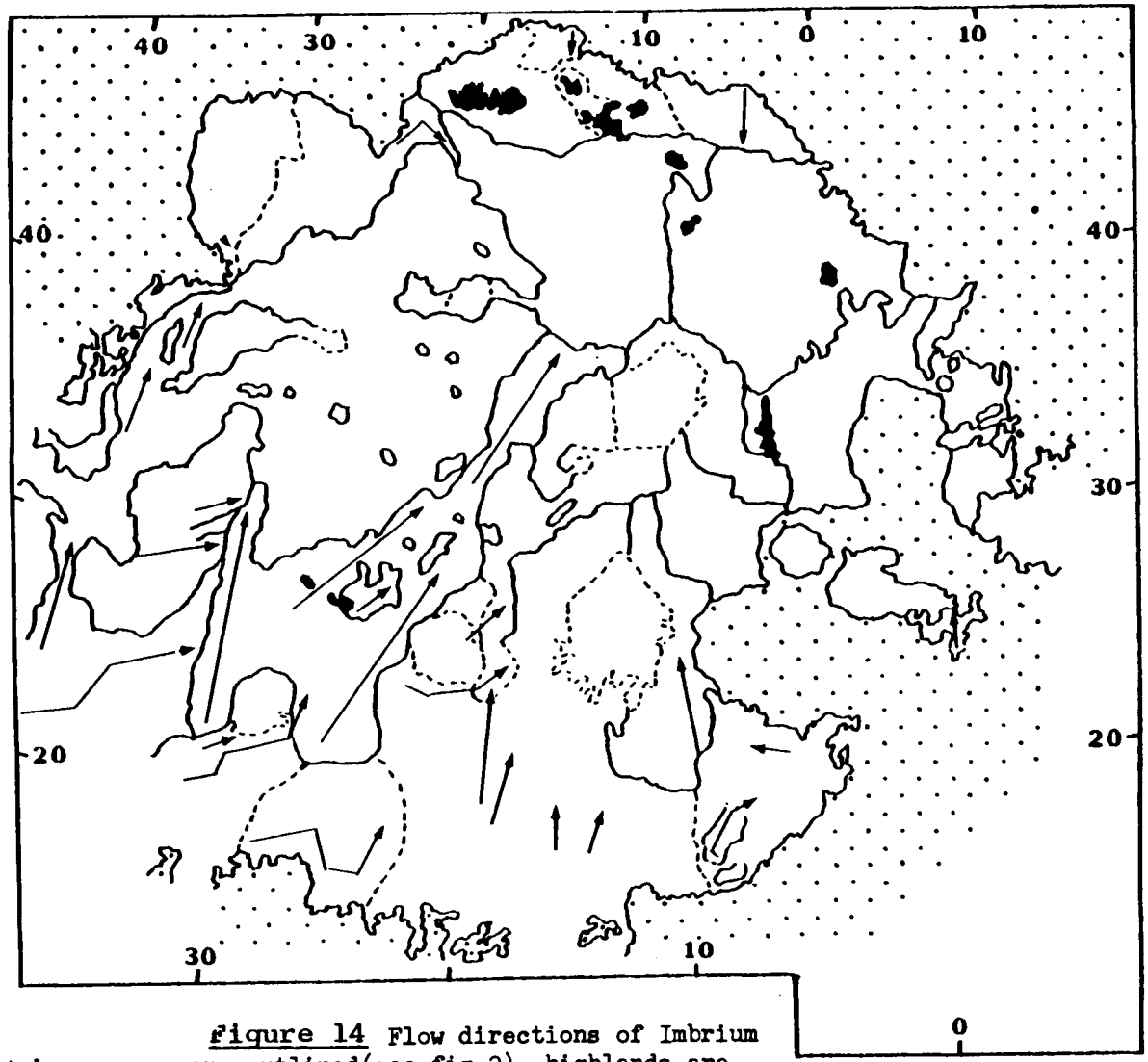

Figure 14 Flow directions of Imbrium
are outlined(see fig.2), highlands are
re solid shading. Note that almost all flows were directed toward the center of Imbrium.

lavas. Unit bc
stipled, and r

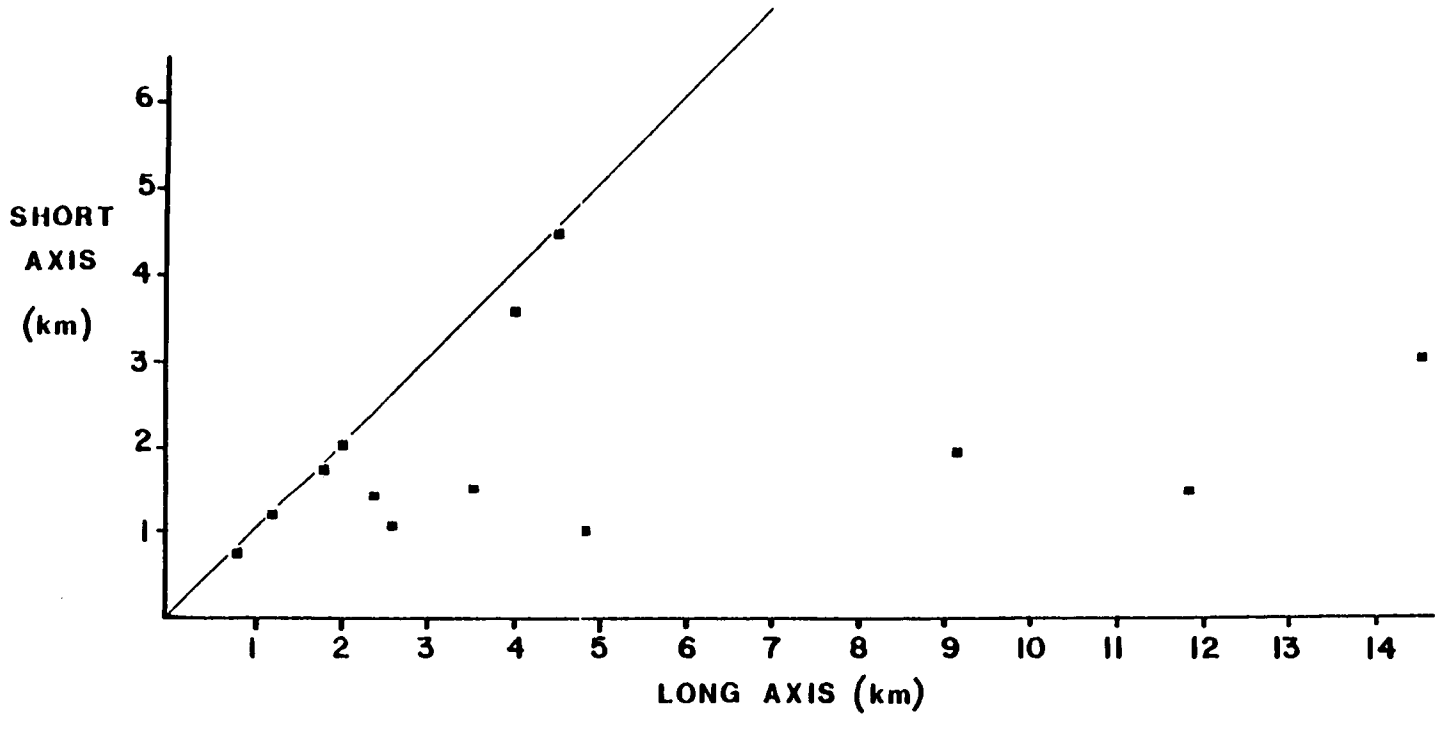

Figure 15 Plot of the axial dimensions of Mare Imbrium sinuous rille source craters. Note the marked deviation from a circular form (45 degree line) of the larger craters.

Sources and flow directions:

Schaber (1973) suggested that the Unit 10 channeled flows appeared to have been derived from a single, 20 km long fissure vent oriented NE-SW within an area bounded by 18-23N, 28-32W, southwest of Euler. Todhunter (1975) has described numerous volcanic vents within this same area; her list includes 4 cones, 7 crater rows, 5 groups of hills or ridges with summit craters, 1 shield volcano, and three linear depressions. Todhunter (1975) also suggested that the linear elements of these vents were aligned either radial or concentric to the center of Imbrium. All of the Unit 10 flows travelled north to northeast, toward the center of the Imbrium basin. Schaber (1973) showed the Unit 9 flows to the immediate east of Sinus Iridum to be derived from this same area of southwest Imbrium. The present mapping, however, indicates that these flows were derived from central west Imbrium (figure 14) and are nearly half the 1,200 km length stated by Schaber.

The sources of sinuous rilles tend to be small and often markedly elongate craters (figure 15). Head and Wilson (1980) argued that the minimum eruption rates implied by such craters are of the order of 10^7 kg/s. Of the 48 rille source craters that could be identified or constrained within reasonable bounds, approximately 6% were located in the Highlands, 17% at the mare/highland boundary, 70% between the inner ring and the mare/high-

Figure 16. Location of Mare ridges within Mare Imbrium. Islands of unflooded ring material are indicated by solid shading. Points A and B mark locations where younger ridges might cross-cut an earlier set. Point C indicates ridges with a very subdued morphology, perhaps a result of flooding by younger flows. Note the markedly circular pattern of ridges defining the inner Imbrium ring.

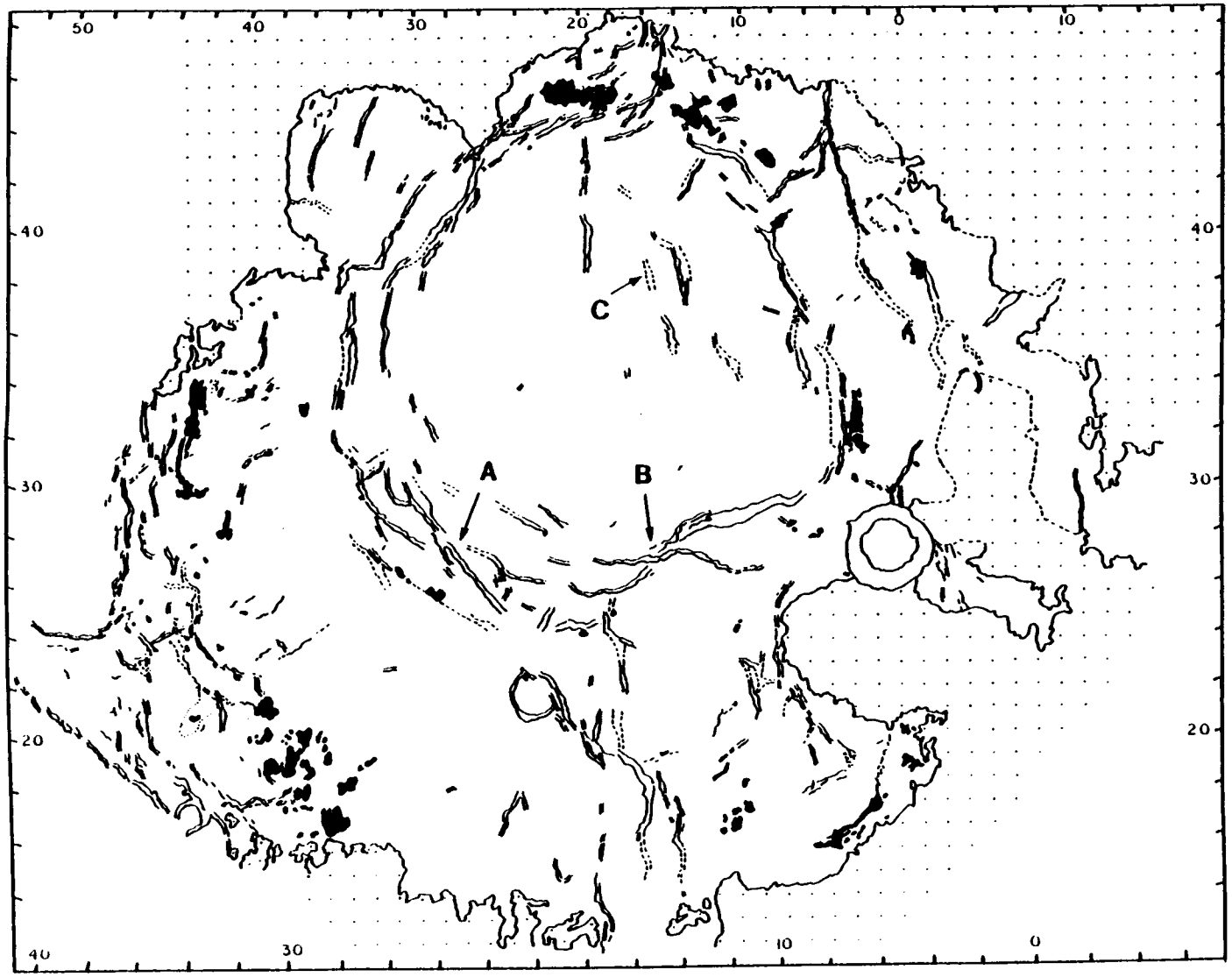

Figure 16

land boundary, 6% at the inner ring, and none inside of the inner ring. In fact, only five of the sinuous rilles could be traced inside of the inner ring (figure 11). This could result from slope reduction making thermal incision less effective (Hulme, 1973), ponding of the lava, or a flood-basalt eruption style. The lack of central rilles could equally result from all three factors. Almost without exception, all of the flows travelled radially toward the center of the mare (figure 14) except where they were diverted by pre-existing obstacles such as mare ridges.

Structure of the Imbrium basin:

The major tectonic elements of Imbrium include mare ridges, tectonic rilles, and faults in the adjacent highlands. The mare ridge system (figure 16) can be separated into that which forms the approximately 280 km radius inner ring of Imbrium and, the remainder. A detailed study of the ridges in the Imbrium-Procellarum area by Lucchitta (1977) showed that ridges defining the Imbrium rings were parallel to contours, and often exhibited different mare surface heights on each side. Fagin et al. (1978) showed there to be a preferential approximately north-south alignment of ridges within central Imbrium while Schaber (1973) demonstrated that ridges both predate and postdate the youngest surface lavas. The present study shows that the ridges are present in each unit. The oldest ridge material that can be shown to have influenced the passage of later basalts is in west-

Figure 17. 0.4/0.56 μm vidicon image of western Mare Imbrium. The bright area to the right represents the titanium-rich Unit 9. The dark area(arrowed) represents titanium-depleted basalts forming a mare ridge around which the younger titanium-rich basalts have flowed. The bright area to the left is the Heraclides Promontory. Circular bright and dark spots are craters. Scale bar is approximately 20 km.

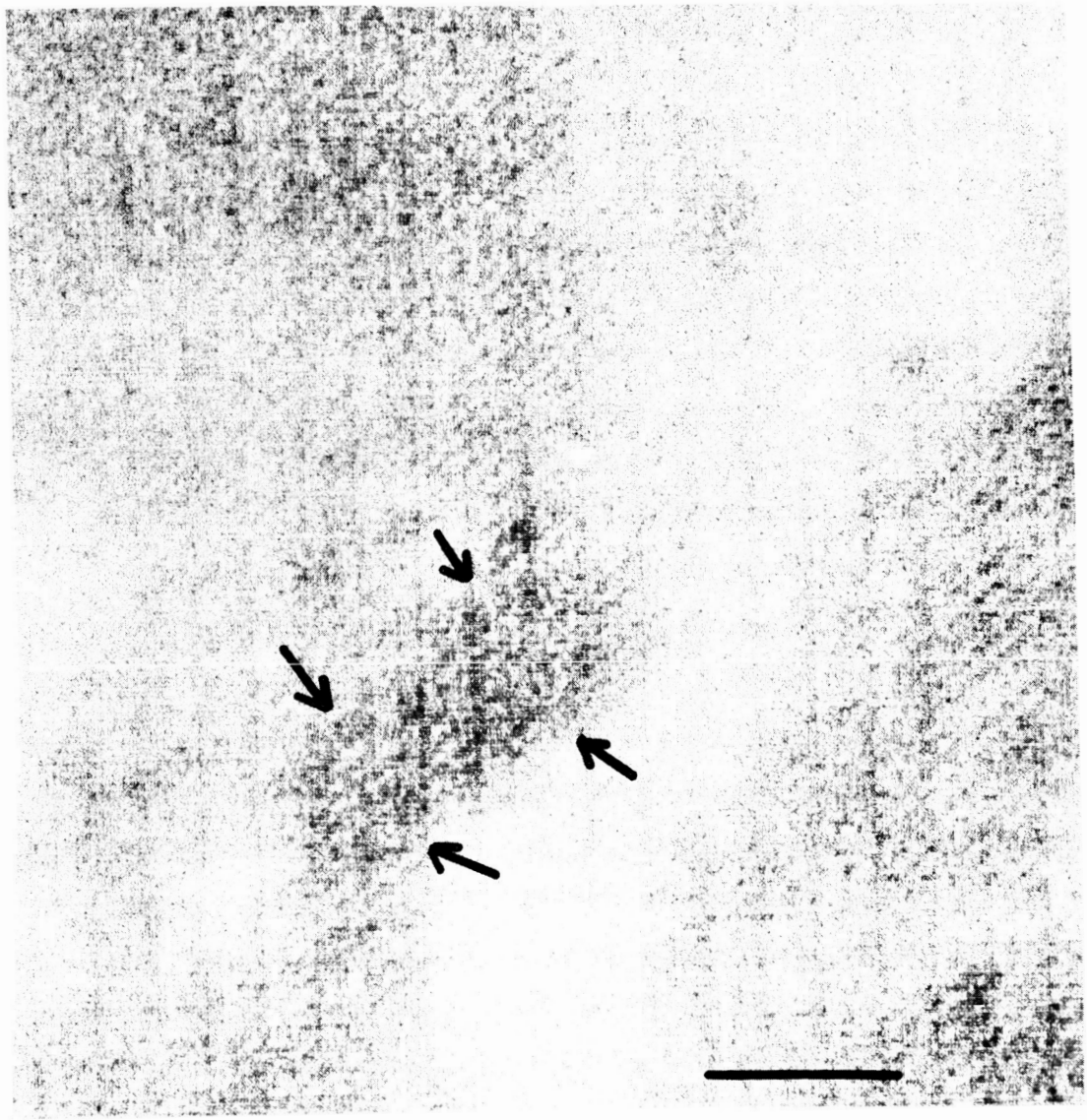

Figure 18. Lunar Orbiter photograph of northwest Mare Imbrium showing a ridge cutting an older sinuous rille(A) and a sinuous rille crossing an older ridge(B). If the two rille sections were originally connected, these relationships would indicate at least two periods of ridge production. Scale bar is 20 km.

ern Imbrium near the Luna 17 landing site, where a ridge of Unit 5 material has channeled flows of Unit 9 material (figure 17). It is possible other such examples exist but they must be below the vidicon imagery resolution. In northwestern Imbrium it appears that a sinuous rille within Unit 6 crosses a ridge but is elsewhere cut by a ridge (figure 18). Additionally, the subdued appearance of ridges in central Imbrium (C in figure 16) within Unit 4 suggests that the surface basalts partially bury an originally more extensive ridge system. The period of ridge formation can therefore be shown to predate the emplacement of Unit 4 and postdate Unit 10 (3.5 ± 0.25 to less than 3.0 b.y.). It is less obvious whether each ridge segment formed in a singular catastrophic event or was produced slowly over a long time period. The generally non cross-cutting relationships exhibited by the ridges (see A and B in figure 16 for possible exceptions) suggests that the stress field influencing their location remained relatively constant in direction over a long time period.

Tectonic rilles are restricted to east Imbrium (figure 11) at a radius of approximately 580 km from the basin center and occur largely within the Apennine Bench Formation (Spudis, 1978). The rilles average 1.75 to 2.0 km in width, though near Cassini they may be as much as 10.95 km wide. Lucchitta and Watkins (1978) found that tectonic rille formation terminated on the moon at about 3.6 ± 0.2 b.y. ago. The present analysis shows that the

Figure 19. Lunar Orbiter photograph of the Apennine Bench area showing graben cutting basalt(A) and being flooded by basalt(B). These relationships indicate termination of graben production between the eruptions of both basalts. Scale bar is approximately 20 km.

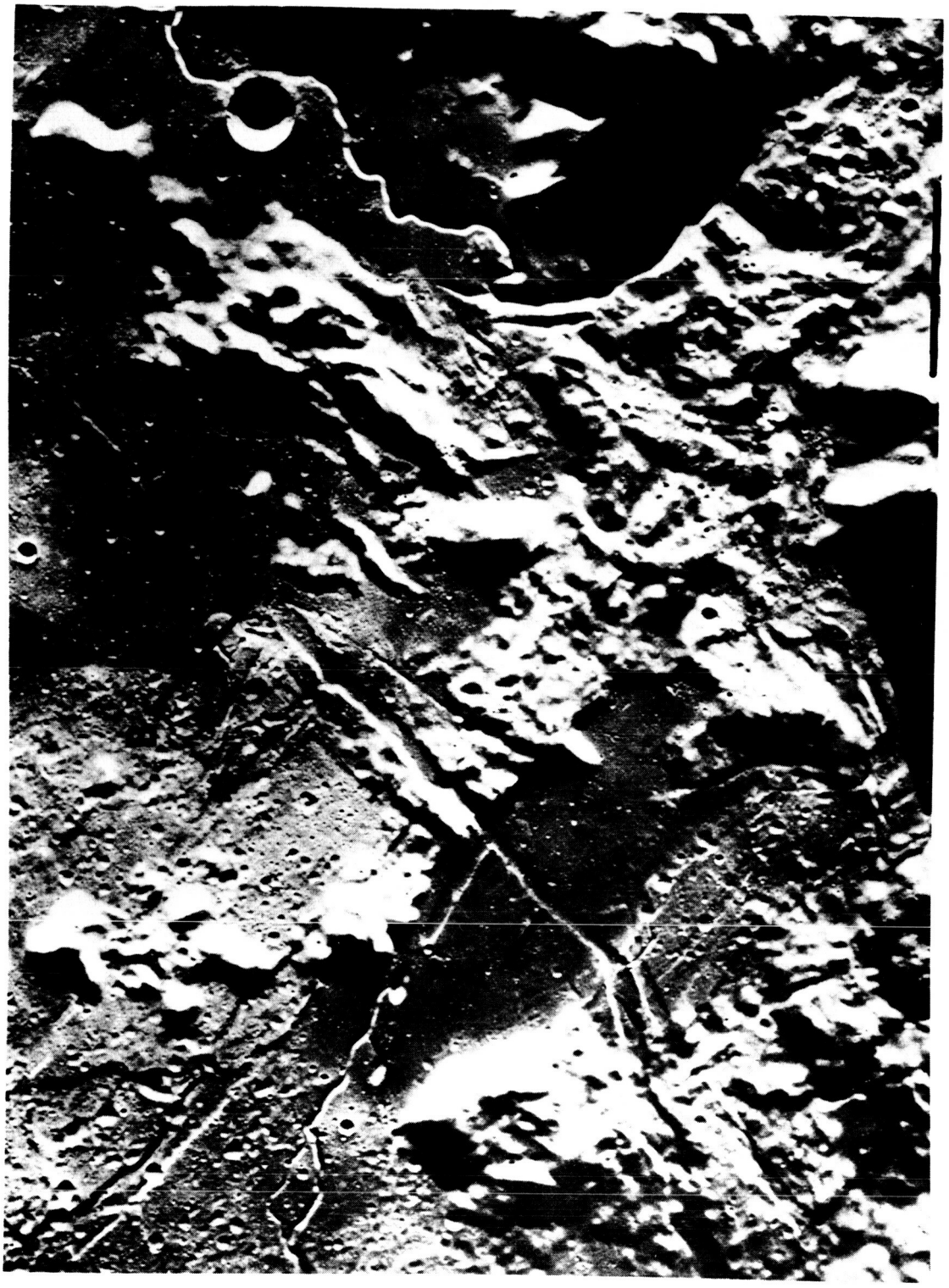

Figure 20. Lunar Orbiter photograph of the Alpine Valley to the immediate north of Mare Imbrium. Note the sinuous rilles on the valley floor and their source craters(arrowed). The lower source fed basalts that flooded the valley floor while the upper source fed lavas which partly covered the earlier rille on the valley floor but mainly drained into Mare Frigoris(top). Scale bar is approximately 20 km.

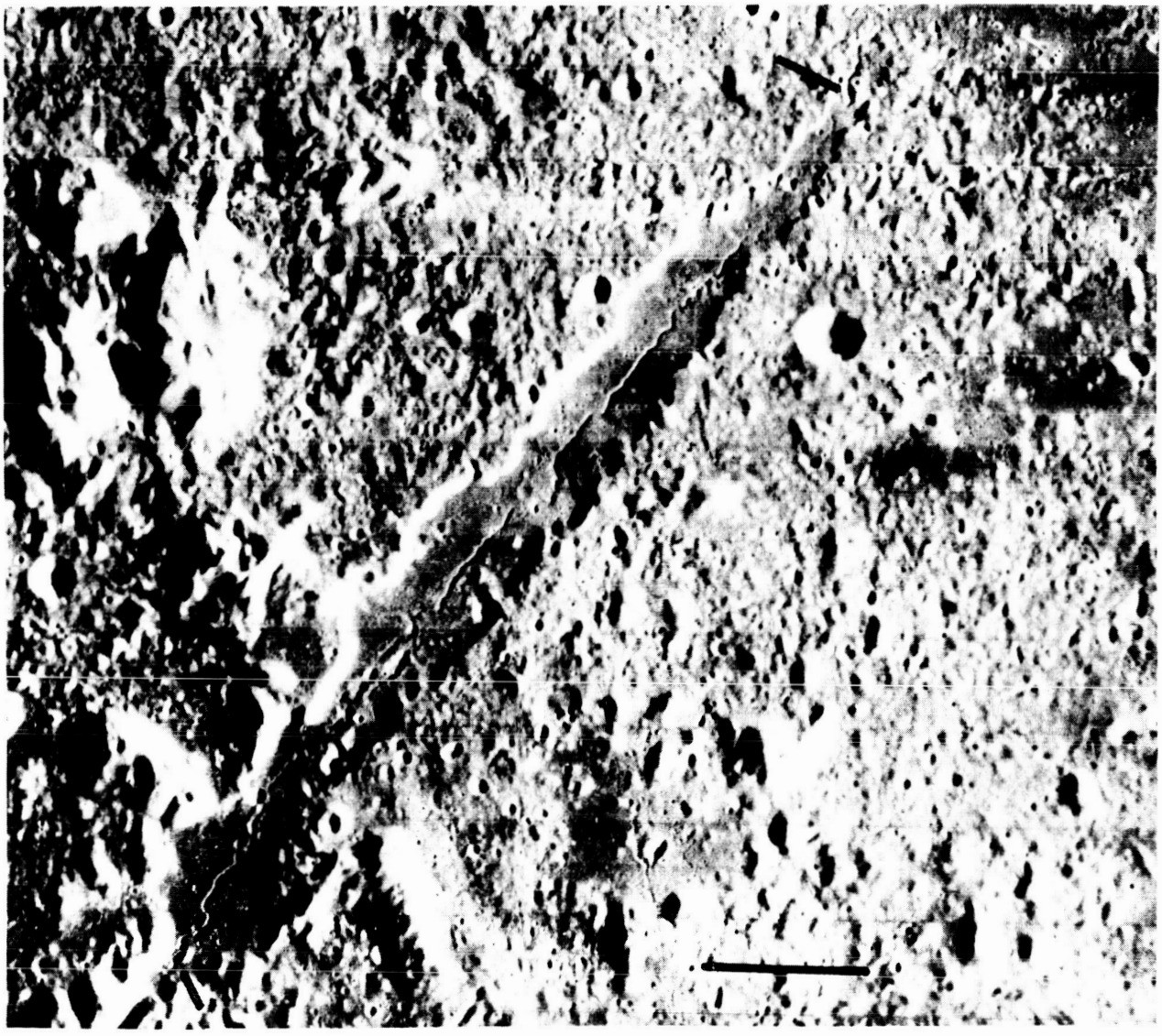

rilles do not cross Unit 6 but do cut Unit 5 (figure 19), both dated at 3.3 ± 0.3 b.y., in agreement with Lucchitta and Watkins' result. Although present in Unit 4, rilles are not seen in northern Imbrium within the older Units 2 and 3. If these early units have been correctly dated, it would imply that crustal conditions were inimical to rille production in that area; possibly a result of a locally thicker lithosphere (Head and Solomon, 1980).

A number of linear structures are distributed radially and concentrically to the Imbrium basin (Mason et al., 1976). Some of these appear to be of sedimentary origin (resulting from the emplacement of the Imbrium basin ejecta) (Head, 1976) while others such as the Sirsalis linear (Whitford-Stark and Head, 1980) and the Alpine Valley are tectonic in origin. The Alpine Valley (figure 20) is some 130 km long, averages 10 km in width, and is floored by basaltic material. The location of the Valley toward the pole and the massif at its southern end render it difficult to determine the basalt composition. There is a slight suggestion from the vidicon images that it is titanium rich. Two possible sinuous rille source craters have been identified in the Valley (figure 20). The older, located at the southern extremity, fed north-flowing lava while the younger erupted basalts which partly covered the earlier rille but mainly drained into Mare Frigoris. Vidicon imagery (Johnson et al., 1977) of basalts within the highland area to the east and west of Plato, and part

of the floor of Plato itself, shows them to be intermediate to high titanium basalts. These units have been assigned variable ages (Ulrich, 1969; M'Gonigle and Schleicher, 1972) and some may be as young as the youngest Imbrium lavas.

Summary:

Following the formation of the Imbrium multi-ring basin at approximately 3.9 b.y. ago, the cavity began to fill with basalt. An estimate of the minimum final fill volume being 2.2 x 10^6 km^3. Early eruptions were possibly of KREEP composition. Initially, the mare basalts were probably concentrated and erupted within the inner ring. None of this thick (+5 km) basalt assemblage appears to be represented by exposed surface units. The oldest (3.5 ± 0.25 b.y.) exposed basalts occur largely outside of the inner ring where their relative altitude has prevented flooding by younger units. Their composition range is from intermediate to high titanium basalt. An older, possibly Very Low Titanium basalt, occurring in Procellarum at the Aristarchus Plateau, may underlie younger units in western Imbrium. The production of tectonic rilles terminated during the eruption of these early units (2-4), reflecting a possible increase in lithosphere thickness.

The remaining units (5-10) all appear to have been derived at or exterior to, the inner Imbrium ring and to have flowed toward the basin center. These units all appear to be less than

100m in thickness and to average 30 to 40 m thickness. They range in composition from very low to high titanium basalts.

Mare ridge production appears to have been a continuous, though possibly episodic, process which commenced at least prior to the eruption of Unit 4(3.5 $\pm$ 0.25 b.y.) and continued after the eruption of the youngest lavas(<3.0 b.y.).Young basalts located in the highlands adjacent to Imbrium appear to be fault-related and may result from the opening of channels in the crust as a consequence of the downwarping of central Imbrium (Solomon and Head,1979).

Unlike Oceanus Procellarum(Whitford-Stark and Head,1980), there appears to be no simple composition - age relationship between the 10 basalt units identified in Imbrium. Basalts of widely varying composition appear to have been synchronously erupted. The identification of numerous vents (+ 50) over a 850,000 km^2 area suggests a widespread subcrustal reservoir for the basalts though does not exclude the possibility of numerous small magma reservoirs, each producing its own compositionally unique basalt.

ACKNOWLEDGEMENTS

We would like to thank Sam Merrell for the hard work he put into the photographic reproduction of the many figures in this text. This work was performed under NASA Grant NGR-40-002-116. The Hawaii Institute of Geophysics is gratefully acknowledged for supplying spectral vidicon images of the Imbrium area to the authors. Carlé Pieters provided helpful discussion on the spectral reflectance data.

REFERENCES

Adams J.B. and Ralph R.L. (1978) Diffuse reflectance of Luna 24 soils. In Mare Crisium: The view from Luna 24 (R.B.Merrill and J.J.Papike eds.) Pergamon Press, New York. 81-87.

Alekseyev V., Lebedev L., and Narimanov G.S. (1973) For Lunar rock. NASA TT-14983 ,119p.

Andre C.G., Bielefeld M.J., Eliason E., Soderblom L.A., Adler I., and Philpotts J.A. (1977) Lunar surface chemistry: A new imaging technique. Science 197, 986-989.

Baldwin R.B. (1970) A new method of determining the depth of lava in the lunar maria. Pub.Astron.Soc.Pacific 82, 857-864.

Bielefeld M.J. (1977) Lunar surface chemistry of regions common to the orbital X-ray and gamma-ray experiments. Proc.Lunar Sci. Conf.8th, 1131-1147.

Bielefeld M.J., Reedy R.C., Metzger A.E., Trombka J.L.,and Arnold J.R.(1976) Surface chemistry of selected lunar regions. Proc.Lunar Sci.Conf.7th,2661-2676.

Bills B.G. and Ferrari A.J. (1975) Frontispiece. Proc. Lunar Sci. Conf.6th.

Bills B.G. and Ferrari A.J.(1977) A lunar density model consistent with topographic, gravitational, librational and seismic data. J.Geophys.Res.82,1306-1314.

Bjorkholm P.J., Golub L., and Gorenstein P.(1973) Distri-

bution of ^{222}Rn and ^{210}Po on the lunar surface as observed by the alpha-particle spectrometer. Proc. Lunar Sci. Conf. 4th.2793-2802.

Boyce J.M.(1976) Ages of flow units in the lunar nearside maria based on Lunar Orbiter IV photographs. Proc.Lunar Sci.Conf.7th.2717-2728.

Boyce J.M. and Dial A.L.(1975) Relative ages of flow units in Mare Imbrium and Sinus Iridum. Proc.Lunar Sci. Conf. 6th.2585-2595.

Carr M.H.(1974) The role of lava erosion in the formation of lunar rilles and martian channels.Icarus, 22,1-23.

Charette M.P.,McCord T.B., Pieters C.M., and Adams J.B.(1974) Application of remote spectral reflectance measurements to lunar geology classification and determination of titanium content of lunar soils.J.Geophys.Res. 79, 1605-1613.

De Hon R.A.(1979) Thickness of the western mare basalts. Proc.Lunar Planet.Sci.Conf.9th. 2935-2955.

Delano J.W.(1979) Apollo 15 green glass: Chemistry and possible origin. Proc.Lunar Planet.Sci.Conf.10th.275-300.

Dyal P. and Daily W.D. (1979) Electrical conductivity anomalies associated with circular lunar maria. Proc. Lunar Planet.Sci.Conf.10th. 2291-2297.

Eggleton R.E.,Schaber G.G., and Pike R.J.(1974) Photogeologic detection of surfaces buried by mare basalts. (abstract) In, Lunar Science V, The Lunar Science Institute,Houston,Texas. 200-202.

Fagin S.W.,Worrall D.M., and Muehlberger W.R.(1978) Lunar

mare ridge orientations. Implications for lunar tectonic models. Proc.Lunar Planet.Sci.Conf.9th. 3473-3479.

Ferrari A.J.(1977) Lunar gravity: A harmonic analysis. J.Geophys.Res. 82, 3065-3084.

Ferrari A.J. and Anada M.P.(1977) Lunar gravity: A long-term Keplerian rate method. J.Geophys.Res.82,3085-3097.

Ferrari A.J.,Nelson D.L.,Sjogren W.L., and Phillips R.J. (1978) The isostatic state of the lunar Apennines and regional surroundings.J.Geophys.Res.83,2863-2871.

Fielder G. and Fielder J.(1971) Lava flows and the origin of small craters in Mare Imbrium. In, Geology and Physics of the Moon(ed.,G.Fielder) Elsevier,Amsterdam.15-26.

Florenskii K.P.,Gurshtein A.A.,Bazilevskii A.T. and Zasetskii V.V.(1971) Preliminary geological-morphological analysis of the Luna 17 landing area.Sov.Phys.Dokladv. 16, 61-65.

Greeley R.(1976) Mode of emplacement of basalt terrains and an analysis of mare volcanism in the Orientale basin. Proc.Lunar Sci.Conf.7th. 2747-2759.

Hartmann W.K.(1967) Lunar crater counts.III: Post mare and "Archimedian" variations.Comm.L.P.L.Univ.of Arizona. 6, 125-129.

Hawke B.R.,MacLaskey D.,McCord T.B.,Adams J.B., Head J.W., Pieters C.M., and Zisk S.H.(1979) Multispectral mapping of the Apollo 15-Apennine region: The identification and distribution of regional pyroclastic

deposits.Proc.Lunar Planet.Sci.Conf.10th.2995-3015.

Head J.W. (1975) Lunar mare deposits: Areas,volumes,sequence, and implication for melting in source areas.(abstract). In, Papers presented to the conference on origins of mare basalts and their implication for lunar evolution. The Lunar Science Institute,Houston,Texas.66-69.

Head J.W. (1976) Lunar volcanism in space and time. Rev. Geophys.Space Phys. 14, 265-300.

Head J.W. (1979) Lava flooding of early planetary crusts: Geometry, thickness, and volumes of flooded impact basins.(abstract) In, Lunar and Planetary Science X. The Lunar and Planetary Science Institute,Houston, Texas. 516-518.

Head J.W. and McCord T.B.(1978) Imbrian-age highland volcanism on the Moon: The Gruithuisen and Mairan domes. Science. 199, 1433-1436.

Head J.W. and Solomon S.C.(1980) Lunar basin structure:Possible influence of variations in lithosphere thickness. (abstract) In, Lunar and Planetary Science XI.The Lunar and Planetary Institute,Houston,Texas.

Head J.W. and Wilson L.(1980) The formation of eroded depressions around the sources of lunar sinuous rilles: Observations. (abstract) In, Lunar and Planetary Science XI. The Lunar and Planetary Institute,Houston,Texas.

Head J.W., Adams J.B.,McCord T.B.,Pieters C.M. and Zisk S.H. (1978) Regional stratigraphy and geologic history of Mare Crisium. In, Mare Crisium: The view from Luna 24. (R.B.Merrill and J.J.Papike, eds.)Pergamon,N.Y. 43-74.

Hood L.L.,Coleman P.J., and Wilhelms D.E.(1979) Lunar near-side magnetic anomalies. Lunar Planet.Sci.Conf.10th. 2235-2257.

Horz F. (1978) How thick are lunar mare basalts ? Proc.Lunar Planet.Sci.Conf.9th. 3311-3332.

Howard K.A., Head J.W., and Swann G.A.(1972) Geology of Hadley Rille. Proc.Lunar Sci.Conf.3rd. 1-14.

Hulme G. (1973) Turbulent lava flow and the formation of lunar sinuous rilles. Modern Geology. 4, 107-117.

Hulme G. (1974) The interpretation of lava flow morphology. Geophys.J.R.Astr.Soc. 39, 361-383.

Hulme G. and Fielder G. (1977) Effusion rates and rheology of lunar lavas. Phil.Trans.R.Soc.Lond.A. 285,227-234.

Johnson T.V.,Mosher J.A., and Matson D.L. (1977a) Lunar spectral units: A northern hemisphere mosaic. Proc. Lunar Sci.Conf.8th. 1013-1028.

Johnson T.V., Saunders R.S., Matson D.L. and Mosher J.A.(1977b) A TiO_2 abundance map for the lunar maria. Proc.Lunar Sci. Conf.8th, 1029-1036.

Kaula W.M.,Schubert G., Lingenfelter R.E.,Sjogren W.L., and Wollenhaupt W.R. (1973) Lunar topography from Apollo 15 and 16 laser altimetry.Proc.Lunar Sci.Conf. 4th. 2811-2819.

Kocharov G.E.,Borodulin N.F.,Victorov S.V.,Vorolaev O.M., Dzevanovskaya A.U.,Ivanov O.G.,Kieryan G.V.,Petrov V.V., and Sakulski V.A. (1971) The lunar automatic spectrometric apparatus "Rectma". In, The mobile laboratory

on the Moon: Lunakhod 1. Nauka, Moskva. 89-95(in Russ.)

Lucchitta B.K. (1977) Topography, structure, and mare ridges in southern Mare Imbrium and northern Oceanus Procellarum. Proc.Lunar Sci.Conf 8th. 2691-2703.

Lucchitta B.K. and Boyce J.M. (1979) Altitude-age relationships of the lunar maria.Proc.Lunar Planet.Sci.Conf. 10th. 2957-2966.

Lucchitta B.K. and Watkins J.A. (1978) Age of graben structures on the Moon. Proc.Lunar Planet.Sci.Conf.9th. 3459-3472.

Ma M-S., Schmitt R.A.,Warner R.D.,Taylor G.J., and Keil K. (1978) Genesis of Apollo 15 olivine normative mare basalts: Trace elements and concentrations. Proc. Lunar Planet.Sci.Conf.9th. 523-533.

Markov M.S., Sukhanov A.L.,Trivonov V.G.,Florenskiy P.V.,and Shkerin L.M. (1974) Geological mapping of the Moon.In, Current concepts regarding the Moon. NASA TT F-766. 97-138.

Marshall C.H. (1961) Thickness of the Procellarum System, Letronne region of the Moon. U.S.Geol.Survey Prof. Paper 424-D, 208-211.

Mason R.,Guest J.E., and Cooke G.N. (1976) An Imbrian pattern of graben on the Moon. Proc.Geol.Ass. 87, 161-168.

McCord T.B.,Pieters C.M., and Feierberg M.A. (1976) Multispectral mapping of the lunar surface using ground-based telescopes. Icarus.29,1-34.

McCord T.B.,Grabow M.,Feierberg M.A.,MacLaskey D. and Pieters C.M. (1979) Lunar multispectral maps: Part II of the

lunar nearside. Icarus.37, 1-28.

Metzger A.E.,Haines E.L.,Etchegaray-Ramirez M.I. and Hawke B.R. (1979) Thorium concentrations in the lunar surface:III. Deconvolution of the Apenninus region. Proc.Lunar Planet.Sci.Conf.10th. 1701-1718.

Metzger A.E.,Johnson T.V., and Matson D.L. (1979) A comparison of mare surface titanium concentrations obtained by spectral reflectance and gamma-ray spectroscopy: An early assessment. Proc.Lunar Planet.Sci.Conf.10th. 1719-1726.

M'Gonigle J.W. and Schleicher D. (1972) Geologic map of the Plato quadrangle of the Moon. U.S.geol.Survey Misc. Inv.Ser. Map I-701.

Moore H.J. and Schaber G.G. (1975) An estimate of the yield strength of the Imbrium flows. Proc.Lunar Sci.Conf.6th. 101-118.

Moore H.J.,Hodges C.A., and Scott D.H.(1974) Multi-ringed basins - illustrated by Orientale and associated features. Proc.Lunar Sci.Conf.5th. 71-100.

Moore H.J.,Arthur D.W.G., and Schaber G.G. (1978) Yield strengths of flows on the Earth, Mars, and Moon. Proc.Lunar Planet.Sci.Conf.9th. 3351-3378.

Muller P.M. and Sjogren W.L. (1968) Mascons: Lunar mass concentrations. Science. 161, 680-684.

Murase T. and McBirney A.R. (1970) Viscosity of lunar lavas. Science. 167, 1491-1493.

Neukum G. and Horn P. (1976) Effects of lava flows on lunar crater populations. The Moon. 15,205-222.

Nyquist L.E. (1977) Lunar Rb-Sr chronology. Phys.Chem.Earth. 10, 103-142.

Papanastassiou D.A. and Wasserburg G.J. (1973) Rb-Sr ages and initial strontium contents in basalts from Apollo 15. Earth Planet.Sci.Letters,17,324-337.

Papike J.J. and Vaniman D.T. (1978) Luna 24 ferrobasalts and the mare basalt suite: Comparative chemistry,mineralogy and petrology. In, Mare Crisium: The view from Luna 24 (R.B.Merrill and J.J.Papike,eds.) Pergamon,N.Y. 371-401.

Pieters C.M. (1978) Mare basalt types on the front side of the Moon: A summary of spectral reflectance data. Proc. Lunar Planet.Sci.Conf.9th 2825-2849.

Pieters C.M., and McCord T.B.(1976) Characterization of lunar mare basalt types: I. A remote sensing study using reflection spectroscopy of surface units. Proc.Lunar Sci.Conf.7th. 2677-2690.

Pike R.J. (1977) Size dependence in the shape of fresh impact craters on the Moon. In,Impact and Explosion Cratering. (eds. D.J.Roddy et al.) Pergamon,N.Y. 489-509.

Pohn H.A. and Wildey R.L. (1970) A photoelectric-photographic study of the normal albedo of the Moon. U.S.Geol.Survey Prof. Paper 599-E.

Pratt D.D.,Moore C.B.,Parsons M.L., and Anderson D.L. (1977) Applications of a new logical search on the lunar data base for use in pattern recognition classification of Apollo 15 mare basalts.Proc.Lunar Sci.Conf.8th.1839-1847

Russell C.T.,Coleman P.J.,Lichtenstein B.R.,Schubert G. and

Sharp L.R. (1974) Apollo 15 and 16 subsatellite measurements of the lunar magnetic field. Space Res. 14, 629-634.

Saito Y. (1977) Sinuous rilles in western Mare Imbrium. Contrb. Kwasan and Hida Obs.Univ.Tokyo, No.234.

Schaber G.G. (1973) Lava flows in Mare Imbrium: Geological evaluation from Apollo orbital photography. Proc. Lunar Sci.Conf.4th. 73-92.

Schaber G.G.,Eggleton R.E., and Thompson T.W. (1970) Lunar radar mapping: Correlation between radar reflectivity and stratigraphy in north-western Mare Imbrium. Nature, 226, 1236-1239.

Schaber G.G.,Thompson T.W., and Zisk S.H. (1975) Lava flows in Mare Imbrium: An evaluation of anomalously low earth-based radar reflectivity. The Moon, 13, 395-423.

Schaber G.G.,Boyce J.M., and Moore H.J. (1976) The scarcity of mappable flow lobes on the lunar maria: Unique morphology of the Imbrium flows. Proc.Lunar Sci.Conf.7th. 2783-2800.

Schubert G.,Smith B.F.,Sonett C.P.,Colburn D.S. and Schwartz, K. (1974) Polarized magnetic field fluctuations at the Apollo 15 site: Possible regional influence on lunar induction. Science,183, 1194-1197.

Schultz P.H. and Spudis P.D. (1979) Evidence for ancient mare volcanism. Proc.Lunar Planet.Sci.Conf.10th.2899-2918.

Settle M. and Head J.W. (1976) Excavation depths of large lunar impacts: Shallow or deep ? In, Interdisciplinary Studies by the Imbrium Consortium,Volume 1. Center for

Astrophysics,Smithsonian,Cambridge,Mass. 139-146.

Settle M. and Head J.W. (1977) Radial variation of lunar crater rim topography. Icarus,31, 123-135.

Settle M. and Head J.W. (1979) The role of rim slumping in the modification of lunar impact craters. J.Geophys. Res. 84, 3081-3096.

Sharp L.R.,Coleman P.J.,Lichtenstein B.R.,Russell C.T. and Schubert G. (1973) Orbital mapping of the lunar magnetic field. The Moon, 7, 322-341.

Sjogren W.L.,Muller P.M.,Gottlieb P.,Wong L.,Buechler G.,Downs, W. and Prislin R. (1971) Lunar surface mass distribution from dynamical point-mass solution. The Moon, 2, 338-353.

Soderblom L.A. and Lebofsky L.A. (1972) Technique for rapid determination of relative ages of lunar areas from Orbiter photography. J.Geophys.Res. 77, 279-296.

Solomon S.C. and Head J.W. (1979) Vertical movement in mare basins: Relation to mare emplacement, basin tectonics, and lunar thermal history.J.Geophys.Res.84, 1667-1682.

Spudis P.D. (1978) Composition and origin of the Apennine Bench Formation. Proc.Lunar Planet.Sci.Conf.9th. 3379-3394.

Thurber C.H. and Solomon S.C. (1978) An assessment of crustal thickness variations on the lunar near side: Models, uncertainties, and implications for crustal differentiation.Proc.Lunar Planet.Sci.Conf.9th.3481-3497.

Todhunter R. (1975) A descriptive account of the geomorphology of southwest Mare Imbrium interpreted with the aid of a comparative study of selected Icelandic lava flows. Unpublished Ph.D. thesis, University of Lancaster.

Turkevich A.L. (1971) Comparison of the analytical results from the Surveyor, Apollo, and Luna missions. Proc. Lunar Sci. Conf.2nd. 1209-1215.

Turner G.(1977) Potassium-argon chronology of the Moon. Phys.Chem.Earth, 10, 145-195.

Ulrich G.E. (1969) Geologic map of the J.Herschel quadrangle of the Moon. U.S.Geol.Survey Misc.Inv.Ser.Map I-604.

Whitaker E.A. (1972) Lunar color boundaries and their relationship to topographic features: A preliminary survey. The Moon, 4, 348-355.

Whitford-Stark J.L. (1979) Charting the Southern Seas: The evolution of the lunar Mare Australe. Proc.Lunar Planet. Sci.Conf.10th. 2975-2994.

Whitford-Stark J.L. and Head J.W. (1980) Stratigraphy of Oceanus Procellarum basalts: Sources and styles of emplacement. J.Geophys.Res. in press.

Wilhelms D.E. and McCauley J.F. (1971) Geologic map of the nearside of the Moon. U.S.Geol.Survey Misc.Inv.Ser. Map I-495.

APPENDIX

Catalog of the morphometric parameters of 372 craters within Mare Imbrium. R is the predicted rim height from equation 1 of the text. R_2 and R_3 are the rim heights predicted from equations 6 through 9 of the text. R_3 values are indicated by *. F is the depth of flooding. E is the excavation depth determined from equation 11 of the text. The symbol # denotes unreliable data due to unusual crater shape.

Crater No.	Name	Location	Diameter (km)	Ejecta width (km)	R (km)	R_2 or R_3 (km)	F (m)	E (km)	Unit
1	-	46.6N 32.6W	4.07	0.68	0.15	0.10	50	0.80	7
2	-	45.2N 34.6W	3.39	1.19	0.12	0.09*	30	0.67	7
3	-	44.5N 33.1W	2.71	0.51	0.10	0.07	30	0.53	7
4	-	43.25N 33.25W	3.05	1.02	0.11	0.08*	20	0.60	7
5	Heraclides E	43.0N 32.6W	4.14	0.99	0.15	0.14	10	0.82	7
6	-	42.5N 32.6W	2.58	0.24	0.09	0.03	60	0.51	7
7	-	41.9N 33.6W	2.37	0.51	0.09	0.07	20	0.46	7
8	-	43.0N 31.0W	1.97	0.24	0.07	0.03	40	0.38	6
9	-	42.8N 30.5W	2.65	0.54	0.10	0.08	20	0.52	6
10	-	42.4N 30.0W	2.37	0.58	0.09	0.08	10	0.46	6
11	-	43.6N 28.6W	2.65	0.54	0.10	0.08	20	0.52	6
12	-	45.7N 32.0W	1.90	0.58	0.07	0.05*	20	0.37	7
13	-	40.5N 30.0W	1.63	0.07	0.06	0.01	50	0.32	9
14	-	40.4N 29.0W	1.29	0.10	0.05	0.01	40	0.25	9
15	-	39.9N 32.5W	2.85	0.48	0.10	0.07	30	0.56	9
16	-	39.3N 31.0W	1.70	0.34	0.06	0.05	10	0.33	5
17	-	39.3N 30.6W	2.37	2.14	0.09	0.10*	-10	0.46	5

18	-	38.8N 32.4W	1.76	0.34	0.06	0.05	10	0.34	5
19	Heraclides F	38.6N 33.8W	3.12	0.48	0.11	0.07	20	0.61	5
20	-	38.3N 36.4W	2.65	0.55	0.10	0.06	40	0.52	7
21	-	37.4N 35.2W	2.85	0.48	0.10	0.07	30	0.56	5
22	C Herschel V	36.5N 33.5W	3.60	0.65	0.13	0.09	40	0.71	5
23	C Herschel C	37.3N 32.6W	7.12	2.89	0.26	0.20*	60	1.42	5
24	-	37.4N 31.8W	2.04	0.41	0.07	0.06	10	0.40	5
25	C Herschel E	34.2N 34.7W	5.42	0.85	0.20	0.12	80	1.08	9
26	-	34.0N 33.2W	1.69	0.31	0.06	0.04	20	0.33	9
27	-	34.0N 32.1W	2.17	0.34	0.08	0.05	30	0.42	5
28	-	34.0N 31.4W	2.03	0.44	0.07	0.06	10	0.40	5
29	C Herschel	34.5N 31.2W	13.89	14.06	0.52	0.74*	-220	2.79	5
30	-	35.0N 32.4W	2.20	0.26	0.08	0.04	40	0.43	9
31	-	33.4N 30.6W	2.03	0.27	0.07	0.04	30	0.40	9
32	Heis	32.4N 31.9W	13.89	18.47	0.52	0.80*	-280	2.79	5
33	Heis A	32.6N 31.85W	6.10	1.36	0.23	0.19	140	1.21	5
34	-	34.6N 36.8W	2.28	0.41	0.08	0.06	20	0.45	9
35	-	32.9N 33.95W	1.69	0.34	0.06	0.05	10	0.33	9
36	-	33.1N 33.9W	1.36	0.27	0.05	0.04	10	0.26	9
37	-	33.3N 32.6W	2.64	0.38	0.10	0.05	50	0.52	5

38	-	35.9N 30.2W	1.69	2.88	0.66	0.12*	-60	0.33	5
39	-	35.3N 37.1W	2.35	0.24	0.09	0.03	60	0.46	9
40	-	45.7N 28.0W	2.04	0.48	0.07	0.07	00	0.40	6
41	Laplace A	43.8N 26.9W	8.42	6.66	0.31	0.34*	-30	1.68	6
42	-	43.8N 24.8W	1.70	0.38	0.06	0.05	10	0.33	9
43	-	44.6N 24.5W	2.38	0.34	0.09	0.05	40	0.47	9
44	-	45.9N 23.8W	1.63	0.27	0.06	0.04	20	0.32	9
45	-	45.5N 22.6W	3.06	0.54	0.11	0.08	30	0.60	9
46	-	45.0N 22.9W	1.43	0.03	0.05	0.00	50	0.28	9
47	-	44.5N 23.2W	1.70	0.07	0.06	0.01	50	0.33	9
48	Laplace FA	44.3N 20.5W	2.65	0.38	0.10	0.05	50	0.52	4
49	-	43.6N 20.8W	1.77	0.03	0.06	0.00	50	0.34	9
50	-	43.8N 21.4W	1.22	0.14	0.04	0.02	20	0.23	9
51	-	42.8N 23.8W	2.45	0.37	0.09	0.05	40	0.48	9
52	Helicon G	41.8N 24.8W	2.58	0.58	0.09	0.08	10	0.51	9
53	-	40.9N 25.4W	1.77	0.24	0.06	0.03	30	0.34	9
54	Helicon C	40.5N 25.6W	2.51	0.21	0.09	0.03	60	0.49	9
55	Helicon E	40.5N 24.1W	2.65	0.38	0.10	0.05	50	0.52	9
56	Helicon	40.5N 23.0W	24.18	2.86	0.84	0.56	280	4.89	9
57	-	40.1N 26.2W	1.22	3.13	0.04	0.12*	-60	0.23	9

58	-	40.05N 25.1W	0.88	1.23	0.03	0.05*	-20	0.17	9
59	-	39.4N 24.3W	1.22	0.11	0.04	0.02	20	0.23	9
60	-	39.3N 24.4W	1.43	0.14	0.05	0.02	30	0.28	9
61	Carlini S	37.9N 27.0W	4.21	0.82	0.15	0.12	30	0.83	5
62	-	38.3N 28.05W	2.24	0.28	0.08	0.04	40	0.44	5
63	-	38.0N 28.2W	1.97	0.31	0.07	0.04	30	0.38	9
64	-	38.8N 28.7W	2.11	0.37	0.08	0.05	30	0.41	5
65	-	38.9N 28.75W	1.83	0.28	0.07	0.04	30	0.36	5
66	-	39.1N 27.8W	1.36	0.24	0.05	0.03	20	0.26	9
67	-	36.0N 29.2W	2.79	0.44	0.10	0.06	40	0.55	9
68	-	35.95N 27.4W	1.77	0.17	0.06	0.02	40	0.34	9
69	-	36.4N 26.3W	2.11	0.03	0.08	0.04	40	0.41	9
70	Carlini A	34.4N 26.5W	6.52	4.55	0.24	0.24*	00	1.30	9
71	-	36.3N 31.5W	3.53	0.45	0.13	0.06	70	0.70	5
72	Carlini C	35.2N 22.8W	3.49	1.95	0.13	0.11*	20	0.69	9
73	-	34.4N 22.7W	1.68	0.20	0.06	0.03	30	0.33	9
74	-	34.9N 19.6W	2.28	0.27	0.06	0.04	20	0.45	9
75	-	33.9N 19.8W	1.48	0.47	0.05	0.04*	10	0.29	9
76	-	33.3N 21.6W	1.34	0.20	0.05	0.03	20	0.26	9
77	-	33.1N 21.6W	1.14	0.30	0.04	0.04	00	0.22	9

78	Carlini	33.8N 24.0W	10.53	1.95	0.39	0.27	120	2.11	9
79	Carlini H	32.3N 24.5W	3.56	0.57	0.13	0.08	50	0.70	9
80	Carlini G	32.6N 25.1W	3.82	0.64	0,14	0.09	50	0.75	9
81	-	32.0N 25.0W	2.42	0.47	0.09	0.07	20	0.47	9
82	-	46.1N 22.5W	2.40	0.34	0.09	0.05	40	0.47	9
83	-	46.8N 20.1W	1.99	0.21	0.07	0.03	40	0.39	4
84	Laplace F	45.6N 19.9W	6.30	1.14	0.23	0.16	70	1,25	4
85	-	44.8N 21.1W	2.33	0.07	0.08	0.01	70	0.46	9
86	-	44.4N 21.8W	1.71	0.04	0.06	0.01	50	0.33	9
87	-	45.1N 18.8W	1.64	0.14	0.06	0.02	40	0.32	4
88	Pico B	46.4N 15.5W	11.86	9.15	0.44	0.47*	-30	2.38	2
89	-	45.1N 16.4W	2.06	0.38	0.07	0.05	20	0.40	4
90	-	44.9N 16.6W	1.51	0.34	0.05	0.05	00	0.29	4
91	-	43.0N 20.4W	2.81	0.24	0.10	0.03	70	0.55	9
92	-	42.3N 19.6W	2.26	2.47	0.08	0.11*	-30	0.44	9
93	Le Verrier E	42.5N 17.0W	6.51	1.72	0.24	0.24	00	1.30	4
94	Le Verrier	40.5N 20.5W	21.24	9.77	0.80	0.88*	-80	4.29	9
95	-	39.9N 20.6W	3.70	0.35	0.14	0.05	90	0.73	9
96	Le Verrier S	38.9N 20.5W	2.47	0.93	0.09	0.07*	20	0.48	9
97	Helicon B	38.0N 21.2W	5.69	2.30	0.21	0.16*	50	1.13	9

98 -	38.1N 22.3W	1.44	0.52	0.05	0.04*	10	0.28	9
99 -	38.1N 22.4W	1.30	0.89	0.05	0.05*	00	0.25	9
100 Helicon BA	36.5N 20.8W	2.47	2.71	0.09	0.12*	-30	0.48	9
101 -	36.5N 20.6W	1.64	0.21	0.06	0.03	30	0.32	9
102 -	37.0N 19.2W	2.19	0.14	0.08	0.02	60	0.43	9
103 Pico BA	46.8N 14.1W	4.04	0.93	0.15	0.13	20	0.80	2
104 -	45.9N 14.7W	1.99	0.28	0.07	0.04	30	0.39	4
105 Le Verrier X	41.6N 12.1W	2.67	0.41	0.10	0.06	40	0.52	4
106 Le Verrier B	40.2N 12.8W	5.00	0.62	0.18	0.09	90	0.99	4
107 Le Verrier D	39.7N 10.5W	9.32	1.85	0.35	0.26	90	1.86	4
108 Le Verrier W	39.4N 13.9W	3.36	0.45	0.12	0.06	60	0.66	4
109 -	39.3N 13.1W	1.99	0.28	0.07	0.04	30	0.39	4
110 Le Verrier A	38.2N 17.2W	4.39	0.55	0.16	0.08	80	0.87	9
111 Le Verrier V	37.8N 14.2W	3.36	0.45	0.12	0.06	60	0.66	10
112 Le Verrier U	37.3N 13.2W	3.56	0.45	0.13	0.06	70	0.70	5
113 -	36.9N 15.8W	1.37	1.37	0.05	0.06*	-10	0.26	10
114 Carlini D	33.0N 16.0W	9.33	10.60	0.35	0.48*	-130	1.86	5
115 Carlini DB	32.9N 15.2W	2.88	0.65	0.11	0.09	20	0.57	5
116 Carlini DA	32.2N 15.0W	3.09	0.38	0.11	0.05	60	0.61	5
117 -	46.6N 12.2W	1.71	0.55	0.06	0.04*	-20	0.33	4

118 Pico G	46.6N 10.4W	4.23	0.69	0.16	0.10	60	0.84	4
119 -	46.6N 9.7W	2.46	0.48	0.09	0.07	20	0.48	4
120 Pico K	44.6N 7.6W	3.21	1.64	0.12	0.10*	20	0,63	4
121 Pico D	43.4N 11.2W	6.42	4.30	0.24	0.23*	-10	1.28	4
122 Pico EA	43.4N 10.5W	3.48	0.38	0.13	0.05	80	0.69	4
123 Pico E	43.0N 10.4W	9.69	7.11	0.36	0.37*	-10	1.94	4
124 -	43.6N 9.5W	1.84	0.52	0.07	0.07	00	0.36	4
125 Picò F	42.4N 10.2W	3.82	1.16	0.14	0.10*	40	0.75	4
126 -	42.5N 7.0W	1.98	0.51	0.07	0.07	00	0.39	7
127 -	41.6N 6.4W	1.98	0.17	0.07	0.02	50	0.39	7
128 Piazzi Smyth M	45.1N 4.2W	2.46	0.24	0.09	0.03	60	0.48	7
129 -	44.6N 4.6W	2.39	0.38	0.09	0.05	40	0.47	7
130 -	44.3N 3.2W	1.71	0.01	0.06	0.00	60	0.33	7
131 -	43.2N 3.1W	2.39	0.38	0.09	0.05	40	0.47	7
132 -	43.1N 2.9W	2.32	0.41	0.08	0.06	20	0.45	7
133 Piazzi Smyth Y	42.8N 3.4W	3.69	0.44	0.14	0.06	80	0.73	7
134 Piazzi Smyth Z	42.1N 4.6W	2.53	0.44	0.09	0.06	30	0.50	7
135 Piazzi Smyth V	40.9N 4.8W	8.06x3.75	0.07	0.30	0.01	290	----	7 #
136 Piazzi Smyth	41.8N 3.3W	12.90	17.79	0.48	0.76*	-280	2.59	7
137 Piazzi Smyth B	40.5N 3.4W	3.82	2.87	0.14	0.15*	-10	0.75	7

138 -	40.05N 5.7W	2.05	0.21	0.07	0.03	40	0.40	7
139 -	39.5N 5.8W	2.18	0.48	0.08	0.07	10	0.43	7
140 Kirch	39.3N 5,8W	11.88	10.79	0.44	0.53*	-90	2,38	7
141 -	39.4N 4.8W	1.71	0.34	0.06	0,05	10	0.33	7
142 Kirch K	39.3N 4.0W	2.46	0.48	0.09	0.07	20	0.48	7
143 Kirch H	39.1N 6.9W	2.87	0.62	0.10	0.09	10	0.56	7
144 -	39.2N 8.0W	1.50	0.41	0.05	0.04*	10	0.29	7
145 -	39.1N 8.2W	1.78	0.34	0.06	0.05	10	0.35	7
146 Kirch M	39.6N 10.0W	3.14	0.58	0.11	0.08	30	0.62	4
147 -	39.8N 9.5W	1.37	0.17	0.05	0.02	30	0.26	4
148 -	40.7N 9.8W	1.91	0.55	0.07	0.05*	20	0.37	4
149 -	41.6N 11.2W	1.57	0.17	0.06	0.02	40	0.30	4
150 -	40.7N 12.1W	2.05	0.41	0.07	0.06	10	0.40	4
151 -	40.6N 10.9W	2.05	0.48	0.07	0.07	00	0.40	4
152 -	39.5N 10.9W	2.12	0.44	0.08	0.06	20	0.41	4
153 -	37.7N 10.8W	2.18	0.45	0.08	0.06	20	0.41	4
154 Kirch G	37.4N 8.05W	2.80	0.51	0.10	0.07	30	0.55	4
155 Kirch E	36.5N 6.9W	3.48	3.04	0.13	0.15*	-20	0.69	9
156 Kirch F	38.0N 6.0W	4.16	0.82	0.15	0.12	30	0.82	7
157 -	35.7N 6.9W	2.25	0.41	0.08	0.06	20	0.44	9

158 -	37.5N 12.1W	2.18	0.11	0.08	0.02	60	0.41	4
159 -	36.6N 11.6W	2.18	0.45	0.08	0.06	20	0.41	4
160 Pico C	47.2N 6.6W	4.78	6.48	0.18	0.28*	-100	0.95	3
161 -	47.5N 4.5W	2.25	0.75	0.08	0.06*	20	0.46	3
162 -	47.4N 4.3W	2.32	0.55	0.08	0.08	00	0.45	3
163 -	47.35N 4.2W	3.21	0.62	0.12	0.09	30	0.63	3
164 Plato KB	47.3N 4.6W	3.75	2.39	0.14	0.13*	10	0.74	3
165 -	47.0N 3.9W	2.66	0.72	0.10	0.10	00	0.52	3
166 -	46.9N 3.9W	2.12	0.82	0.08	0.06*	20	0.41	3
167 Plato KA	46.8N 3.8W	5.80	4.27	0.21	0.22*	-10	1.15	3
168 Plato K	46.85N 3.4W	6.82	5.46	0.25	0.28*	-30	1.36	3
169 -	43.4N 0.4W	2.46	0.65	0.09	0.09	00	0.48	7
170 -	43.25N 0.6E	1.98	0.58	0.07	0.05	20	0.39	7
171 -	42.4N 0.05W	2.32	0.72	0.08	0.05*	30	0.45	7
172 Piazzi Smyth W	42.2N 1.9W	3.21	0.44	0.12	0.06	60	0.63	7
173 -	41.9N 2.05W	2.18	0.48	0.08	0.07	10	0.43	7
174 Piazzi Smyth U	40.9N 2.8W	2.87	0.44	0.10	0.06	40	0.56	7
175 Piton A	39.8N 0.9W	5.73	0.72	0.21	0.10	110	1.14	7
176 Piton B	39.4N 0.2W	4,64	3.48	0.17	0.18*	-10	0.92	4
177 Spitzbergensis D	33.3N 8.6W	3.25	0.68	0.12	0.10	20	0.64	5

178	Spitzbergensis C	32.9N	8.7W	6.23	1.05	0.23	0.15	80	1.24	5
179	-	33.6N	8.4W	1.35	0.55	0.05	0.04*	10	0.26	9
180	Spitzbergensis A	32.8N	7.2W	6.23	5.69	0.23	0.28*	-50	1.24	5
181	-	33.5N	5.4W	1.76	0.00	0.60	0.00	60	0.34	9
182	-	33.3N	5.5W	1.83	0.27	0.07	0.04	30	0.36	9
183	-	32.7N	5.9W	1.76	0.21	0.06	0.03	30	0.34	9
184	-	33.4N	4.3W	2.23	0.45	0.08	0.06	20	0.44	4
185	Archimedes V	32.9N	3.95W	2.71	0.51	0.10	0.07	30	0.53	4
186	Aristillus B	34.8N	1.9W	7.86	0.81	0.29	0.11	180	1.57	4
187	-	34.5N	0.9W	2.71	0.37	0.10	0.05	50	0.53	4
188	Archimedes U	32.9N	1.95W	2.64	0.07	0.10	0.01	90	0.52	4
189	Archimedes D	32.2N	2.6W	4.74	1.36	0.17	0.12*	50	0.94	4
190	Cassini	40.2N	4.6E	55.97	11.61	1.18	1.09	90	-	-
191	Aristillus	33.8N	1.1E	54.20	182.90	1.16	1.85*	-690	-	-
192	Aristillus A	33.8N	4.4E	4.25	0.28	0.16	0.04	120	0.84	7
193	Angstrom	29.8N	41.7W	6.27	9.41	0.23	0.39*	-160	1.25	1
194	-	29.6N	39.5W	1.88	0.35	0.07	0.05	20	0.37	9
195	-	29.5N	39.0W	1.82	0.19	0.07	0.03	40	0.35	9
196	-	29.0N	38.2W	3.01	0.44	0.11	0.06	50	0.59	9
197	-	28.6N	38.8W	1.63	0.32	0.06	0.04	20	0.32	9

198 -	29.5N 38.1W	1.88	0.03	0.07	0.00	70	0.37	9
199 -	27.8N 39.2W	2.01	0.56	0.07	0.07*	00	0.39	1
200 Diophantus A	27.7N 36.5W	7.77	5.99	0.29	0.31*	-20	1.55	5
201 -	26.8N 37.0W	2.13	0.32	0.08	0.04	40	0.42	5
202 -	24.5N 40.7W	2.32	0.66	0.08	0.06*	20	0.45	-
203 -	21.9N 39.2W	1.94	0.97	0.07	0.04*	30	0.38	-
204 Brayley C	21.4N 39.4W	8.40	2.70	0.31	0.22*	90	1.68	-
205 Brayley E	21.3N 39.7W	4.89	5.08	0.18	0.24*	-60	0.97	-
206 -	20.2N 38.1W	2.19	1.26	0.08	0.07*	10	0.43	9
207 -	20.1N 38.3W	1.82	0.35	0.07	0.05	20	0.35	9
208 -	19.8N 38.7W	2,57	0.47	0.09	0.07	20	0.50	-
209 -	19.8N 37.8W	2.70	0.41	0.10	0.06	40	0.53	-
210 Bessarion D	19.8N 41.6W	9.53	1,51	0.35	0.21	140	1.91	-
211 -	20.7N 41.4W	2.13	0.66	0.08	0.05*	30	0.42	-
212 Brayley K	21.2N 41.7W	3.26	0.57	0.12	0.08	40	0.64	-
213 -	22.2N 41.0W	1.88	0.03	0.07	0.00	70	0.37	-
214 -	22.3N 40.9W	1.69	0.01	0.06	0.00	60	0.33	-
215 Diophantus B	29.0N 32.4W	6.04	4.14	0.22	0.22*	00	1.20	5
216 -	28.5N 34.2W	2.05	2.40	0.07	0.11*	-40	0.40	5
217 Diophantus	27.6N 34.3W	17.55	33.55	0.74	0.98*	-240	3.53	5

218 Diophantus C	27.3N 34.6W	4.73	1.37	0.17	0.12*	50	0.94	5
219 -	27.9N 31.5W	1.87	1.09	0.07	0.06*	10	0.37	9
220 -	27.6N 35.4W	1.74	0.25	0.06	0.04	20	0.34	5
221 Diophantus D	26.9N 36.3W	3.98	0.66	0.15	0.09	60	0.79	5
222 -	26.2N 35.7W	2.36	0.32	0.09	0.04	50	0.46	5
223 -	26.8N 35.1W	1.62	0.34	0.06	0.05	10	0.31	5
224 -	26.2N 34.9W	1.18	0.97	0.04	0.05*	-10	0.23	5
225 -	26.3N 33.1W	1.56	0.28	0.06	0.04	20	0.30	9
226 -	25.3N 32.9W	1.80	0.28	0.07	0.04	30	0.35	9
227 Euler E	24.7N 34.0W	6.16	3.30	0.23	0.20*	30	1.22	9
228 Brayley S	25.1N 36.6W	2.92	0.50	0.11	0.07	40	0.57	9
229 -	23.8N 33.1W	1.93	0.30	0.07	0.04	30	0.38	9
230 -	24.4N 32.9W	1.49	1.75	0.05	0.08*	-30	0.29	10
231 -	23.5N 30.9W	2.43	0.65	0.09	0.09	00	0.48	10
232 Euler J	23.3N 31.7W	3.67	0.53	0.13	0.07	60	0.72	10
233 -	22.6N 32.8W	1.99	0.56	0.07	0.05*	20	0.39	9
234 -	22.8N 35.5W	1.99	0.28	0.07	0.04	30	0.39	9
235 -	23.1N 36.6W	1.93	0.28	0.07	0.04	30	0.38	9
236 Brayley	20.9N 36.9W	14.13	2.58	0.53	0.36	170	2.84	9
237 Brayley F	21.1N 34.0W	4.42	1.53	0.16	0.12*	40	0.87	9

238 Brayley B	20.8N 34.3W	9.46	8.34	0.35	0.41*	-60	1.89	9
239 -	20.1N 33.7W	2.24	0.44	0.08	0.06	20	0.44	-
240 Brayley	20.0N 32.8W	7.47	3.11	0.28	0.21*	70	1.49	0
241 Euler K	20.6N 31.9W	4.67	2.96	0.17	0.16*	10	0.92	0
242 -	19.5N 34.1W	2.12	0.25	0.08	0.04	40	0.41	-
243 -	19.45N 34.5W	1.93	0.44	0.07	0.06	10	0.38	-
244 -	18.2N 32.8W	2.61	0.28	0.10	0.04	60	0.51	0
245 -	30.5N 31.0W	2.03	0.25	0.07	0.04	30	0.40	10
246 -	29.9N 30.8W	2.60	0.33	0.09	0.05	40	0.51	10
247 -	29.8N 30.7W	2.85	0.16	0.10	0.02	80	0.56	10
248 La Hire D	29.8N 29.4W	2.91	0.16	0.11	0.02	90	0.57	9
249 -	27.2N 29.9W	2.22	0.48	0.08	0.07	10	0.43	10
250 -	26.7N 30.7W	1.77	0.26	0.06	0.04	20	0.34	10
251 -	27.3N 31.8W	1.96	0.48	0.07	0.07	00	0.38	9
252 -	26.0N 29.5W	2.22	0.63	0.08	0.05*	30	0.43	10
253 Euler H	25.4N 28.2W	3.86	2.19	0.14	0.13*	10	0.76	10
254 Euler	23.3N 29.3W	26.91	48.30	0.88	0.86*	20	5.45	0
255 -	22.6N 29.4W	2,41	0.54	0.09	0.08	10	0.47	0
256 Euler P	20.0N 31.1W	11.40	1.42	0.42	0.20	220	2.28	0
257 Heis D	31.7N 30.9W	7.85	4.37	0.29	0.26*	30	1.57	5

258 -	31.8N 33.8W	2.44	0.51	0.09	0.07	20	0.48	5
259 -	31.85N 34.3W	1.76	0.65	0.06	0.05*	10	0.34	5
260 -	31.95N 35.0W	2.37	1.05	0.09	0.07*	20	0.46	5
261 -	31.7N 35.8W	2.23	0.44	0.08	0.06	20	0.44	5
262 Delisle	30.0N 34.5W	24.03	32.65	0.84	1.00	-160	4.86	5
263 -	29.7N 35.1W	2.44	0.41	0.09	0.06	30	0.48	5
264 -	29.4N 26.1W	1.67	0.44	0.06	0.06	00	0.32	10
265 -	29.0N 27.0W	1.79	0.38	0.06	0.05	10	0.35	10
266 -	27.5N 27.7W	2.10	0.62	0.08	0.05*	30	0.41	10
267 -	26.9N 28.2W	2.17	0.62	0.08	0.05*	30	0.42	10
268 -	26.4N 27.6W	1.67	0.25	0.06	0.04	20	0.32	10
269 -	25.9N 28.2W	2.17	0.65	0.08	0.05*	30	0.42	10
270 Euler L	21.5N 29.0W	3.96	2.04	0.15	0.13*	20	0.78	0
271 Euler G	20.4N 27.6W	3.90	0.74	0.14	0.10	40	0.77	0
272 -	19.5N 25.5W	2.23	0.47	0.08	0.07	10	0.44	0
273 Carlini L	31.3N 24.9W	2.94	0.47	0.11	0.07	40	0.58	9
274 Carlini K	31.1N 23.8W	3.35	0.33	0.12	0.05	70	0.66	9
275 La Hire A	28.6N 23.7W	4.62	1.87	0.17	0.13*	40	0.91	5
276 La Hire B	27.8N 23.0W	3.68	0.84	0.13	0.12	10	0.73	5
277 -	27.5N 23.0W	2.48	0.60	0.09	0.08	10	0.49	10

278 -	27.3N 23.8W	2.34	0.34	0.12	0.05	70	0.46	10
279 -	28.8N 22.0W	2.41	0.30	0.09	0.04	50	0.47	10
280 Carlini B	30.3N 21.0W	7.28	2.06	0.27	0.18*	90	1.45	5
281 Carlini E	31.7N 20.6W	1.24	1.92	0.04	0.08*	-40	0.24	10
282 -	31.2N 19.4W	2.33	0.42	0.08	0.06	20	0.46	5
283 -	31.8N 20.2W	1.85	0.01	0.07	0.00	70	0.36	5
284 Timocharis F	31.3N 14.8W	6.18	5.15	0.23	0.26*	-30	1.23	0
285 Lambert I	28.5N 20.2W	3.02	0.45	0.11	0.06	50	0.59	5
286 -	29.0N 20.6W	2.26	0.25	0.08	0.04	40	0.44	10
287 Lambert S	27.6N 21.1W	2.47	0.48	0.09	0.07	20	0.48	5
288 Lambert A	26.5N 21.5W	3.84	0.55	0.14	0.08	60	0.76	0
289 Lambert	25.9N 20.9W	30.20	44.25	0.92	0.92*	00	6.12	5
290 -	27.5N 18.8W	1.99	0.89	0.07	0.06*	10	0.39	9
291 Timocharis E	24.7N 17.1W	4.05	0.72	0.15	0.10	50	0.80	0
292 -	24.6N 22.4W	2.47	0.35	0.09	0.05	40	0.48	0
293 -	30.6N 13.6W	2.19	0.62	0.08	0.05*	30	0.43	0
294 Archimedes Y	30.0N 9.6W	2.47	0.14	0.09	0.02	70	0.48	5
295 Sampson	29.6N 16.5W	1.85	0.31	0.07	0.04	30	0.36	0
296 -	28.3N 16.3W	2.19	0.48	0.08	0.07	10	0.43	0
297 -	26.6N 16.1W	2.33	0.41	0.08	0.06	20	0.46	0

298 Timocharis AA	25.7N 15.0W	2.40	0.52	0.09	0.07	20	0.47	0
299 -	25.3N 15.3W	2.47	0.34	0.09	0.05	40	0.48	0
300 -	25.2N 15.6W	3.29	0.45	0.12	0.06	60	0.65	0
301 Timocharis A	24.9N 15.5W	7.20	1.71	0.27	0.24	30	1.43	0
302 Timocharis C	24.9N 14.2W	3.63	0.76	0.13	0.11	20	0.72	0
303 Timocharis	26.8N 13.0W	33.92	58.43	0.96	1.23*	-270	6.88	0
304 Timocharis B	27.9N 12.2W	5.07	1.07	0.19	0.15	40	1.00	0
305 Feuillee	27.4N 9.9W	9.32	1.00	0.35	0.14	210	1.86	8
306 Beer	27.2N 9.1W	8.91	1,24	0.33	0.17	260	1.78	-
307 -	26.0N 10.1W	2.54	0.48	0.09	0.07	20	0.50	8
308 -	23.9N 22.4W	1.98	0.13	0.07	0.02	50	0.39	0
309 -	23.4N 23.2W	2.10	0.19	0.08	0.03	50	0.41	0
310 Pytheas W	21.9N 23.8W	2.85	1.24	0.10	0.08*	20	0.56	10
311 -	21.8N 22.2W	2.17	0.19	0.08	0.03	50	0.42	0
312 Pytheas J	21.8N 21.1W	3.34	0.47	0.12	0.07	50	0.66	0
313 Pytheas N	22.6N 20.4W	3.16	0.59	-.12	0.08	40	0.62	0
314 Pytheas D	21.2N 20.5W	5.08	0.56	0.19	0.08	110	1.01	0
315 Pytheas A	20.5N 21.7W	5.76	1.15	0.21	0.16	50	1.14	0
316 Pytheas	20.5N 20.5W	18.39	18,05	0.75	0.82*	-70	3.71	0
317 Timocharis D	24.0N 15.2W	2.98	0.40	0.11	0.06	50	0.59	0

318 Timocharis H	23.8N 16.6W	2.25	0.24	0.08	0.03	50	0.44	0
319 -	21.4N 16.7W	1.94	0.85	0.07	0.06*	10	0.38	0
320 Pytheas G	21.8N 17.8W	3.64	0.49	0.13	0.07	60	0.72	0
321 Pytheas M	20.0N 17.8W	2.79	0.43	0.10	0.06	40	0.55	0
322 Pytheas H	20.6N 16.6W	2.43	0.55	0.09	0.08	10	0.48	0
323 Pytheas K	20.0N 16.2W	2.19	0.49	0.08	0.07	10	0.43	0
324 -	24.5N 8.9W	2.29	0.35	0.08	0.05	30	0.45	8
325 Timocharis K	23.8N 11.0W	2.16	0.11	0.08	0.03	50	0.42	8
326 Wallace H	21.3N 9.0W	2.03	0.38	0.07	0.05	20	0.40	0
327 -	20.8N 11.7W	1.65	0.48	0.06	0.04*	20	0.32	0
328 -	17.6N 25.6W	2.11	0.06	0.08	0.01	70	0.41	0
329 -	17.5N 24.9W	1.98	0.25	0.07	0.04	30	0.39	0
330 -	17.4N 24.9W	1.67	0.25	0.06	0.04	20	0.32	0
331 Draper A	17.9N 23.4W	3.96	0.87	0.15	0.12	30	0.78	0
332 -	17.2N 22.8W	2.23	0.44	0.08	0.06	20	0.44	0
333 Draper	17.6N 21.7W	8.55	0.68	0.32	0.10	210	1.71	0
334 Draper C	17.1N 21.5W	7.43	3.41	0.28	0.22*	60	1.48	0
335 -	16.9N 21.6W	3.10	0.31	0.11	0.04	70	0.61	0
336 -	16.4N 22.1W	3.28	0.59	0.12	0.08	40	0.65	0
337 Tobias Mayer GA	18.2N 27.7W	4.62	0.77	0.17	0.11	60	0.91	0

338 Tobias Mayer G	17.4N 27.2W	6.78	4.47	0.25	0.25	00	1.35	O
339 -	18.7N 16.9W	2.54	0.48	0.09	0.07	20	0.50	O
340 Pytheas L	18.7N 16.9W	2.79	0.67	0.10	0.09	10	0.55	O
341 -	16.8N 15.1W	2.47	0.42	0.09	0.06	30	0.48	O
342 Eratsothenes C	17.0N 12.8W	5.20	0.57	0.19	0.08	110	1.03	O
343 -	17.9N 12.3W	2.54	0.32	0.09	0.04	50	0.50	O
344 -	17.0N 11.8W	2.18	0.32	0.08	0.04	40	0.43	O
345 Eratosthenes D	17.5N 10.9W	3.99	0.35	0.15	0.05	100	0.79	O
346 Eratosthenes B	18.6N 8.8W	5.40	1.11	0.20	0.16	40	1.07	9
347 Eratosthenes A	18.3N 8.4W	6.03	1.43	0.22	0.20	20	1.20	9
348 Wallace	20.4N 8.7W	24.12	2.39	0.84	0.51	330	4.88	O
349 Wallace T	21.9N 5.1W	2.54	0.35	0.09	0.05	40	0.50	O
350 Wallace B	20.2N 5.1W	3.76	0.63	0.14	0.09	50	0.74	O
351 Archimedes AA	28.7N 6.3W	2.51	0.47	0.09	0.07	20	0.49	5
352 Archimedes	29.5N 4.0W	82.80	13.18	1.37	1.16	210	-	5
353 Archimedes Q	28.5N 2.4W	2.45	0.35	0.09	0.05	40	0.48	5
354 Archimedes K	27.9N 1.2W	12.86	1.10	0.48	0.15	330	2.58	5
355 -	26.6N 2.2E	2.01	0.31	0.07	0.04	30	0.39	5
356 -	26.5N 2.2E	2.07	0.22	0.08	0.03	50	0.40	5
357 Archimedes T	30.3N 5.0W	2.51	0.25	0.09	0.04	50	0.49	5

358	Archimedes AB	28.8N	7.0W	2.19	0.28	0.08	0.04	40	0.43	5
359	Archimedes G	29.2N	8.2W	3.15	0.55	0.12	0.08	40	0.62	5
360	Archimedes X	31.0N	8.0W	2.12	1.51	0.08	0.08*	00	0.41	5
361	Archimedes C	31.6N	1.6W	7.88	1.37	0.29	0.19	100	1.57	4
362	Autolycus	30.5N	1.3E	39.26	34.52	1.02	1.08*	-60	7.98	-
363	-	30.6N	4.8E	2.46	0.41	0.09	0.06	30	0.48	8
364	Autolycus K	31.2N	5.5E	2.94	0.28	0.11	0.04	70	0.58	4
365	-	25.5N	5.9E	2.46	0.41	0.09	0.06	30	0.48	4
366	Hadley	30.9N	2.7E	5.68	1.61	0.21	0.14*	70	1.13	7
367	Plato D	49.7N	14.5E	9.36	5.69	0.35	0.32*	30	1.87	2
368	Plato E	49.8N	16.2W	6.69	4.68	0.25	0.25*	00	1.33	9
369	Plato X	50.2N	13.8W	4.55	1.74	0.17	0.12*	50	0.90	2
370	-	50.7N	17.8W	2.54	0.34	0.09	0.05	40	0.50	2
371	-	50.8N	17.0W	2.14	0.40	0.08	0.06	20	0.42	9
372	-	49.2N	22.3W	3.01	0.57	0.11	0.08	30	0.59	2

STORMS AND RAINS: A COMPARISON OF THE LUNAR MARE IMBRIUM AND OCEANUS PROCELLARUM

J.L.WHITFORD-STARK

Dept of Geological Sciences
Brown University
Providence, R.I., 02912, U.S.A.

ABSTRACT

The origin and development of the irregular Oceanus Procellarum and circular Mare Imbrium is compared. Imbrium is shown to be a deeply flooded(3 to 8 km), multi-ring basin with a complex eruption history involving at least ten major basalt units with no apparent simple chemical trend. Procellarum is hypothesized to be a down-faulted region of highland crust; the motion a direct result of the Imbrium basin-forming event. The basalt fill in Procellarum is thin (average 550 m) and is separated into four chemically distinct formations. KREEP basalts formed an important additional component of the early fill of both basins. Breccia fragments returned from the landing sites indicate pre-basinal basaltic volcanism. In both maria the youngest basalts were erupted from vents near the periphery and the styles in both were similar though Procellarum lacks the young, titanium-rich, short-duration, flood-style basalts of Imbrium and contains three unique volcanic complexes. Basalts of differing chemistries were synchronously erupted in each mare.

The tectonic evolution of both maria was similar; mare ridges being synchronously produced and graben formation terminating at 3.3 $\pm$ 0.3 b.y. in both. The distribution of the tectonic products in both maria differed as a result of the different distribution of the basalt loads and crustal thickness variations. The sub-

Procellarum lithosphere being less than 25 km thick at the time of graben production while that of Imbrium being 50 to 75 km thick. Currently available models for mare basalt petrogenesis do not satisfy the remote-sensing and photogeologic observations of basin filling.

Introduction:

Mare basalts flood the topographically low areas of the lunar surface; the majority of these lows were circular basins, though irregular, non-basinal areas were also flooded. It appears that a lunar crustal thickness asymmetry (Kaula et al,1972) has led to the preferential emplacement of mare basalts on the lunar near side which overall, relative to a 1738 km radius sphere, is lower than the far. The purpose of this paper is to outline the development of a circular and a non-circular mare area in terms of the volumes and chemistries of erupted materials, the chronology of eruptions, and the varying styles of volcanism. The evolution of the basaltic fill is further related to the tectonic history. Mare Imbrium is used as the type example of a circular mare and Oceanus Procellarum, the irregular mare. The basaltic fill of other lunar maria are employed to illustrate specific points which, because of a lack of data, cannot be made by reference to Imbrium and Procellarum alone.

Morphology of the basins prior to mare flooding.

The presence of isolated peaks and mare ridges forming circular patterns plus a mountain ring denote Imbrium as a multi-ring basin (figure 1). There is little

Figure 1. Distribution of mare ridges and islands of highland material(solid shading) within Mare Imbrium. A circle of mare ridges(through points A and B) demarcates the inner Imbrium ring and the surrounding highlands(dotted) an outer ring. A possible third, intermediate ring follows the western edge of the Apennine Bench(projecting into eastern Imbrium) and continues as highland islands. Points A and B denote locations where the ridge systems may be cross-cutting while point C is an area where the ridges could be partially flooded by younger basalts.

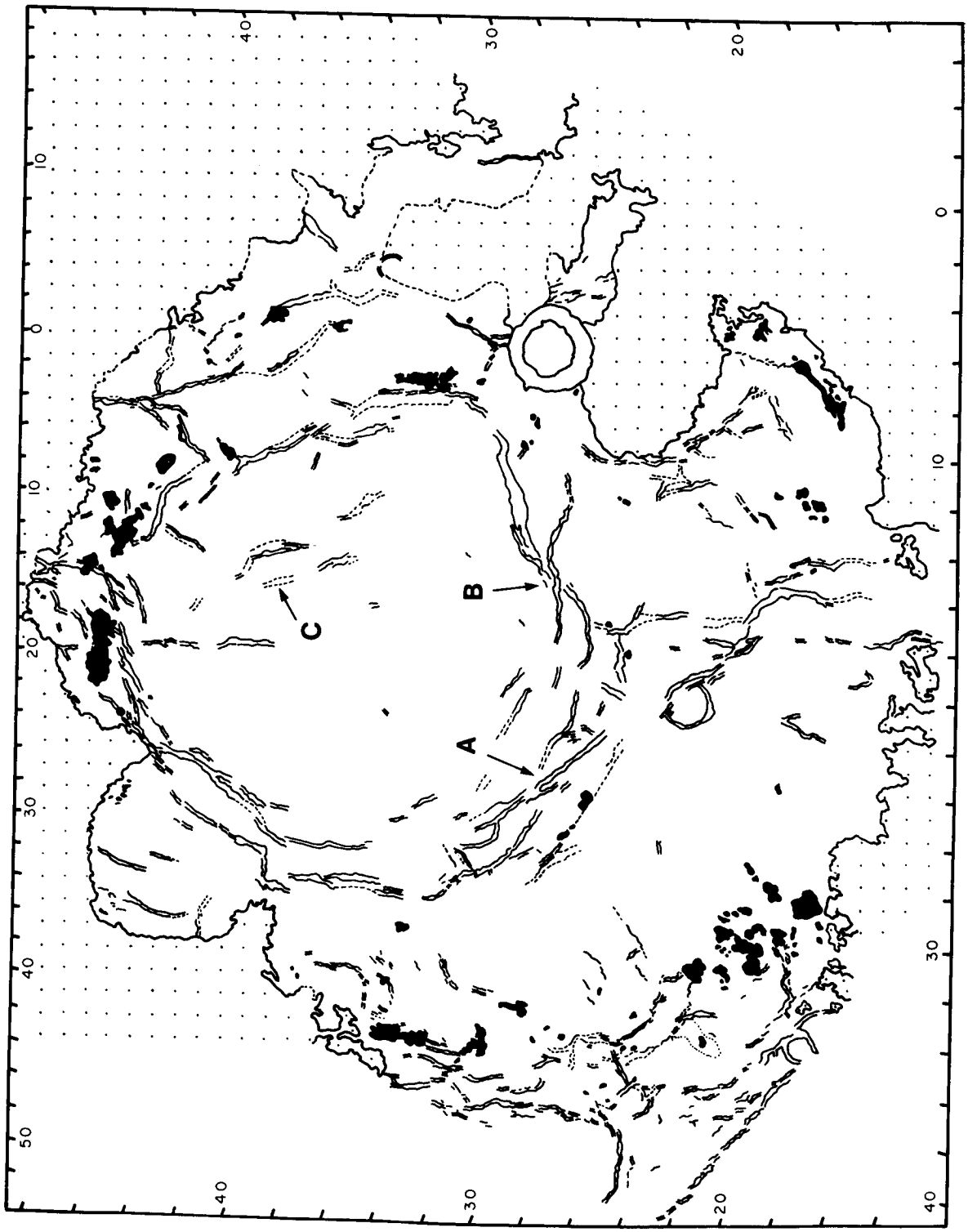
A
B
C

agreement as to which, if any, of the rings represents the rim crest of the original cavity of excavation (see for example, Head,1977; Hodges and Wilhelms,1978).Furthermore, there is a great divergence of opinion as to the depth/diameter ratio of the transient cavity; proposed values include less than 1/5 (Settle and Head,1976), 1/10 to 1/15 (Hodges and Wilhelms,1978), 1/33 (Chao,1977), and 1/113 (Pike,1974). Rock fragments in Apollo 17 breccias appear to be derived from depths of about 60 km (Warner et al,1978). If this represents the maximum excavation depth of Serenitatis and the second ring, with a diameter 0f 610 km (Head,1977), represents the original transient cavity rim, a minimum depth/diameter ratio of 1/10 is derived. Applying this value to the Imbrium cavity would indicate an excavation depth close to 100 km based on the 970 km diameter intermediate ring(Head,1977). Rebound, collapse, and deposition of impact melt would have shallowed this cavity essentially instantaneously. The present height differential between the outer scarp and the center of Mare Orientale is approximately 9 to 10 km while it has been estimated (Head,1974) that impact melt and mare basalt infil central Orientale to a depth of about 2 km. These data suggest a post-impact depth of the order of 12 km for the Orientale multi-ring basin. The complexity of the processes involved in post transient cavity modifications of such large basins render it difficult to define whether the resultant cavity scaled to the size of the basin or whether an approximately similar depth was achieved in

each. The present height differential between the Imbrium mountain ring and the mare center is about 7 km. Reasonable estimates of the fill thickness at the center of Imbrium fall in the range of 3 to 8 km (Thurber and Solomon,1978; Baldwin, 1963; Head, 1979; Whitford-Stark and Head, 1980b). Post modification depths of Imbrium and Orientale appear therefore to have been comparable despite the fact that the latter was only two thirds the diameter of the Imbrium transient cavity.

An estimate of the amount of impact melt contributing toward the early basin fill can be made by extrapolation from terrestrial craters (Head,1974) with the proviso that less melt was produced in comparably-sized lunar craters; Hawke and Head(1979) proposed that the volume of impact melt in lunar craters was 15 to 44 % that of terrestrial craters. Employing the curves in Head's(1974) paper, the volume of impact melt in Imbrium is of the order of 10^6 km^3 and has a thickness approaching 2 km.

Other contributions to the early post-impact fill were made by ejecta from large craters and basins. The only basin to post-date Imbrium was Orientale. Employing a diameter of 620 km for the Orientale impact cavity (Head,1974) and the equation describing the variation of ejecta thickness of McGetchin et al (1973), less than 2 m of Orientale ejecta would be found at the center of the Imbrium basin. A more significant contribution to the fill of Imbrium would have been the ejecta of the Sinus Iridum impact. This event, however, appears to be of mid-Imbrian age (Ulrich,1969) and

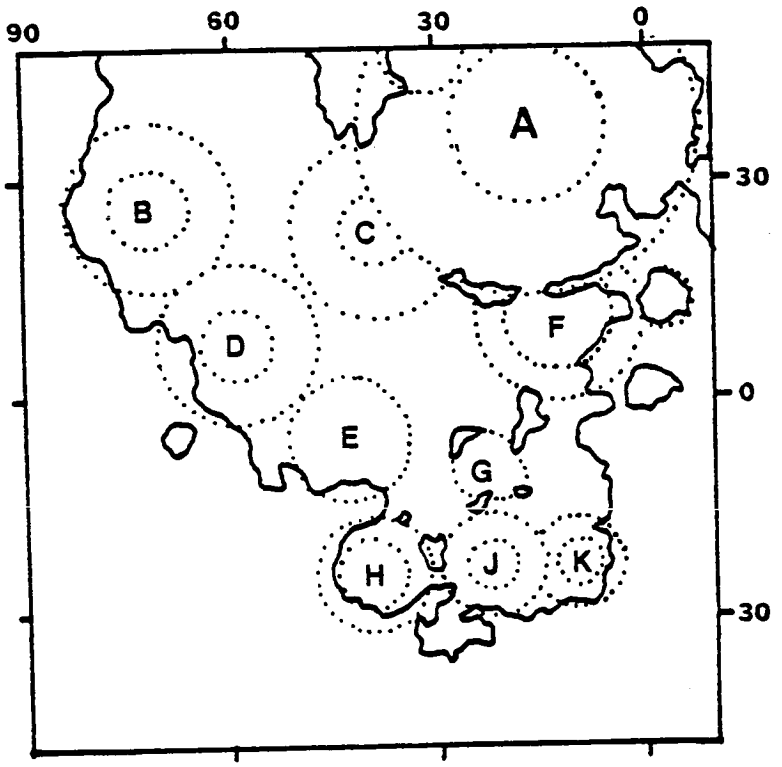

Figure 2 Location of possible basins in and around Procellarum and Imbrium(A) based on the work of De Hon(1979). There appears to be good evidence supporting the existence of the south Imbrium basin(F), Cognitum basin(G), Humorum basin(H), and the east and west Nubium basins(J,K). Evidence for the existence of basins B, C, D, and E is minimal and discussed in the text.

possibly post-dates early mare basalt eruptions.

The pre mare basalt morphology of the irregular Oceanus Procellarum is less readily defined. Three alternative scenarios have been proposed: 1) that Procellarum was a series of overlapping basins (De Hon, 1979), 2) that Procellarum lies within what was a very large early basin called Gargantuan (Cadogan,1974), and 3) that Procellarum was tectonically lowered following the Imbrium impact (Whitford-Stark and Head,1980 c).

The existence of large craters and basins prior to mare flooding in southeast Procellarum can be readily recognized from remanent rim material (e.g.,Hawke and Head, 1977). Such an identification is less readily made in central Procellarum since there is an apparent total lack of unflooded highland material (Whitford-Stark and Head, 1977 a). De Hon (1979) has located four large basins in the central Procellarum area (figure 2) on the basis of calculated basalt thickness variations. The paucity of data points, lack of consistent thickness variations, and lack of any supplemental evidence lead the present author to question the existence of such basins. Furthermore it is not necessary to invoke the presence of a basin to account for a topographic low; there is no evidence for the presence of any basins along the entire length of the irregular western Mare Frigoris (Whitford-Stark and Fryer, 1975).

The validity of the Gargantuan basin (center at 29W, 23 N) cannot be definitively resolved. If such a structure

did exist, its diameter of 2400 km (Cadogan,1974) would make it the largest impact structure so far recognized on the Moon (or, for that matter, any other solar system body); 400 km greater than the South Pole-Aitken basin (Stuart-Alexander,1978) and approximately twice the size of Imbrium. The most compelling evidence against the Gargantuan basin hypothesis is that its existence presents difficulties in accounting for the present topographic variation of highland terrain around Procellarum. Specifically the highlands are topographically high in the southeast quadrant of what would have been the Gargantuan basin (the Fra Mauro area) but are completely buried in the central Procellarum area (except at the anomalous Aristarchus Plateau) which is equidistant from the proposed basin center. It is therefore necessary to invoke an additional mechanism to account for the height variations around Gargantuan. Smaller basins superimposed on the Gargantuan basin would satisfy this condition but then the same arguments used against the De Hon model arise. In summary, although the former presence of the Gargantuan basin cannot be disproved by the present author, its presence requires further modifying parameters which alone may satisfy the observed characteristics of Procellarum.

The model favored by the present author is one which requires Procellarum to be a tectonic basin; essentially a large graben structure. This graben was initiated as a direct result of the Imbrium impact event. Assuming the Imbrium transient cavity to have a radius of 480 km, a depth of 100 km, and a parabaloid shape, the volume of that

cavity would have been approximately 3.6 x 10^7 km^3. Post-impact modification then led to the production of a multi-ring basin with a radius of about 670 km and a depth of 15 km. Again, assuming a parabaloid shape, the volume of this multi-ring basin cavity is approximately 1.0 x 10^7 km^3. Neglecting the fallback of ejecta, lunar curvature, and appreciating that these are order of magnitude estimates, the volume defficiency between the transient cavity and multi-ring basin is approximately 2.5 x 10^7 km^3. This volume corresponds to a circular plate with a radius of 1,000 km and thickness of 8 km or a cylinder with a 480 km radius and 35 km height. A substantial quantity of subsurface material was therefore required to facilitate the transition from the transient cavity to the multi-ring basin. This material would probably have been derived from both directly beneath the basin and by sub-lithospheric flow from surrounding areas (Hulme,1974a). Phase changes accompanying the change in depth of this sub-lithospheric material would lessen the total volume of material required to infil the transient cavity. This process, plus the presence of an extremely thin lithosphere(less than 25 km) beneath Procellarum(Head et al, 1980) might have been the cause of significant vertical(Whitford-Stark and Head, 1977a) and horizontal (Whitford-Stark and Fryer,1975) motions of the circum-Imbrium lithosphere. The origin of the Procellarum topographic low is therefore ascribed to downfaulting of the lunar highlands as a consequence of sub-lithospheric flow of material toward the Imbrium transient cavity. The effects of this process are not noticeable

to the east of Imbrium because of the prior-existence of the Serenitatis and Tranquillitatis basins and a thicker lithosphere to the east. The magnitude of the downfaulting varied around Procellarum, being greatest in the central section and least in the southeast. It is difficult to place values on the actual displacement because of topographic variation through the highlands resulting from the presence of pre-displacement impact craters. If the buried parts of the walls of craters such as Letronne and Repsold C are topographically low because they were down-dropped, the magnitude of the displacement may have been of the order of 500 m to 1.0 km. It is necessary, however, to bear in mind that subsidence also resulted from the emplacement of mare basalts and therefore the final displacement is a combination of both mechanisms.

Age of the topographic lows:

The age of the Imbrium cavity can be determined both stratigraphically (e.g.,Hartmann and Wood,1971;Wilhelms, 1979) and by radiometric dating of returned samples. Rocks returned from the Apollo 14 site were considered to be ejecta from the Imbrium cavity although a substantial volume of locally-derived material may be present at that site(Oberbeck et al,1974; Hawke and Head,1977). The ages of the Apollo 14 rocks have been summarized by Turner(1977) and Nyquist(1977) who quote ages for the Imbrium impact event of 3.95 $\pm$ 0.04 b.y., 3.90 $\pm$ 0.05 b.y., and 3.88 $\pm$ 0.04 b.y. An alternative

argument by Schonfield and Meyer(1973) is that the majority of the Apollo 14 rocks are not Imbrium ejecta and that the formation of the Imbrium basin pre-dates the initial extrusion of KREEP basalt at 4.3 to 4.4 b.y. Although their argument has some attractive qualities, it does not appear to explain the lack of non-mare rocks with ages greater than about 4.0 b.y. (Turner,1977) at the Apollo 15 site close to an Imbrium ring. It is extremely unlikely that no Imbrium ejecta or Imbrium ring material was collected at that site. Similarly Imbrium is stratigraphically younger than Serenitatis yet the non-mare boulders at the Apollo 17 site cluster in age around 3.98 $\pm$ 0.03 b.y.(Turner,1977; Nyquist,1977) and more recently ages of 3.87 $\pm$ 0.03 b.y. have been obtained on breccia samples(Staudacher et al,1979). Again it is extremely unlikely that no rocks related to the formation of the basin were collected from the Apollo 17 site where the Serenitatis ejecta has been estimated (McGetchin et al, 1973) to form a layer in excess of 1500 m thick. Additionally, although mare basalts were probably erupted prior to the formation of all the large basins, no presently observed mare surface has a crater density or crater degredation age in excess of 4.0 b.y. Although the earliest erupted basin-filling basalts are undoubtedly buried by younger flows, it would seem too co-incidental to find not one basalt surface with an age in the range 4.0 to 4,3 b.y. It is therefore concluded that the majority of available evidence points to the formation of the Imbrium impact cavity at about 3.9 b.y. ago. Since Procellarum is here

envisaged as a direct product of the Imbrium basin-forming event, the production of the Procellarum topographic low is considered to closely follow 3.9 b.y.

Composition of the early basin fill:

The eruption of mare basalts did not commence at the same time that the formation of large multi-ring basins terminated; there is now abundant evidence for pre-Imbrium basin mare basalts. The earliest mare basalts (10003,10029) returned from a mare landing site have an age of 3.90 ± 0.03 b.y. (Guggisberg et al, 1979). The extrusion of these basalts in Tranquillitatis therefore took place at approximately the same time as the formation of Imbrium and may have pre-dated it.

Other direct evidence of pre-basinal volcanism is provided by KREEP basalts and fragments incorporated within breccias (Ryder and Spudis,1979). KREEP basalts (15382,15386) from the Apollo 15 site have been assigned crystallization ages of 3.94 ± 0.01 b.y.(Nyquist et al, 1975) and 3.85 ± 0.08 b.y. (Carlson and Lugmair,1979) and so are also of similar age to the Imbrium impact event. KREEP basalts may therefore represent some of the earliest lavas lining the Imbrium cavity (Spudis,1978). The large thorium contents associated with large south-east Imbrium craters(e.g., Lambert,Timocharis,Archimedes) indicate KREEP underlies a significant area of mare basalt(Metzger et al,1979). Furthermore, a postulated

correlation with red spots(Malin,1974), the presence of KREEP fragments in the Apollo 12 regolith, at the Apollo 14 site, and as KREEPy fragments in Apollo 17 breccias (Norman and Ryder,1979) suggests a widespread distribution for KREEP basalts on the Moon. Although major concentrations of KREEP are found in the Imbrium-Procellarum region, Spudis(1979) has argued, on the basis of high radioactive element concentrations derived from orbital gamma-ray data, that KREEP materials are also widespread on the lunar farside. Variations in initial strontium isotope ratios(Meyer,1977) indicate that KREEP was derived from several discrete eruptions. If, as Malin(1974) proposed, the Gruithuisen domes in Procellarum are KREEP extrusions, an age of 3.3 to 3.6 b.y. assigned to them (Head and McCord,1978) would mean that KREEP volcanism also postdated the eruption of mare basalts. Warner et al (1977) argue that the earliest KREEP rocks must post-date the formation of "feldspathic granulitic impactites" since those rock contain essentially no KREEP component. The age of KREEP volcanism is thereby constrained to a period extending from about 4.1 b.y. to possibly 3.3 b.y.

Other fragments with mare basalt affinities have been recovered from the lunar breccias(e.g., Ryder and Taylor, 1976; Blanchard and Budahn,1979) dated at 3.87 $\pm$ 0.03 b.y. (Staudacher et al,1979). Like samples of post-basin mare basalts, these older basalts exhibit a divergent chemistry with TiO_2 concentrations ranging up to 7 wt%. Further

materials that may have been extruded at the lunar surface include those variously described as quartz monzodiorite, monzonite, felsite, and granitic. These appear to have been volumetrically small and derived as immiscible liquids(Rutherford et al,1976).

Photogeologic evidence for the possible existence of pre-basinal volcanic deposits is the existence of dark halo craters thought to excavate mafic extrusive material from beneath basin ejecta(Schultz and Spudis,1979) and the presence of plains deposits of possible volcanic origin within old basins(Gifford and El-Baz,1979). Although not all plains deposits are volcanic, as was found out at the Apollo 16 site, morphologic criteria alone are not capable of distinguishing their mode of origin(Whitford-Stark,1980). Moonwide orbital geochemical remote sensing may possibly resolve this problem. At present it is only possible to state that the plains and dark halo material, if of volcanic origin, indicate the former existence of an early moonwide volcanic episode.

In summary, eruptions of KREEP and mare basalt appear to have taken place at the lunar surface possibly 200 million years prior to the formation of the Imbrium basin. Synchronous eruptions of basalts with extremely divergent chemistries were possibly accompanied by minor eruptions of more silicic magma. The Imbrium-Procellarum region appears to have been a particularly favorable area for KREEP basalt eruption at about the time of the Imbrium basin-forming event and such materials probably underlie

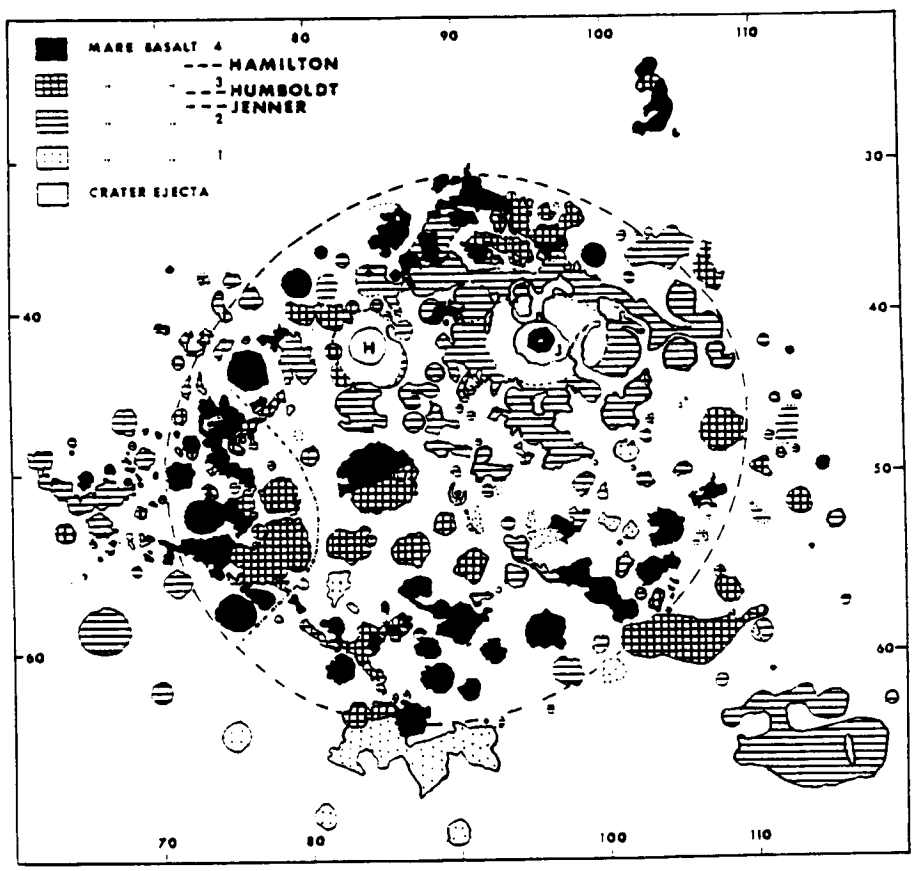

Figure 3 Geologic map of the basalt units within Mare Australe. The units in the key are in their relative stratigraphic positions except for that labeled crater ejecta. J and H mark the locations of the craters Jenner and Hamilton. The dashed line encloses an annulus of the youngest(Basalt 4) basalt exposures and is approximately 900 km in diameter. The dash-dot line marks a slope inflection which may be associated with an old basin.

and interdigitate with mare basalts in both maria.

Location of early vents:

In neither Procellarum nor Imbrium can the extrusion sites of early basalts be identified; either because they have been eroded or obscured by later deposits. The location of vents in multi-ring basins appears to have been largely dependent on the time interval between the impact event and the initiation of basalt eruption. At one extreme stands Mare Australe where the observed surface basalts appear to post-date basin formation by a significant period and at the other is Mare Orientale where basalt eruption appears to have closely followed the impact event. This scenario is complicated by the fact that, because of the increased early impact flux, the older basins were degraded at a much more rapid rate than the later. As purely hypothetical examples, a basin produced 4.1 b.y. ago may have been totally destroyed by 4.05 b.y. while a basin formed at 3.85 b.y. may be preserved in relatively pristine condition to the present. In Australe, mare basalts have been erupted within nearly 200 separate craters superimposed on the degraded ring structure (Whitford-Stark,1979). Apart from the fact that early eruptions appear to have been preferentially located near the basin center(figure 3), the structure of the basin appears to have played but a minor role in determining vent distribution. At the other extreme, in the Orientale basin

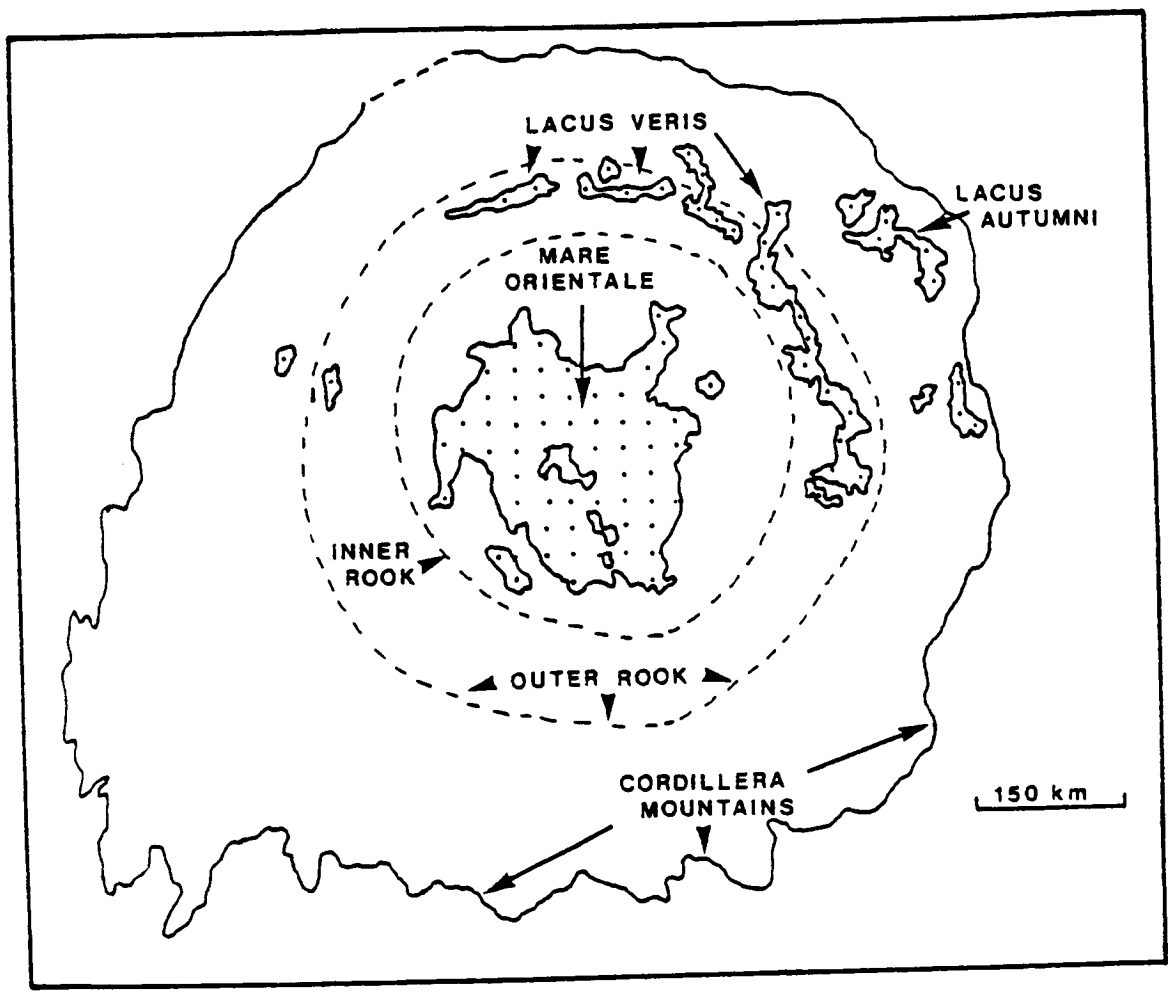

Figure 4 Distribution of mare basalts(dotted) within the young Orientale basin. The Orientale rings are outlined in solid and dashed lines. Note how the rings restrict the basalts to the basin center and between the ring mountains.

the location of vents and distribution of erupted products was strongly influenced by the basin morphology (figure 4). The earliest basalts in Orientale occupy the basin center, have no obvious vents, and appear to be at least 1.0 km thick (Greeley,1976). Further basalts were erupted in Lacus Veris between the basin center and the Rook Mountains. These basalts contain sinuous rilles and shield-like structures and appear to have originated from vents at the Rook Mountains (Greeley,1976). The youngest eruptions in Orientale were small patches of basalt emplaced in Lacus Autumni between the Rook and Cordillera Mountains. Like those of Lacus Veris, the Autumni basalts contain sinuous rilles suggesting similar, though volumetrically smaller, eruptions (Greeley,1976).

The relative youth of the Imbrium basin, the short (if any) time period between basin formation and basalt eruption, and the relatively pristine condition of the ring structure, combine to suggest that Imbrium was more akin to Orientale than Australe in terms of vent and early basalt distribution. That is, early basalts were erupted within the basin center and from the rings to infil the inter-ring topographic lows. The great thickness of basalt in Imbrium precludes identification of any possible large (greater than 35 km diameter) post-basin,pre-basalt craters which may also have been eruption sites.

Procellarum is inferred to have been a topographically low highland area punctuated by small basins and craters. In this respect it would have resembled Australe but

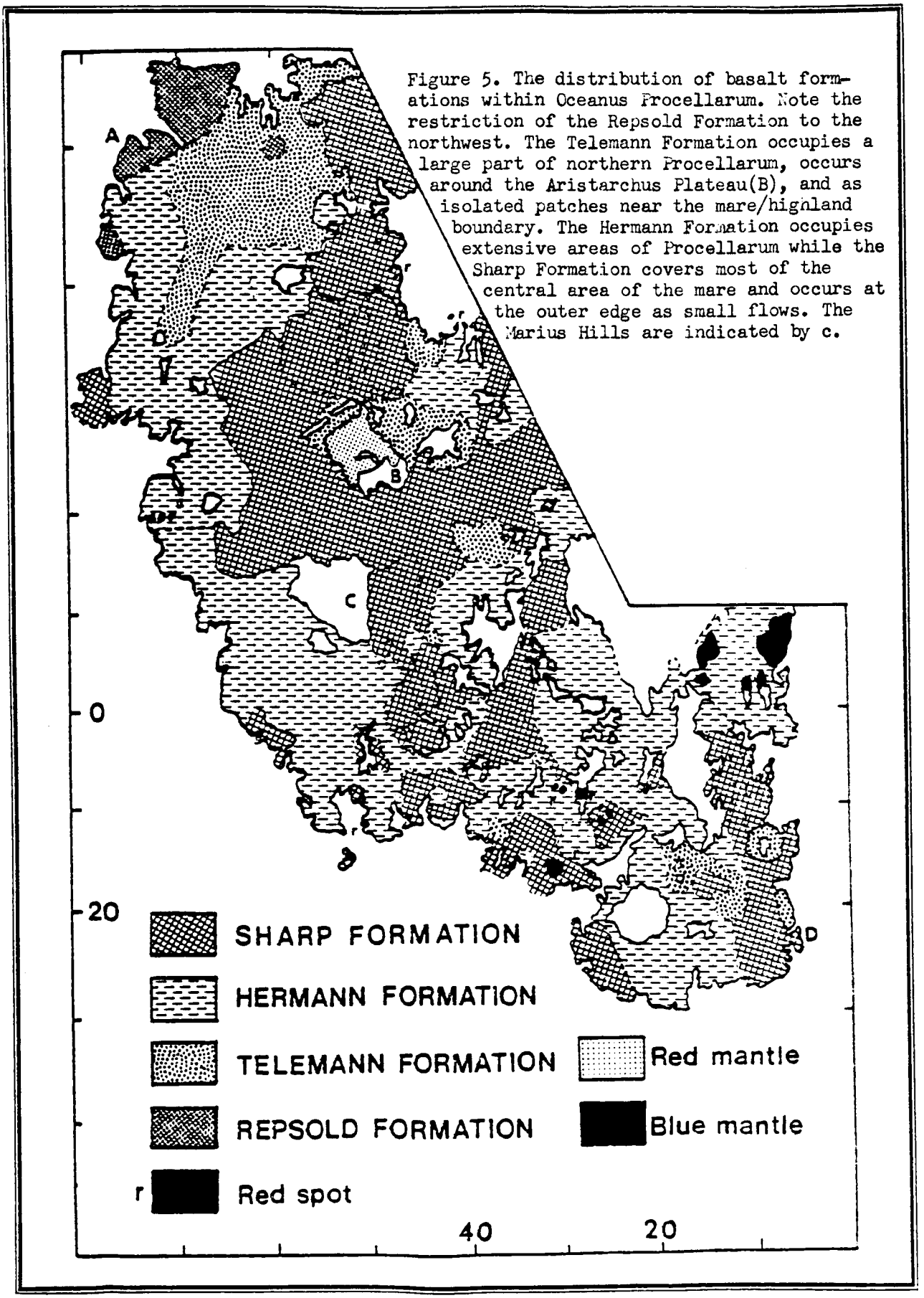

Figure 5. The distribution of basalt formations within Oceanus Procellarum. Note the restriction of the Repsold Formation to the northwest. The Telemann Formation occupies a large part of northern Procellarum, occurs around the Aristarchus Plateau(B), and as isolated patches near the mare/highland boundary. The Hermann Formation occupies extensive areas of Procellarum while the Sharp Formation covers most of the central area of the mare and occurs at the outer edge as small flows. The Marius Hills are indicated by c.

lacked the basinal structure. That is, vents were initially located on the floors of craters. It is not known whether the large volcanic complexes within Procellarum were erupting from the time of initiation of the topographic low. No early volcanic materials can be traced to the complexes but such materials may simply be buried by younger basalts.

Composition and nature of surface-exposed, early mare fill:

Early (pre-3.8 b.y. ; Turner,1977) mare basalts (10003,70215) returned from Apollo sites are characterized by high TiO_2 contents (> 10 wt%), low Al_2O_3 contents(< 11 wt%) low FeO contents(< 20 wt%), and average MgO contents (about 8 wt%)(Papike et al,1976). At the Apollo 17 site the basalts are accompanied by similarly-aged, titanium-rich glass spherules interpreted to be pyroclastic deposits(e.g., Heiken et al,1974). Similar pyroclastic deposits are believed (Head,1974 b) to comprise the extensive dark mantle deposits developed across the lunar surface. In Procellarum, early (3.75 $\pm$ 0.05 b.y.) titanium-rich basalts form the Repsold Formation(Whitford-Stark and Head,1980 a) developed as surface basalts in the northwest of the mare and as dark mantle deposits in the Sinus Aestuum region (figure 5). A magnesium-rich, titaniferous (3.5 to 5.5 wt% TiO_2) basalt has been interpreted (Head et al,1978) to form the early (3.75 $\pm$ 0.05 b.y. ;Boyce and Johnson,1977) fill of the Crisium basin while titaniferous basalts may have

been erupted early in the history of Mare Frigoris (Hawke and Head,1980). Undated titanium-rich glasses were also found(Reid et al,1972) to comprise about 5% of the Apollo 12 regolith glasses. Comparably-aged, titanium-rich basalts are not observed in Mare Imbrium although an early (3.5 ± 0.25 b.y.), titanium-rich basalt does occur in the northeast(figure 6)(Whitford-Stark and Head,1980 b). Furthermore, undated, titanium-rich(>13 wt%) glasses were found in Apollo 15 samples(e.g.,Ridley et al, 1973) albeit in minor quantities. An old, titanium-rich basalt could therefore be present but be buried by younger basalts in Imbrium. The available evidence therefore suggests that early, post-Imbrium basalts(about 3.75 to 3.9 b.y.) erupted across most of the lunar nearside were titanium-rich.

The titanium-rich basalts contrast significantly in composition with the Imbrian-aged basalts and Imbrian or possibly Nectarian-aged (Wilhelms and El-Baz,1977) plains of Mare Smythii. Conca and Hubbard (1979) show these materials to be enriched in Al_2O_3 (16 to 24 wt%) and to have MgO contents up to 16 wt%. No returned lunar mare basalt sample has this composition. The chemically closest materials are samples from the Apollo 14 site(14053,14072) which have Al_2O_3 contents approaching 14 wt% and MgO contents up to 12.2 wt% and which are considered by Ridley(1975) to be pristine igneous rocks with ages of about 3.95 to 4.04 b.y. (Turner,1977; Nyquist,1977). Closer, chemically, are the KREEP basalts (15 to 20 wt% Al_2O_3 and 7 to 15 wt% MgO)

Figure 6. The distribution of basalt units within Mare Imbrium. Unit 10 is the youngest and 1 the oldest. Also indicated are the approximate TiO_2 concentrations and ages of the units. Note that the older units are largely restricted to the mare periphery while the center is occupied by the younger units.

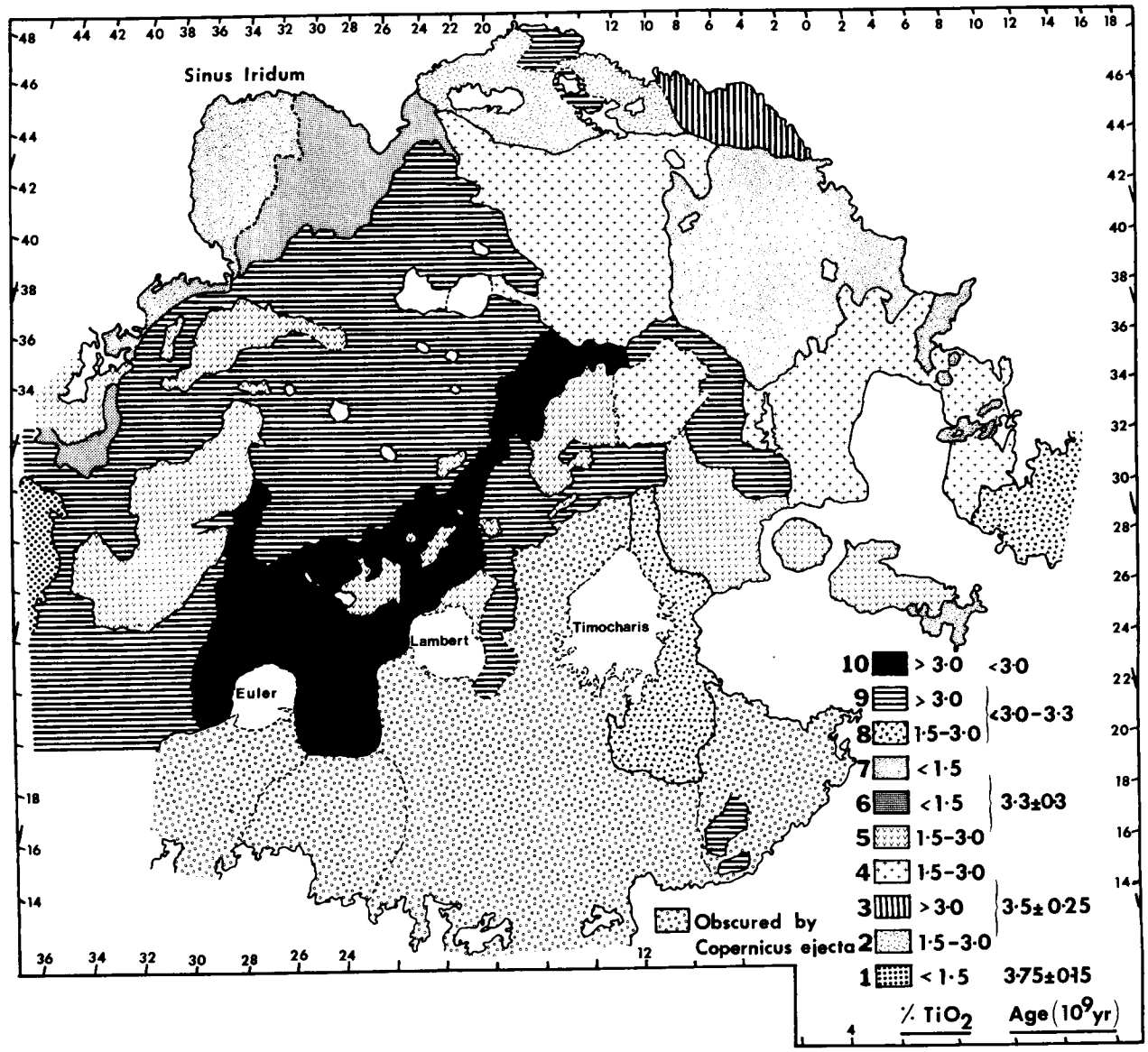
Sinus Iridum
Lambert
Timocharis
Euler
Obscured by Copernicus ejecta
10 > 3·0 <3·0
9 > 3·0
8 1·5-3·0 <3·0-3·3
7 < 1·5
6 < 1·5 3·3±03
5 1·5-3·0
4 1·5-3·0
3 > 3·0 3·5± 0·25
2 1·5-3·0
1 < 1·5 3·75±0·15
% TiO2
Age (10^9 yr)

(Meyer,1977) but the orbital gamma-ray data(Metzger et al, 1977) indicates that Mare Smythii does not have the high thorium contents required of KREEP basalts. It would therefore appear that Mare Smythii contains an unsampled type of mare basalt and that eruptions of widely divergent chemistry were taking place synchronously at the lunar surface.

Eruption style of the early titanium-rich unit:

No vents have been observed in the Repsold Formation of Procellarum. It, and the early titanium-rich basalts of Crisium and Serenitatis are all preserved near the topographically high highland/mare boundary. Evidence of basin-center subsidence (Solomon and Head,1979), subsurface mare basalt layering(Peeples et al,1978), and excavation from beneath the mare surface layers by recent impacts (Whitford-Stark and Head,1980 a), all serve to indicate that the old titanium-rich basalt was areally extensive and has been largely covered by younger materials. Maxwell and Phillips(1978) argue, on the basis of radar-detected subsurface layering, that the unit in Crisium could be from 1.0 to 2.0 km thick. In Procellarum the unit has been assigned an average thickness of 125 m and a total volume of 2.1×10^5 km^3 (Whitford-Stark and Head,1980a). The great volumes and apparent lack of identifiable vents combine to suggest a flood-style(Greeley,1976) eruption for the early titanium-rich basalts. Associated dark mantle deposits

appear to have exhibited continuous or strombolian-style eruptions(Wilson and Head,1980).

Further pre-graben basalts:

The early titanium-rich basalts of Procellarum were followed by the Telemann Formation basalts(Whitford-Stark and Head,1980a). These younger(3.6 ± 0.2 b.y.) basalts appear to have a low or Very Low Titanium content, similar to VLT basalts(Papike and Vaniman,1978). Basalts with similar compositions are common at the Luna 24 site in Crisium, have been found in Apollo 17 samples(Papike and Vaniman,1978), and may be present at the Apollo 15 site(Steele et al,1977). Similarly low titanium contents also characterize the green glass at the Apollo 15 site (Papike and Vaniman,1978). Ages obtained on green glass include 3.79 ± 0.08 b.y.(Husain,1972), 3.38 ± 0.06 b.y., and 3.29 ± 0.06 b.y. (Podosek and Huneke,1973; Huneke et al, 1974) while Luna 24 VLT samples cluster at 3.30 ± 0.05 b.y. (The Lunatic Assylum,1978). Delano (1979) has argued that the Apollo 15 green glass was derived from at least five separate magma chambers. Furthermore, Grove and Vaniman (1978) suggest that the Luna 24, Apollo 17 VLT basalts and Apollo 15 green glass compositional differences required three distinct source regions and/or different degrees of partial melting in each source. In the light of these arguments it is possible that the age variation recorded in the Apollo 15 green glass is real and that the similar

age of the younger Apollo 15 green glasses and Crisium VLT basalts may be fortuitous. Additionally the Apollo 17 VLT basalts occur in breccias dated at 4.0 b.y. and as two chemically distinct, young(?) series of glasses in the regolith (Warner et al,1979). It would therefore appear that titanium-poor basalts were erupted in distinct episodes ranging in age from perhaps 3.0 to 4.0 b.y. with probably repeated eruptions of the same composition in each mare. At least two, perhaps three episodes of titanium-depleted basalts have been recognized in Mare Imbrium on the basis of photogeologic and remote-sensing criteria(Whitford-Stark and Head,1980b). The younger two of these episodes appear to have been preceded by perhaps three episodes of intermediate basalt eruption and an episode of titanium-rich basalt volcanism(Whitford-Stark and Head,1980b).

The Telemann Formation in Procellarum was followed by the eruption of intermediate basalts belonging to the Hermann Formation with an estimated age of 3.3 $\pm$ 0.3 b.y. (Whitford-Stark and Head,1980a). The Hermann Formation appears to have been erupted in at least two major episodes and graben formation terminated during its emplacement (Whitford-Stark and Head,1980c). Rocks returned from the Apollo 12 site, which constitute part of the Hermann Formation, have argon ages in the range 3.15 $\pm$ 0.06 to 3,27 $\pm$ 0.05 b.y.(Turner,1977) and Rb/Sr ages most closely bracketed by 3.16 $\pm$ 0.09 and 3.36 $\pm$ 0.10 b.y.(Nyquist,1977).

In Imbrium, the last mare unit that can be shown to be

cut by graben is the intermediate Unit 5 with an estimated age of 3.3 ± 0.3 b.y.(Whitford-Stark and Head,1980b). It would therefore appear that the termination of graben production was approximately synchronous in both Imbrium and Procellarum and occured during the eruption of similar composition basalts in each. The recognition of at least five (perhaps seven,including KREEP and a possible high titanium basalt) basalts in Imbrium predating the termination of graben production but only three in Procellarum, suggests that the magmatic evolution of the former was more complex.

Eruption of VLT and intermediate basalts in Procellarum and intermediate basalts in Imbrium appears to have been approximately synchronous with the eruption of feldspathic basalts in Mare Fecunditatis at about 3.4 to 3.6. b.y. (Turner,1977) and the younger VLT basalts in Crisium.

Eruption style of pre-graben basalts:

The Telemann Formation titanium-depleted basalts can be definitively shown to have been locally derived from the Aristarchus Plateau(Whitford-Stark and Head,1980a) where they are associated with at least 36 sinuous rilles (Whitford-Stark and Head,1977b). Other areas of northern Procellarum and patches at the mare/highland boundary and mare ridge crests(Pieters et al,1980) cannot be related to identifiable vents. It is extremely doubtful, however, that all the Telemann Formation basalts in the 1,700,000 km^2

Procellarum were derived from the Aristarchus Plateau. A study by Head and Wilson(1980) indicates that the most likely mass eruption rates for the sinuous rilles with large source craters at the Aristarchus Plateau was of the order of 10^7 to 10^{10} kg/s. Whitford-Stark and Head (1980a) estimated an average thickness of 250 m for the Telemann Formation. This, plus the earlier Repsold Formation appears to have been sufficiently thick to flood the majority of the pre-existing topography in central Procellarum except at the volcanic complexes themselves. In southeast Procellarum, however, the preservation of the Telemann Formation around highland remanents demonstrates that it obviously did not eradicate prior topographic variations.

The proximity of the Aristarchus Plateau to Mare Imbrium suggests that the former could also have provided VLT basalts to the early infil of the latter. An indeterminable volume of these basalts were then covered by younger Imbrium lavas. The possible early age quoted for a green glass fragment from the Apollo 15 site is also suggestive of early titanium-poor magmas being locally derived within Imbrium. Other pre-graben basalts within Imbrium are largely confined in the area defined by the outer mare edge and the inner ridge ring; this is largely because the mare center is occupied by younger surface basalts. It also implies ,however, that a sufficient thickness of basalt has accumulated between the basin rings that either the hydrostatic head was incapable of lifting further magma above

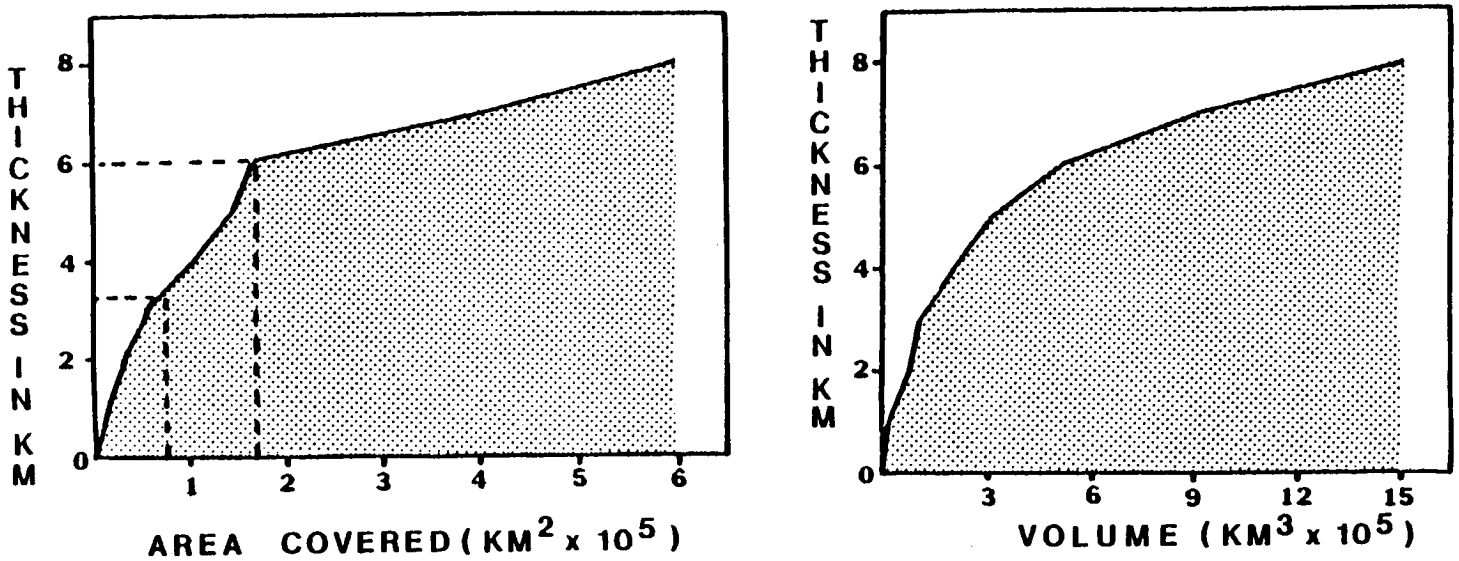

Figure 7 Volumes and areas of basalts required to fill the Orientale basin (from Head,1979). The dotted lines in the left diagram indicate the depth of flooding at the stage that the inner ring is flooded (80 km) and the inner Rook is reached (180 km). The maximum values in each diagram indicate the volumes, areas, and thicknesses obtained when basalt floods to the Cordillera Mountains.

the existing basalts or that the local slope prevented further basalt deposition. By artificially flooding a topographic model of the Orientale basin, Head(1979) showed that flooding of central Orientale to the peak ring accounted for less than one third the lava area and less than one third of the volume required to make Orientale similar in appearance to Imbrium. Further flooding to the Cordillera Scarp tripled the lava area and doubled its volume(figure 7). Although Head's model is an over-simplification of the emplacement locations, it excellently illustrates that by the time of graben termination, the bulk of the volume of basalts occupying Imbrium had been erupted. Additionally, the apparent youth(3.5 $\pm$ 0.25 b.y.) of the earliest identified surface basalts suggests that most of this volume is unrepresented by presently observed lavas. Those surface basalts which are observed appear to be predominantly of intermediate composition(figure 6), generally are defficient in surface features such as sinuous rilles, and appear, on average, to be thicker than basalts of other compositions(Whitford-Stark and Head,1980b).It would therefore appear that not only were basalts of differ-

ing composition being synchronously erupted but also that the styles of the eruptions differed.

The initiation and termination of graben production:

Both Imbrium and Procellarum have associated graben structures, supporting the observations of Lucchitta and Watkins(1978) that graben formation is related neither to basin shape nor the presence or absence of a mascon. In Imbrium the graben are confined to the mare side of the Apennine Mountains while in Procellarum, though present on the mare surface, extend up to 450 km into the adjacent highlands. The Procellarum graben are best developed to the southwest and around Mare Humorum, exhibiting patterns both concentric and radial to the mare fill. Golombek(1979) related the average width of the graben to the thickness of the megaregolith layer, arguing that the two sides of the graben converged at a depth corresponding to the base of the megaregolith. One product of his analysis was that the southwest Procellarum graben appeared to indicate a thickening of the megaregolith toward the Orientale basin; a result to be expected from the increased Orientale ejecta thickness. The values he obtained were about 1.9 km thickness near Procellarum, rising to 3.9 km near Orientale.

Whitford-Stark(1974) showed that both floor-fractured craters and graben were distributed around, and were therefore related to, the lunar maria. More recently Solomon and Head(1979) have shown that graben location is a function of

the global thermal stress and local stresses resulting from mare basalt loading. That is, the location, extent, and age of graben formation are related to the relative thickness of the elastic lithosphere and the basalt load. Lucchitta and Watkins(1978) determined that lunar graben production terminated at 3.6 ± 0.2 b.y. while Whitford-Stark and Head(1980a,b) showed that it terminated in Procellarum during the deposition of the Hermann Formation(3.3 ± 0.3 b.y.) and in Imbrium between the eruption of Units 5 and 6(3.3 ± 0.3 b.y.). The apparently synchronous termination of graben production in Imbrium and Procellarum would be best explained as a result of a moonwide process such as cooling of the interior(Solomon and Head,1979). However, since the basalt thickness in Imbrium is substantially greater than that in Procellarum, a difference in lithosphere thickness between each is required to satisfy the Solomon and Head(1979) model. Head and Solomon(1980) found that at the time of graben formation, the elastic lithosphere was 50 to 75 km thick beneath Imbrium but less than 25 km thick beneath Procellarum (Head et al,1980). The preferential development of graben adjacent to central Procellarum and the volcanic complexes developed there suggest a variable lithosphere thickness beneath the mare. A similarly variable lithosphere thickness beneath Imbrium has been proposed (Head and Solomon,1980); it being thickest beneath central, eastern and southern Imbrium. This greater lithosphere thickness may be the cause for the apparent lack of graben in Units 2 and 3 of northern Imbrium.

Composition of post-graben basalts:

The post-graben basalts of Procellarum include the younger members of the intermediate composition Hermann Formation(3.3 ± 0.3 b.y.) and the Sharp Formation titanium-rich basalts(2.7 ± 0.7 b.y.)(Whitford-Stark and Head,1980a). Spectra (Pieters et al,1980) suggest that the different members of the Hermann Formation could be compositionally distinct with varying pyroxene concentrations.Alternatively, the spectral variations could result from glass concentration or composition differences in the regolith. Similarities in the opaque mineral modes for the three main basalt types returned from the Apollo 12 site, but extremely variable but consistent pyroxene and olivine modes(Papike et al,1976) would support a pyroxene variation as the cause of the spectral differences. Likewise, although the Sharp Formation basalts are characterized by high titanium concentrations, there appear to be some compositional differences between them. In particular, one group has TiO_2 concentrations of about 4.0 to 6.0 wt% , while another 6.0 to 8.0 wt%(Pieters et al,1980).

The relatively simple chemistries of the Procellarum post-graben basalts are not reflected by those of Imbrium. In Imbrium there appears to have been at least two phases of VLT basalts, one of intermediate basalts, and two of titanium-rich basalts(Units 5 - 10, figure 6). Rocks returned from the Apollo 15 site include compositionally distinct olivine and pigeonite basalts (TiO_2,1.0 to 3.0 wt%)

and the very low titanium (TiO_2 less than 1.0 wt%) green glass (Papike et al,1976). Other yellow, brown, and orange glasses from the Apollo 15 regolith may represent locally derived pyroclastic deposits(Hawke et al,1979). The young (less than 3.3 b.y.) titanium-rich basalts(Units 9 and 10, figure 6) of central Imbrium are spectrally similar to those of central Procellarum and, indeed, are in part derived from the same sources. The titanium-depleted basalts of Imbrium (Units 6 and 7; 3.3 $\pm$ 0.3 b.y.), however, appear to be spectrally similar to the older (3.6 $\pm$ 0.2 b.y.) Telemann Formation basalts of Procellarum. Thus, not only do the post-graben basalt eruptions in Imbrium appear to have been more chemically diverse than those of Procellarum, the compositional sequences also differed.

Post-graben basalt eruptive style:

In Imbrium, none of the post-graben basalts can be shown to have been erupted within the mare ridge ring. Of the 48 identified sinuous rille source locations, about 6% are in the highlands, 17% at the mare/highland boundary, 70% between the inner ring and the mare edge, and 6% at the inner ring(Whitford-Stark and Head,1980b). Such a distribution is consistent with an extensional bending stress toward the periphery of Imbrium resulting from basin center subsidence(Solomon and Head,1979). Further volcanic constructs(cones, shields, crater rows, hills and ridges with summit craters, and linear depressions) located in southwest Imbrium have

have been described in detail by Todhunter(1975) and also appear to have been associated with this late peripheral extension stage. Almost all of the young lava flows went directly toward the center of Imbrium indicating that in this area, in spite of voluminous early eruptions, there was still a topographic low. Additionally the flow directions imply that the Imbrium basin rings at this stage were sufficiently flooded as to not form a barrier to the lavas. An exception is in the Apennine Bench region where a further 2.7 km of basalt is still required to flood the Montes Archimedes section of the second basin ring (Head,1979).

Estimates of mass eruption rates at the source of Hadley Rille fall in the range 10^8 to 10^{10} kg/s (Head and Wilson,1980) while estimates of the flow rates of the Unit 10 Imbrium flows fall in the range 10^4 to 10^5 m^3/s (Hulme 1974b;Hulme and Fielder, 1977).

In Procellarum, a large part of the Hermann Formation appears to have been derived from the Marius Hills and

possibly the Rümker Hills(Whitford-Stark and Head,1980a). Over 20 separate sinuous rille sources have been identified near the Marius Hills associated with the Hermann Formation. Additionally the hills contain the densest concentration of volcanic domes and cones on the Moon, including 135 low domes, 127 steep domes, and 59 cones(Whitford-Stark and Head,1977b). The smaller size of the Marius rilles and their source craters suggests lower mass eruption rates than those of the earlier titanium-depleted, Telemann Formation basalts. The sinuous rilles originating at the Marius Hills cannot be traced far from the complex; suggesting either a decrease in pre-emplacement slope or ponding of the lava led to a decrease in the efficiency of thermal incision by the flows(Hulme,1974b) The associat- of these intermediate basalts with rilles contrasts with Imbrium where, most commonly, the intermediate basalts are rille-less. Like Imbrium, however, the younger Hermann Formation basalts appear to have been relatively thin; an average thickness of only 150 m being derived (Whitford-Stark and Head,1980a) for both the pre- and post-graben members of the Formation. Sources of the Hermann Formation were not confined to the complexes; cones, domes, and sinuous rilles occur in the Flamsteed region(Pieters et al,1980) and sinuous rille sources are located along a ring of the south Imbrium basin(Whitford-Stark and Head,1980a).

The titanium-enriched, Sharp Formation basalts of Procellarum are commonly, though not exclusively, associated with sinuous rilles. These youngest Procellarum lavas were,

like those of Imbrium, largely erupted from mare/highland boundary locations; exceptions being those erupted at or near mare ridge crests and close to the complexes(Whitford-Stark and Head,1980a). The Sharp Formation basalts appear to be relatively thin with an estimated average thickness of only 25 m(Whitford-Stark and Head,1980a). This thinness is reflected by their having not been able to cross minor topographic highs such as mare ridges(Pieters et al,1980).

In summary, the post-graben basalts of both Imbrium and Procellarum are characteristically thin and were erupted from locations near the mare periphery. Eruption styles differed for different units within either mare though Imbrium appears to have been peculier in having late flood-style eruptions of short duration(Unit 10) (Schaber et al,1976). Procellarum is unique in its possesion of three large volcanic complexes; possibly a result of a thin elastic lithosphere(Head et al,1980). The difficulties in distinguishing the early from the late Hermann Formation away from the mare periphery do not allow the authors to determine whether eruptions terminated at the complexes at the same time as termination of graben formation. Sharp Formation basalts do have sources near, but not on, the Marius Hills while no post-Telemann Formation basalts can be traced to the Aristarchus Plateau. A synchronous termination of eruptions at the complexes and graben production would satisfy the Solomon and Head(1979) model whereby after the achievement of bulk lunar volume, global comp-

Figure 8. Distribution of mare ridges in Oceanus Procellarum. Note the parallel central zone of ridges in central Procellarum, the polygonal pattern in the north, and the reticulate pattern in the southeast. Also indicated are the Rumker(R), Aristarchus Plateau(A), and Marius Hills(M) volcanic complexes. S and T mark the mare extension of Rima Sirsalis from Sirsalis E (S) to Tobias Mayer W (T), the postulated fault boundary separating central and southeastern Procellarum.

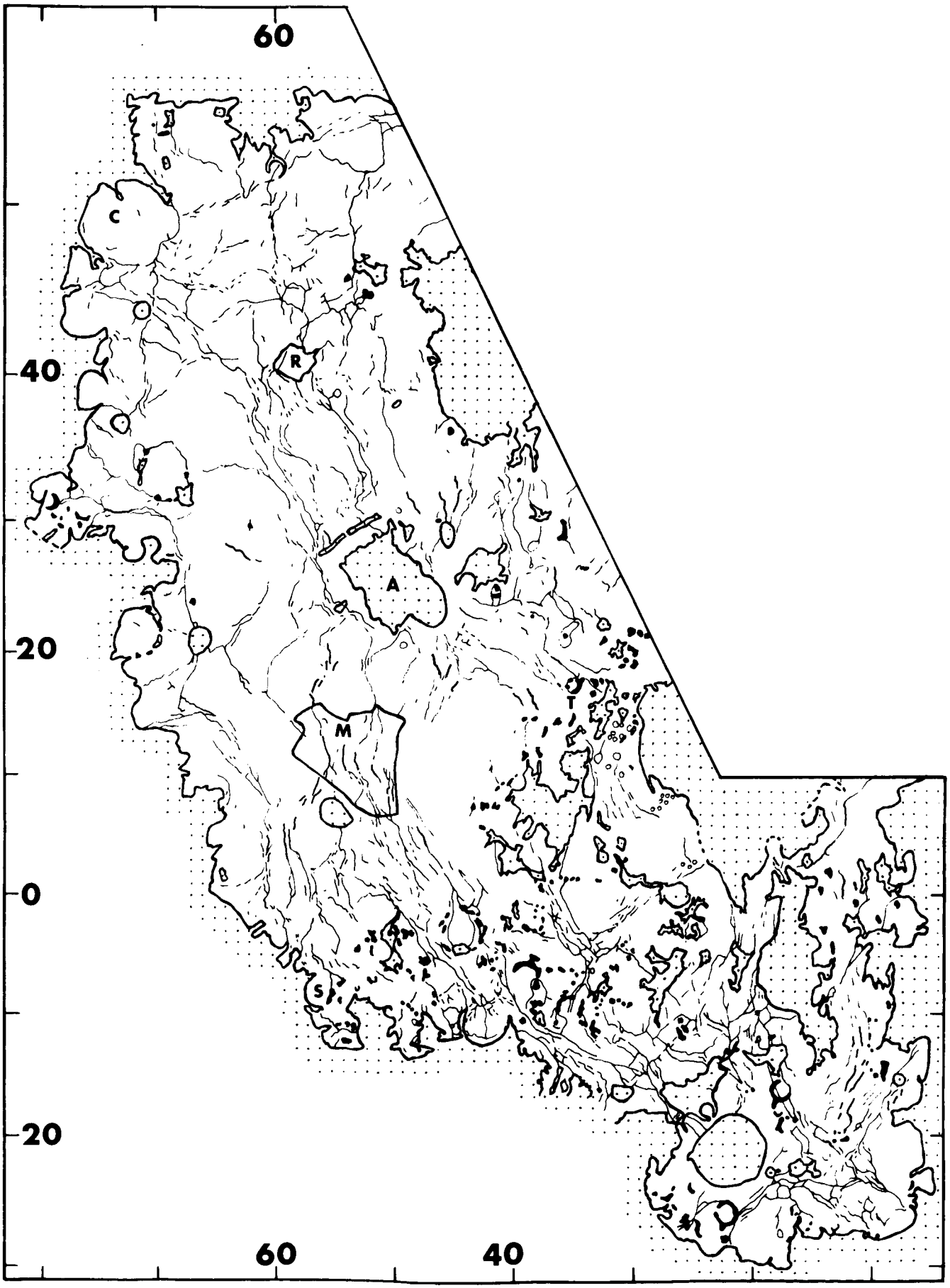
60
40
20
0
20
60
40
C
R
A
M
T
S

ression acted to reduce the zone of extensional stress outside the mare load and to enhance the compression within the load area; the horizontal compressive stresses acting to shut off volcanism.

A further consequence of post-graben volcanism appears to have been that the lunar crust was unable to completely compensate isostatically. A small positive gravity anomaly appears to be associated with the Sharp Formation in Procellarum (Whitford-Stark,1980) while the centers of the mascon maria (Imbrium,Serenitatis,Crisium,Humorum, and Smythii) are all occupied by young basalts(Whitford-Stark and Head,1980a; Howard et al,1973; Head et al,1978; Pieters et al,1975; Boyce and Johnson,1978) in spite of their vents being at the mare periphery. The situation is complicated by the apparent lack of graben in Crisium, Smythii, and Nectaris(Lucchitta and Watkins,1978) and a suggested uniformity both in age(Wilhelms and McCauley,1971) and composition(Pieters,1978) of the Nectaris surface basalts. Such a scenario would not be inconsistent, however, with a thicker lithosphere beneath the eastern mascon maria(Head and Solomon,1980) preventing the development of graben.

Mare ridge production:

Both Imbrium and Procellarum contain mare ridges (figures 1 and 8). In Imbrium the major portion of the ridges outline a basin ring, largely now buried by mare basalts, while in Procellarum the ridges exhibit three

distinct patterns in each of the three mare subdivisions; reticulate in the southeast, a parallel centrally-located zone in the center, and a polygonal pattern in the north. The various arguments for a tectonic or volcanic origin for the ridges have been summarized by Sharpton and Head (1980) and will not be repeated here.

In both Imbrium and Procellarum ridge production can be shown (Schaber,1973; Whitford-Stark and Head,1980c) to post-date the emplacement of the youngest basalts. The evidence for the earliest period of ridge formation, however, is less clear-cut. In Imbrium the apparent smoothing of centrally-located ridges by Unit 4(3.5 $\pm$ 0.25 b.y.) suggests that ridge formation pre-dated the emplacement of those basalts. The initiation of ridge formation in Imbrium therefore pre-dated the termination of graben production. In Procellarum, the period of major ridge production pre-dated the emplacement of the Sharp Formation(Pieters et al, 1980). Furthermore, deformation of the Telemann Formation (3.6 $\pm$ 0.2 b.y.) appears to have pre-dated emplacement of the Hermann Formation(Whitford-Stark and Head,1980a).Ridge production in Procellarum therefore also appears to have pre-dated the termination of graben production. Such a scenario is consistent with the thick mare loads of the pre-graben period and decrease in subsidence with time as the lithosphere thickened(Solomon and Head,1979).

Although an age range of at least 0.5 b.y. can be demonstrated for ridge production, it is difficult to define whether individual ridges were formed gradually or

in short, discrete intervals. Both in Imbrium and Procellarum it has been shown that ridges grew between successive basalt eruptions(Schaber,1973; Bryan,1973; Greeley,1971). Since the ages of these flows are indistinguishable by currently available dating techniques, it would imply that individual ridges could have grown extremely rapidly. However, the generally non cross-cutting nature and regular offsets of the ridges also suggests that they were formed within a uniform stress field(Whitford-Stark and Head,1980c). Since the distribution of ridges in Imbrium and Procellarum differs, it follows that the stress distribution in each differed. Such a result is to be expected because of the differences in morphology of the two maria; the Imbrium ridges reflecting the circular basalt distribution, and the Procellarum ridges the oblong outline of the mare. It would appear, however, that a global component of stress was superimposed on the local stress patterns causing a preferential north-south alignment of the ridge pattern(Fagin et al,1978).

In summary, mare ridges grew over a substantial time period though individual ridges may have grown quite rapidly, the major period of ridge production appears to pre-date or be synchronous with the termination of graben production though ridges continued to form after the eruption of the youngest basalts in both maria, the ridge distribution appears to have been controlled by the basin shape(therefore basalt thickness variation) and a global stress component. These observations are best supported by a tectonic origin

for the ridges even though they have also been the sites of volcanic eruptions(e.g.,Greeley and Spudis,1978).

Post-basalt history:

Subsequent to the emplacement of the youngest basalts in each mare, the basaltic pile has continued to deform. This deformation included the formation of the previously described mare ridges and the more widespread gradual subsidence of the mare surface(Scott et al,1978). In general it appears that basinal areas where the basaltic pile is thickest continued to preferentially subside with respect to areas of thin fill. In places, however, reversed topography along sinuous rilles suggests that formerly basinal areas did not remain so(Whitford-Stark and Head,1980c).

Other post-basalt events include the formation of impact craters. In comparison with syn- and pre-mare craters they are generally small(less than 30 km diameter; though Copernicus has a diameter of 93 km) and have prominent ejecta blankets. These cratering events served to excavate and redistribute the mare basalts and highland rocks, leading to the formation of multi-layered regoliths(e.g.,Basu and Bower,1977).

Summary and implications for basalt petrogenesis:

The main features of the evolution of Imbrium and Procellarum are outlined in figure 9. Procellarum is an

Figure 9. Summary of events in the evolution of Mare Imbrium and Oceanus Procellarum. The central column denotes age in 10^9 years. The length of the bars on each side of the central column indicates the estimated time range of the event specified.

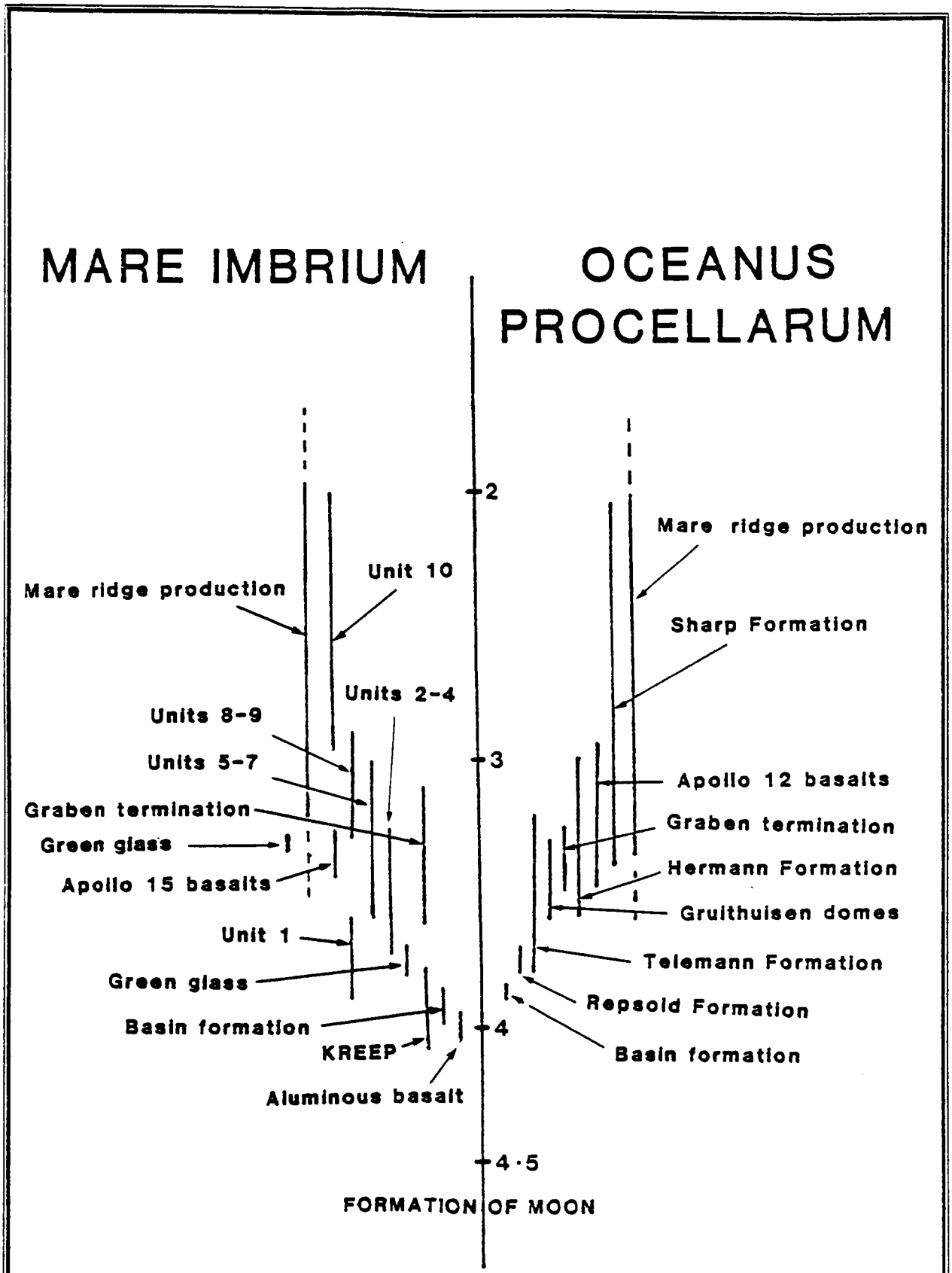
MARE IMBRIUM
OCEANUS PROCELLARUM
2
3
4
4·5
Mare ridge production
Unit 10
Units 2-4
Units 8-9
Units 5-7
Graben termination
Green glass
Apollo 15 basalts
Unit 1
Green glass
Basin formation
KREEP
Aluminous basalt
Mare ridge production
Sharp Formation
Apollo 12 basalts
Graben termination
Hermann Formation
Gruithuisen domes
Telemann Formation
Repsold Formation
Basin formation
FORMATION OF MOON

Figure 9

irregular mare with an area of about 1,700,000 km^2 and has a basalt fill estimated at 0.87 x 10^6 km^3 while Imbrium is a circular mare with a basalt area of approximately 850,000 km^2 and a volume of about 2.2 x 10^6 km^3(Whitford-Stark and Head,1980a,b). The chemical evolution of Procellarum lavas appears to have been relatively simple with early titanium-rich basalts followed by titanium-depleted basalts, in turn followed by intermediate basalts and concluding with titanium-rich basalts. Non-mare, highlands basalts were erupted synchronously with these materials. In contrast, although the earliest basalts of Imbrium are unexposed, the surface basalts exhibit no simple chemical trend; different chemistries appear to have been synchronously erupted, at least ten distinctive eruptive phases can be identified, and KREEP basalts formed an important component of the early basalt fill. Eruption styles in the two maria were similar though Procellarum lacks the short-duration flood basalts peculier to Imbrium and contains three unique igneous complexes. The youngest basalts in both areas were preferentially erupted from vents near the mare periphery and were titanium-rich. Tectonic deformation in both maria was essentially similar both in timing and morphologic result. A major difference, however, was the areal distribution of the deformed products; this being locally controlled by the basin morphology, basalt thickness variation, and elastic lithosphere thickness differences.

Currently available models of mare basalt petrogenesis

have been reviewed by Papike et al(1976). Three basic types of models have been proposed: one with a cumulate source, one with a primitive source, and one invoking assimilation processes. Each model has its attractive qualities but, additionally, each can be questioned on the basis of chemical or isotopic data(Papike et al,1976). Furthermore, samples returned from the lunar landing sites were generally understood by experimental petrologists to be representative of mare basalts in general. These samples suggested a fairly simple relationship between basalt chemistry and age. By synthesizing remote-sensing data, Pieters(1978) was able to show that there are many basalt types at the lunar surface which remained unsampled. More recently, by combining remote-sensing and photogeologic data, the present and other authors(Whitford-Stark and Head,1980a,b; Pieters et al,1980) have shown that there is no simple relationship between basalt chemistry and age; basalts of different chemistry were erupted simultaneously both within and between maria and the chemical sequences differed between maria. Additionally it was shown that even the surface basalts may not represent the entire lunar basaltic suite; the early eruptives being buried by younger materials. The emerging picture is one of early(pre- 3.3 $\pm$ 0.3 b.y.) voluminous eruptions, perhaps with little chemical diversity(KREEP and titanium-rich basalts) and subsequent, volumetrically small($\leq$ 1,500 km^3), chemically diverse eruptions. The ubiquity of vents and complex age and composition relationships of lunar mare basalts suggests

that they had chemically heterogeneous, perhaps unconnected, source regions. These observations are not readily reconcilable with existing petrogenetic models. Moreover, there is now ample evidence that basaltic volcanism did not commence following the "terminal lunar cataclysm" but may have preceded it by in excess of 200 million years and may have continued, albeit in small volumes, to at least 2.0 b.y. ago, a duration of 1.2 b.y.

ACKNOWLEDGEMENTS

I would like to thank Jim Head for the encouragement to persue this topic and the advice and criticism that he offered during its development. I would also like to thank Sam Merrell for the photographic reproduction of the figures. This work was performed under NASA grant NGR-40-002-116.

REFERENCES

Baldwin R.B. (1963) The Measure of the Moon.The Univ. of Chicago Press,Chicago. 488p.

Basu A. and Bower J.F. (1977) Provenance of Apollo 15 deep drill core sediments. Proc.Lunar Sci.Conf.8th.2841-2867.

Blanchard D.P. and Budahn J.R. (1979) Remnants from the ancient lunar crust: Clasts from Consortium breccia 73255. Proc.Lunar Planet.Sci.Conf.9th. 803-816.

Boyce J.M. and Johnson D.A. (1977) Ages of flow units in Mare Crisium based on crater density. Proc.Lunar Sci.Conf. 8th. 3495-3502.

Boyce J.M. and Johnson D.A. (1978) Ages of flow units in the far eastern maria and implications for basin-filling history. Proc.Lunar Planet.Sci.Conf.9th.3275-3284.

Bryan W.B, (1973) Wrinkle ridges as deformed surface crust on ponded mare lavas. Proc.Lunar Sci.Conf.4th.93-106.

Cadogan P.H. (1974) Oldest and largest lunar basin ? Nature, 250, 315-316.

Carlson R.W. and Lugmair G.W. (1979) Sm-Nd constraints on early lunar differentiation and the evolution of KREEP. Earth Planet.Sci.Letters 45, 123-132.

Chao F.C.T. (1977) The Ries Crater of Southern Germany - a model for large craters on planetary surfaces. Geologisches Jahrbuch, 43, 3-85.

Conca J. and Hubbard N (1979) Evidence for early volcanism in

Mare Smythii. Proc.Lunar Planet.Sci.Conf.10th. 1727-1737.

De Hon R.A. (1979) Thickness of the western mare basalts. Proc.Lunar Planet.Sci.Conf.10th. 2935-2955.

Delano J.W. (1979) Apollo 15 green glass: Chemistry and possible origin. Proc.Lunar Planet.Sci.Conf.10th.275-300.

Fagin S.W.,Worrall D.M., and Muehlberger W.R. (1978) Lunar mare ridge orientations. Implications for lunar tectonic models. Proc.Lunar Planet.Sci.Conf.9th. 3473-3479.

Gifford A.W. and El-Baz F. (1979) Distribution and ages of light-colored plains on the Moon.(abstract) In, Conference on the lunar highlands crust. The Lunar and Planetary Institute,Houston,Texas. 21-23.

Golombek M.P. (1979) Structural analysis of lunar grabens and the shallow crustal structure of the Moon. J.Geophys. Res. 84, 4657-4666.

Greeley R. (1971) Lava tubes and channels in the lunar Marius Hills. The Moon, 3, 289-314.

Greeley R. (1976) Modes of emplacement of basalt terrains and an analysis of mare volcanism in the Orientale basin. Proc.Lunar Sci.Conf.7th. 2747-2759.

Greeley R. and Spudis P.D. (1978) Mare volcanism in the Herigonius region of the Moon. Proc.Lunar Planet Sci.Conf. 9th. 3333-3350.

Grove T.L. and Vaniman D.T. (1978) Experimental petrology of very low Ti (VLT) basalts. In, Mare Crisium: The view

from Luna 24. (R.B.Merrill and J.J.Papike,eds.)Pergamon, New York. 445-471.

Guggisberg S.,Eberhardt P.,Geiss J.,Grogler N.,Stettler A., Brown G.M., and Peckett A. (1979) Classification of the Apollo 11 mare basalts according to Ar^{39}-Ar^{40} ages and petrological properties. Proc.Lunar Planet.Sci. Conf.10th. 1-39.

Hartmann W.K. and Wood C.A. (1971) Moon: Origin and evolution of multi-ring basins. The Moon, 3, 3-78.

Hawke B.R. and Head J.W. (1977) Pre-Imbrian history of the Fra Mauro region and Apollo 14 sample provenance. Proc. Lunar Sci.Conf.8th. 2741-2761.

Hawke B.R. and Head J.W. (1979) Impact melt volumes associated with lunar craters.(abstract) In, Lunar and Planetary Science X. The Lunar and Planetary Institute,Houston, Texas. 510-512.

Hawke B.R. and Head J.W. (1980) Small dark mantle deposits of possible pyroclastic origin: Geologic setting,composition and relation to regional stratigraphy.(abstract). In, Lunar and Planetary Science XI. The Lunar and Planetary Institute,Houston,Texas.

Hawke B.R.,MacLaskey D.,McCord T.B.,Adams J.B.,Head J.W., Pieters C.M.,and Zisk S.H. (1979) Multispectral mapping of the Apollo 15 - Apennine region: The identification and distribution of regional pyroclastic deposits.Proc. Lunar Planet.Sci.Conf.10th. 2995-3015.

Head J.W. (1974) Orientale multi-ringed basin interior and impl-

implications for the petrogenesis of lunar highland samples. The Moon, 11, 327-356.

Head,J.W.(1974b) Lunar dark mantle deposits: Possible clues to the distribution of early mare deposits. Proc. Lunar Sci.Conf.5th., 207-222.

Head,J.W.(1977) Origin of the outer rings in lunar multi-ringed basins: Evidence from morphology and ring spacing. In,Impact and explosion cratering (eds. D.J.Roddy et al.) Pergamon,N.Y. 563-573.

Head,J.W.(1979) Lava flooding of early planetary crusts: Geometry,thickness, and volumes of flooded impact basins (abstract). In,Lunar and Planetary Science X, The Lunar and Planetary Institute,Houston,Texas.516-518

Head,J.W. and McCord,T.B.(1978) Imbrian-age highland volcanism on the Moon: The Gruithuisen and Mairan domes. Science, 199, 1433-1436.

Head,J.W. and Solomon,S.C.(1980) Lunar basin structure: Possible influence of variations in lithospheric thickness (abstract). In,Lunar and Planetary Science XI, The Lunar and Planetary Institute,Houston, Texas. 421-423.

Head,J.W. and Wilson,L.(1980) The formation of eroded depressions around the sources of lunar sinuous rilles: Observations (abstract). In,Lunar and Planetary Science XI, The Lunar and Planetary Institute, Houston, Texas. 426-428.

Head,J.W.,Adams,J.B.,McCord,Y.B.,Pieters,C. and Zisk,S. (1978) Regional stratigraphy and geologic history of Mare Crisium.In,Mare Crisium: The View from Luna 24.

(R.B.Merrill and J.J.Papike,eds.). Pergamon,N.Y.43-74.

Head J.W.,Solomon S.C. and Whitford-Stark J.L. (1980) Oceanus Procellarum region: Evidence for an anomalously thin early lunar lithosphere.(abstract). In, Lunar and Planetary Science XI. The Lunar and Planetary Institute, Houston, Texas.

Heiken G.H.,McKay D.S., and Brown R.W. (1974) Lunar deposits of possible pyroclastic origin. Geochim.Cosmochim.Acta 38, 1703-1718.

Hodges C.A. and Wilhelms D.E. (1978) Formation of lunar basin rings. Icarus,34, 294-323.

Howard K.A.,Carr M.H., and Muehlberger W.R. (1973) Basalt stratigraphy of southern Mare Serenitatis. Apollo 17 Preliminary Science Report. NASA SP-330. 29.1-29.12.

Hulme G. (1974a) Generation of magma at lunar impact crater sites. Nature, 252, 556-558.

Hulme G. (1974b) The interpretation of lava flow morphology. Geophys.J.R.Astr.Soc. 39, 361-383.

Hulme G. and Fielder G. (1977) Effusion rates and rheology of lunar lavas. Phil.Trans.R.Soc.Lond.A. 285, 227-234.

Huneke J.,Jessberger E.K., and Wasserburg G.J. (1974) The age of metamorphism of a highland breccia(65015) and a glimpse at the age of its protolith. (abstract) In, Lunar Science V. The Lunar Science Institute,Houston, Texas. 375-377.

Husain L. (1972) The ^{40}Ar-^{39}Ar and cosmic ray exposure ages of Apollo 15 crystalline rocks, breccias and glasses. (abstract). In, The Apollo 15 Lunar Samples.(eds.J.W.Chamberlain and C.Watkins)The Lunar Science Institute,Houston,

Texas. 375-377.

Kaula W.M.,Schubert G.,Lingenfelter R.E.,Sjogren W.L., and Wollenhaupt W.R. (1972) Analysis and interpretation of lunar laser altimetry. Proc.Lunar Sci.Conf.3rd.2189-2204.

Lucchitta B.K. and Watkins J.A. (1978) Age of graben systems on the Moon.Proc.Lunar Planet.Sci.Conf.9th.3459-3472.

Malin M.C. (1974) Lunar red spots: Possible pre-mare materials. Earth Planet.Sci.Letters, 21, 331-341.

Maxwell T.A., and Phillips R.J.(1978) Stratigraphic correlation of the radar-detected subsurface interface in Mare Crisium. Geophys.Res.Letters, 5,811-814.

McGetchin T.R.,Settle M. and Head J.W. (1973) Radial thickness variations in impact crater ejecta: Implications for lunar basin deposits. Earth Planet.Sci.Letters,20,226-236.

Metzger A.E.,Haines E.L.,Parker R.E.,and Radocinski R.G.(1977) Thorium concentration in the lunar surface.I: Regional values and crustal content. Proc.Lunar Sci.Conf.8th. 949-999.

Metzger A.E.,Haines E.L.,Etchegaray-Ramirez M.I. and Hawke R.B. (1979) Thorium concentrations in the lunar surface:III. Deconvolution of the Apenninus region. Proc.Lunar Planet. Sci.Conf.10th. 1701-1718.

Meyer C. (1977) Petrology, mineralogy, and chemistry of KREEP basalt. Phys.Chem.Earth, 10, 239-260.

Norman M.D. and Ryder G.(1979) A summary of the petrology and geochemistry of pristine highland rocks. Proc.Lunar

Planet.Sci.Conf.10th. 531-559.

Nyquist L.E. (1977) Lunar Rb-Sr chronology. Phys.Chem.Earth, 10, 103-142.

Nyquist L.E.,Bansal B.M., and Wiesman H. (1975) Rb-Sr ages and initial $^{87}Sr/^{86}Sr$ for Apollo 17 basalts and KREEP basalt 15386. Proc.Lunar Sci.Conf.6th.1445-1465.

Oberbeck V.R.,Morrison R.H.,Horz F.,Quaide W.L., and Gault D.E. (1974) Smooth plains and continuous deposits of craters and basins. Proc.Lunar Sci.Conf.5th. 111-136.

Papike J.J. and Vaniman D.T. (1978) Luna 24 ferrobasalts and the mare basalt suite: Comparative chemistry,mineralogy, and petrology. In, Mare Crisium: The view from Luna 24. (eds.R.B.Merrill and J.J.Papike)Pergamon,N.Y.371-401.

Papike J.J.,Hodges F.N.,Bence A.E.,Cameron M., and Rhodes J.M. (1976) Mare basalts: Crystal chemistry, mineralogy and petrology.Rev,Geophys.Space Phys. 14, 475-540.

Peeples W.J.,Sill W.R.,May T.W.,Ward S.H.,Phillips R.J.,Jordan R.L.,Abbott E.A., and Killpack T.J. (1978) Orbital radar evidence for lunar subsurface layering in Maria Serenitatis and Crisium. J.Geophys.Res. 83,3459-3468.

Pieters C.M. (1978) Mare basalt types on the front side of the Moon: A summary of spectral reflectance data. Proc.Lunar Planet.Sci.Conf.9th. 2825-2849.

Pieters C.M.,Head J.W.,McCord T.B.,Adams J.B. and Zisk S.H. (1975) Geochemical and geological units of Mare Humorum: Definition using remote sensing and lunar sample information. Proc.Lunar Sci.Conf.6th. 2689-2710.

Pieters C.M.,Head J.W.,Adams J.B.,McCord T.B.,Zisk S.H.,and Whitford-Stark J.L. (1980) Late high titanium basalts of the western maria: Geology of the Flamsteed region of Oceanus Procellarum. J.Geophys.Res. in press.

Pike R.J. (1974) Depth/diameter relations of fresh craters: Revision from Spacecraft data.Geophys.Res.Letters, 1, 291-294.

Podosek F.A. and Huneke J.C. (1973) Argon in Apollo 15 glass spherules(15426) , ^{40}Ar-^{39}Ar age and trapped argon. Earth Planet.Sci.Letters, 19, 413-421.

Reid A.M.,Warner J.,Ridley W.I.,Johnson D.A.,Harmon R.S.,Jakes P., and Brown R.W. (1972) The major element compositions of lunar rocks as inferred from glass compositions in the lunar soils. Proc.Lunar Sci.Conf.3rd.363-378.

Ridley W.I. (1975) On high-alumina mare basalts. Proc.Lunar Sci.Conf.6th. 131-145.

Ridley W.I.,Reid A.M.,Warner J.L.,and Brown R.W. (1973) Apollo 15 green glass. Phys.Earth Planet.Int. 7,133-136.

Rutherford M.J.,Hess P.C.,Ryerson F.J.,Campbell H.W. and Dick P.A. (1976) The chemistry, origin and petrogenetic implications of lunar granite and monzonite. Proc.Lunar Sci.Conf.7th. 1723-1740.

Ryder G. and Spudis P.D. (1979) Volcanism prior to the termination of the heavy bombardment: Evidence, characteristics, and concepts.(abstract). In, Conference on the Lunar Highlands Crust.The Lunar and Planetary Institute, Houston,Texas. 132-134.

Ryder G. and Taylor G.J. (1976) Did mare-type volcanism commence early in lunar history ? Proc.Lunar Sci.Conf.7th. 1741-1755.

Schaber G.G. (1973) Lava flows in Mare Imbrium: Geologic evaluation from Apollo orbital photography. Proc.Lunar Sci.Conf.4th. 72-92.

Schaber G.G.,Boyce J.M., and Moore H.J. (1976) The scarcity of mappable flow lobes on the lunar maria: Unique morphology of the Imbrium flows. Proc.Lunar Sci.Conf.7th. 2783-2800.

Schonfield E. and Meyer C. (1973) The old Imbrium hypothesis. Proc.Lunar Sci.Conf.4th. 125-138.

Schultz P.H. and Spudis P.D. (1979) Evidence for ancient mare volcanism. Proc.Lunar Planet.Sci.Conf.10th.2899-2918.

Scott D.H.,Watkins J.A.,and Diaz J.M. (1978) Regional deformation of mare surfaces. Proc.Lunar Planet.Sci.Conf.9th. 3527-3539.

Settle M. and Head J.W. (1976) Excavations depths of large lunar impacts: Shallow or deep ? In, Interdisciplinary Studies by the Imbrium Consortium, Volume 1. Center for Astrophysics, Smithsonian,Cambridge,Mass. 139-146.

Sharpton V.L. and Head J.W. (1980) Lunar mare arches and ridges: Relation of ridge lobes to small pre-existing craters. (abstract). In, Lunar and Planetary Science XI.The Lunar and Planetary Institute,Houston,Texas.

Solomon S.C. and Head J.W. (1979) Vertical movement in mare basins: Relation to mare emplacement, basin tectonics,

and lunar thermal history. J.Geophys.Res.84,1667-1682.

Spudis P.D. (1978) Composition and origin of the Apennine Bench Formation.Proc.Lunar Planet.Sci.Conf.9th. 3379-3394.

Spudis P.D. (1979) The extent and duration of lunar KREEP volcanism.(abstract) In, Conference on the Lunar Highlands Crust. The Lunar and Planetary Institute,Houston, Texas. 157-159.

Staudacher Th.,Jessberger E.K.,Flohs I., and Kirsten T.(1979) ^{40}Ar-^{39}Ar age systematics of consortium breccia 73255. Proc.Lunar Planet.Sci.Conf.10th. 745-762.

Steele I.M.,Irving A.J., and Smith J.V. (1977) Apollo 15 breccia rake samples - mineralogy of lithic and mineral clasts. Proc.Lunar Sci.Conf.8th. 1925-1941.

Stuart-Alexander D.E.(1978) Geologic map of the central far side of the Moon. U.S.Geol.Survey Misc.Inv.Map Ser. I-1047.

The Lunatic Assylum (1978) Petrology, chemistry, age and irradiation history of Luna 24 samples. In, Mare Crisium: The view from Luna 24.(eds.R.B.Merrill and J.J.Papike). Pergamon,N.Y. 657-678.

Thurber C.H. and Solomon S.C. (1978) An assessment of crustal thickness variations on the lunar near side: Models, uncertainties, and implications for crustal differentiation. Proc.Lunar Planet.Sci.Conf.9th.3481-3497.

Todhunter R. (1975) A descriptive account of the geomorphology of southwest Mare Imbrium interpreted with the aid of

a comparative study of selected Icelandic lava flows. Unpublished Ph.D.Thesis, University of Lancaster.

Turner G. (1977) Potassium-argon chronology of the Moon. Phys.Chem.Earth.,10, 145-195.

Ulrich G.E. (1969) Geologic map of the J.Herschel quadrangle of the Moon. U.S.Geol.Survey Misc.Geol.Inv.Map I-604.

Warner J.L.,Phinney W.C.,Bickel C.E., and Simonds C.H. (1977) Feldspathic granulitic impactites and pre-final bombardment lunar evolution. Proc.Lunar Sci.Conf.8th.2051-2066.

Warner R.D.,Taylor G.J.,Mansker W.L. and Keil K.(1978) Clast assemblages of possible deep-seated(77517) and immiscible-melt(77538) origins in Apollo 17 breccias. Proc. Lunar Planet.Sci.Conf.9th. 941-958.

Warner R.D.,Taylor G.J., and Keil K. (1979) Composition of glasses in Apollo 17 samples and their relation to known lunar rock types. Proc.Lunar Planet.Sci.Conf.10th. 1437-1456.

Whitford-Stark J.L. (1974) Internal origin for lunar rilled craters and the maria ? Nature,248, 573-574.

Whitford-Stark J.L. (1979) Charting the Southern Seas: The evolution of the lunar Mare Australe. Proc.Lunar Planet. Sci.Conf.10th. 2975-2994.

Whitford-Stark J.L. (1980) Problems associated with the identification of magma composition from volcanic landforms. (abstract). In, Reports of the Planetary Geology Program, 1979-1980. NASA TM-81776. 195-197.

Whitford-Stark J.L. (1980) The gravity anomalies of Oceanus

Procellarum. (abstract) In, Reports of the Planetary Geology Program, 1979-1980. NASA TM-81776 22-24.

Whitford-Stark J.L. and Fryer R.J. (1975) Origin of Mare Frigoris. Icarus, 26, 231-242.

Whitford-Stark J.L. and Head J.W. (1977) Oceanus Procellarum: Volcanic and tectonic evolution.(abstract) In, Lunar Science VIII. The Lunar Science Institute,Houston, Texas. 1011-1013.

Whitford-Stark J.L. and Head J.W. (1977b) The Procellarum volcanic complexes: Contrasting styles of volcanism. Proc.Lunar Sci.Conf.8th. 2705-2724.

Whitford-Stark J.L. and Head J.W. (1980a) Stratigraphy of Oceanus Procellarum basalts: Sources and styles of emplacement. J.Geophys.Res. in Press.

Whitford-Stark J.L. and Head J.W. (1980b) The stratigraphy of Mare Imbrium. This thesis.

Whitford-Stark J.L. and Head J.W. (1980c) The tectonic evolution of the Oceanus Procellarum basin.This thesis.

Wilhelms D.E. (1979) Relative ages of lunar basins.(abstract) In, Reports of the Planetary Geology Program,1978-1979. NASA TM-80339. 135-137.

Wilhelms D.E. and El-Baz F. (1977) Geologic map of the east side of the Moon.U.S.Geol.Survey Misc.Inv.Ser.Map I-948.

Wilhelms D.E. and McCauley J.F. (1971) Geologic map of the nearside of the Moon.U.S.Geol.Survey Misc.Geol.Inv.Map I-495.

Wilson L. and Head J.W. (1980) Ascent and emplacement of basaltic magma on the Earth and Moon. Submitted to J.Geophys.Res.

☆U.S. GOVERNMENT PRINTING OFFICE: 1983-639-008/ 23

1. Report No.	2. Government Accession No.	3. Recipient's Catalog No.
NASA TM-85630		

4. Title and Subtitle	5. Report Date
Advances in Planetary Geology	February 1983
	6. Performing Organization Code

7. Author(s)	8. Performing Organization Report No.
Alex Woronow, Editor	
	10. Work Unit No.

9. Performing Organization Name and Address	11. Contract or Grant No.
University of Houston Department of Geology Houston, Texas	
	13. Type o Report and Period Covered
12. Sponsoring Agency Name and Address	Technical Memorandum
NASA Office of Space Science and Applications Solar System Exploration Division Washington, DC 20546	14. Sponsoring Agency Code

15. Supplementary Notes

16. Abstract

Part I: Martin Global Tectonics.

Scarps, ridges, and grabens within the heavily cratered terrain of Mars define distinct groups of structural trends on a regional scale, and a pattern of crustal deformation on a global scale. These trends are the result of regional deformations of the crust, rather than the imposition of a single planet-wide stress system, and reflect a fundamental global organization of volcanic and tectonic activity.

Part II: A Comparison of the Origin and Evolution of a Circular and Irregular Lunar Mare.

The origin and development of the circular Mare Imbrium and the irregular Oceanus Procellarum is compared. Imbrium is a deeply flooded (3-8 km), multi-ring basin with a complex eruption sequence of at least 10 major basalt units. Procellarum is hypothesized to be a down-faulted region of highland crust - a direct result of the Imbrium basin forming event. The basalt fill in Procellarum is thin (average 550m) and is separated into four chemically distinct formations.

17. Key Words (Suggested by Author(s))	18. Distribution Statement
Planetary Geology Planetology	Unclassified-Unlimited Subject Category 91

19. Security Classif. (of this report)	20. Security Classif. (of this page)	21. No. of Pages	22. Price
Unclassified	Unclassified	357	A16

N-305

For sale by the National Technical Information Service, Springfield, Virginia 22161